UNIVERSIDAD AUTÓNOMA DE MADRID

INSTITUTO DE FÍSICA TEÓRICA

TESIS DOCTORAL

Entanglement in inhomogeneous quantum chains

Autor: Daniel Nadir SAMOS SÁENZ DE BURUAGA

Directores: Dr. Germán SIERRA y Dr. Javier RODRÍGUEZ-LAGUNA

Memoria de Tesis Doctoral presentada
ante el Departamento de Física Teórica
de la Universidad Autónoma de Madrid
para optar al título de Doctor en Física Teórica

Diciembre, 2021

De hecho, podríamos decir que el todo
sólo es el resultado de la suma de las partes
cuando las partes se ignoran entre sí.

El corazón helado,
ALMUDENA GRANDES

Para mamá y papá

About this thesis

This document collects part of the work developed during my Ph.D. at the Instituto de Física Teórica in Madrid under the direction of Prof. Germán Sierra and Prof. Javier Rodríguez-Laguna. The main goal of this thesis is to improve our understanding of the quantum entanglement properties of low-dimensional inhomogeneous systems. The thesis is based on the following publications:

- N. Samos Sáenz de Buruaga, S. N. Santalla, J. Rodríguez-Laguna and G. Sierra, *Symmetry protected phases in inhomogeneous spin chains*, JSTAT 093102 (2019).
- N. Samos Sáenz de Buruaga, S. N. Santalla, J. Rodríguez-Laguna and G. Sierra, *Piercing the rainbow state: Entanglement on an inhomogeneous spin chain with a defect*, Phys. Rev. B **101**, 205121 (2020).
- N. Samos Sáenz de Buruaga, S. N. Santalla, J. Rodríguez-Laguna and G. Sierra, *Entanglement in noncritical inhomogeneous quantum chains*, Phys. Rev. B **104**, 195147 (2021).

I declare that this thesis is the result of my own original work and that it has not been submitted for any other degree or academic award. In cases where the work of others is presented, appropriate citations are used.

Quantum entanglement has recently become a cornerstone in theoretical physics, being, therefore, a very rich and complex subject. This is why I have made a theoretical introduction in some detail that is intended to be useful for a student or researcher entering this field. The thesis presents appendices in each chapter that collect either the most laborious calculations or a review of basic content that the expert reader can skip.

The characterization of inhomogeneous systems requires different techniques, both numerical and analytical. All figures presented in this paper have been created expressly or belong to the aforementioned papers. Likewise, all the results have been obtained using codes written in C++ with the Hvb library[1] or in Python. Do not hesitate to contact me if you want any code.

[1] Hvb is free software, and is released under the GPL. You can download it from the github repository:
http://github.com/jvrlag/hvb

Agradecimientos

El proceso de escritura de tesis se me antoja como una travesía larga a pie que recorre varios parajes. Por supuesto, ha tenido sus tramos difíciles y menos bonitos, pero incluso esos, con el tiempo, se tornan interesantes al contemplarlos y tratar de aprender de ellos. He disfrutado y aprendido muchísimo y me siento agradecido por la oportunidad. Acabo cansado del viaje, con las botas muy desgastadas pero con una gran sonrisa.

Así, a estas alturas, soy muy consciente de la gran suerte que he tenido de que mis directores fueran Germán Sierra y Javier Rodríguez Laguna. Ellos han estado siempre ahí, sosteniéndome, exigiéndome y señalándome el camino. Mi gratitud por su cercanía, disponibilidad y dedicación. Esta tesis existe gracias a ellos. Guardo con muchísimo cariño las discusiones en la mesa redonda del despacho 118 y maldita esta pandemia que nos privó de unas cuantas. Desearía seguir siendo el pupilo de Germán toda la vida. Agradezco a Javi su disponibilidad plena y sus enseñanzas sobre física y tantas otras cosas. Mi agradecimiento también a Silvia por su simpatía, buenas ideas y por compartir su extraordinaria habilidad para crear buenas figuras. My gratitude to Erik Tonni for allowing me to get to know SISSA. Living in Trieste was a very enriching experience.

Agradezco a toda la gente del IFT, i.e, personal de limpieza, de conserjería, secretaría e investigador, con la que he tratado a lo largo de estos años. Gracias por crear un ambiente agradable y exigente. Extiendo mi agradecimiento a los profesores que he tenido a lo largo de mi vida, especial mención a Mariano Santander, Andrés Vega y Carlos Sabín porque me ayudaron a elegir este camino.

Gracias de corazón a mi familia. No quiero poner una retahíla de nombres, así que todos mis primos y tíos se den por aludidos. Gracias por todo el apoyo y cariño. Mención especial para mi tío David, por su eterna disponibilidad, buen ánimo y cariño. También me gustaría dedicar esta tesis a mis abuelas, Concha y Pilar, por su amor infinito.

Gracias a mis viejos amigos, Pablo, Dani y Jara, después de tanto tiempo ahí seguimos, y aunque no hablemos tanto como antes, siento su cariño y apoyo, y espero que también sientan el mío. Gracias a Fabián por tanta música y conversaciones. A Diego, por esos buenos partidos de tenis y pimpón y a Jorge por mostrarme la ejemplaridad. A Raquel, Adri y Chuchi porque jugar y hablar con vosotros ha supuesto una escapatoria a momentos en que esta travesía atravesaba

zonas desérticas. Gracias infinitas. Óscar *el maquinarias* merece mención a parte. Le agradezco enormemente todo el apoyo que me ha dado estos años.

Dejo en el tintero muchos nombres de amigos y espero que me disculpen por ello, así como por mi más que probable distanciamiento ocasionado por desarrollar esta tesis. Es sólo espacial.

Un párrafo aparte se merecen mis amigos de O'Donnell. A Christian le agradezco que reconociera yo era el tío más elegante del piso. Pero no, lo era él. A Javier, por esos buenos momentos viendo el fútbol. A Roi por enseñarme tantas cosas y por esas cenas de productos leoneses que compartía conmigo. A Beatriz, que tal como dijo Christian, ha dado un equilibrio a nuestra curiosa configuración. Es una bellísima persona y nunca olvidaré las conversaciones de balcón. A Simón, mi querido Simón, le agradezco muchísimas cosas, desde descubrirme recetas y música hasta entrenamientos y actitudes vitales. Solo lamento que no me gustase el cilantro. Ellos han sido mis compañeros de viaje del día a día, y nunca les olvidaré.

Mi agradecimiento a Maria José por todo su cariño, hospitalidad y esas tortillas de patata tan deliciosas.

Gracias a mis padres, José Manuel y Hungría, por su apoyo constante, su amor y comprensión y porque no perdieron la confianza en mí cuando tuve mis (pocos) momentos de desfallecimiento. Soy lo que soy gracias a a ellos.

Y finalmente, gracias a Marta. Hemos tenido la suerte de hacer la tesis a la vez y no tengo duda de que hemos sido oasis el uno del otro. Guardo en el recuerdo con muchísimo cariño esas largas videollamadas, trabajando, cada uno a lo nuestro o ayudándonos como podíamos. Gracias por esos ánimos constantes y esa predisposición a escuchar mis movidas sobre el arco-iris y los Majoranas. No tengo palabras para expresar todo lo que me ha dado y todo lo que me da.

Resumen

En esta tesis caracterizamos las propiedades de entrelazamiento cuántico de estados fundamentales de sistemas inhomogeneos en 1D. En particular consideramos modelos inhomogeneos de cadenas de fermiones libres y sus correspondientes versiones de espín obtenidas con la transformación de Jordan-Wigner. Las versiones homogéneas de estos modelos han sido ampliamente estudiadas y constituyen una buena referencia a la hora de estudiar la nueva física debida a la inhomogeneidad. Por ejemplo, la mayoría de los estados fundamentales obedecen la llamada ley del área de la entropía de entrelazamiento, la cual establece que la cantidad de entrelazamiento presente entre un subsistema y su entorno es proporcional a la medida de su frontera. Los estados fundamentales de ciertos sistemas inhomogeneos constituyen un ejemplo de violación de la ley del área. Un caso paradigmático se conoce asimismo como modelo arco-iris que describe una cadena de espín XX cuyos acoplos decrecen exponencialmente con una tasa h desde el centro de la cadena hacia los extremos. Su estado fundamental es el llamado estado arco-iris debido a que en el régimen de alta inhomogeneidad $h \gg 1$, el grupo de Renormalización de Fuerte Desorden predice un sólido de valencia de enlace formado por estados máximamente entrelazados (pares de Bell) concéntricos como puede verse en la Fig. 1.

El estado arco-iris presenta entrelazamiento de largo alcance y viola (máximamente) la ley del área. Ademas, la teoría de campos que describe el modelo en el régimen de baja inhomogeneidad $h \ll 1$ se corresponde con una teoría de campos conforme con carga central $c = 1$. En esta tesis usamos este estado como punto de partida para explorar los efectos que genera la inhomogeneidad, caracterizando las propiedades de entrelazamiento con diversas herramientas. En particular estudiamos las entropias de Rényi, el Hamiltoniano de entrelazamiento, el espectro de entrelazamiento y también el contorno de entrelazamiento. Los cuatro primeros capítulos son introductorios y presentan la tecnología básica ya introducida en la literatura[2]. Así, el Capítulo 1 pretende hacer una introducción general, no técnica del campo. En el Capítulo 2 se introduce el entrelazamiento cuántico y su caracterización. El Capítulo 3 discute en detalle la caracterización del entrelazamiento en una cadena homogenea XX, y finalmente en el Capítulo

[2]Es justo decir que la sección 4.2 es una generalización presentada por primera vez en este documento.

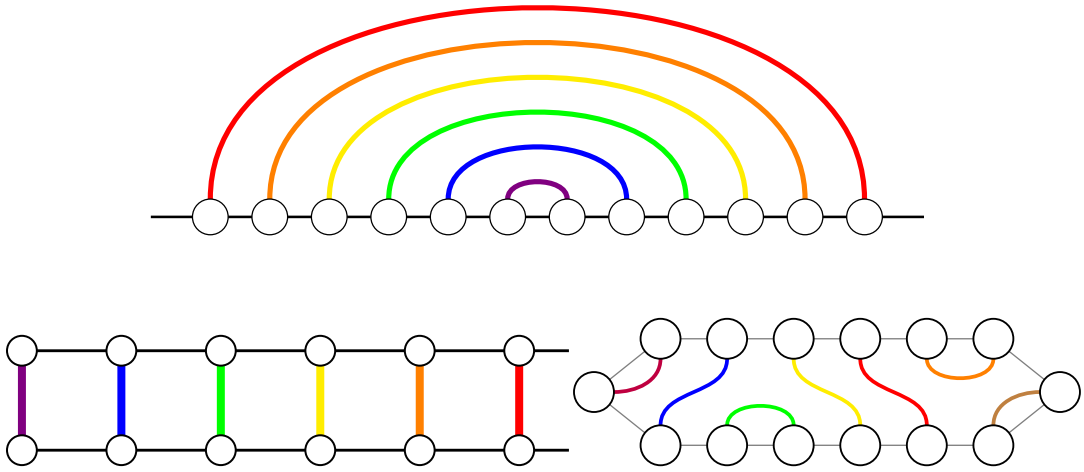

Figure 1: Arriba. Ilustración del estado arco-iris. Los sitios conectados por los arcos están entrelazados. Abajo izquierda (derecha) los estados plegados respecto al acoplo (sitio) central. El estado de la izquierda es topologicamente trivial mientras que el estado de la derecha es no-trivial.

4 introducimos una familia de modelos inhomogeneos y en particular el modelo arco-iris. Los tres capítulos siguientes presentan contenido original de esta tesis.

En el Captítulo 5 exploramos las implicaciones de añadir un defecto con intensidad variable γ en el modelo arco-iris. En el régimen de alta inhomogeneidad, mostramos que es posible generar transiciones entre fases con entrelazamiento corto (fases dimerizadas) y largo (fase arco-iris) sólo con cambiar la intensidad del defecto. Calculamos parámetros de orden y energías del Hamiltoniano de primera cuantización para apoyar este hecho. En lo que concierne al régimen de baja inhomogeneidad, mostramos que el sistema puede ser descrito con una teoría de campos conforme en espacio-tiempo curvo pero con una carga central efectiva dependiente de γ.

En el Capítulo 6 discutimos la posibilidad de caracterizar las fases críticas en el marco de las llamadas fases topológicas protegidas por simetría. Mostramos que una transformación de plegado de la cadena convierte el entrelazamiento de largo en entrelazamiento de corto alcance, permitiendo la descripción eficiente en término de estados producto de matrices (MPS) y la clasificación en fases topológicas protegidas por simetría. Aquellas fases que presentan una simetría de reflexión respecto al acoplo central son topologicamente triviales, mientras que las que presentan una simetría de reflexión respecto al sitio central son no triviales (vea la Fig. 1). De hecho, encontramos un estado fundamental que pertenecen a la fase AIII de la clasificación de aislantes topológicos cuyo representante paradigmático es el modelo de Su-Schrieffer-Heeger y un estado fundamental de una cadena inhomogénea con simetría $SU(2)$ muy similar al estado AKLT, perteneciente a la fase de Haldane. Además, proponemos una extensión de este resultado a cadenas

con espín mayor, encontrando una correspondencia entre fases con y sin gap de la protección topológica por simetría.

En el Capítulo 7 proponemos un modelo arco-iris de Ising con campo transverso. En el régimen de inhomogeneidad fuerte, el estado fundamental es un estado arco-iris de fermiones de Majorana, i.e. una colección de singletes de $SU(2)_2$. El régimen de baja inhomogeneidad es descrito por una teoria conforme con carga central $c = 1/2$ en espacio-tiempo hiperbólico. Por otro lado, consideramos una modificación de los acoplos del modelo arco-iris de Ising con nuevo parametro δ. Así, el régimen de baja inhomogeneidad se describe por una teoría cuántica de campos con una masa proporcional a δ en el espacio-tiempo hiperbólico. El régimen de alta inhomogeneidad es rico y variado. En función de δ se obtienen estados pertenecientes a la fase D de invariantes topológicos cuyo modelo más representativo es la cadena de Kitaev. Asimismo, obtenemos estados con una estructura de entrelazamiento de alto y bajo alcance.

El Capítulo 8 contiene las conclusiones en inglés y castellano del trabajo hecho y los resultados obtenidos en esta tesis. Finalmente, una lista de todas las referencias citadas a lo largo del documento concluye la tesis.

Summary

In this thesis we characterize the quantum entanglement properties of ground states of 1D inhomogeneous systems. In particular, we consider free fermion inhomogeneous chains and their corresponding spin versions obtained through the Jordan-Wigner transformation. Homogeneous models have been extensively studied, so they constitute a good reference when studying new physics due to inhomogeneity. For example, many ground states obey the so-called area law of entanglement entropy, which establishes that the amount of entanglement present between a subsystem and its environment is proportional to the measure of its boundary. Ground states of certain inhomogeneous systems constitute an example of a violation of the area law. A paradigmatic case is the so-called rainbow model describing an XX spin chain whose couplings decay exponentially with a rate h from the center towards the edges of the chain. Its ground state is the so-called rainbow state because in the regime of strong inhomogeneity $h \gg 1$, the strong disorder Renormalization Group predicts a valence bond solid formed by concentric maximally entangled states (Bell pairs) as it can be seen in Fig. 2.

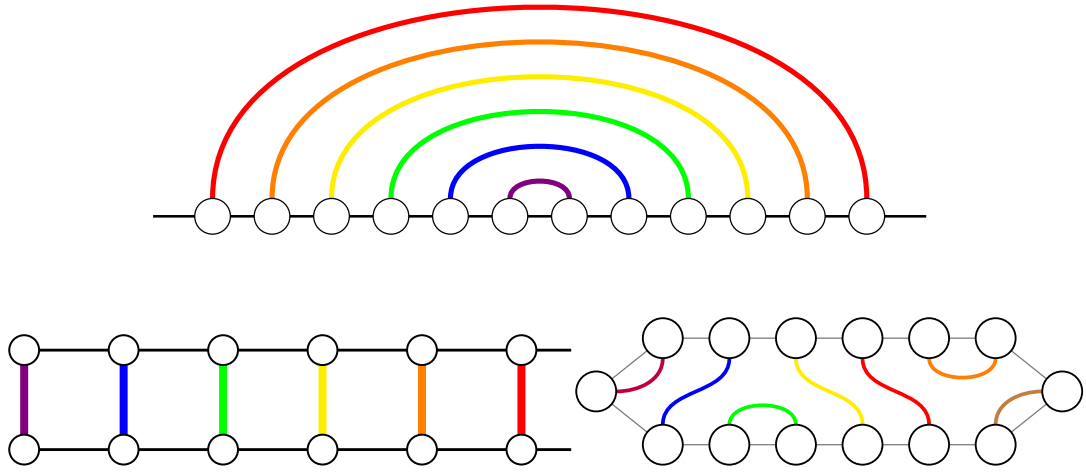

Figure 2: Top. Illustration of the rainbow state. The sites connected by the bonds are entangled. Bottom left (right). Folded version of the states with respect to the central coupling (site). The state on the left is topologically trivial while the state on the right is non-trivial.

The rainbow state exhibits long-range entanglement and violates (maximally)

the area law. Moreover, the field theory describing the model in the weak inhomogeneity regime $h \ll 1$ corresponds to a conformal field theory with central charge $c = 1$. In this thesis we use this state as a starting point to explore the effects generated by inhomogeneity, characterizing the entanglement properties with various tools. In particular we study the Rényi entropies, the entanglement Hamiltonian, the entanglement spectrum and also the entanglement contour.

The first four chapters are introductory and present the basic technology already presented in the literature[3]. Thus, Chapter 1 is intended to give a general, non-technical introduction to the field. Chapter 2 introduces quantum entanglement and its characterization. Chapter 3 discusses in detail the characterization of entanglement in a homogeneous XX chain, and finally in Chapter 4 we introduce a family of inhomogeneous models and in particular the rainbow model. The following three chapters present the original content of this thesis.

In Chapter 5 we explore the implications of adding a central defect with varying intensity γ in the rainbow model. In the strong inhomogeneity regime, we show that it is possible to generate transitions between phases with short (dimerized phases) and long (rainbow phase) entanglement just by changing the defect intensity. We calculate order parameters and single-body energies to support this fact. As far as the weak inhomogeneity regime is concerned, we show that the system can be described through a conformal field theory in curved space-time but with an effective central charge dependent on γ.

In Chapter 6 we discuss the possibility of characterizing the critical phases in the framework of the so-called symmetry-protected topological phases. We show that a folding transformation converts long-range entanglement into short-range entanglement, allowing an efficient description in terms of matrix product states (MPS) and classification into symmetry-protected topological phases. Those states presenting a reflection symmetry with respect to the central coupling are topologically trivial, while those presenting a reflection symmetry with respect to the central site are non-trivial (see Fig. 2). In fact, we find a ground state belonging to the AIII phase of the classification of topological insulators whose paradigmatic representative is the Su-Schrieffer-Heeger model and a ground state of an inhomogeneous chain with $SU(2)$ symmetry very similar to the AKLT state which belongs to the Haldane phase. Furthermore, we propose an extension of this result to chains with higher spin, finding a correspondence between the symmetry protection of gapped and gapless phases.

In Chapter 7 we propose a rainbow Ising model with transverse magnetic field. In the strong inhomogeneity regime, the fundamental state is a rainbow state of Majorana fermions, i.e. a collection of $SU(2)_2$ singlets. The low inhomogeneity regime is described by a conformal theory with central charge $c = 1/2$ in hyperbolic space-time. On the other hand, we consider a modification of the couplings of the Ising rainbow model adding a new parameter δ. Thus, the weak inhomogeneity

[3]Section 4.2 is a generalization presented for the first time in this thesis.

regime is described by a massive quantum field theory in the hyperbolic space-time. The high inhomogeneity regime is rich and varied. As a function of δ we obtain states belonging to the D phase of topological invariants whose most representative model is the Kitaev chain. Likewise, we obtain states with a high and low range entanglement structure.

Chapter 8 contains a discussion in English and Spanish of the work done and the results obtained in this thesis. Finally, a list of all references cited throughout the document concludes the thesis.

Contents

Chapter 1

Introduction and motivation

This chapter aims to present a global, non-technical view of quantum entanglement in many-body systems and to introduce the concepts that will appear in the thesis. It is intended to provide a general intuition and to prevent one from not being able to see the forest from the trees.

Entanglement is a meeting point between quantum information, condensed matter, and quantum gravity and is, therefore, a vast and complex subject. The narrative we present has a condensed matter perspective.

A bird's eye view of theoretical condensed matter

The purpose of condensed matter physics is to characterize material systems where the interaction among a very large number of constituent particles is crucial. They are called interacting many-body systems and their properties may differ remarkably from those of a system with the same number of constituent elements but isolated. We can make the distinction between those systems where the interactions can be averaged yielding an effective non-interacting system and those where this is not possible. The former case is developed in Landau-Fermi liquid theory (Landau 1957) that has been extremely successful in explaining the properties of metals. The theory is based on the assumption that a system of interacting fermions presents elementary excitations called quasiparticles and quasiholes that behave in a similar way to electrons and holes in a Fermi gas. Widespread mean-field (self-consistent) numerical methods like Hartree-Fock or density functional theory are suitable for systems that follow the Fermi liquid paradigm. Systems that belong to the second group of our classification are usually called non-Fermi liquids, or more generally, strongly correlated systems, such as the so-called Luttinger liquid that describes certain many-body interacting system in one dimension. Phenomenologically, the quasiparticle picture fails as they are confined to move along the line, so they cannot move freely –as dictated by the Fermi gas– without "pushing" others , as can be seen in Fig. 1.1. As a consequence, only collective wave-like excitations can exist. Indeed, low-dimensional systems,

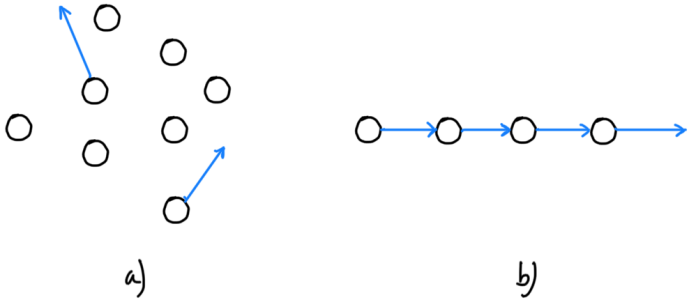

Figure 1.1: (a) In high dimensions, almost free individual quasiparticles are allowed so Fermi-liquid theory satisfactorily describes metals in high dimensional systems. In one dimension, however, quasiparticles cannot be properly defined as they cannot move without affecting their neighbours. Hence, only collective excitations can exist.

and in particular two-dimensional ones that encompass $(1+1)$D quantum[1] or classical equilibrium 2D systems are often dominated by strong correlations and non-perturbative effects. So there is the surprising situation where the approximate methods that best characterize physics in high-dimensional systems very often fail to explain the low-dimensional models that were initially proposed as toy models.

Indeed, low dimensional systems are interesting in themselves, and constitute a good arena where a large variety of theoretical physics methods and disciplines –such as integrability, quantum field theory (QFT), conformal field theory (CFT), renormalization group, and perturbation approaches among others– and numerical methods –like exact diagonalization, quantum Monte Carlo or density matrix renormalization group (DMRG)– find common ground. Thanks to the discovery of the fractional quantum Hall effect, high-temperature superconductors as well as the recent possibility of synthesizing (effective) low-dimensional materials, the study of low-dimensional systems has become of paramount importance for applications and is a very active field of research.

It is fair to say that the field of low-dimensional magnetism was born with the Ising model (Ising 1925) and the Heisenberg model (Heisenberg 1928). These models were proposed as toy models that would help to explain magnetic materials. Despite the simplicity of the Hamiltonians which at most involve quadratic terms of spins with local interactions, these models capture a wide variety of magnetic phenomena. Bethe (1931) found an exact solution for the spin-1/2 1D Heisenberg model by means of what is now known as Bethe ansatz. This method allows us to solve systems whose many-body scattering matrix is non-trivial (i.e., non-Fermi liquids), but can be obtained by successive products of scattering matrices of two quasiparticles. These quasiparticles are the magnons with spin $s = 1$ for the ferromagnetic case and the spinons with spin $s = 1/2$ for the antiferromagnetic case.

[1] In this thesis, we will work with quantum spin chains, and we shall generally use the term one-dimensional systems.

In fact, spinons are fermionic gapless excitations that constitute an example of the *fractionalization* phenomena appearing in low dimensional physics. Moreover, Onsager (1944) obtained an analytical expression for the free energy of the 2D classical Ising model in a square lattice using the theory of Lie algebras. Later, Schultz *et al.* (1964) rederived it by considering an analogous many-body fermionic system. We can also mention the Hubbard model (Hubbard 1963) which was proposed to describe electrons in solids whose solution for the 1D case was also found via the Bethe ansatz, and the Kondo model (Kondo 1964) that describes a localized quantum impurity coupled to a large reservoir of non-interacting electrons. The solution of this model came instead from renormalization group ideas.

The renormalization group. Critical points

One of the main purposes of condensed matter physics is the distinction and characterization of phases of matter. The perspective provided by the renormalization group[2] (RG) is crucial in this topic. The RG scheme focuses on how the physical phenomena change with the length scale. Starting from a physical Hamiltonian $H(\{g\})$ depending on a set of coupling constants $\{g\}$, the RG scheme characterizes how $H(\{g\})$ changes under a re-scaling[3] $\mathcal{R}$ of the lattice spacing a (or UV-cutoff) $a \to ba$ with $b > 1$. The RG transformation $\{g'\} = \mathcal{R}(\{g\})$ can be seen as a flow from point $\{g\}$ to $\{g'\}$. A fixed point is reached when $\{g^*\} = \mathcal{R}(\{g^*\})$. The correlation length of the system does not change with the scale transformation, but it must be measured with respect to the new scale, so it has to be shrinked $\mathcal{R}(\xi) = (1/b)\xi$. Thus, in the fixed point $\xi = 0$ or $\xi = \infty$. For systems in equilibrium, the first case is a trivial fixed point and it characterizes a phase, as the short-distance physics cannot be neglected. On the contrary, if $\xi = \infty$, short distances are irrelevant and the fixed points characterize a critical point or phase transition. Due to their scale invariance, critical points can be characterized with conformal field theories. Belavin *et al.* (1984) laid down the foundations of two-dimensional conformal field theory. In this thesis we will make special use of Kadanoff's real space approach (Kadanoff 1966): a lattice of spins can be partitioned into blocks each of which behaves similarly to single spin with modified coupling constants. Thus, the number of degrees of freedom is reduced exponentially as we proceed, simplifying the problem considerably. However, the practical implementation of this scheme was (and is) complicated. The first successful implementation of the RG was carried out by Wilson (1975) to solve the Kondo model mentioned above. Wilson designed

[2]The renormalization group has a misleading name: it is not a group in the mathematical sense and it is not strictly related to eliminating divergencies of a quantum field theory. It has a broader scope and, as Cardy (1996) wrote, *It cannot be stressed too strongly that the renormalization group is merely a framework, a set of ideas, which has to be adapted to the nature of the problem at hand*.

[3]It is convenient to start the RG procedure with a Hamiltonian that respects the same symmetries as the physical Hamiltonian but which incorporates all the necessary coupling constants that guarantee that the functional form of the Hamiltonian is invariant under the scale transformation.

the numerical renormalization group (NRG), which proceeds by conveniently slicing the system into shells corresponding to different length scales, selecting the lowest energy state of the deepest shell, and promoting it to the next one, creating thus a new effective Hamiltonian, which is diagonalized in the next step.

However, the application of the NRG to other systems yielded erroneous results. White (1992, 1993) realized that the less energetic state which is selected on each step of the NRG does not have to be the optimal one. Why? Because the blocks or shells into which the system is divided can be (strongly) correlated with the environment. With this idea, White developed the density matrix renormalization group (DMRG) which has made it possible to numerically find the ground state of many 1D systems with very high accuracy. In this method, the most representative state of each block is not the one with minimum energy but the one with the largest eigenvalue of the density matrix. Thus, the DMRG provided a link between condensed matter physics and quantum information[4].

Entanglement meets condensed matter physics

Given two systems A and B, a quantum state defined on them exhibits entanglement if the measurement of a local observable on A (B) alters the probabilities of obtaining different results on B (A), regardless of the distance between A and B. This attribute of entanglement led Einstein *et al.* (1935) to pose the famous EPR thought experiment and to doubt that quantum mechanics provides a complete description of reality. Local hidden variable theories were proposed to guarantee *local realism*[5] of quantum mechanics. Bell (1964) proved that the statistical correlations between measurements of any two observers must satisfy an inequality provided that local realism holds. Next, he showed that an entangled quantum state can violate this inequality. Thanks to Bell's work, the debate ceased to be strictly philosophical as it was possible to check the validity of Bell's inequality in the lab. The first experiment carried out by Freedman and Clauser (1972) with entangled photons concluded that there was a violation of the inequality. Since then, there has been a battle between loophole finders and improved experiments that has lasted until recently (Giustina *et al.* 2015; Rosenfeld *et al.* 2017). In all the experiments, the violation of Bell's inequality has been found.

During the last quarter of the past century, various works have appeared where entanglement is used as a resource to develop technologies unattainable with classical devices. This is the emerging domain of quantum technologies

[4]Although it is worth to say that that the word "entanglement" is not present in White's seminal papers.

[5]Local realism encompasses two requisites: all measurable properties of a system are well defined prior to any measurement, and these properties depend exclusively on the past lightcone of the system (realism) and there are no physical influences traveling faster than the speed of light (locality).

which contains the field of quantum information[6] (Nielsen and Chuang 2010). The reader interested in the quantum information perspective of entanglement can refer to the review by Horodecki *et al.* (2009).

As we have anticipated, entanglement and other concepts of quantum information have made their appearance into the field of condensed matter (Amico *et al.* 2008; Laflorencie 2016; Rachel *et al.* 2015), becoming essential to understanding the strongly correlated systems presented in the first subsection, and giving rise to the birth of the field known as quantum matter (Preskill 2000; Zeng *et al.* 2019) –to which this manuscript hopes to contribute–. It is important to note that the development of these interdisciplinary domains aids to explore new physics. As an example, we can consider quantum computation where the objects of study are many-body systems whose Hamiltonians can be manipulated.

Given a many-body system $\mathcal{S}$ and a bipartition $\mathcal{S} = A \bigcup B$, the state that describes A is given by the so-called reduced density matrix $\rho_A = \mathrm{tr}_B\, \rho_{AB}$. Its spectrum[7] $\{\omega_k\}$ codify the entanglement properties of A. The entanglement entropy is one of the most widespread characterizations of entanglement in condensed matter. It is defined as

$$S(A) = -\,\mathrm{tr}\left(\rho_A \log \rho_A\right). \tag{1.1}$$

The entanglement entropy $S(A)$ measures the amount of information associated to the fact that the state ρ_A is not pure. It is important to note that the concept of information has made it possible to connect the (apparently far) fields of quantum gravity and condensed matter by means of the area law of entanglement entropy (Eisert *et al.* 2010).

The area law of entanglement entropy

Bekenstein (1973) proposed that the entropy of a black hole is proportional to the area of its event horizon $\mathcal{A}$ and Hawking (1975) found the constant of proportionality:

$$S_{\mathrm{BH}} = \frac{1}{4\ell_P^2}\mathcal{A}, \tag{1.2}$$

where ℓ_P is the Planck length. Bekenstein interpreted this expression from an information theory point of view and wrote[8]: *It is then natural to introduce the concept of black-hole entropy as the measure of the inaccessibility of information (to an exterior observer) as to which particular internal configuration of the black hole is actually realized in a given case.*

Bekenstein's work motivated the investigation of the relation between information theory and quantum field theory. First, Bombelli *et al.* (1986) and later

[6] In fact, quantum information encompasses quantum computation and quantum cryptography. Other examples of quantum technologies (Dowling and Milburn 2003) are, quantum imaging (Lugiato *et al.* 2002) and quantum sensing (Degen *et al.* 2017).

[7] And a related one called entanglement spectrum (Li and Haldane 2008).

[8] In page 2336 of Bekenstein 1973.

Srednicki (1993) explored the entropy of a the ground state of a real scalar field satisfying the Klein-Gordon equation on a fixed background. They found that the entropy of a subsystem A with volume ℓ^D with ℓ much greater than the correlation length is proportional to the measure of its boundary

$$S(A) = C|\partial A| = C\ell^{D-1}, \tag{1.3}$$

where D is the space dimension, and in contrast to (1.2), C is a non-universal cut-off dependent constant.

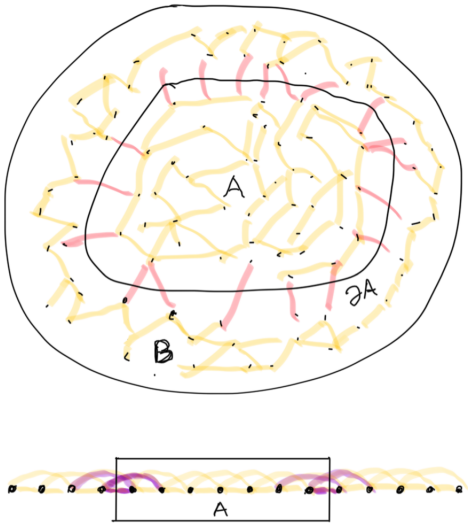

Figure 1.2: Schematic representation of the area law of entanglement entropy for two dimensions (top) and one dimension (bottom). For the one dimensional system, the boundary ∂A are just two points.

Hence, the area law can provide some intuition on how the correlations are distributed in ground states. To see it, let us consider a spatially extended system divided in two subsystems A and B as can be seen in Fig. 1.2. Then, the state that describes the system is said to satisfy the area law if the only degrees of freedom belonging to A that are correlated with B are those near the boundary ∂A.

Now we can understand the main reason behind the success of DMRG that we introduced previously. The goal of the DMRG (and of any RG scheme) is to describe the system effectively while keeping the dimensionality of the effective Hilbert space small. Hence, the more representative the retained states are, the more effective the DMRG is. Those states that fulfill the area law meet precisely this requirement: most of the entanglement is encoded in a few eigenvalues of the reduced density matrix. Nowadays the success of the DMRG is understood in the framework of tensor networks, and in particular in their 1D realization: the matrix products states (MPS) (Dukelsky *et al.* 1998; Östlund and Rommer 1995; Verstraete *et al.* 2004).

Before briefly introducing the MPS, it is worth to mention that its origin is

very related to the so-called Haldane conjecture[9] (Haldane 1983) which states that integer spin Heisenberg chains are gapped whereas half-integer ones are gapless. Affleck *et al.* (1988) proposed a gapped spin 1 Hamiltonian whose ground state (AKLT state) is a valence-bond state with finite correlation length. Fannes *et al.* (1992) and Lange *et al.* (1994) extended the AKLT ideas and introduced the finitely-correlated states which are precursors of MPS. As a matter of fact, tensor networks (Orús 2014; Schollwöck 2011) describe many-body wave functions in a *basis* in which the properties of entanglement and correlation lengths are the central features. Hence, a tensor network is composed of tensors (multidimensional arrays of complex numbers) interconnected in a particular way. For instance, the MPS is a one dimensional tensor network where the tensors are matrices that are contracted with the usual matrix multiplication, and the projected entangled pair states (PEPS) are the two dimensional generalization of the MPS, proposed by Verstraete and Cirac (2004).

The dimension of the contracted indices, known as ancillary indices, is called bond dimension, and it is related to the amount of entanglement that a given state possesses. In general, the bond dimension scales exponentially with the system size N, making it computationally infeasible for being represented with an MPS. However, Vidal (2003) showed that states with a saturated bond dimension[10] are efficiently simulated in classical computers by describing them using an MPS. He called these states *slightly-entangled*, and intuitively we can think that states that satisfy the area law are of this kind. Indeed this was rigorously proved by Hastings (2007): the ground state of a local, gapped and finite strength Hamiltonian obeys the area law and can be approximated with an MPS (Verstraete and Cirac 2006).

Violations of the area law

Page (1993) showed that the entanglement entropy of a bipartition of $N/2$ constituents of a system described by a random state is $S(A) \sim (N/2)\log d - 1/2$ where d is dimension of the local Hilbert space. And indeed, excited states of ergodic Hamiltonians present the same behaviour. These states, which fill up almost entirely the Hilbert space are said to satisfy the *volume law*[11]. The states that satisfy the area law represent a small corner of the whole Hilbert space.

As we have said above, Hastings proved that all the ground states of 1D gapped Hamiltonians belong to this small corner. A ground state that violates

[9] *It was rejected by multiple journals, and was labeled a "conjecture" even though it was, in my mind, a clear prediction. I recall that one referee pontificated that my claims "were in manifest contradiction to fundamental principles such as renormalization and continuity"! Of course, my predictions were later vindicated both by numerical studies and experiments.* . Duncan M. Haldane – Biographical. NobelPrize.org. Nobel Prize Outreach AB 2021. Wed. 11 Aug 2021.

[10] Indeed, Vidal (2003) showed that the states whose bond dimension grows polynomially with the number of sites are efficiently simulated.

[11] There is, however, a notorious exception with the excited states of many-body localized systems which also follow the area law (Abanin *et al.* 2019).

the area law must break at least one of the hypothesis of Hastings theorem. For instance, non-local terms may yield ground states that violate the area law (Gori *et al.* 2015; Shiba and Takayanagi 2014). The next paragraphs describe different physical models whose Hamiltonians are local but gapless and their ground states constitute examples of violation of the area law.

The ground state and low energy excitations of critical Hamiltonians are expected to violate the area law. This is so because even the degrees of freedom far from the boundary ∂A can be correlated with the environment B since the correlation length diverges at the critical point. Indeed, Srednicki (1993) showed that the expression (1.3) is not valid for the massless case in $D = 1$ and that there is a logarithmic dependency with the volume ℓ. Holzhey *et al.* (1994) first computed the entanglement entropy in a CFT in two dimensions and showed that

$$S \approx \frac{c}{3} \log \ell, \tag{1.4}$$

where c is the central charge of the associated CFT. A few years later, explicit calculations of the entanglement behavior in critical systems confirmed and extended the predictions given by CFT (Calabrese and Cardy 2004; Jin and Korepin 2004; Lambert *et al.* 2004; Latorre *et al.* 2003; Vidal *et al.* 2003) showing a logarithmic violation of the area law (1.4). The same logarithmic scaling was found by Wolf 2006 for Fermi liquids for an arbitrary dimension. Because of the divergence of the correlation length, ground states of critical systems cannot be described efficiently with MPS. Does this mean that tensor networks can not describe critical points? Vidal (2007) developed the multiscale entanglement renormalization ansatz (MERA) which is able to describe efficiently states of a D dimensional lattice with a tensor network in $D + 1$ dimensions. Layers of tensors are stacked along the additional dimension where each layer describes a different length scale. In addition, Swingle (2012) proposed that MERA is a discrete realization of the holographic-principle (Ryu and Takayanagi 2006).

We may also find violations of the area law when considering disordered systems. On one hand Anderson (1958) established that one-dimensional systems with an uncorrelated disorder in the local potential display localization. Hence, this kind of disorder respects the area law. However, correlated or off-diagonal disordered systems –such as spin chains with random local couplings– lead in certain cases to long-range correlations and to a logarithmic violation of the area law (Refael and Moore 2004).

Another interesting example is provided by the ground states of the (colorful) Motzkin spin-chains (Bravyi *et al.* 2012; Movassagh and Shor 2016) which exhibit a violation of the area law $S \sim \sqrt{N}$ that is not related to conformal invariance. Their construction is based on Motzkin paths. These comprise all possible ways to connect two points of the lattice $(0, 0)$ and $(N, 0)$ without crossing the x axis. The connection with spins is done with the mapping $\{|{+}1\rangle, |0\rangle, |{-}1\rangle\}$ to the degrees of freedom for forming the path $\{ /, —, \backslash \}$.

Finally, and more importantly for this thesis, the ground state of some inhomogeneous systems violates the area law. Historically, disordered systems have been confronted with homogeneous systems. This is misleading since disordered systems do not include those whose inhomogeneity does not depend on a probability distribution, i.e. it is not random. In this thesis we are interested in non-disordered inhomogeneous systems. Indeed, inhomogeneous systems with engineered couplings can violate the area law, even maximally. The paradigmatic example is the *rainbow state* that was proposed by Vitagliano *et al.* (2010) and studied profusely by our research group (Ramírez *et al.* 2015, 2014; Rodríguez-Laguna *et al.* 2017). In fact, the rainbow state is a central pillar of this manuscript, so we will devote a chapter to explaining it in detail.

Entanglement and quantum phases

In addition to the contributions of the renormalization group that we have mentioned above, a crucial step in understanding and classifying the phases of matter was given by Landau (1937) with his theory of symmetry-breaking. According to this theory, two symmetry-breaking phases are distinguishable because they present different symmetries that can be classified via symmetry groups. The continuous phase transition or critical point is usually the point at which there is a change in the number of symmetries describing the system. At this point, the gap of the Hamiltonian closes, and the theory becomes gapless, whereas it remains finite outside the critical point. Hence, using symmetry and the related group theory it is possible to describe many different phenomena, ranging from the 230 different crystals that can exist in three dimensions, to ferromagnetic and paramagnetic phases, to superfluid phases, etc. The existence of different phases is manifested in a local order parameter $\Delta(x)$ (for instance magnetization for ferromagnet) that vanishes in the paramagnetic phase, but not in the ferromagnetic one. In addition, the symmetry breaking also provides the origin of many collective gapless excitations by the mechanism of spontaneous symmetry breaking of a continuous symmetry.

Physicist use to believed that Landau symmetry-breaking theory characterizes all continuum phase transitions. However, important experimental results obtained in the eighties such as the discovery of the fractional quantum Hall (FQH) effect (Tsui *et al.* 1982) and high-temperature superconductors (Bednorz and Muller 1986) opened the door to new phases of matter that are beyond the so-called Landau paradigm. Indeed, FQH systems contain different phases at zero temperature with the same symmetry. As we have mentioned, the entanglement has proven to be a useful tool for improving the characterization of phases belonging to the Landau paradigm. But it has become *essential* for distinguishing and understanding phases of matter that cannot be explained in terms of changes in symmetries.

They key concept is the distinction between short-range entanglement (SRE) and long-range entanglement (LRE) in ground states of gapped Hamiltonians. A state is said to present SRE if it can be connected to a product state by means of a unitary local evolution, i.e. by means of a quantum circuit whose depth does not depend on the system size. If this is not possible, i.e., the depth of the quantum circuit grows with the system size, the system presents LRE. The *topological order* (Chen *et al.* 2010) quantifies the different patterns of LRE that ground states of gapped Hamiltonians present. Changes in these patterns imply topological phase transitions, which are characterized by quasiparticles with different fractional statistics. These are the topological phases of matter first encountered with the discovery of the fractional quantum Hall effect (Laughlin 1983).

Observe that gapped systems that satisfy the area-law *necessarily* present SRE. Hastings theorem therefore ensures that there cannot be gapped one dimensional states with LRE[12] and, we can conclude that 1D gapped systems do not possess topological order. However, $1D$ systems may possess non-trivial topological properties. The entanglement of all gapped ground states can be removed using local unitaries. Yet, if we impose that the unitaries must preserve some symmetries of the system, some states cannot be transformed into a product state because of constraints imposed by symmetry. Thus, the states belong to *symmetry protected topological* (SPT) phases that we will encounter in this thesis. This terminology can be misleading, as one might think that an SPT is identified by a topological order[13] but it is very accepted by the community. If the system is closed, the ground state belonging to an SPT phase does not spontaneously break the symmetry, and it is not degenerate. On the contrary, if the system is open, non-trivial edge modes make the ground state degenerate. In fact, a relevant example of SPT phase is the Haldane phase for spin 1 that we have mentioned above, with the AKLT state being the most representative. The entanglement spectrum has also proven to be a reliable detector of this kind of phases (Pollmann *et al.* 2010), so we can conclude this short tour by emphasizing the prominence that entanglement has taken in understanding strongly correlated many-body systems.

Inhomogeneous systems

Non-homogeneous systems are the rule rather than the exception in nature. Real materials present local random impurities that can dramatically change their properties. This is the reason why frozen – also known as quenched – disorder has received much interest (Iglói and Monthus 2005). The characterization of non-disordered inhomogeneous systems has intensified since the experimental

[12]Notice that the definition of LRE and SRE applies exclusively to systems with finite correlation length, so critical systems are not included in this distinction. However, as in these systems the correlation length diverges, the depth of the quantum circuit grows with the system size.

[13]In fact, to emphasize the distinction, Wen (2017) coined the term symmetry protected trivial (SPT) order.

realization of ultracold quantum gases which offers a unique setting for quantum simulation of interacting many-body systems (Bloch *et al.* 2012). The local potential and hopping amplitudes that these atoms experience can be fine-tuned by making use of the interference pattern of overlapping laser beams. This has made it possible to explore phenomena of QFT in curved spacetime by placing the atoms with inhomogeneous hopping amplitudes simulating a position-dependent index or refraction (Boada *et al.* 2011). Moreover, inhomogeneous models such as the celebrated Sadchev-Ye-Kitaev (SYK) model (Maldacena and Stanford 2016) or experiments with Rydberg atoms (Bernien *et al.* 2017) which are governed by long-range interactions are useful tools in the understanding of quantum chaos.

This thesis explores the entanglement properties of inhomogeneous spin chains. In particular, we will work with Hamiltonians whose parameters vary locally, depending on an inhomogeneity parameter $h \geq 0$. Standard numerical tools can be used to characterize the system for any values of h. Yet, from the analytical perspective it is convenient to distinguish between two asymptotic regimes.

- In the strong inhomogeneity regime $h \gg 1$ there exist many different energy scales, so it is possible to apply an RG scheme that decimates the degrees of freedom associated to each energy scale, in decreasing order. This RG is the strong-disorder renormalization group (SDRG) that was proposed by Dasgupta and Ma (1980) and Ma *et al.* (1979) and characterized in detail by Fisher (1995).

- The opposite situation is the weak inhomogeneity regime where $h \to 0$. The system is thus almost homogeneous so it is possible to study the differences due to the inhomogeneity by studying the continuum limit of the theory defined in the same region where the field theory of the homogeneous system is relativistic.

In the following chapters we develop in more detail some of the topics raised in this bird's eye view of condensed matter and entanglement theories. We begin by defining entanglement and its characterization by means of the reduced density matrix in Chapter 2. In Chapter 3 we analyze the entanglement properties of homogeneous spin chains. We shall focus on the XX model and work it out in some detail as it is important for the correct understanding of this thesis. In Chapter 4 we shall describe the SDRG and its validity regime. We shall also illustrate the characterization of the strong and weak inhomogeneity regimes of an inhomogeneous XX model whose ground state is the rainbow state: a concentric valence-bond state which violates maximally the area law in the strong inhomogeneity regime. The weak inhomogeneity regime can be in turn understood as a massless fermion placed on a curved spacetime that reproduces the inhomogeneity of the model. The rainbow model will be our starting point in the following chapters.

Chapter 2

Quantum Entanglement

2.1 Entanglement in pure states.

Given a quantum system composed of two subsystems A and B with finite dimensional Hilbert spaces $\mathcal{H}_A$ and $\mathcal{H}_B$ respectively, a pure state is given by the vector $|\psi\rangle_{AB} \in \mathcal{H}_{AB}$ with $\mathcal{H}_{AB} = \mathcal{H}_A \otimes \mathcal{H}_B$. We can distinguish two situations:

- If the state can be written as

$$|\psi\rangle_{AB} = |\phi\rangle_A \otimes |\varphi\rangle_B , \quad |\phi\rangle_A \in \mathcal{H}_A, \quad |\varphi\rangle_B \in \mathcal{H}_B, \tag{2.1}$$

  then the state is said to be *separable*.

- If the above does not hold,

$$|\psi\rangle_{AB} \neq |\phi\rangle_A \otimes |\varphi\rangle_B , \tag{2.2}$$

  the system is said to be non-separable that is *entangled*.

Let us mention here that the characterization of entanglement and other kinds of quantum correlations is richer and harder in mixed states. The reason is that the mixed states that are said to be separable do not present entanglement but they display other kind of quantum correlations (Adesso *et al.* 2016) in contrast with pure states. The characterization of these correlations via quantum coherence (Streltsov *et al.* 2017), quantum discord (Modi *et al.* 2012), and others have recently attracted great attention. Moreover, we have described the so-called bipartite entanglement as it concerns two subsystems A and B. We mention here that it is possible to study also the multipartite entanglement (Karlsson and Bourennane 1998) that appears when more than two subsystems A, B, C, etc. are considered. Multipartite entanglement requires the additional distinctions of partially-entangled and partially-separable states besides the classes defined above.

In this thesis, we will work with ground states of spin chains, that is, with pure states and we shall only consider bipartite entanglement so we will ignore the term bipartite throughout the entire thesis.

2.2 Reduced density matrix

Given a state Ψ_{AB}, the state that describes the degrees of freedom of A is in general mixed, so it is convenient to use the density matrix formalism. In particular, the entanglement can be characterized by means of the reduced density matrix ρ_A. Let us recall that the density operator ρ is a Hermitian, positive-semidefinite operator that verifies $\mathrm{tr}\,\rho = 1$. The density matrix ρ_{AB} of the pure state $|\psi\rangle_{AB}$ is

$$\rho_{AB} = |\psi\rangle_{AB} \langle\psi|_{AB} . \tag{2.3}$$

Let us now define the reduced density matrix ρ_A (and ρ_B). Consider an operator $\tilde{O}_A = O_A \otimes \mathbb{1}_B$ whose support lies in A. The expectation value is given by $\langle \tilde{O}_A \rangle = \mathrm{tr}_{AB} \left(\rho_{AB} \tilde{O}_A \right)$. The reduced density matrix ρ_A is a density operator acting on $\mathcal{H}_A$ such that:

$$\langle \tilde{O}_A \rangle = \mathrm{tr}_{AB} \left(\rho_{AB} \tilde{O}_A \right) = \mathrm{tr}_{AB} \left(\rho_A O_A \right) . \tag{2.4}$$

Thus, the reduced density matrix ρ_A (ρ_B) describes the state for an observer restricted to the subsystem A (B). It is obtained by tracing out the inaccessible degrees of freedom belonging to B (A):

$$\rho_A = \mathrm{tr}_B \, \rho_{AB}, \qquad \rho_B = \mathrm{tr}_A \, \rho_{AB}. \tag{2.5}$$

Owing to its hermiticity, ρ_A can be diagonalized:

$$\rho_A = \sum_{k=1}^{N_A} \omega_k |\phi_k\rangle \langle\phi_k| , \quad 0 \leq \omega_k \leq 1, \quad \text{and} \quad \sum_{k=1}^{N_A} \omega_k = 1. \tag{2.6}$$

Notice that $\{\phi_k\}_{k=1}^{N_A}$ is a orthonormal basis of $\mathcal{H}_A$ with dimension N_A.

A pure state $|\psi\rangle \in \mathcal{H}_{AB}$ can be written by means of the so-called Schmidt decomposition

$$|\psi\rangle = \sum_{k=1}^{r} s_k |k\rangle_A |k\rangle_B , \tag{2.7}$$

where $s_k > 0$ are the Schmidt values, and $\{|k\rangle_A\}_{k=1}^{N_A}$ ($\{|k\rangle_B\}_{k=1}^{N_B}$) is an orthogonal basis of $\mathcal{H}_A$ ($\mathcal{H}_B$) and $r \leq \min(N_A, N_B)$ is the Schmidt number. The Schmidt decomposition is intimately related with the singular value decomposition and we refer to appendix 2.A for a more detailed derivation.

Finally, using (2.7) and (2.4) the reduced density matrices are

$$\rho_A = \sum_{k=1}^{r} s_k^2 |k\rangle_A \langle k|_A , \quad \rho_B = \sum_{k=1}^{r} s_k^2 |k\rangle_B \langle k|_B \tag{2.8}$$

We can compare (2.8) with the general expression of the diagonalization of the density operator (2.6). It follows that the nonzero eigenvalues $\omega_k = s_k^2$ with $k = 1 \ldots, r$ are the same for both matrices ρ_A and ρ_B and that they may differ in the degeneracy of zero eigenvalues $\omega_k = 0$ for $k = r+1, \ldots, N_A - r$ ($k = r+1, \ldots, N_B - r$).

The eigenvalues of the reduced density matrix codify the whole entanglement structure of a system. Notice that if the Schmidt number $r = 1$, the sum in (2.7)

reduces to one term and the state is a product state (2.1). In the other cases the state is entangled and it is *maximally entangled* when $s_k^2 = 1/\min(N_A, N_B)$.

The reduced density matrix ρ_A, as every density operator, possesses non-negative spectrum and it is Hermitian. As a consequence, it can be written as:

$$\rho_A = e^{-\mathcal{H}_A}, \tag{2.9}$$

where $\mathcal{H}_A$ is a Hermitian operator[1] which is known as *entanglement Hamiltonian*. Notice that by taking the logarithm in (2.8) we find the spectrum of the entanglement Hamiltonian which is also known as *entanglement spectrum*[2]:

$$E_k = -2 \log s_k. \tag{2.10}$$

Having obtained the spectrum of ρ_A, we can introduce the entanglement entropy.

2.3 Entanglement entropy

There are many measures to characterize entanglement by means of the reduced density matrix [3]. It is a fundamental object from which correlations between A and the exterior of A are obtained. For instance, the purity $P(\rho_A) = \mathrm{tr}_A\, \rho_A^2$ measures the degree of mixedness of the partition: if $P(\rho_A) = 1$ it means that ρ_A describes a pure state and $|\psi\rangle_{AB}$ is separable (2.1). On the contrary, if $P(\rho_A) < 1$ then ρ_A describes a mixed state and $|\psi\rangle_{AB}$ is entangled (2.2). Purity is thus bounded:

$$\frac{1}{N_A} \leq P(\rho_A) \leq 1. \tag{2.11}$$

The entanglement entropy is the most widespread magnitude in the characterization of bipartite entanglement. The concept of entropy was born in the fields of thermodynamics (Clausius) and classical statistical physics (Boltzmann and Gibbs). In this context, the macroscopic state that describes a system is characterized by a probability distribution of microstates. The entropy of the system is

$$S = -\sum_k p_k \log p_k, \tag{2.12}$$

[1] Note that for $\mathcal{H}_A$ to be well defined, ρ_A must be positive.

[2] The term was coined by Li and Haldane (2008)

[3] The are other measures that do not use the reduced density matrix. For instance, the *negativity* is based on the partial transpose criterion (Horodecki *et al.* 1996; Peres 1996) which establishes that if a state is separable, the partial transpose matrix ρ^{T_B} (ρ^{T_A}) is a valid density matrix (i.e. positive semidefinite). Given a density matrix ρ acting on $\mathcal{H}_A \otimes \mathcal{H}_B$

$$\rho = \sum_{ijkl} M_{kl}^{ij} \, |i\rangle_A \langle j|_A \otimes |k\rangle_B \langle l|_B \,,$$

the associated partial transpose matrix ρ^{T_B} (ρ^{T_A}) is obtained by leaving untouched the degrees of freedom of A (B) and transposing those of B (A)

$$\rho^{T_B} \coloneqq \sum_{ijkl} M_{lk}^{ij} \, |i\rangle_A \langle j|_A \otimes |k\rangle_B \langle l|_B$$

where p_i is the probability associated to the occurrence of the microstate i. Shannon (1948) introduced the concept of entropy (2.12) into the field of classical information theory. Shannon entropy quantifies the amount of uncertainty or the amount of information that a message possesses. Von Neumann extended the concept of entropy to quantum physics. The entropy is given in terms of the density matrix ρ as $S = -\operatorname{tr}(\rho \log \rho)$. Thus, the von Neumann entropy of the subsystem A is

$$S(\rho_A) = -\operatorname{tr}(\rho_A \log \rho_A) = -\sum_{k=1}^{N_A} \omega_k \log \omega_k, \tag{2.13}$$

where $\{\omega_k\}_{k=1}^{N_A}$ is the set of eigenvalues of ρ_A (2.6). Revisiting the von Neumann entropy 2.13 under the perspective of Shannon theory leads to interpret $S(\rho_A)$ as the amount of information necessary to describe the subsystem A as a pure state starting with the mixed state ρ_A. Or, in other words, it quantifies the correlations that prevents describing A as a pure state. It is for that reason the von Neumann entropy is nowadays called *entanglement entropy*.

Observe that the eigenvalues $\omega_k = 0$ do not contribute to the entanglement entropy (2.13), so it can be given in terms of the Schmidt singular values s_k (2.8):

$$S(\rho_A) = -\sum_{k=1}^{r} s_k^2 \log s_k^2 = S(\rho_B). \tag{2.14}$$

Notice that if $r = 1$, the state is a product state, and $S(\rho_A) = 0$. The entanglement entropy satisfies a series of mathematical properties which are the result of physical requirements (Wehrl 1978). For instance, additivity:

$$S(\rho_A \otimes \rho_B) = S(\rho_A) + S(\rho_B), \tag{2.15}$$

and subbaditivity:

$$S(\rho_{AB}) \leq S(\rho_A) + S(\rho_B), \tag{2.16}$$

which establishes that the entropy of a given state $\rho_{AB} \in \mathcal{H}_A \otimes \mathcal{H}_B$ is bounded by the entropy of a product state $\rho_A \otimes \rho_B$. Rényi (1961) proposed a generalization of the entropy which fulfills all the properties of the entropy but with the relaxation of the subadditivity[4]. They are known as Rényi entropies:

$$S_\alpha(\rho_A) = \frac{1}{1-n} \log \rho_A^n, \quad \text{with } n > 0, n \neq 1, \tag{2.18}$$

and it can be shown that the entanglement entropy can be obtained as a limit

$$\lim_{n \to 1^+} S_n(\rho_A) = S(\rho_A). \tag{2.19}$$

[4]Indeed subadditivity is a weak version of the strong-subadditivity which is also fulfill by the entanglement entropy. It relates the entanglement entropy of three subsystems A, B, and C:

$$S(\rho_{ABC}) + S(\rho_B) \leq S(\rho_{AB}) + S(\rho_{BC}) \tag{2.17}$$

Rényi entropies are very useful in quantum field theory as they can be computed directly with the so-called replica trick. Having introduced the quantum entanglement and its characterization by means of the reduced density matrix, we shall apply these concepts in the next chapter to characterize the entanglement in homogeneous spin chains.

Appendices

2.A Schmidt decomposition

A pure state can be written as

$$|\psi\rangle = \sum_{m=1}^{N_A}\sum_{n=1}^{N_B} \psi_{mn} |m\rangle_A \otimes |n\rangle_B , \tag{2.A.1}$$

where $\{|m\rangle_A\}_{m=1}^{N_A}$ and $\{|n\rangle_B\}_{n=1}^{N_B}$ are orthonormal basis of the Hilbert spaces $\mathcal{H}_A$ and $\mathcal{H}_B$ respectively, and the coefficients ψ_{mn} can be arranged in a rectangular $N_A \times N_B$ matrix ψ.

Attending to the definition of the reduced density matrix (2.5) we have:

$$\rho_A = \mathrm{tr}_B \rho_{AB} = \sum_{n=1}^{N_B} {}_B\langle n|\psi\rangle \langle\psi|n\rangle_B = \sum_{m,m'=1}^{N_A}\sum_{n=1}^{N_B} \psi_{mn}\psi^*_{m'n} |m\rangle_A \langle m'|_A . \tag{2.A.2}$$

Then $\rho_A = \psi\psi^\dagger$ in the $\{|m\rangle_A\}$ basis and, in similar way $\rho_B = \psi^\dagger\psi$ in the $\{|n\rangle_B\}$ basis. As the $N_A \times N_B$ matrix ψ is in general rectangular, it admits a singular value decomposition (SVD):

$$\psi = UDV^\dagger, \tag{2.A.3}$$

where U (V) is a $N_A \times N_A$ ($N_B \times N_B$) unitary matrix, and D is a $N_A \times N_B$ rectangular matrix with $s_i \geq 0$ with $i = 1, \ldots, \min(N_A, N_B)$ in the diagonal [5]. Applying the SVD (2.A.3) to (2.A.1):

$$|\psi\rangle = \sum_{k=1}^{\min(N_A,N_B)} s_k \left(\sum_{m=1}^{N_A} U_{mk} |m\rangle_A\right)\left(\sum_{n=1}^{N_B} V^*_{nk} |n\rangle_B\right) = \sum_{k=1}^{\min(N_A,N_B)} s_k |k\rangle_A |k\rangle_B , \tag{2.A.4}$$

where the sets $\{|k\rangle_{A(B)}\}$ are orthonormal basis of $\mathcal{H}_{A(B)}$. If we consider the

$$r \leq \min(N_A, N_B)$$

non-zero singular values $s_k > 0$ (i.e. the rank of M) we arrive at the *Schmidt decomposition*

$$|\psi\rangle = \sum_{k=1}^{r} s_k |k\rangle_A |k\rangle_B , \tag{2.A.5}$$

where r is called the *Schmidt number*.

[5] Alternatively we can consider the D matrix to be square $\min(N_A, N_B) \times \min(N_A, N_B)$. Then U (V) is a $N_A \times \min(N_A, N_B)$ ($\min(N_A, N_B) \times N_B$) isometry $UU^\dagger = \mathbb{1}$ ($V^\dagger V = \mathbb{1}$).

Chapter 3

Entanglement in homogeneous spin chains

A spin chain is a collection of interacting spins arranged in a line that can be closed or open. It is a realization of a many-body system and it helps to understand a wide range of physical models. A paradigmatic example is the spin $1/2$ Heisenberg model

$$H = -\sum_{m=1}^{N} J\, \mathbf{S}_m \cdot \mathbf{S}_{m+1} = -\sum_{m=1}^{N} \frac{J}{4} \left(\sigma_m^x \sigma_{m+1}^x + \sigma_m^y \sigma_{m+1}^y + \sigma_m^z \sigma_{m+1}^z\right), \tag{3.1}$$

where σ_m^i with $i = x, y, z$ are the Pauli matrices that describe the spin $1/2$ degrees of freedom. It is an homogeneous spin chain because the exchange coupling J does not depend on the position. In the next chapter we shall present the inhomogeneous spin chains where $J \to J_m$. The purpose of this chapter is to discuss the entanglement properties of homogeneous spin chains. In order to compute the entanglement entropy of a given subsystem or block A of the chain, we need to first obtain the ground state of the theory and the density matrix, and then compute the entanglement spectrum of the reduced density matrix ρ_A.

In general this is a hard task from a computational point of view. The reason is that the Hilbert space that accommodates the ground state and the excited states of a given spin $1/2$ chain of N sites grows as 2^N. If we could store information on every atom of the universe, we would be able to diagonalize the Hamiltonian of 270 spins. It thus seems a priori an impossible task to diagonalize spin Hamiltonians such as (3.1) by classical computational methods. We can see here the convenience and necessity of developing quantum computation and quantum simulation, but, as long as this technology is not available it is needed to resort to numerical methods –such as exact diagonalization (Lanczos), DMRG, or quantum Monte Carlo– or to search for exactly solvable systems such as (3.1) or the XX model that we shall present in the next section.

With the objective of computing the entanglement properties of the XX model, we shall first introduce and diagonalize this model in Section 3.1, showing that it is gapless and that it can be described via CFT. We shall extract the leading

order of the Rényi entropies which is fixed by conformal invariance, and we shall obtain the non-universal properties by means of diagonalizing the two-point correlation matrix in Section 3.2. We will also compute the entanglement Hamiltonian, entanglement spectrum, and the so-called entanglement contour in Section 3.3.

3.1 The XX model

The Hamiltonian of the XX model is given by

$$H = -\sum_{m=1}^{N-1} \frac{J}{4} \left(\sigma_m^x \sigma_{m+1}^x + \sigma_m^y \sigma_{m+1}^y\right) - \eta \frac{J}{4} \left(\sigma_N^x \sigma_1^x + \sigma_N^y \sigma_1^y\right), \tag{3.2}$$

where the parameter η takes account of possible boundary conditions of the system. In particular, $\eta = 0$ yields a Hamiltonian that describes a chain with open boundary conditions (OBC) and $\eta = 1$ a closed chain with periodic boundary conditions (PBC) $\sigma_{N+1}^i = \sigma_1^i$, $i = x, y$. It is called the XX model because the Hamiltonian (3.2) involves only the x and y components of the spin operators coupled with the same exchange coupling J. It is convenient to write (3.2) in terms of the ladder operators $\sigma_m^{\pm} = (1/2)(\sigma_m^x \pm i\sigma_m^y)$.

$$\begin{aligned} H &= -\sum_{m=1}^{N-1} \frac{J}{2} \left(\sigma_m^+ \sigma_{m+1}^- + \sigma_m^- \sigma_{m+1}^+\right) - \eta \frac{J}{2} \left(\sigma_N^+ \sigma_1^- + \sigma_N^+ \sigma_1^-\right) \\ &= H^{\text{OBC}} - \eta \frac{J}{2} \left(\sigma_N^+ \sigma_1^- + \sigma_N^- \sigma_1^+\right). \end{aligned} \tag{3.3}$$

Let us analyze the symmetries of the model. The total third component of the spin S_z^{tot}, also known as total magnetization

$$\mathcal{M} = \frac{1}{2} \sum_{m=1}^{N} \sigma^z, \tag{3.4}$$

commutes with the Hamiltonian $[H, \mathcal{M}] = 0$. As a consequence, the Hamiltonian (3.2) is invariant under rotations around the z axis. Moreover, the Hamiltonian commutes with the parity operator

$$\mathcal{P} = \prod_{m=1}^{N} \sigma^z, \tag{3.5}$$

so it is invariant under spin inversion. The Hamiltonian (3.3) acts non-trivially only between nearest neighbour opposite spins, i.e.

$$|\uparrow\downarrow\rangle \leftrightarrow |\downarrow\uparrow\rangle,$$

but it is insensitive to the sign[1] of J so we can consider for now on $J > 0$. In addition, if the system is closed, the system presents translational invariance.

[1] Observe that in general this is not true. For instance, the Heisenberg Hamiltonian (3.1) presents different physics depending on the sign of J.

In this case (3.3) also commutes with the translation operator by one site and therefore momentum k is a good quantum number to label the spectrum.

The XX model corresponds to a particular case of the more general XY model, where the exchange couplings of each spin component can vary independently. Indeed, Lieb *et al.* (1961) solved exactly this model – in the sense of finding its ground state and their elementary excitations – by considering an analogous system of free fermions. The mapping between spins and fermions is done by means of the Jordan-Wigner transformation (Jordan and Wigner 1928), which relates the spin and fermionic degrees of freedom:

$$\begin{aligned}\sigma_m^+ &= \exp\left\{-i\pi \sum_{k=1}^{m-1} c_k^\dagger c_k\right\} c_m \\ \sigma_m^- &= \exp\left\{i\pi \sum_{k=1}^{m-1} c_k^\dagger c_k\right\} c_m^\dagger \\ \sigma_m^z &= 1 - 2c_m^\dagger c_m.\end{aligned} \tag{3.6}$$

At a single site the correspondence between the eigenstates of σ^z and the empty and occupied sites of a fermion is

$$|\uparrow\rangle \leftrightarrow |0\rangle\,, \quad |\downarrow\rangle \leftrightarrow |1\rangle = c^\dagger |0\rangle\,. \tag{3.7}$$

Observe that the Fock vacuum corresponds to the state with $\mathcal{M} = N/2$

$$|0\rangle \longleftrightarrow |\uparrow, \ldots, \uparrow\rangle\,. \tag{3.8}$$

The phase factor $\exp\left\{\pm i\pi \sum_{k=1}^{m-1} c_k^\dagger c_k\right\}$ is a non-local operator that transforms the commutation relations of the spins

$$\left[\sigma_m^+, \sigma_{m'}^-\right] = \delta_{mm'}\sigma_m^z, \quad \left[\sigma_m^z, \sigma_{m'}^\pm\right] = \pm 2\delta_{mm'}\sigma_m^\pm, \tag{3.9}$$

into anticommutation relations satisfied by the fermions (see Appendix 3.A for more details):

$$\left\{c_m^\dagger, c_{m'}\right\} = \delta_{mm'}, \quad \left\{c_m, c_{m'}\right\} = \left\{c_m^\dagger, c_{m'}^\dagger\right\} = 0. \tag{3.10}$$

With the Jordan-Wigner transformation we find that the magnetization (3.4) and the parity (3.5) become

$$\begin{aligned}\mathcal{M} &= \frac{1}{2}\sum_{m=1}^{N}(1 - 2c_m^\dagger c_m) = \frac{N}{2} - N_f, \\ \mathcal{P} &= \prod_{m=1}^{N}(1 - 2c_m^\dagger c_m) = (-1)^{N_f},\end{aligned} \tag{3.11}$$

where

$$N_f = \sum_{m=1}^{N} c_m^\dagger c_m, \tag{3.12}$$

is the operator that counts the total number of fermions. Hence, since $[H, \mathcal{M}] = 0$, the number of particles, and therefore the parity of the system, are fixed. Applying the transformation (3.6) to the open XX Hamiltonian (3.3) leads to:

$$H^{\text{OBC}} = -\frac{J}{2}\sum_{m=1}^{N-1}\left(c_m^\dagger c_{m+1} + c_{m+1}^\dagger c_m\right). \tag{3.13}$$

Thus, despite the non-local nature of the Jordan-Wigner transformation, (3.13) is a local fermionic Hamiltonian that shares the same structure that the spin Hamiltonian. However, when the spin Hamiltonian (3.3) describes a closed spin chain, the non-locality of the transformation makes a big difference. The reason is that the product of the localized spins at the ends of the chain gives

$$\sigma_N^- \sigma_1^+ = (-1)^{N_f+1} c_N^\dagger c_1, \tag{3.14}$$

where we have taken into account (3.11). Hence, the fermionic map of (3.3) for PBC $\eta = 1$ is:

$$H^{\text{PBC}} = H^{\text{OBC}} - \frac{J}{2}(-1)^{N_f+1}(c_N^\dagger c_1 + \text{h.c}). \tag{3.15}$$

Hence, given that parity is conserved, it is possible to split the Hilbert space and consider a Hamiltonian in each parity sector. They exclusively differ on the boundary conditions applied to the fermionic system

$$\begin{aligned} &N_f \quad \text{even} \Rightarrow H_{\mathcal{P}=1} = H^{\text{OBC}} + \frac{J}{2}(c_N^\dagger c_1 + \text{h.c}) \quad \Rightarrow \text{APBC} \quad c_{N+1} = -c_1, \\ &N_f \quad \text{odd} \Rightarrow H_{\mathcal{P}=-1} = H^{\text{OBC}} - \frac{J}{2}(c_N^\dagger c_1 + \text{h.c}) \quad \Rightarrow \text{PBC} \qquad c_{N+1} = c_1. \end{aligned} \tag{3.16}$$

Hence, each sector is determined by the same Hamiltonian but the Fock spaces are different due to the boundary conditions imposed. Let us see it more in detail.

3.1.1 Periodic boundary conditions

To diagonalize the Hamiltonians (3.16) we can exploit translational invariance. This is done defining the discrete Fourier transform of the fermionic operators c_m

$$d_k = \frac{1}{\sqrt{N}}\sum_m e^{-ikm} c_m. \tag{3.17}$$

The set of allowed values of the allowed values of the momentum $\Omega_{\mathcal{P}}$ is determined by the boundary conditions (3.16):

$$\left.\begin{aligned} \Omega_{-1} &= \{k \mid k = \frac{2m\pi}{N}\} \\ \Omega_1 &= \{k \mid k = \frac{(2m-1)\pi}{N}\} \end{aligned}\right\} \text{ with } \begin{aligned} &m = -L+1, \ldots, L, && \text{if } N = 2L, \\ &m = -L, \ldots, L, && \text{if } N = 2L+1. \end{aligned} \tag{3.18}$$

Inverting (3.17) and plugging it in (3.16) yields:

$$H_{\mathcal{P}} = -J\sum_{k\in\Omega_{\mathcal{P}}} \cos(k) d_k^\dagger d_k, \tag{3.19}$$

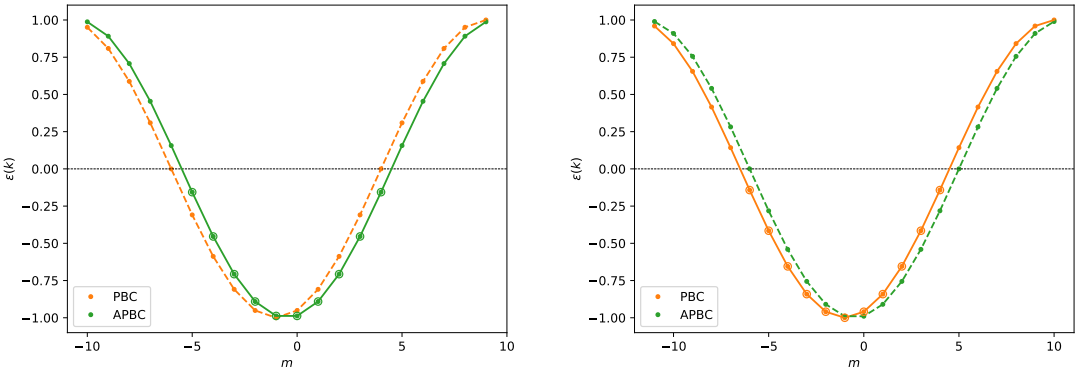

Figure 3.1: Dispersion relation $\epsilon(k) = -J\cos k$ with $J = 1$ of the two parity sectors given by (3.18) for chain (left) $N = 20$ and (right) $N = 22$. $\mathcal{P} = 1$ imposes antiperiodic boundary conditions on the fermionic chain and $\mathcal{P} = -1$ periodic ones. The solid line with circled points corresponds to the ground state of the XX chain.

The states of each fermionic Hamiltonian are constructed by filling the Fock vacua.

$$|\psi\rangle_{\mathcal{P}} = \prod_{k\in\mathcal{K}_{\mathcal{P}}} d_k^\dagger |0\rangle_{\mathcal{P}}\,, \tag{3.20}$$

where $\mathcal{K}_{\mathcal{P}} \subseteq \Omega_{\mathcal{P}}$ is a set of allowed values of momenta. In particular, the ground state of each $H_{\mathcal{P}}$ is obtained by filling all the negative energy levels (see Table 3.1). Since the ground state of an even XX chain has zero magnetization, it follows from (3.11) that $N_F = N/2$. Then, if $N = 4n$, the ground state must be sought in the $\mathcal{P} = 1$ sector that imposes antiperiodic boundary conditions (see (3.16)) on the fermionic Hamiltonian whereas the ground state of a $N = 4n + 2$ spin chain must be sought in the $\mathcal{P} = -1$ sector. Observe that the Fermi momentum for even chains is:

$$k_F \equiv \pi\frac{N_f}{N} = \frac{\pi}{2}. \tag{3.21}$$

N	$\mathcal{K}_{\mathcal{P}=-1}\quad \{k \mid \frac{2m\pi}{N}\}$	$\mathcal{K}_{\mathcal{P}=1}\quad \{k \mid \frac{(2m-1)\pi}{N}\}$
$4n$	$m \in [-n, n]$	$m \in [-n+1, n]$
$4n+2$	$m \in [-n, n]$	$m \in [-n, n+1]$

Table 3.1: The negative energy levels depend on the parity of the total number of fermions N and the boundary conditions. The coloured cells denote the subspace where the ground state of the XX spin chain must be sought.

Notice that the dimension of the Hilbert space of the XX spin chain is 2^N and that the dimension of the fermionic Hilbert space of each parity sector is also 2^N. As a consequence, there are 2^{N+1} fermionic states meaning that half of them are redundant. Therefore, from each parity sector one has to keep only those 2^{N-1} fermionic states with the right parity.

3.1.2 Open boundary conditions

The OBC chain is not translationally invariant due to the existence of boundaries. Nevertheless, the dispersion relation of H^{OBC} (3.13) can be obtained by diagonalizing the hopping matrix (also known as first-quantized Hamiltonian)

$$-\frac{J}{2}\begin{pmatrix} 0 & 1 & & & \\ 1 & 0 & 1 & & \\ & \ddots & \ddots & \ddots & \\ & & 1 & 0 & 1 \\ & & & 1 & 0 \end{pmatrix}\begin{pmatrix} \phi_1 \\ \phi_2 \\ \vdots \\ \phi_{N-1} \\ \phi_N \end{pmatrix} = \epsilon \begin{pmatrix} \phi_1 \\ \phi_2 \\ \vdots \\ \phi_{N-1} \\ \phi_N \end{pmatrix} \Rightarrow \begin{cases} -\frac{J}{2}\phi_2 = \epsilon\phi_1 \\ -\frac{J}{2}\left(\phi_{l-1}+\phi_{l+1}\right) = \epsilon\phi_l, \; l\in[2,N-1] \\ -\frac{J}{2}\phi_{N-1} = \epsilon\phi_N, \end{cases} \tag{3.22}$$

that it is diagonalized using the ansatz

$$\phi_l = Ae^{ikl} + Be^{-ikl}. \tag{3.23}$$

It follows that $\epsilon(k) = -J\cos(k)$, and imposing the OBC conditions $\phi_0 = \phi_{N+1} = 0$ we obtain the following set of allowed momenta:

$$\Omega_0 = \{k \;|\; k = \frac{m\pi}{N+1},\; m \in [1, N]\}, \tag{3.24}$$

where we have assigned $\mathcal{P} = 0$ to the OBC case in order to systematize notation. Hence, we can write the Hamiltonian (3.13) as

$$H^{\text{OBC}} = -J\sum_{k\in\Omega_0}\cos(k)b_k^\dagger b_k, \tag{3.25}$$

where

$$b_k = \sqrt{\frac{2}{N+1}}\sum_{l=1}^{N}\sin(kl)\,c_l. \tag{3.26}$$

Notice that the fermions $\{b_k\}$ satisfy the anticommutation relations (3.10) and that they define the same Fock vacuum $b_k|0\rangle = c_m|0\rangle = 0$. As in the PBC case, the ground state is obtained by filling the negative energy levels as in (3.20)

$$\mathcal{K}_0 = \{k \in \Omega_0 \;|\; m \in [1, L]\}, \quad \text{if } N = 2L. \tag{3.27}$$

If the system has an odd number of spins, there is a zero mode, that is a state with zero energy corresponding to the momentum $k = \pi/2$ ($m = L+1$). As a consequence, the ground state is degenerate since it is possible to define a ground state with and without the zero mode. Indeed, observe that the definition of the Fermi momentum $k_F \equiv \frac{\pi N_F}{N}$ leads to $k_F = \pi/2$ if $N = 2L$ but there is an ambiguity in its definition for odd systems $N = 2L+1$ since $N_F = L$ or $N_F = L+1$. As a consequence,

$$k_F = \frac{\pi}{2} - \frac{\pi}{2N}, \;\text{ or }\; k_F = \frac{\pi}{2} + \frac{\pi}{N}. \tag{3.28}$$

Note that in the thermodynamic limit $N \to \infty$ and $k_F = \pi/2$ for both parities and both boundary conditions.

3.1.3 The continuum limit

From what we have seen above it is clear that in the thermodynamic limit $N \to \infty$ the XX model is gapless for both PBC and OBC cases since it is possible to add fermions with an energy arbitrarily close to the Fermi level $k_F = \pi/2$. Indeed we shall see that the model is described by a CFT with central charge $c = 1$. To do so, we shall restrict ourselves to the region near the Fermi level, so we shall consider:

$$\frac{c_m}{\sqrt{a}} \approx e^{ik_F x/a}\psi_L(x) + e^{-ik_F x/a}\psi_R(x), \tag{3.29}$$

where we define the coordinate $x = ma$, where a is the lattice spacing and $\psi_L(x)$ and $\psi_R(x)$ describe left and right moving Dirac fermionic fields which vary slowly on the lattice scale, while the terms $e^{\pm ik_F x/a} = i^m$ carry the rapid oscillations. Plugging the above parametrization in (3.13) and taking into account that the sum of the highly oscillating crossed term can be neglected[2], and taking in addition the usual continuum limit $a \to 0$, $N \to \infty$ with $\mathcal{N} = Na$ kept constant yields:

$$H \approx -\frac{iJa}{2}\int_0^{\mathcal{N}} dx \left[(\partial_x\psi_R)^\dagger\psi_R - (\partial_x\psi_L)^\dagger\psi_L + \psi_L^\dagger\partial_x\psi_L - \psi_R^\dagger\partial_x\psi_R\right], \tag{3.30}$$

where $\psi_{L(R)}(x+a) = \psi_{L(R)}(x) + a\partial_x\psi_{L(R)}(x) + o(a^2)$. Integrating by parts,

$$H \approx -iaJ\int_0^{\mathcal{N}} dx \left(\psi_L^\dagger\partial_x\psi_L - \psi_R^\dagger\partial_x\psi_R\right) = -v_F\int_0^{\mathcal{N}} dx\Psi^\dagger(x)\sigma_3\partial_x\Psi(x), \tag{3.31}$$

where $v_F = Ja$ is the Fermi velocity, $\sigma_3 \equiv \sigma_z$, and we have defined the spinor

$$\Psi(x) = \begin{pmatrix}\psi_L(x)\\ \psi_R(x)\end{pmatrix}. \tag{3.32}$$

The expression (3.31) is called the masless Dirac Hamiltonian and it describes a massless Dirac fermion field theory with "speed of light" given by v_F. The equations of motion are:

$$\partial_t\Psi(x,t) = -v_F\sigma_3\partial_x\Psi(x,t). \tag{3.33}$$

Defining $\Psi(x,t) \equiv \Psi(x)e^{iEt}$ and plugging into (3.33) yields

$$\begin{aligned}\psi_L(x) &= A_L e^{i\frac{E}{v_F}x},\\ \psi_R(x) &= A_R e^{-i\frac{E}{v_F}x}.\end{aligned} \tag{3.34}$$

Imposing the boundary conditions $c_{N+1} = c_0 = 0$ with (3.29) yields

$$e^{i2\frac{E}{v_F}Na} = (-1)^{N+1} \quad \Rightarrow \begin{cases} E = \frac{(m+1/2)\pi J}{N}, & m = 0, \pm 1, \dots \quad \text{if } N = 2L,\\ E = \frac{m\pi J}{N}, & m = 0, \pm 1, \dots \quad \text{if } N = 2L+1\end{cases}. \tag{3.35}$$

[2] If we would instead consider $J = 1 + (-1)^m\delta$, the oscillation is canceled, so the right and left moving fermions are coupled originating a mass $m \propto \delta$ in the theory.

It is convenient for us to rescale time and to perform a Wick rotation $t = -iv_F x^0$ and $x = x^1$. The equations of motion (3.33) can thus be written as

$$(i\partial_{x^0} + \sigma_3 \partial_{x^1})\, \Psi(x^0, x^1) = 0. \tag{3.36}$$

We can write them in terms of the complex coordinates $z = x^1 + ix^0$ and $\bar{z} = x^1 - ix^0$:

$$\begin{aligned} \partial_z \psi_L(z, \bar{z}) = 0 \quad &\Rightarrow \quad \psi_L(z, \bar{z}) = \psi_L(\bar{z}) \\ \partial_{\bar{z}} \psi_R(z, \bar{z}) = 0 \quad &\Rightarrow \quad \psi_R(z, \bar{z}) = \psi_R(z). \end{aligned} \tag{3.37}$$

It can be shown that the holomorphic part of the stress energy tensor is

$$T_R(z) = -\frac{1}{2} : \psi_R^\dagger(z) \partial_z \psi_R(z) - \partial_z \psi_R^\dagger(z) \psi_R(z) :, \tag{3.38}$$

where :: denotes the normal ordered product. The central charge c of the conformal field theory appears in the operator product expansion (OPE) of the stress energy tensor:

$$T(z_1)T(z_2) = \frac{c/2}{(z_1 - z_2)^4} + \frac{2}{(z_1 - z_2)^2} T(z_2) + \frac{1}{z_1 - z_2} \partial T(z_2), \tag{3.39}$$

Then, taking in account that $\langle T(z) \rangle = 0$ we have that the two-point correlator is

$$\langle T(z_1)T(z_2) \rangle = \frac{c/2}{(z_1 - z_2)^4}. \tag{3.40}$$

It is possible to show that $c = 1$ by computing $\langle T(z_1)T(z_2) \rangle$ with (3.38), using Wick's theorem and the two-point correlation functions

$$\left\langle \psi_R(z_1) \psi_R^\dagger(z_2) \right\rangle = \frac{1}{z_1 - z_2}, \quad \left\langle \psi_L(\bar{z}_1) \psi_L^\dagger(\bar{z}_2) \right\rangle = \frac{1}{\bar{z}_1 - \bar{z}_2}.$$

Due to the constraints imposed by conformal invariance, it is possible to obtain a large amount of information from the system with CFT. In particular, we can obtain the universal properties of entanglement entropy.

3.2 Entanglement entropy

In this section we shall discuss the entanglement entropy of the XX model in detail. As we have shown in Chapter 2 the computation of the entanglement entropy requires finding the singular values of the reduced density matrix. In the spin chain case, this means that ρ_A scales as 2^{N_A}. We face then the same computational difficulty that we encountered when diagonalizing the Hamiltonian of a spin chain. A crucial simplification was found by Peschel (2003). He showed that the reduced density matrices of free fermionic and bosonic states can be determined from their two-point correlation function. Since the fermionic mapping of the XX model yields a free fermion Hamiltonian (3.13), we can follow this strategy to compute the entanglement entropy. Thus, in the next subsection we shall explain in detail this procedure that has been employed to obtain all the numerical data appearing in this thesis. Next, we shall describe the features of the entanglement entropy that are fixed by conformal invariance, and finally the non-universal contributions whose analytical expression is known.

3.2.1 Entanglement entropy in free fermion systems

A fermionic or bosonic state is completely determined by the expectation values of all the admissible operators acting on it. Thus, knowing the n point-functions is equivalent to knowing all the expectation values and thus characterizing completely the state. Moreover, using Wick's theorem, the n-point functions can be written in terms of the two-point correlator. For instance

$$\left\langle c_m^\dagger c_n^\dagger c_k c_l \right\rangle = \left\langle c_m^\dagger c_l \right\rangle \left\langle c_n^\dagger c_k \right\rangle - \left\langle c_m^\dagger c_k \right\rangle \left\langle c_n^\dagger c_l \right\rangle . \tag{3.41}$$

Then, the state is known as a Gaussian state as it is fully characterized by expectation values of quadratic operators. All the two-point correlators $C_{ij} = \langle c_i^\dagger c_j \rangle$ can be arranged in the correlation matrix

$$\mathbf{C} = \begin{pmatrix} \langle c_1^\dagger c_1 \rangle & \cdots & \langle c_1^\dagger c_N \rangle \\ \vdots & \ddots & \vdots \\ \langle c_N^\dagger c_1 \rangle & \cdots & \langle c_N^\dagger c_N \rangle \end{pmatrix}, \tag{3.42}$$

which completely characterizes the state[3]. The correlation matrix associated to the block A that is denoted by $\mathbf{C}_A$ is obtained by the corresponding restriction of $\mathbf{C}$:

$$\mathbf{C}_A = \{C_{mn} \mid m, n \in A\}. \tag{3.43}$$

The correlation matrix of the XX model is obtained with the fermionic operators (3.17) and (3.26):

$$C_{ij} = \left\langle c_i^\dagger c_j \right\rangle = \frac{1}{N} \sum_{k \in \mathcal{K}_\mathcal{P}} e^{ik(i-j)}, \quad \text{PBC} \tag{3.44}$$

$$C_{ij} = \left\langle c_i^\dagger c_j \right\rangle = \frac{2}{N+1} \sum_{k \in \mathcal{K}_0} \sin(ki)\sin(kj), \quad \text{OBC}, \tag{3.45}$$

where $\mathcal{K}_\mathcal{P}$ with $\mathcal{P} = \pm 1, 0$ are the corresponding sets of allowed momenta that define the ground states for PBC (see Table 3.1) and for OBC (3.27). If we consider the thermodynamic limit $N \to \infty$ we can approximate the sums above by integrals and find:

$$C_{ij} = \frac{\sin(k_F(i-j))}{\pi(i-j)}, \qquad \text{PBC} \tag{3.46}$$

$$C_{ij} = \frac{\sin(k_F(i-j))}{\pi(i-j)} - \frac{\sin(k_F(i+j))}{\pi(i+j)}, \qquad \text{OBC}. \tag{3.47}$$

Since the state is Gaussian, the eigenvalues of $\mathbf{C}_A$ must be related to the eigenvalues of ρ_A. To see it, let us first diagonalize $\mathbf{C}_A$:

$$\sum_{m,n=1}^{N_A} U_{mk}^* (C_A)_{mn} U_{nl} = \nu_{kl} \delta_{kl}, \tag{3.48}$$

[3]For free fermion systems that do not conserve the number of particles, the correlator $F_{ij} = \left\langle c_i^\dagger c_j^\dagger \right\rangle$ must also be considered.

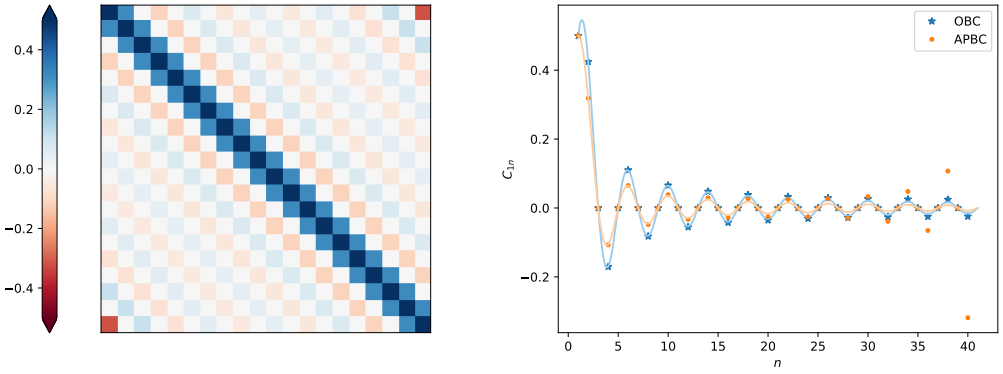

Figure 3.2: Left. Color plot of the correlation matrix $\mathbf{C}$ of a closed chain of $N = 20$. It can be seen that it is a Toeplitz matrix since all the entries along each diagonal take the same value. Right. Matrix elements C_{1n} for all values of n. In pale colors we plot the asymptotic result (3.47),(3.47). The discrepancies are due to the finite size.

where $\mathbf{U}$ is a unitary matrix. Thus, the two-point correlator of a new set of fermions $\{f_k\}_{k=1}^{N_A}$ with

$$f_k = \sum_{m=1}^{N_A} U_{mk} c_k, \tag{3.49}$$

is diagonal $\langle f_k^\dagger f_l \rangle = \nu_k \delta_{kl}$. Using the definition of the density matrix, $\langle O \rangle = \mathrm{tr}(O\rho)$ (2.4):

$$\langle f_k^\dagger f_l \rangle = \mathrm{tr}\left(f_k^\dagger f_l \rho_A \right) = \nu_k \delta_{kl} \tag{3.50}$$

The above equation implies that $\rho_A = \varrho_1 \otimes \cdots \otimes \varrho_{N_A}$ in the chosen basis, so we can focus on the eigenvalues of

$$\varrho_k = \begin{pmatrix} \alpha_k & \beta_k \\ \beta_k^* & 1 - \alpha_k \end{pmatrix}.$$

Expressing the fermionic operators in its matrix representation

$$f_k = \begin{pmatrix} 0 & 0 \\ 1 & 0 \end{pmatrix}, \quad f_k^\dagger = \begin{pmatrix} 0 & 1 \\ 0 & 0 \end{pmatrix}, \tag{3.51}$$

and imposing $\langle f_k \rangle = 0$ yields $\mathrm{tr}\{f_k \rho_A\} = \beta_k = 0$. Moreover, computing (3.50) leads to $\alpha_k = \nu_k$. So we can write

$$\rho_A = \bigotimes_{k=1}^{N_A} \varrho_k = \bigotimes_{k=1}^{N_A} \begin{pmatrix} \nu_k & 0 \\ 0 & 1 - \nu_k \end{pmatrix} \tag{3.52}$$

Then, it follows that

$$\mathrm{tr}\, \rho_A^n = \prod_{k=1}^{N_A} \mathrm{tr}\, \varrho_k^n = \prod_{k=1}^{N_A} \left(\nu_k^n + (1 - \nu_k)^n \right), \tag{3.53}$$

so the Rényi entropies (2.18) are

$$S_n(A) = \frac{1}{1-n} \sum_{k=1}^{N_A} \log\left(\nu_k^n + (1-\nu_k)^n\right), \tag{3.54}$$

and the Von Neumann (2.19) is:

$$S(A) = -\sum_{k=1}^{N_A} \left(\nu_k \log \nu_k + (1-\nu_k)\log(1-\nu_k)\right). \tag{3.55}$$

The above expressions allow to compute numerically the Rényi entropies with low computational cost. We can summarize the steps:

1. Compute the correlation matrix $\mathbf{C}_A$ of the subsystem A.
2. Diagonalize $\mathbf{C}_A$.
3. Use (3.54) and (3.55).

This procedure can be also applied to spin chains by means of the Jordan-Wigner transformation. However, it is only valid for connected blocks. For disjoint blocks, the spin density matrix is different from that of fermions. This is due to the non-locality of the transformation (3.6).

3.2.2 Universal properties of entanglement entropy

Let us consider an infinite fermionic chain. We are interested in computing the Rényi entropies (2.18) of a subsystem $A = [u, v]$ of length $\ell = |u - v|$ delimited by the points $x = u$ and $x = v$ that are called *entangling points* as it can be seen in Fig.3.3

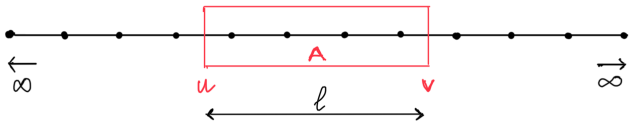

Figure 3.3: The block or subsystem $A = [u, v]$ of an infinite chain.

Thanks to the conformal invariance, is possible to get insight into the entanglement even without diagonalizing explicitly the reduced density matrix ρ_A as it was shown by Holzhey *et al.* (1994) and later by Calabrese and Cardy (2004). Conformal field theory can provide the universal behaviour of the Rényi entropies $S_n(\rho_A)$ (2.18) but the non-universal one cannot be captured by CFT and, in general, it cannot be neglected. The starting point is to write the density matrix of a thermal state with inverse temperature β

$$\rho = \frac{e^{-\beta H}}{Z}, \quad Z = \operatorname{tr} e^{-\beta H}, \tag{3.56}$$

as a Euclidean path integral on the imaginary time interval $(0, \beta)$. The constant Z corresponds to the partition function that ensures the correct normalization and it corresponds to a cylinder of circumference β obtained by sewing together the edges along $\tau = 0$ and $\tau = \beta$. Thus, the reduced density matrix (2.5) corresponds to the same cylinder but with an open cut in A. Next we consider n copies or replicas (labelled by $k = 1, \ldots, n$) of this cylinder sewed together along the cuts. Hence, $\operatorname{tr} \rho^n$ corresponds to sewing the copies $k = 1$ and $k = n$ together. This construction defines a path integral denoted by $Z_n(A)$ over an n-sheeted Riemmann surface $\mathcal{R}_n$. Then $\operatorname{tr} \rho_A^n = Z_n(A)/Z_1(A)$ and the Rényi entropies (2.18) are given by

$$S_n(A) = \frac{1}{1-n} \log(Z_n(A)) + \frac{n}{1+n} \log Z_1(A). \tag{3.57}$$

Furthermore, it can be shown that

$$Z_n(A) \propto \left\langle \mathcal{T}_n(u,0) \tilde{\mathcal{T}}_n(v,0) \right\rangle, \tag{3.58}$$

where $\mathcal{T}_n(u,0)$ ($\tilde{\mathcal{T}}_n(v,0)$) is a local field called *twist field*. Hence, the Rényi entropies take the form:

$$S_n(A) = \frac{1}{1-n} \log\Big(\left\langle \mathcal{T}_n(u,0) \tilde{\mathcal{T}}_n(v,0) \right\rangle \Big) + c_n'. \tag{3.59}$$

So far we have not used yet the conformal invariance. It can be shown that the twist fields are primary fields. They transform under an arbitrary conformal transformation $\omega = f(z)$, $\bar{\omega} = \bar{f}(\bar{z})$ as

$$\mathcal{T}_n(z,\bar{z}) = \left(\frac{df}{dz}\right)^{\Delta_n} \left(\frac{d\bar{f}}{d\bar{z}}\right)^{\bar{\Delta}_n} \mathcal{T}_n'(\omega,\bar{\omega}), \tag{3.60}$$

with

$$\Delta_n = \bar{\Delta}_n = \frac{c}{24}\left(n - \frac{1}{n}\right).$$

Furthermore, the two-point correlator of primary fields is completely fixed by conformal invariance:

$$\left\langle \mathcal{T}_n(u,0) \tilde{\mathcal{T}}_n(v,0) \right\rangle = \left(\frac{|u-v|}{a}\right)^{-2(\Delta_n + \bar{\Delta}_n)} = \left(\frac{\ell}{a}\right)^{-\frac{c}{6}(n-1/n)}, \tag{3.61}$$

where the lattice spacing a acts as an UV cut-off that makes the final result dimensionless and it corresponds to the normalization of $Z_1(A)$. Finally, plugging (3.61) into (3.59) leads to

$$S_n(A) = S_n(\ell) = \frac{1}{1-n} \log\left(\frac{\ell}{a}\right)^{-\frac{c}{6}(n-1/n)} + c_n' = \frac{c}{6}\left(1 + \frac{1}{n}\right) \log\left(\frac{\ell}{a}\right) + c_n', \tag{3.62}$$

Using (2.19) we obtain the entanglement entropy:

$$S(\ell) = \frac{c}{3} \log \frac{\ell}{a} + c_1', \tag{3.63}$$

which is the expression found for the first time by Holzhey *et al.* (1994). By considering different conformal mappings Calabrese and Cardy (2004) were able

to compute the correlators of the twist fields associated to other geometries. For instance, the entanglement entropy of a thermal state in an infinite long strip is

$$S(\ell) = \frac{c}{3} \log\left(\frac{\beta}{\pi a} \sinh\left(\frac{\pi \ell}{\beta}\right)\right) + c_1', \tag{3.64}$$

that interpolates from (3.62) for $\ell \ll \beta$ to the thermal (extensive) entropy $S(\ell) = c\pi\ell/(3\beta)$ for $\ell \gg \beta$. The Rényi entropies associated with subsystem A of length ℓ in a finite system of length N with periodic boundary conditions is

$$S_n(\ell) = \frac{c}{6}\left(1 + \frac{1}{n}\right) \log\left(\frac{N}{\pi a} \sin\left(\frac{\pi \ell}{N}\right)\right) + c_n'. \tag{3.65}$$

The quantity inside the logarithm

$$\frac{D(\ell, N)}{a} = \frac{N}{\pi a} \sin\left(\frac{\pi \ell}{N}\right), \tag{3.66}$$

is the *chord length* and tends to ℓ for $N \gg 1$, recovering thus the result for the infinite system (3.62).

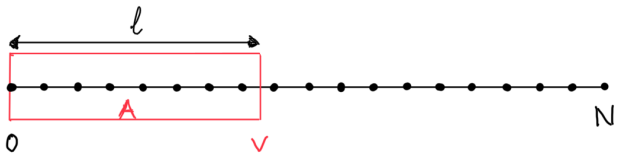

Figure 3.4: The subsystem $A = [0, \ell]$ of a finite chain of lenght N.

The computation of the Rényi entropies in systems with open boundary conditions is similar. Let us consider an open finite system of length N and a subsystem $A = [0, \ell]$ of length ℓ. Observe that in this case there is only one entangling point $v = \ell$ since $u = 0$ corresponds to the physical boundary of the system, as it can be seen in Fig. 3.4. As a consequence, the computation of the partition function $Z_n(A)$ over $\mathcal{R}_n$ is related to the correlator $\langle \mathcal{T}_n(\ell, 0) \rangle$. It can be shown (Calabrese and Cardy 2004) that

$$S_n(\ell) = \frac{c}{12}\left(1 + \frac{1}{n}\right) \log\left(\frac{2N}{\pi a} \sin\left(\frac{\pi \ell}{N}\right)\right) + \tilde{c}_n'. \tag{3.67}$$

The non-universal constants of (3.67) and (3.65) are not the same, but they are related by the so called *boundary entropy* proposed by Affleck and Ludwig (1991)

$$\log g = \tilde{c}_n' - c_n/2 \tag{3.68}$$

which is a universal magnitude related to the boundary conformal field theory, which in turn is related to the degeneracy of the ground state. For the XX model $g = 1$ (Affleck and Ludwig 1991) and we have that $\tilde{c}_n' = c_n'/2$ as it can be seen in

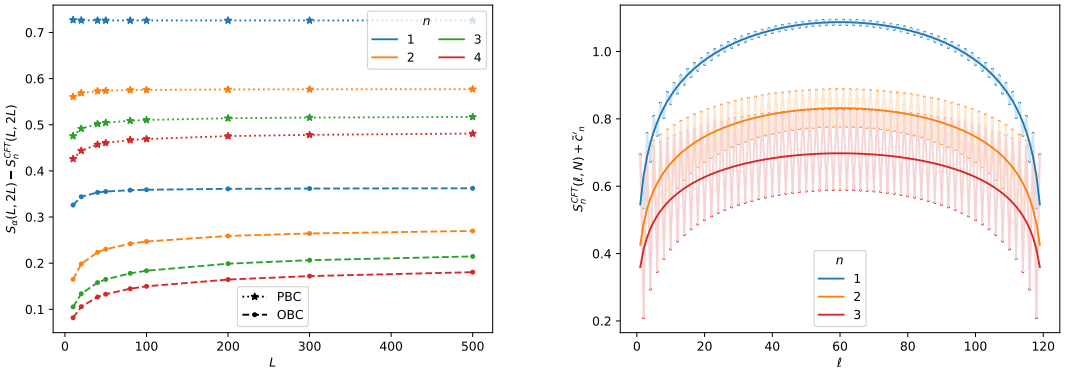

Figure 3.5: (Left) The difference $S_n(L,2L) - S_n^{\text{CFT}}(L,2L)$ converges to a different constant for PBC and OBC. Notice that for the entanglement entropy case $n = 1$, $c'_1 \approx 0.72$ and $\tilde{c}'_1 \approx 0.36$ which is in agreement with the relation of these constants fixed by the universal boundary entropy (3.68) with $g = 1$ $\tilde{c}'_n = c'_n/2$. (Right) Reading the asymptotic value of this constant and adding it to the conformal prediction (3.67) leads to the solid lines. Observe that the parity oscillations (pale color lines) of the Rényi entropies are not captured by (3.67).

Fig. 3.5 left. Thus, the part of the entanglement entropy that is completely fixed by conformal invariance can be written as

$$S_n^{\text{CFT}}(\ell) = \begin{cases} \frac{c}{6}\left(1+\frac{1}{n}\right)\log\left(\frac{D(\ell,N)}{a}\right) & \text{(closed chain)}, \\ \frac{c}{12}\left(1+\frac{1}{n}\right)\log\left(\frac{2D(\ell,N)}{a}\right) & \text{(open chain)}. \end{cases} \tag{3.69}$$

In Fig. 3.5 (left) we plot the difference between the Rényi entropies obtained by numerical methods – that we shall explain below – and the conformal prediction $S_n(L,2L) - S_n^{\text{CFT}}(L,2L)$ for different values of $N = 2L$. As it can be seen the outcome converges to a constant. Let us identify then these numerical values of the OBC case with $\tilde{c}'_n$. As it can be seen in Fig. 3.5 (right), the expression (3.67) captures satisfactorily the leading behaviour but there is an oscillating term whose amplitude increases with the Rényi order n that it is not captured by the CFT and the additive constant, meaning that (3.67) is incomplete.

3.2.3 Finite-size corrections to entanglement entropy

Jin and Korepin (2004) showed that the entanglement entropy can be written as a contour integration in the complex plane with poles at ν_k

$$S(A) = \frac{1}{2\pi i}\lim_{\epsilon\to 0^+}\sum_{k=1}^{N_A}\oint_\gamma \frac{f_n(\lambda+2\epsilon+)}{\lambda-\nu_k}d\lambda, \tag{3.70}$$

where γ is a closed circuit that surround the poles $\nu_k \in [0,1]$, and the shift 2ϵ is used for avoiding the logarithmic cuts in

$$f_1(x) = -x\log(x) - (1-x)\log(x), \quad \text{or} \quad f_{n>1}(x) = \frac{1}{1+n}\log\left(x^n + (1-x)^n\right).$$

Observe that

$$\sum_{k=1}^{N_A} \frac{1}{\lambda - \nu_k} = \frac{d}{d\lambda}\left(\prod_{k=1}^{N_A} \log(\lambda - \nu_k)\right) = \frac{d}{d\lambda}\left(\det\left(\lambda \mathbb{1} - \mathbf{C}_A\right)\right) = \frac{d}{d\lambda}\left(D_{N_A}(\lambda)\right). \tag{3.71}$$

Then we can write (3.70) in terms of the determinant of the resolvent of $\mathbf{C}_A$

$$S(A) = \frac{1}{2\pi i} \lim_{\epsilon \to 0^+} \oint_\gamma f_n(\lambda + 2\epsilon) \frac{d}{d\lambda}\left(D_{N_A}(\lambda)\right), \tag{3.72}$$

The problem of computing the Rényi entropies is therefore mapped to computing a determinant $D_{N_A}(\lambda)$. Observe that the correlation matrix of the PBC case (3.47) verifies that $C_{i,j} = C_{i+1,j+1}$ with $i < j$. This property defines the class of Toeplitz matrices which has been extensively studied in physics (Deift *et al.* 2013). Jin and Korepin (2004) used an important result on Toeplitz determinants called the Fisher-Hartwig conjecture (Fisher and Hartwig 1969) to evaluate the asymptotic behaviour of the entanglement entropy ($N_A = \ell$). They found the expression

$$S(\ell) = \frac{1}{3}\log(\ell) + \frac{1}{3}\log 2 + \Upsilon_1, \tag{3.73}$$

with

$$\Upsilon_1 = -\int_0^\infty dt \left(\frac{e^{-t}}{3t} + \frac{1}{t\sinh^2(t/2)} - \frac{\cosh(t/2)}{2\sinh^3(t/2)}\right) \approx 0.49502.$$

Comparing expression (3.73) with the result obtained with CFT (3.63) leads us to identify the non-universal constant $c_1' = 1/3\log 2 + \Upsilon_1 \approx 0.726$ which coincides with the blue line of Fig. 3.5. Jin and Korepin provided also expressions for Rényi entropies with $n > 1$. For instance

$$\Upsilon_2 \approx 0.40405, \quad \Upsilon_3 \approx 0.366365, \quad \Upsilon_4 \approx 0.346061. \tag{3.74}$$

Observe that the oscillating behaviour of the Rényi entropies of Fig.3.5 is not captured by the above result. However, the amplitude of the oscillations increases with the Rényi parameter n, even blurring the universal behavior given by the CFT. Cardy and Calabrese (2010) showed that these terms contain more information about the underlying CFT, so they have been studied and computed for certain spin chains (Xavier and Alcaraz 2011). In particular, for the infinite XX model – and in general for infinite Lutinger liquids – Calabrese *et al.* (2010) proposed that the oscillations obey a universal scaling law

$$S_n(\ell) \approx S_n^{\mathrm{CFT}}(\ell) + c_n' + f_n \cos(2k_F\ell)|2\ell \sin k_F|^{-p_n}, \tag{3.75}$$

where $p_n = 2K/n$ is a universal parameter. Here $K = 1$ is the Luttinger parameter for the XX model, k_F is the Fermi level and f_n is a non-universal term which is known exactly for the XX model:

$$f_n = \frac{2}{1-n}\left(\frac{\Gamma(\frac{1}{2} + \frac{1}{2n})}{\Gamma(\frac{1}{2} - \frac{1}{2n})}\right)^2. \tag{3.76}$$

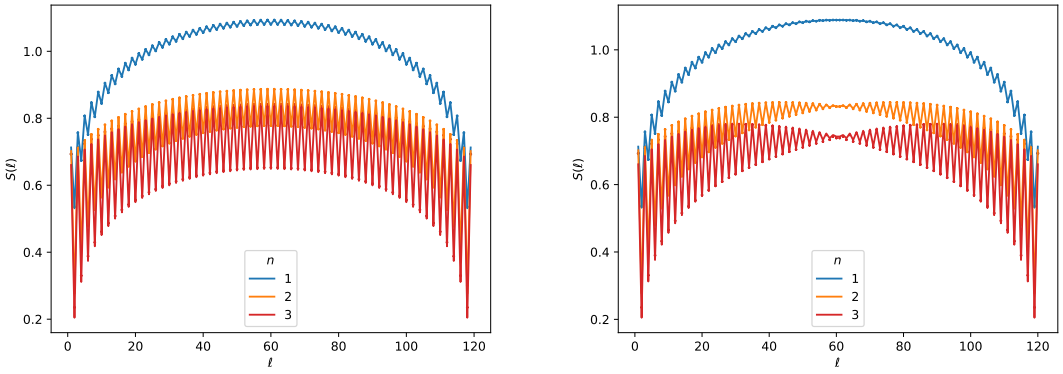

Figure 3.6: Rényi entropies for open chains of $N = 120$ with $k_F = \pi/2$ (left) and $N = 121$ (right) sites with k_F given by (3.28). The dots are data from numerics while the colored lines are theoretical predictions.

Note that $f_1 = 0$ and there are no oscillating terms in the entanglement entropy of a closed (or infinite) system. Hence, the full expression for a closed XX chain is:

$$\begin{aligned} S_n(\ell, L) \approx \frac{1}{6}\left(1+\frac{1}{n}\right)\log\left(\frac{D(\ell,L)}{a}\right) \\ +\Upsilon_n + \frac{1}{6}\left(1+\frac{1}{n}\right)\log 2 + f_n \cos(2k_F\ell)|2D(\ell,L)\sin k_F|^{-2/n}, \end{aligned} \tag{3.77}$$

where $D(\ell, L)$ is the chord length (3.66). Notice that the universal behavior predicted by the CFT is expressed in the first row, while the second contains the non-universal corrections. The constant term proportional to $\log 2$ is usually absorbed in the logarithm of the first row. It is explicitly detached in order to emphasize that it is not fixed by the CFT. Let us mention that the oscillatory behaviour where obtained by considering a generalized version of Fisher-Hartwig conjecture (Basor and Tracy 1991). Fagotti *et al.* (2011) studied the subleading corrections of the infinite and finite OBC chain by applying also a generalized Fisher-Hartwig conjecture. However they modified it accordingly to take into account that the correlation matrix of the OBC case (3.47) is composed by a Toeplitz matrix plus a Hankel matrix[4]:

$$\begin{aligned} S_n(\ell, L) \approx \frac{1}{12}\left(1+\frac{1}{n}\right)\log\left(\frac{2D(2\ell+1, 2(L+1))}{a}|\sin k_F|\right) + \frac{\Upsilon_n}{2} + \frac{1}{12}\left(1+\frac{1}{n}\right)\log 2 \\ + f_n \cos(2k_F\ell)(4D(2\ell+1, 2(L+1))|\sin k_F|)^{-1/n}, \end{aligned} \tag{3.78}$$

where $k_F = \pi/2$ if $N = 2L$ and $k_F = \pi/2 + \pi/(2(N+1))$ if $N = 2L+1$ as we discussed in (3.28). In this case,

$$f_n = \frac{2}{1-n}\left(\frac{\Gamma(\frac{1}{2}+\frac{1}{2n})}{\Gamma(\frac{1}{2}-\frac{1}{2n})}\right), \tag{3.79}$$

[4]A matrix M is a Hankel matrix if $M_{i,j} = M_{i+1,j-1}$ with $i < j$.

allowing oscillations for $n = 1$ as $f_1 = -1$. Notice the good agreement of this expression with the numerical data in Fig. 3.6. Observe that the chord length of the above expression considers an effective closed system of length $2(N + 1)$ that is composed as the open chain and its mirrored image reflected by the boundaries plus two additional sites (Fagotti *et al.* 2011).

3.3 Beyond entanglement entropy

In this section we shall characterize the entanglement properties of the XX model with the entanglement Hamiltonian, entanglement spectrum and the entanglement contour.

3.3.1 Entanglement Hamiltonian

In this section we shall consider more in detail the entanglement Hamiltonian that we introduced in (2.9). The structure of the entanglement Hamiltonian $\mathcal{H}_A$ depends on the quantum state and on the subsystem A, so it differs in general from the physical Hamiltonian H, since $\mathcal{H}_A$ describes in general an inhomogeneous system. The complete form of these parameters depends on each state, but there is a common pattern: the intensity of the couplings increases with the distance to the entangling points. This behaviour is well captured in the seminal works by Bisognano and Wichmann (1975, 1976) where they computed $\mathcal{H}_A$[5] of an infinite subsystem A embedded in an infinite system described by a relativistic quantum field theory in arbitrary dimensions. Particularizing for the one-dimensional case with $A = [0, \infty)$

$$\mathcal{H}_A = 2\pi \int_0^\infty x T_{00}(x) dx, \tag{3.80}$$

where the time-time component of the energy-momentum tensor $T_{00}(x)$ i.e. the energy density of the physical system is modulated by a weight function x. The expression (3.80) is referred as Bisognano-Wichmann theorem. The presence of the physical Hamiltonian density motivates the interpretation of ρ_A as a thermal state (3.56) with an inverse local temperature $T(x) = 1/\beta(x) = 1/x$ which is referred as *entanglement temperature* (Arias *et al.* 2017; Wong *et al.* 2013). The entanglement temperature is thus maximal at the entangling point and decreases as $1/x$ moving away from it.

It is possible to extend the Bisognano-Wichmann theorem (3.80) to conformally invariant systems. Cardy and Tonni (2016) computed $\mathcal{H}_A$ by mapping the spacetime geometry associated to the Euclidean path integral formulation of ρ_A into an annulus described by a complex coordinate $w = f(z)$ for different system

[5]The work of Bisognano and Wichmann is previous to the proposal of the entanglement Hamiltonian. It was obtained in the context of modular theory and that is why the entanglement Hamiltonian is also known as modular Hamiltonian.

geometries. The reason for choosing an annulus is that the theory is regularized by removing infinitesimal disks around the entangling points that separate A and B. Cardy and Tonni found the relation

$$\mathcal{H}_{\mathcal{A}} = 2\pi \int_A dx \beta(x) T_{00}(x), \tag{3.81}$$

where the weight function $\beta(x)$ is related to the conformal mapping to the annulus $f(z)$:

$$\beta(x) = \frac{1}{f'(x)}. \tag{3.82}$$

Hence, each geometry requires a different conformal mapping $f(z)$ which leads to a different $\beta(x)$. For instance, the weight function associated to a finite subsystem of length ℓ with entangling points at 0 and ℓ of an infinite subsystem (see Fig. 3.3) is

$$\beta(x) = \frac{x}{\ell}(\ell - x), \quad A = [0, \ell]. \tag{3.83}$$

The above expression can be extended to a closed finite system of length $2L$:

$$\beta(x) = \frac{D(\ell - x, 2L) D(x, 2L)}{D(\ell, 2L)}, \quad A = [0, \ell]. \tag{3.84}$$

where $D(x, 2L)$ is the chord length (3.66). Finally, the weight function associated to a subsystem $A = [x_0, L]$ of a finite system of length $2L$ centered at the origin $[-L, L]$ with the same boundary conditions at $\pm L$ is[6]:

$$\beta(x) = \frac{2L}{\pi} \frac{\sin\left(\frac{\pi x}{2L}\right) - \sin\left(\frac{\pi x_0}{2L}\right)}{\cos\left(\frac{\pi x_0}{2L}\right)}, \quad A = [x_0, L] \tag{3.85}$$

Observe that the above result (3.85) can also be derived from the result of the closed chain (3.84) with the parametrization $x \to x - x_0$ and $\ell \to 2(2L - x_0)$ since the computation of the open system is equivalent to the computation of the closed system composed by the original system plus its mirror image reflected by the boundaries, as we also discussed below (3.78).

As we have mentioned in section 3.2.3, a fermionic state is Gaussian since it is fully characterized by the expectation values of quadratic operators. Therefore it must be also the ground state – or a thermal state – of a fermionic Hamiltonian which is quadratic in the creation and annihiliation operators:

$$\mathcal{H}_{\mathcal{A}} = \mathbf{c} \boldsymbol{\mathcal{H}} \mathbf{c} = \sum_{mn} \mathcal{H}_{mn} c_m^\dagger c_n. \tag{3.86}$$

Since $\rho_A = \varrho_1 \otimes \cdots \otimes \varrho_{N_A}$ in the basis of fermions $\{f\}_{k=1}^{N_A}$ that diagonalizes the correlation matrix (3.48), $\mathcal{H}_A$ is diagonal also in terms of these fermions:

$$\mathcal{H}_A = -\sum_{k=1}^{N_A} \epsilon_k f^\dagger f_k, \tag{3.87}$$

[6]Notice that it is the system represented in Fig. 3.4 with different coordinates

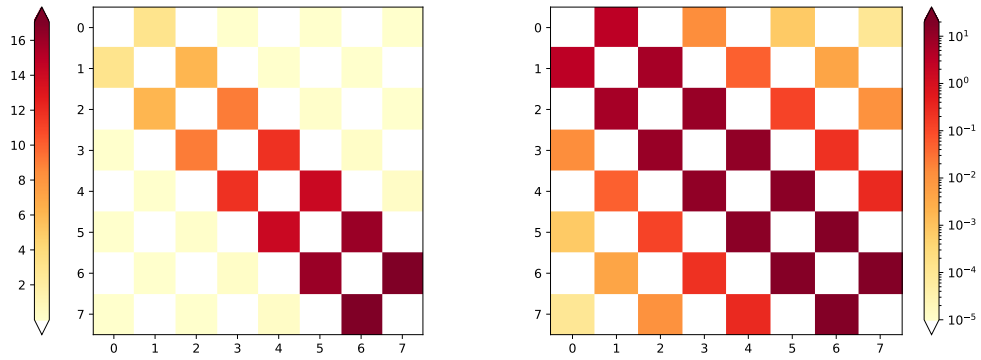

Figure 3.7: First quantized entanglement Hamiltonian $\mathcal{H}$ (3.86) associated to the half system of $N = 16$ fermions. As it can be seen in the left panel, the first neighbours terms are the largest. However, there are non-zero 3th, 5th, etc neighbour interactions, as it can be seen with logarithmic scale in the right panel.

where $\{\epsilon_k\}_{k=1}^{N_A}$ is the single-body entanglement spectrum. Hence, from (3.50) it follows that

$$\nu_k \delta_{kl} = \mathrm{tr}\left(f_k^\dagger f_l \rho_A\right) = \prod_{m \neq k} \mathrm{tr}(\varrho_m)\, \mathrm{tr}\left(f_k^\dagger f_k \varrho_k\right)\delta_{kl} = \frac{e^{-\epsilon_k}}{1 + e^{-\epsilon_k}}\delta_{kl}. \tag{3.88}$$

Hence, there is a relation between the eigenvalues of the correlation matrix and the single-body entanglement spectrum

$$\nu_k = \frac{1}{1 + e^{\epsilon_k}}, \quad \epsilon_k = \log\left(\frac{1 - \nu_k}{\nu_k}\right), \tag{3.89}$$

that allows us to compute the entanglement Hamiltonian with the correlation matrix (3.42) following these steps:

1. Diagonalize $\mathbf{C}_A$
$$\mathbf{U}^\dagger \mathbf{C}_A \mathbf{U} = \mathbf{D}_\nu. \tag{3.90}$$
2. Define the matrix
$$\mathbf{D}_\epsilon = \log\left(\frac{\mathbb{1} - \mathbf{D}_\nu}{\mathbf{D}_\nu}\right) \tag{3.91}$$
3. Compute the first-quantized Hamiltonian
$$\mathcal{H} = \mathbf{U}\mathbf{D}_\epsilon\mathbf{U}^\dagger \tag{3.92}$$

.

Although Bisognano-Wichmann's theorem is strictly defined for infinite and continuum systems, some recent works extend its scope to lattice Hamiltonians (Dalmonte *et al.* 2018; Giudici *et al.* 2018). In Fig. 3.7 we show the first quantized entanglement Hamiltonian $\mathcal{H}$ corresponding to the subsystem $A = [8, 16]$ of an open system of $N = 16$ fermionic sites described by the Hamiltonian (3.13). As it

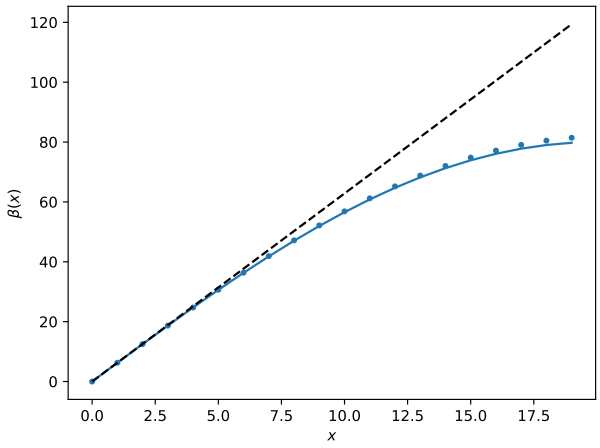

Figure 3.8: Couplings $\boldsymbol{\beta}$ of the effective entanglement Hamiltonian (3.93) of the half system $x_0 = 0$ of a chain of $2L = 80$. The continuous line corresponds to the analytical result (3.85). The dashed black line is the Bisognano-Wichmann prediction (3.80).

can be seen in the left panel, the most relevant terms connect sites that are first neighbors but there are also non-zero long-range terms, in apparent contradiction with Bisognano-Wichmann. Eisler and Peschel (2017) obtained the analytical form of all couplings (short and long-range) for free fermion systems and then Eisler *et al.* (2019) took the continuum limit recovering the Bisognano-Wichmann prediction.

The obtainment of the first quantized Hamiltonian $\boldsymbol{H}$ requires to numerically distinguish between eigenvalues ν_k that can be exponentially close to 0 and 1. This fact poses a very demanding computational task, since it requires a precision of at least N digits for N sites (Arias *et al.* 2017; Eisler *et al.* 2020)[7]. Tonni *et al.* (2018) developed an alternative way of obtaining an effective entanglement Hamiltonian. As it can be seen in Fig. 3.7 left, the first neighbours interactions are the strongest ones. The result of Bisognano-Wichmann ensures that if the physical Hamiltonian involves exclusively first-neighbor interactions, the entanglement Hamiltonian must present the same structure. These facts motivates the ansatz

$$\mathcal{H}_A = \mathbf{c}^\dagger \boldsymbol{\mathcal{H}}(\boldsymbol{\beta})\mathbf{c} = \sum_{m=1}^{N_A} \beta_m \left(c_m^\dagger c_{m+1} + c_{m+1}^\dagger c_m \right). \tag{3.93}$$

The set of couplings $\boldsymbol{\beta}$ that defines the entanglement Hamiltonian is found minimizing the norm

$$\|\mathbf{C}_A - \mathbf{C}_A(\boldsymbol{\beta})\| \tag{3.94}$$

using Powell's method (Powell 1964), where

$$\mathbf{C}_A(\boldsymbol{\beta}) = \mathbf{U}^\dagger(\boldsymbol{\beta})\mathbf{D}_\nu(\boldsymbol{\beta})\mathbf{U}(\boldsymbol{\beta}).$$

[7]Note that the computation of the entanglement entropy does not require this high-precision numerics since the eigenvalues close to 0 and 1 contribute minimally to it.

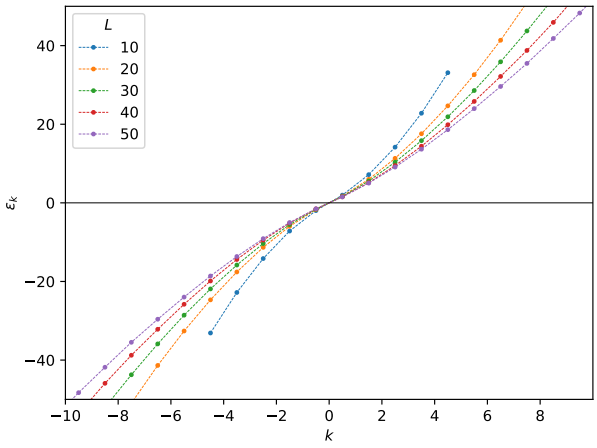

Figure 3.9: Entanglement spectrum $\{\epsilon_k\}$ from half-chain subsystems of length $N_A = L$. Observe that the dispersion relation is not linear, but the curvature decreases with the size, as expected from the asymptotic result (3.97).

The matrix $\mathbf{D}_\nu(\boldsymbol{\beta})$ is obtained from (3.91) and $\mathbf{U}(\boldsymbol{\beta})$ is the unitary matrix that diagonalizes $\boldsymbol{\mathcal{H}}(\boldsymbol{\beta})$ (3.92). In Fig. 3.8 we present the couplings $\boldsymbol{\beta}$ that correspond to the half chain subsystem of a chain of $N = 40$ and the prediction (3.85).

3.3.2 Entanglement spectrum

The full entanglement spectrum (2.10) can be obtained from the spectrum of the single-body entanglement Hamiltonian, which we may call the single-body entanglement spectrum.

$$E(\{n_j\}) = \sum \epsilon_k n_k + r_0 \tag{3.95}$$

where r_0 is a constant that ensures that $\operatorname{tr} \rho_A = 1$, and each E_j is specified by the set $\{n_j\}$ of occupied single-body levels. The term *entanglement spectrum* was coined by Li and Haldane (2008) and they suggested that it contains more physical information than the entanglement entropy. Indeed, in some cases, its low part can be regarded as the energy spectrum of a boundary CFT (Läuchli 2013) and Pollmann *et al.* (2010) showed that it can be used to detect of symmetry protected topological phases. We shall use this result in Chapter 6. It is worth to say that in this thesis we work exclusively with the single-body entanglement spectrum, so we shall refer to it as entanglement spectrum. Peschel (2004) showed using CFT arguments that the entanglement spectrum of a subsystem of length ℓ of an infinite chain of free fermions described by (3.13) is equispaced:

$$\epsilon_k = \frac{\pi^2}{\log \ell/a} k, \quad k = \pm\frac{1}{2}, \pm\frac{3}{2}, \dots \tag{3.96}$$

Hence, the first gap $\Delta_1 = \epsilon_{k+1} - \epsilon_k$ is

$$\Delta_1 = \frac{\pi^2}{\log \ell/a}. \tag{3.97}$$

Cardy and Tonni (2016) extended this result for other geometries with the formalism developed for computing the entanglement Hamiltonian finding

$$\Delta_1 \approx \frac{2\pi^2}{\log \frac{4L}{\pi a} \cos \frac{\pi x}{2L}}, \quad x \in A = [x_0, L] \tag{3.98}$$

for an open finite chain defined in the interval $[-L, L]$ with the same boundary conditions. Observe that we recover (3.97) by considering the half-chain block $x_0 = 0$.

However, the above behavior (3.97) is only expected when both ℓ and $\log \ell$ are large. If this is not the case, the eigenvalues vary as

$$\epsilon_k = \frac{\pi^2}{\log \ell + b_k} k, \quad k = \pm\frac{1}{2}, \pm\frac{3}{2}, \dots$$

rather than (3.96). As a consequence, the dispersion relation of ϵ_k shows some curvature – as it can be seen in Fig. 3.9 – for $N \sim O(10^3)$ and (3.97) must be modified with sub-leading corrections

$$\Delta_1 = \frac{\pi^2}{\log \gamma_1 \ell}, \tag{3.99}$$

where $\gamma \geq 1$.

3.3.3 Entanglement Contour

The Rényi entropies allow us to determine whether a state is entangled or not. Let us consider a discrete system with N sites and suppose that subsystem A is entangled $S_n(A) > 0$. How is the entanglement distributed over the sites $m \in A$? Do all of them contribute equally? In order to address that question Chen and Vidal (2014) proposed to define an entanglement contour as

$$S_n(A) = \sum_{m \in A} s_A^{(n)}(m), \tag{3.100}$$

although to define its properties it is more useful to define the contour for subregions $A_i \subseteq A$.

$$s_A^{(n)}(A_i) = \sum_{m \in A_i} s_A^{(n)}(m). \tag{3.101}$$

It is important to emphasize that $s_A^{(n)}(A_i)$ describes the entanglement of the region A_i with $B = \bar{A}$ and it does not provide information about the entanglement of A_i with the rest of A. Chen and Vidal proposed five requierements that the contour function must verify

1. Positivity: $s_A^{(n)}(A_i) \geq 0$.
2. Normalization: $s_A^{(n)}(A_i \to A) = S_n(A)$.
3. Upper bound: $s_A^{(n)}(A_i) \leq S_n(A_i)$

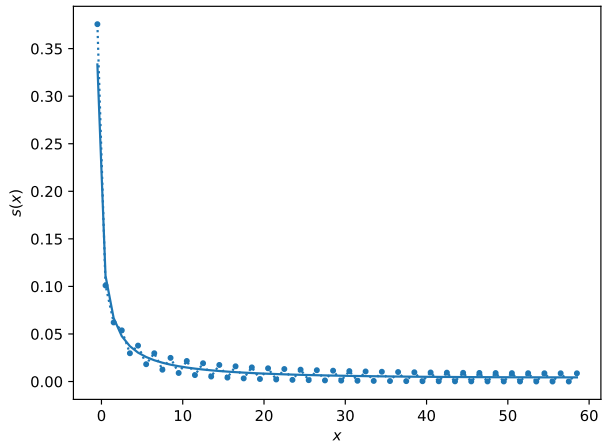

Figure 3.10: Entanglement contour $s_A^{(1)}(x)$ where A corresponds to the half-chain block of a system of $N = 120$. The data-points have been obtained with (3.102) and the line is the prediction (3.105). Of course, the oscillations are not captured with (3.105) since they are subleading corrections.

4. Correct behavior under symmetries of the system: Given a symmetry $\mathcal{T}$ such that $\mathcal{T}A = A'$ and $\mathcal{T}A_i = A'_i$ then $s_A^{(n)}(A_i) = s_{A'}^{(n)}(A'_i)$.

5. Correct behavior under unitaries: $s_A^{(n)}(A_i)$ must be invariant under an unitary that acts on A_i or in B.

These five conditions do not uniquely define a contour function. However, Wen (2020) added a new condition that claimed to lead to a univocal definition of the contour.

6. It must hold that $s_A^{(n)}(A_i) = s_{\bar{A}_i}^{(n)}(B)$. where $\bar{A}_i$ is the complementary of A_i,

Chen and Vidal (2014) proposed a contour function for free fermions that verifies all of the requisites. It is a weighted average of the eigenstates of the correlation matrix (and therefore of the entanglement Hamiltonian)

$$s_A^{(n)} = \frac{1}{1-n}\sum_{k=1}^{N_A} |U_{mk}|^2 \log\left(\nu_k^n + (1-\nu_k)^n\right), \quad m \in A, \tag{3.102}$$

where U_{mk} is an element of the unitary matrix $\mathbf{U}$ that diagonalizes the correlation matrix (3.48). From (3.100) we can write a continuous version of the entanglement contour.

$$S_n(A) = \int s_A^{(n)}(x)dx \tag{3.103}$$

Coser *et al.* (2017) proposed a candidate for the entanglement contour for the conformal systems

$$s_A^{(n)}(x) = \frac{c}{12}\left(1+\frac{1}{n}\right)\frac{1}{\beta(x)} + \frac{c_n}{\ell}. \tag{3.104}$$

Hence, the entanglement contour is proportional to the inverse of the weight function – i.e. entanglement temperature $T(x) = 1/\beta(x)$ – of the entanglement Hamiltonian (3.82). Therefore, the contour of the subsystem $A = [x_0, L]$ of the chain $[-L, L]$ is given by the inverse of (3.85)

$$s_A^{(n)}(x) \approx \frac{c\pi}{24L}\left(1+\frac{1}{n}\right)\frac{\cos\left(\frac{\pi x_0}{2L}\right)}{\sin\left(\frac{\pi x}{2L}\right)-\sin\left(\frac{\pi x_0}{2L}\right)}. \tag{3.105}$$

In Fig. 3.10 we present the entanglement contour corresponding to the half-chain block ($A = [0, 60]$). Observe that the sites that are close to the entangling point contribute more to the entanglement, as expected from Bisognano-Wichmann.

Appendices

3.A Jordan-Wigner transformation

In this appendix we provide a more detailed explanation of the Jordan-Wigner (JW) transformation. Let us start by pointing out that the commutation relations of two spin operators (3.9) is another spin operator. On the contrary, the commutation (anticommutation) relations of bosons (fermions) are numbers (0 or 1). Therefore, it seems advantageous to map a spin chain to a bosonic or fermionic chain. This process is known as bosonization or fermionization respectively.

A priori, bosonization seems more convenient since both bosons and spins have commutation relations like spins. However, the Fock space associated with a site can accommodate an arbitrary number of bosons. This does not make sense in the spin language since a spin $1/2$ has only two allowed states. To solve this inconsistency, one must impose an infinite repulsion between bosons (hard-core boson approximation) which makes the problem very difficult. Thus, fermionization is more advantageous[8], since the Pauli exclusion principle imposes what we need.

As we have said, the Hilbert space of the spin $1/2$ and a spinless fermion c satisfying $\{c, c^\dagger\} = 1$ have the same dimension. We can make the identification $|\downarrow\rangle = |1\rangle$ and $|\uparrow\rangle = |0\rangle$ where

$$c\,|0\rangle = 0, \quad c^\dagger\,|0\rangle = |1\rangle\,, \tag{3.A.1}$$

The parallelism in the eigenvalues of S^z and the number operator $n = c^\dagger c$ leads to define

$$\sigma^z = 1 - 2c^\dagger c, \tag{3.A.2}$$

and also $\sigma^- = c^\dagger$ and $\sigma^+ = c$. However, this mapping is not valid for more than one spin. The reason is that spin ladder operators at different positions commute while fermionic operators anticommute. The transformation derived by Jordan and

[8]It turns out that bosonization is applied to convert interacting systems of fermions in (1+1) dimensions to a system of massless, non-interacting bosons.

Wigner (1928) solves this inconsistency by adding a phase to the transformation:

$$\begin{aligned}
\sigma_m^- &= \exp\left\{-i\pi \sum_{k=1}^{m-1} c_k^\dagger c_k\right\} c_m^\dagger = (-1)^{N_{m-1}} c_m^\dagger \\
\sigma_m^+ &= \exp\left\{i\pi \sum_{k=1}^{m-1} c_k^\dagger c_k\right\} c_m = (-1)^{N_{m-1}} c_m \\
\sigma_m^z &= 1 - 2c_m^\dagger c_m.
\end{aligned} \tag{3.A.3}$$

We see that the phase depends on the total number of fermions $N_{m-1} = \sum_{k=1}^{m-1} n_k$ placed at the left of the site m. Taking in account that $(-1)^{N_{m-1}}$ commutes with a fermionic operator on site m, that $c_m^\dagger (-1)^{n_m} = c_m^\dagger$, and that[9] $c_m (-1)^{n_m} = -c_m$, the commutation relations of the spins are mapped into anticommutation relations:

$$\{c_m^\dagger, c_{m'}\} = \delta_{mm'}, \quad \{c_m, c_{m'}\} = \{c_m^\dagger, c_{m'}^\dagger\} = 0. \tag{3.A.4}$$

For what follows it will be useful to compute the nearest neighbors spin-spin terms:

$$\sigma_m^- \sigma_{m+1}^+ = c_m^\dagger (-1)^{n_m} c_{m+1} = c_m^\dagger c_{m+1} \tag{3.A.5}$$

$$\sigma_m^+ \sigma_{m+1}^- = c_m (-1)^{n_m} c_{m+1}^\dagger = -c_m c_{m+1}^\dagger \tag{3.A.6}$$

$$\sigma_m^- \sigma_{m+1}^- = c_m^\dagger (-1)^{n_m} c_{m+1}^\dagger = c_m^\dagger c_{m+1}^\dagger \tag{3.A.7}$$

$$\sigma_m^+ \sigma_{m+1}^+ = c_m (-1)^{n_m} c_{m+1} = -c_m c_{m+1}, \tag{3.A.8}$$

Let us discuss the mapping of the boundary conditions of the spin system to the fermionic chain. The periodic boundary conditions (PBC) are common $\mathbf{S}_{N+1} = \mathbf{S}_1$ for the spin operators. If we impose them in the fermionic chain

$$\begin{aligned}
\sigma_N^- \sigma_1^+ &= (-1)^{N_{N-1}} c_N^\dagger c_1 = (-1)^{N_N} (-1)^{n_N} c_N^\dagger c_1 = -(-1)^{N_N} c_N^\dagger c_1, \\
\sigma_N^- \sigma_1^- &= (-1)^{N_{N-1}} c_N^\dagger c_1^\dagger = (-1)^{N_N} (-1)^{n_N} c_N^\dagger c_1^\dagger = -(-1)^{N_N} c_N^\dagger c_1^\dagger,
\end{aligned} \tag{3.A.9}$$

we see that the kind of boundary condition depends on the number of fermions $n_f = N_N$, namely antiperiodic boundary conditions (ABC) if n_f is even and periodic boundary conditions (PBC) if n_f is odd.

To summarize, thanks to the JW transformation it is possible to map the spin chain into a spinless fermion chain. It is, therefore, a different but equivalent physical system. Its usefulness is manifest if the fermionic Hamiltonian has no interaction term (free fermion Hamiltonian) as one has to diagonalize at most a $2N \times 2N$ matrix instead of a $2^N \times 2^N$ of the spin Hamiltonian.

[9] The term $c_m^\dagger (-1)^{n_m} = c_m^\dagger$ because $c_m^\dagger c_m$ must be 0, as it acts before $c_m^\dagger$. With the same reasoning, we have that $c_m (-1)^{n_m} = -c_m$

Chapter 4

Entanglement in inhomogeneous spin chains. The rainbow state

In the previous chapter, we have studied the entanglement properties of the ground state of the homogeneous XX spin chain. In the present chapter, we shall do the same with the inhomogeneous XX spin chain. The inhomogeneous models that we shall consider are obtained by a deformation of the critical models for which the entanglement entropy violates the area law as it scales logarithmically (Calabrese and Cardy 2004; Latorre *et al.* 2003) as we discussed in Chapter 1. The effect of the lack of homogeneity may be, for some models, to increase this violation that becomes linear in the size of the blocks, like a thermal entropy. This mechanism has a geometrical interpretation related to the underlying conformal field, according to which the inhomogeneity may correspond to a curvature of spacetime (Rodríguez-Laguna *et al.* 2017; Tonni *et al.* 2018).

Let us consider the inhomogeneous XX spin chain whose Hamiltonian is given by

$$H = -\sum_{m=1}^{N-1} \frac{J_m(h)}{4} \left(\sigma_m^x \sigma_{m+1}^x + \sigma_m^y \sigma_{m+1}^y\right) - \eta \frac{J_N(h)}{4} \left(\sigma_N^x \sigma_1^x + \sigma_N^y \sigma_1^y\right), \tag{4.1}$$

where $\eta = 0$ ($\eta = 1$) sets open (periodic) boundary conditions. Notice that the couplings $J_m(h)$ vary with the lattice position and that they depend on a parameter $h \geq 0$ that we shall call the inhomogeneity parameter. We impose that

$$J_m(0) = J, \quad \forall m, \tag{4.2}$$

recovering thus the homogeneous Hamiltonian (3.2). We can write (4.1) in terms of spinless fermions by means of the Jordan-Wigner transformation (3.6):

$$H = -\sum_{m=1}^{N-1} \frac{J_m(h)}{2} \left(c_m^\dagger c_{m+1} + c_{m+1}^\dagger c_m\right) - \eta(-1)^{N_f+1} \frac{J_N(h)}{2} \left(c_N^\dagger c_1 + c_1^\dagger c_N\right), \tag{4.3}$$

where we should recall that N_f is the total number of fermions present in the fermionic chain. Observe that, since the parity operator (3.11) commutes with

the above Hamiltonian, the discussion that we made in Section 3.1.1 about the treatment of the homogeneous PBC case applies also here albeit there is no translational invariance symmetry and the analysis in Fourier space does not simplify the problem. From now on we will restrict our attention to the open case $\eta = 0$.

As we anticipated in Chapter 1, it is convenient to distinguish between the *strong inhomogeneity regime* $h \gg 1$ and the *weak inhomogeneity regime* $h \ll 1$ as they require different theoretical approaches. It is worth to say that the numerical approach is the same for all values of h and we refer to Appendix 4.A.2 for a detailed explanation regarding the obtainment of the ground state and its associated correlation matrix of free fermion Hamiltonians. In the remainder of this chapter, we shall explain the theoretical approaches for each regime, particularizing the discussions for the so-called rainbow model that was originally proposed by Vitagliano *et al.* (2010) and studied in detail by Ramírez *et al.* (2015, 2014). It describes a fermionic chain with $N = 2L$ sites whose Hamiltonian H_R is given by (4.3) with the engineered couplings

$$J_m(h) = e^{-h|m-L|}, \quad m \neq L, \quad J_L(h) = e^{-\frac{h}{2}}. \tag{4.4}$$

Since $h > 0$, the intensity of the couplings decreases from the center of the chain toward the edges. Additionally, observe that the above couplings are symmetric under inversion around the central coupling $J_L(h)$, i.e. the system possesses left-right symmetry. It is then convenient to label the fermions c_m from the origin with $m = \pm 1/2, \ldots, \pm(L - 1/2)$

$$H_R = -\frac{e^{-\frac{h}{2}}}{2}\left(c^\dagger_{-1/2}c_{1/2} + \sum_{m=1/2}^{L-3/2} e^{-hm}\left(c^\dagger_m c_{m+1} + c^\dagger_{-(m+1)}c_{-m}\right) + \text{h.c.}\right), \tag{4.5}$$

where h.c. refers to the Hermitian conjugate. The ground state of the rainbow model (4.5) is the rainbow state which is of paramount importance for this thesis dissertation.

4.1 Strong inhomogeneity regime

In this section we shall introduce the strong disorder renormalization group and apply it to the rainbow model introduced above.

4.1.1 The strong disorder renormalization group

As we have mentioned, the inhomogeneity prevents us from diagonalizing the Hamiltonian (4.5) with the ansatz (3.23). However, it is possible to obtain the ground state by implementing a real space renormalization group (see Chapter 1) scheme called the strong disorder renormalization group (SDRG) that allows us to sequentially decimate the spins that are strongly coupled with the largest

absolute value $J_{\max}$. Although it was designed for solving the antiferromagnetic Heisenberg spin chain with random couplings by Dasgupta and Ma (1980), it can be extended to the XX spin chain.

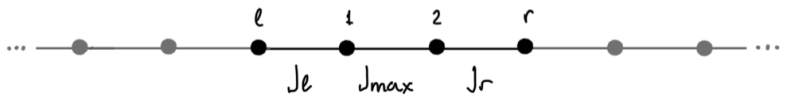

Figure 4.1: The subsystem composed of four sites (spins or fermions) considered at each step of the SDRG.

Let us consider the inhomogeneous XX spin chain and a subsystem of four spins (see Fig. 4.1) that involves the largest coupling $J_{\max}$ and the first neighbors whose Hamiltonian is

$$H_4 = -J_{\max}\left(\sigma_1^+\sigma_2^- + \sigma_1^-\sigma_2^+\right) - J_l\left(\sigma_l^+\sigma_1^- + \sigma_l^-\sigma_1^+\right) - J_r\left(\sigma_2^+\sigma_r^- + \sigma_2^-\sigma_r^+\right). \tag{4.6}$$

Let us assume that $J_{\max} \gg J_l, J_r$. The spins coupled by $J_{\max}$ are strongly correlated and they form a state

$$|\psi_0\rangle = \frac{1}{\sqrt{2}}\left(|+-\rangle + \text{sign}(J_{\max})\,|-+\rangle\right), \tag{4.7}$$

with energy $E_0 = -|J_{\max}|$. Notice that $|\psi_0\rangle$ corresponds to the $SU(2)$ singlet if $J_{\max} < 0$. Therefore the spins are decoupled from the neighboring spins placed at l and r. It is possible to show with degenerate (second order) perturbation theory that the decimation induces an effective Hamiltonian

$$H^{(1)} = -J_{lr}(\sigma_l^+\sigma_r^- + \sigma_l^-\sigma_r^+), \tag{4.8}$$

with

$$J_{lr} = \frac{J_l J_r}{J_{\max}}, \tag{4.9}$$

Note that J_{lr} presents the same sign as $J_{\max}$ and that we have described a single

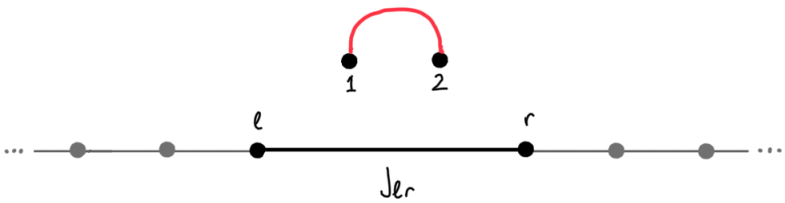

Figure 4.2: Sites 1 and 2 are detached inducing a coupling between sites l and r. State (4.7) is represented with a red bond.

step of the SDRG on which the two spins coupled with the largest coupling are decimated inducing a chain with two spin less, as it can be seen in Fig. 4.2. Hence, each step k is composed of three actions:

1. Identify the strongest coupling $J_{\max}^{(k)}$ in the chain formed by $N-2(k-1)$ spins which is described by the Hamiltonian $H^{(k)}$. It should be understood that the original Hamiltonian corresponds to $k=0$, i.e $H \equiv H^{(0)}$.

2. Decimate the involved spins by creating a state (4.7).

3. Define a new effective Hamiltonian $H^{(k)}$ which describes a chain with $N-2k$ spins. $H^{(k)}$ presents the same functional form and the same set of couplings that $H^{(k-1)}$ with the exception of the removed spins coupled by $J_{\max}^{(k)}$ and the new term (4.8).

Assuming that we can use the SDRG at every step of the process[1], we obtain the ground state of a chain with $2L$ sites after L iterations. Each further step allows the formation of states (4.9) that involve spins that are far apart from each other. The ground state obtained by this process is called a valence bond state. If the inhomogeneous couplings are positive and obey a given random distribution, the Hamiltonian (4.1) describes a disordered system and the ground state belongs to the so-called random singlet phase, which is an example of an infinite randomness fixed point (Fisher 1995, 1994) and is in close analogy with the fixed critical point discussed in Chapter 1. However, it presents unique scaling properties [2] (Iglói and Monthus 2005). Nonetheless, in this thesis we are interested in non-random inhomogeneities such as (4.4) and we will not treat this kind of phase.

The SDRG can also be applied to free fermionic chains and the procedure that we have explained for spins is also valid. However, the anticommutation relation of the fermions induces a change in the sign of the effective coupling

$$J_{lr} = -\frac{J_l J_r}{J_{\max}}. \tag{4.10}$$

As a consequence, the ground state is a tensor product of both bonding/anti-bonding operators $(b^{\pm})^{\dagger}$,

$$|GS\rangle = \prod_{k=1}^{L} (b_{m,n}^{\eta_k})^{\dagger} |0\rangle , \tag{4.11}$$

with

$$(b_{m,n}^{\eta_k})^{\dagger} = \frac{1}{\sqrt{2}} \left(c_m^{\dagger} + \eta_k c_n^{\dagger} \right), \tag{4.12}$$

and it follows that the phase $\eta_k = \pm$ depends on the sign of $J_{\max}^{(k)}$.

[1] We shall discuss in the following chapters situations where the SDRG cannot be applied.

[2] Whereas the standard energy-length scaling is $E \sim 1/L^z$, where z is called the dynamical critical exponent. A critical point described by a CFT is characterized by $z=1$. In turn, the scaling of the infinite randomness fixed point case is $\log 1/E \sim L^{\psi}$, where $\psi = 1/2$ in the case of the random singlet phase.

The SDRG applied to the rainbow model

Let us apply the ideas presented in the previous paragraphs to the concrete example of the rainbow model (4.5). Since $h > 0$, the strongest coupling is the central one, $J^{(1)}_{\max} = J_{-1/2} = e^{-h/2}$, so we decimate the central fermionic sites

$$(b^{+}_{-\frac{1}{2},\frac{1}{2}})^{\dagger}\,|0\rangle\,. \tag{4.13}$$

The effective Hamiltonian is

$$H^{(1)}_{R} = -\frac{e^{-\frac{h}{2}}}{2}\left(J_{-3/2}c^{\dagger}_{-3/2}c_{3/2} + \sum_{m=3/2}^{L-3/2} e^{-hm}\left(c^{\dagger}_{m}c_{m+1} + c^{\dagger}_{-(m+1)}c_{-m}\right) + \text{h.c.}\right), \tag{4.14}$$

where $J_{-3/2} = -e^{-3h/2}$ follows from (4.10).

In the second step, the strongest coupling is indeed the effective one created in the previous step $J^{(2)}_{\max} = J_{-3/2} = -e^{-3h/2}$. We thus decimate the sites with an antibonding operator

$$(b^{-}_{-\frac{3}{2},\frac{3}{2}})^{\dagger}\,|0\rangle\,, \tag{4.15}$$

and

$$H^{(2)}_{R} = -\frac{e^{-\frac{h}{2}}}{2}\left(e^{-2h}c^{\dagger}_{-5/2}c_{5/2} + \sum_{m=5/2}^{L-3/2} e^{-hm}\left(c^{\dagger}_{m}c_{m+1} + c^{\dagger}_{-(m+1)}c_{m}\right) + \text{h.c.}\right). \tag{4.16}$$

The strongest coupling at each RG step lies at the center of the effective chain, so the k-th step yields

$$b^{\eta_k}_{\frac{1}{2}-k,-\frac{1}{2}+k}\,|0\rangle = \left(c^{\dagger}_{\frac{1}{2}-k} + \eta_k c^{\dagger}_{-\frac{1}{2}+k}\right)|0\rangle \qquad k = 1,\ldots,L. \tag{4.17}$$

We can now see the reason why (4.5) is called the rainbow Hamiltonian and its ground state the rainbow state. If we represent each fermionic operator (4.17) by a bond that links the fermionic sites as in Fig. 4.2, the outcome of the SDRG is a concentric set of bonds that reminds the shape of a rainbow, as it can be seen in Fig. 4.3.

Using the left-right symmetry we shall simplify the notation $b^{\eta_k}_{1/2-k,-1/2+k} \to b^{\eta_k}_{k-1/2}$. Hence, particularizing (4.11) to this case yields

$$|RS\rangle = (b^{\eta_L}_{L-\frac{1}{2}})^{\dagger}\ldots(b^{-}_{\frac{3}{2}})^{\dagger}(b^{+}_{\frac{1}{2}})^{\dagger}\,|0\rangle\,, \tag{4.18}$$

where $\eta_L = (-1)^{L+1}$.

Once we have obtained the ground state of an inhomogeneous chain (4.3), and in particular the rainbow state (4.18), we shall focus on their entanglement properties.

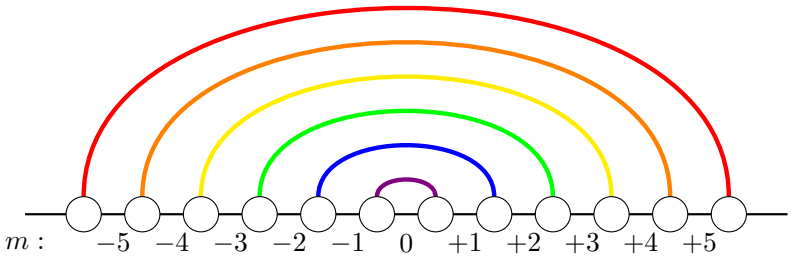

Figure 4.3: Illustrating the rainbow state, GS of H_R given by (4.5) with $L = 6$, for $h \gg 1$. Links are indexed by the integer m. The bonds are established between sites n and $-n$ for $n \in \{\pm 1/2, \cdots, \pm(L - 1/2)\}$.

4.1.2 Entanglement in valence bond states

As we discussed in the previous chapter (see Section 3.2.1), the entanglement entropy can be obtained from the eigenvalues of the correlation matrix associated to a given block. We refer to Appendix 4.A.1 for a detailed derivation of the obtaining of the correlation matrix.

However, the computation of the entanglement entropy is particularly simple for valence bond states. Observe that (4.12) creates a Bell state or *maximally entangled state* (Nielsen and Chuang 2010). Hence, the entanglement entropy associated to cutting a bond is maximal, namely, $\log 2$. As a consequence, the entanglement entropy of a block A is

$$S(A) = n_A \log 2, \tag{4.19}$$

where n_A is the number of outgoing bonds from A (Refael and Moore 2009).

Entanglement in the rainbow

Let us compute the entanglement entropy of lateral blocks of the rainbow state

$$A_\ell = \{m \mid m \geq -(L + 1/2) + \ell\}, \quad \ell \in [1, 2L]. \tag{4.20}$$

According to (4.19),

$$S(\ell) = \ell \log 2, \tag{4.21}$$

where we have simplified $S(A_\ell) = S(\ell)$. Notice that the entanglement entropy of these blocks is proportional to their volume – length in 1D – constituting one example of the (maximal) violation of the area law. As we mentioned in Chapter 1 the rainbow state does not challenge Hastings theorem since (4.5) is a gapless Hamiltonian. Indeed, notice that the lowest energy scale in the system is given by the smallest coupling constant, which is proportional to e^{-hL} and tends to zero in the thermodynamic limit for all values of h.

In Fig. 4.4 we plot the correlation matrices at half-filling for $h = 10$ and $h = 1$ for a chain with $N = 22$. Notice that the restriction of the correlation matrix associated

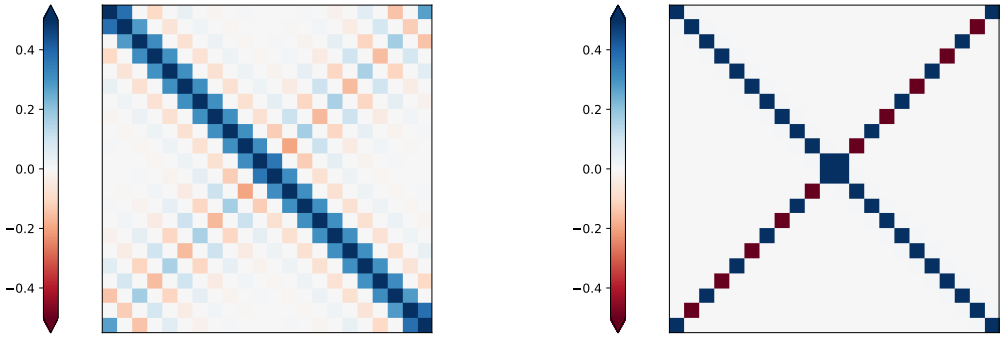

Figure 4.4: Correlation matrix $C_{mn} = \langle c_m^\dagger c_n \rangle$ (3.42) obtained from the rainbow state (4.18) at half filling. We refer to 4.A.1 for details of the computation of the correlation matrix. (Left) $h = 1$ and (Right) $h = 10$ for a chain with $N = 22$. It is worth to compare them with Fig. (3.2) corresponding to $h = 1$. Observe that for $h = 10$, the restriction of a lateral block A_ℓ (4.20) is $\mathbf{C}_\ell = 1/2\mathbb{1}_\ell$. As a consequence, the entanglement entropy is given by (4.21).

to the lateral block A_ℓ (4.20) with $\ell < L$ in the valence bond picture is

$$(\mathbf{C}_\ell)_{mn} \overset{h\to\infty}{\longrightarrow} \frac{1}{2}\delta_{mn},$$

and the eigenvalues are $\nu_k = 1/2$ with $k = 1, \ldots, \ell$ for $\ell = 1, \ldots, L$, as it can be seen in Fig. 4.4 (right). Hence, using the expression of the Rényi entropies in terms of the eigenvalues of the correlation matrix (3.54) yields (4.21).

In Fig. 4.5 we plot the entanglement entropy corresponding to all possible lateral blocks (4.20) for different values of h. As we have mentioned, the validity of the SDRG and the associated valence bond picture increases with h.

To summarize, we have described satisfactorily the strong inhomogeneity regime by means of the SDRG leading to the linear growth prediction of the entanglement entropy. In addition, the blue points of Fig. 4.5 correspond to the entanglement entropy of the homogeneous case $h = 0$ that has been described in the previous chapter (see Fig. 3.6). We shall now describe the regime of weak inhomogeneity $h \ll 1$ and study the crossover between both regimes.

4.2 Weak inhomogeneity regime

In this section we shall consider the regime $h \ll 1$ where the SDRG and the valence bond interpretation do not hold. As we have noticed, for $h = 0$ the inhomogeneous Hamiltonian (4.3) becomes the homogeneous one (3.17) whose continuum limit has been studied in Section 3.1.3 by defining $x = ma$ and imposing $x \to 0$ and $N \to \infty$ while keeping constant $\mathcal{N} = Na$. Here we shall impose the additional

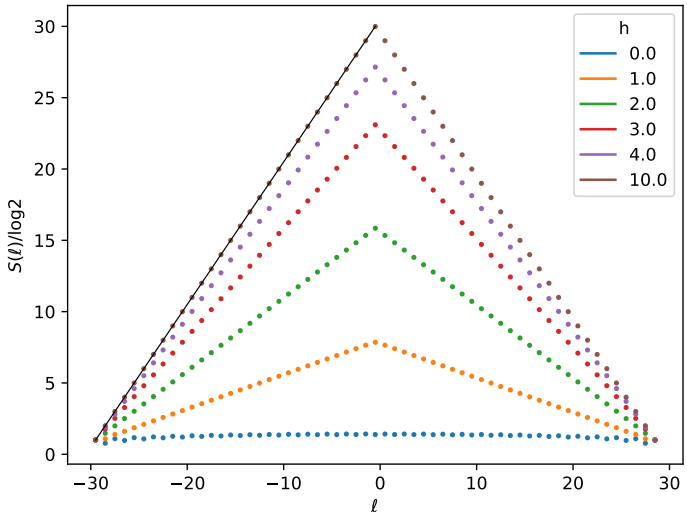

Figure 4.5: Entanglement entropy of lateral blocks (4.20) over the rainbow state with $N = 60$ at half filling for different values of h. The black line corresponds to (4.21). Let us recall that the left-right $S(\ell) = S(N-\ell)$ symmetry of the plot is consequence of $S(A) = S(B)$ for a bipartition $A \cup B$ as was discussed in Chapter 2 see (2.14).

constrain $h \to 0$, so we define

$$\hat{h} = \frac{h}{a}, \tag{4.22}$$

that remains constant in the continuum limit. We shall make the assumption that the lattice couplings tend to a continuous function

$$J_m(h) \to J(x, \hat{h}), \quad J \in C^0 \text{ for } x \in [0, \mathcal{N}]. \tag{4.23}$$

In addition, we assume that we can write the lattice fermions as in (3.29),

$$\frac{c_m}{\sqrt{a}} \approx e^{ik_F x/a}\psi_L(x) + e^{-ik_F x/a}\psi_R(x),$$

where the the fermionic fields $\psi_{L,R}(x)$ vary slowly on the spatial scale $1/k_F$. Finally, if the lattice system is centered at the origin $[-(N+1)/2, (N+1)/2]$, the continuum limit maps to the interval $[-\mathcal{L}, \mathcal{L}]$ with $\mathcal{L} = La$ for $N = 2L$. Performing an analogous analysis to the one discussed in Section 3.1.3 we arrive at

$$H \approx -\frac{ia}{2}\int_{-\mathcal{L}}^{\mathcal{L}} J(x,\hat{h})dx\left[(\partial_x\psi_R)^\dagger\psi_R - (\partial_x\psi_L)^\dagger\psi_L + \psi_L^\dagger\partial_x\psi_L - \psi_R^\dagger\partial_x\psi_R\right]. \tag{4.24}$$

Integrating the above expression by parts yields

$$H \approx -ia\int_{-\mathcal{L}}^{\mathcal{L}} dx J(x,\hat{h})\Psi^\dagger(x)\sigma_3\left(\partial_x + \frac{J'(x,\hat{h})}{2J(x,\hat{h})}\right)\Psi(x), \tag{4.25}$$

where $\Psi^T(x) = (\psi_L(x), \psi_R(x))$ and $f'(x) = (d/dx)f(x)$. The equations of motion are

$$\partial_0 \Psi(x^0, x^1) = -J(x^1, \hat{h})\sigma_3 \left(\partial_1 + \frac{J'(x^1, \hat{h})}{2J(x^1, \hat{h})} \right) \Psi(x^0, x^1), \tag{4.26}$$

where we have rescaled the time coordinate $t \to ax^0$ and relabeled the space coordinate $x \to x^1$. Observe that (4.26) becomes (3.33) if $h = 0$ with the assumption (4.2).

It is convenient to consider the massless Dirac equation on a curved spacetime described by the static metric $g_{\mu\nu}$ with signature $(-,+)$

$$(i\not{D} - m)\Psi = 0, \tag{4.27}$$

where $\not{D}$ is the slashed covariant derivative (see details in Appendix 4.B). More explicitly,

$$\left(\gamma^0 \partial_0 + \frac{1}{2}\omega_0^{01}\gamma^0\gamma^3 + \frac{E_1^1}{E_0^0}\left(\gamma^1 \partial_1 + \frac{1}{2}\omega_1^{01}\gamma^1\gamma^3 \right) \right) \Psi = 0, \tag{4.28}$$

where γ^μ, $\mu = 0, 1, 3$ are the usual gamma matrices that generate the Clifford algebra

$$\{\gamma^\mu, \gamma^\nu\} = -2\eta^{\mu\nu}\mathbb{1},$$

where $\eta^{\mu\nu}$ is the Minkowski metric with signature $(-,+)$, and E_a^μ is the inverse of the *zweibein* e_μ^a, i.e. the *vielbein* formalism particularized for two dimensions

$$\begin{aligned} E_a^\mu &= g^{\mu\nu}\eta_{ab}e_\nu^b, \\ g_{\mu\nu} &= e_\mu^a e_\nu^b \eta_{ab}, \end{aligned} \tag{4.29}$$

and ω_μ^{ab} is the spin connection

$$\omega_\mu^{ab} = e_\nu^a \partial_\mu E^{b\nu} + e_\nu^a E^{b\sigma}\Gamma_{\sigma\mu}^\nu, \tag{4.30}$$

where η_{ab} is the flat spacetime metric and $\Gamma_{\sigma\mu}^\nu$ are the Christoffel symbols. We refer to Appendix 4.B for more details.

From now on we shall consider $a = 1$ which implies $\hat{h} = h$. Multiplying (4.26) by σ_2 and comparing it with (4.28) yields $\gamma^0 = \sigma_2$ and $\gamma^1 = \sigma_1$ and

$$\frac{E_1^1}{E_0^0} = J(x^1, h), \quad \omega_1^{01} = 0, \quad \omega_0^{01} = J'(x^1, h). \tag{4.31}$$

Using the expressions (4.29) and (4.31) leads the condition

$$\frac{E_1^1}{E_0^0} = -\sqrt{-\frac{g_{00}}{g_{11}}} \tag{4.32}$$

where we have assumed that the metric is static so it only has diagonal entries. In addition, from (4.30) we obtain

$$\frac{\partial_1 g_{00}}{g_{00}} = -\frac{2J'(x^1, h)}{J(x^1, h)}. \tag{4.33}$$

Integrating the above expression we find that

$$g_{00} = -J^2(x^1, h). \tag{4.34}$$

Plugging (4.34) in (4.32) yields $\sqrt{g_{11}} = 1$.

Additionally, we shall characterize more in detail the curved background by computing its curvature. The Christoffel symbols are all zero except

$$\begin{aligned} \Gamma^0_{01} &= \Gamma^1_{10} = \frac{J'(x^1, h)}{J(x^1, h)}, \\ \Gamma^1_{00} &= J(x^1, h)J'(x^1, h). \end{aligned} \tag{4.35}$$

With them, we can compute the diagonal entries of the Ricci tensor $R_{\mu\nu}$

$$R_{00} = J(x^1, h)J''(x^1, h), \tag{4.36}$$

$$R_{11} = -\frac{J''(x^1, h)}{J(x^1, h)}, \tag{4.37}$$

where $f''(x) = d^2 f(x)/dx^2$. Finally, the Ricci scalar, which completely characterizes the curvature of the spacetime is

$$R(x, h) = g^{\mu\nu} R_{\mu\nu} = -2\frac{J''(x^1, h)}{J(x^1, h)}. \tag{4.38}$$

The Euclidean version of the metric is

$$ds^2 = J^2(x, h)dt^2 + dx^2, \tag{4.39}$$

where we have restored the (t, x) coordinates for convenience. Observe that (4.39) is Weyl equivalent to the flat metric

$$ds^2 = \Omega^2(x, h)\left(dt^2 + d\tilde{x}^2\right), \;\Rightarrow\; \Omega(x, h) = J(x, h), \tag{4.40}$$

where $\Omega(x, h)$ is the Weyl factor, and we have introduced a new spatial coordinate $\tilde{x}(x)$

$$d\tilde{x} = \Omega^{-1}(x, h)dx \;\Rightarrow\; \tilde{x}(x) = \int_0^x \frac{dy}{J(y, h)}, \tag{4.41}$$

that we shall call tilded or deformed coordinate. Expressions (4.39) and (4.41) are the most important of this section. With the key assumption (4.23), we have shown that the continuum limit of the inhomogeneous lattice Hamiltonian (4.3) describes a massless Dirac fermion on a curved background whose metric (4.39) with curvature (4.38) depend on the (continuous version of) the couplings.

The rainbow model as a Dirac fermion in curved spacetime

Let us particularize the previous discussion to the rainbow model (4.5). The analysis of the weak inhomogeneity regime was done firstly by Ramírez *et al.* (2015) and later, Rodríguez-Laguna *et al.* (2017) proposed the rainbow model as

a massless Dirac fermion in curved spacetime with an analogous formalism to the one presented above. However, Rodríguez-Laguna *et al.* (2017) obtained the resulting metric by comparing the generic Dirac Lagrangian with the rainbow model Lagrangian. It turns out that it is more convenient to compare the equations of motion rather than the Lagrangian in order to extend these results to models of Majorana fermions, as we will see in Chapter 7.

The continuum limit of the rainbow model couplings is

$$J(x,h) = e^{-h|x|}. \tag{4.42}$$

Plugging (4.42) in (4.25) yields the continuum version of the rainbow Hamiltonian (4.5):

$$H_R \approx -i \int_{-L}^{L} dx e^{-h|x|} \Psi^\dagger(x) \sigma_3 \left(\partial_x - \frac{h}{2} \operatorname{sign}(x) \right) \Psi(x). \tag{4.43}$$

The Weyl factor is thus

$$\Omega(x,h) = J(x,h) = e^{-h|x|}, \tag{4.44}$$

and the Euclidean metric generated by the couplings is obtained from (4.39)

$$ds^2 = e^{-2h|x|}(dt^2 + d\tilde{x}^2), \tag{4.45}$$

with the new spatial coordinate given by (4.41)

$$\tilde{x}(x) = \frac{\operatorname{sign}(x)}{h} \left(e^{h|x|} - 1 \right). \tag{4.46}$$

The metric has a scalar curvature (4.38)

$$R(x) = 4h\delta(x) - 2h^2,$$

i.e. except at the origin, it is an homogeneous manifold with negative curvature that can be mapped to the Poincaré metric in the upper half-plane (Rodríguez-Laguna *et al.* 2017) or the anti-de Sitter (AdS) metric in 1+1D (MacCormack *et al.* 2019).

Finally, observe that the rainbow Hamiltonian (4.43) can be written in terms of the deformed coordinate $\tilde{x}$. Using that

$$\tilde{\psi}_{L,R}(\tilde{x}) = \left(\frac{dx}{d\tilde{x}} \right)^{1/2} \psi_{L,R}(x), \tag{4.47}$$

and (4.46) yields

$$H_R \approx -i \int_{-\tilde{L}}^{\tilde{L}} d\tilde{x} \left(\tilde{\psi}_L^\dagger \partial_{\tilde{x}} \tilde{\psi}_L - \tilde{\psi}_R^\dagger \partial_{\tilde{x}} \tilde{\psi}_R \right), \tag{4.48}$$

with

$$\tilde{L} = \frac{1}{h}(e^{hL} - 1). \tag{4.49}$$

Notice that (4.48) presents the same functional form than the Dirac Hamiltonian on Minkowski spacetime (3.31). In the next section we shall compute the entanglement properties in the weak inhomogeneity regime.

4.2.1 Entanglement entropy

In the previous section we have shown that the weak inhomogeneity regime of a lattice inhomogeneous system (4.3) where the assumption of continuity of the continuous version of the couplings (4.23) holds is described by a massless Dirac fermion over a curved background whose metric is given by (4.39). As a consequence, we can apply all the results presented in the previous chapter with the substitution of flat space quantities by the deformed ones associated to the curved space. In particular, the distance measured from the origin is given by $\tilde{x}(x)$ (4.41). We shall refer to this as a *deformed length*.

The entanglement entropy can be obtained by means of the correlators of the twist operators placed at the entangling points. The Rényi entropies associated to (the continuous version) of the lateral blocks (4.20) $A = [-L, x_0]$ for a given chain is (Rodríguez-Laguna *et al.* 2017)

$$S_n(A) = \frac{1}{1-n} \log \langle \tau_n(x_0, 0) \rangle_{\text{curved}} + c'_n. \tag{4.50}$$

We can rewrite the above expression in terms of the flat metric by means of a Weyl transformation

$$\langle \tau_n(x_0, 0) \rangle_{\text{curved}} = \left(\frac{1}{\Omega(x_0, h)} \right)^{\Delta_n} \langle \tau_n(\tilde{x}(x_0), 0) \rangle_{\text{flat}} . \tag{4.51}$$

Observe that $\langle \tau_n(\tilde{x}(x_0), 0) \rangle_{\text{flat}}$ is completely fixed by conformal invariance (Calabrese and Cardy 2004). Hence

$$S_n(A) \equiv S_n(x) = \frac{1}{12} \left(1 + \frac{1}{n} \right) \log \left(\frac{2\tilde{D}(x, 2L)}{a\Omega(x_0, h)} \right) + c'_n, \tag{4.52}$$

where $D(x, 2L)$ denotes the chord length (3.66) centered at the origin

$$D(x, 2L) = \frac{2L}{\pi} \cos \left(\frac{\pi(2x+1)}{4L} \right) = \frac{2L}{\pi} \cos \left(\frac{\pi(x+1/2)}{2L}, \right) \tag{4.53}$$

and $\tilde{D}(x, 2L)$ corresponds to the deformed chord length

$$\tilde{D}(x, 2L) = \frac{2\tilde{x}(L)}{\pi} \cos \left(\frac{\pi x + \tilde{1}/2}{2\tilde{L}} \right), \tag{4.54}$$

where we have taken into account that $\tilde{x}(x)$ deforms lengths from the origin, so the the deformed length $\tilde{N}$ of the chain centered at the origin is not $\tilde{x}(N)$ but $2\tilde{x}(N/2)$. Expression (4.52) shall be compared with[3] (3.67). Besides the change $x \to \tilde{x}$, there is an additional term

$$\frac{1}{12} \left(1 + \frac{1}{n} \right) \log \left(\frac{1}{\Omega(x_0, h)} \right)$$

[3]Observe that in (3.67) we have written the non-universal constant as $\tilde{c}'_n$ in order to distinguish from the non universal constant of the closed system. Here we avoid the tilde in order to not generate confusion with the tilded quantities.

proportional to the Weyl factor $\Omega(x_0, h)$. Observe that we recover the functional form of (3.67) if we define

$$\tilde{a}(x_0) \equiv \Omega(x_0, h)a, \tag{4.55}$$

i.e. if the UV cutoff is also deformed accordingly.

In fact, we can extend this reasoning beyond the CFT result. Applying the recipe that all distances from the origin $x = 0 = \tilde{x}(0)$ must be deformed with $\tilde{x}(x)$ (4.41), we consider the expression of the entanglement entropy of an open finite chain (3.78) obtained by Fagotti *et al.* (2011), which includes the non-universal leading constant[4] computed by Jin and Korepin (2004) (3.73) and the subleading terms that account for the parity oscillations. In flat space, the entanglement entropy of the open finite chain is computed by embedding it on a periodic one. The resulting chain is composed of the physical chain with N sites, its mirror image and two additional sites (Fagotti *et al.* 2011) yielding $2(N+1)$ sites. We obtain the entanglement entropy in the curved space case by appropriately deforming the flat case. The length of the physical chain plus the two additional sites is $2\tilde{x}((N+1)/2)$. Hence the total length of a chain with $N = 2L$ sites is $4\tilde{x}(L+1/2)$, and the chord length (4.53) to be deformed is $D(2x+1/2, 4(L+1/2))$. Thus, the entanglement entropy is

$$\begin{aligned} S_n(x) = \frac{1}{12}\left(1+\frac{1}{n}\right)\log Y(x) + \frac{\Upsilon_n}{2} \\ + f_n \cos\left(2k_F\left(x+\frac{N+1}{2}\right)\right)\left(\frac{1}{Y(x)}\right)^n, \quad x \in [-L, x_0], \end{aligned} \tag{4.56}$$

with f_n given by (3.79) and

$$\begin{aligned} Y(x) \equiv & \frac{2\tilde{D}(2x+1/2, 4(L+1/2))}{\pi\Omega(x_0,h)}|\sin k_F| \\ = & \frac{8\tilde{x}(L+1/2)}{\Omega(x_0,h)\pi}\cos\left(\frac{\pi\tilde{x}(x+1/2)}{2\tilde{x}(L+1/2)}\right)|\sin k_F|. \end{aligned} \tag{4.57}$$

Entanglement entropy of the rainbow state

Let us particularize the discussion for the rainbow model (4.43). To do so, we have to plug the tilded spatial coordinate (4.46) and particularize the Weyl factor to (4.44) into the general expression of the entanglement entropy (4.56). In Fig. 4.6 we plot the von Neumann entropy of a chain with $N = 60$ for different values of h. Observe that the entropy grows faster towards the center of the chain as the inhomogeneity increases.

[4]Notice that the constant computed by Jin and Korepin does not depend on the spacetime metric whereas the subleading parity oscillations are strongly modified. These facts suggest that the asymptotic results do not depend on the curvature of the spacetime.

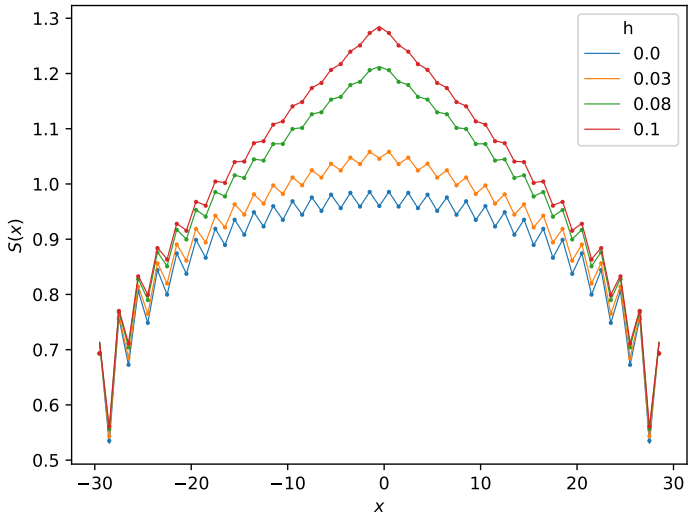

Figure 4.6: Von Neumann entropy of lateral blocks $A = [-L, x_0]$ for different values of h. The points are obtained numerically with the eigenvalues of the correlation matrix (3.54). The lines correspond to the theoretical prediction (4.56) particularized for the rainbow model.

It is instructive to analyze the half-chain entanglement entropy $x_0 = 0$ in the regime $hL \gg 1$

$$S_n(0, 2L) \approx \frac{1}{12}\left(1 + \frac{1}{n}\right)\log\left(\frac{8(e^{hL} - 1)}{h\pi}\right) \sim \frac{1}{12}\left(1 + \frac{1}{n}\right)hL, \quad \text{for } hL \gg 1, \tag{4.58}$$

and to compare it with the entanglement entropy of a thermal state (3.64) with inverse temperature β of an open system in the limit $L/\beta \gg 1$

$$S_A(\beta) = \frac{1}{12}\left(1 + \frac{1}{n}\right)\log\left(\frac{\beta\pi}{a}\sinh\left(\frac{2\pi L}{\beta}\right)\right) \sim \frac{1}{12}\left(1 + \frac{1}{n}\right)\frac{2\pi L}{\beta}. \tag{4.59}$$

It follows that we can define a temperature T_R that depends on the inhomogeneity parameter h.

$$\frac{2\pi}{\beta} = h \;\Rightarrow\; T_R = \frac{h}{2\pi}. \tag{4.60}$$

Finally, in Fig. (4.7) we plot the von Neumann entropy of the half-chain rainbow state for different values of h as a function of L. We can see the extensive linear behavior given by (4.58).

4.2.2 Entanglement Hamiltonian, entanglement spectrum and entanglement contour

Tonni *et al.* (2018) carried out a rigorous study of the entanglement Hamiltonian associated to ground states of inhomogeneous systems, mainly extending the results obtained by Cardy and Tonni (2016), which we have described in 3.3.1

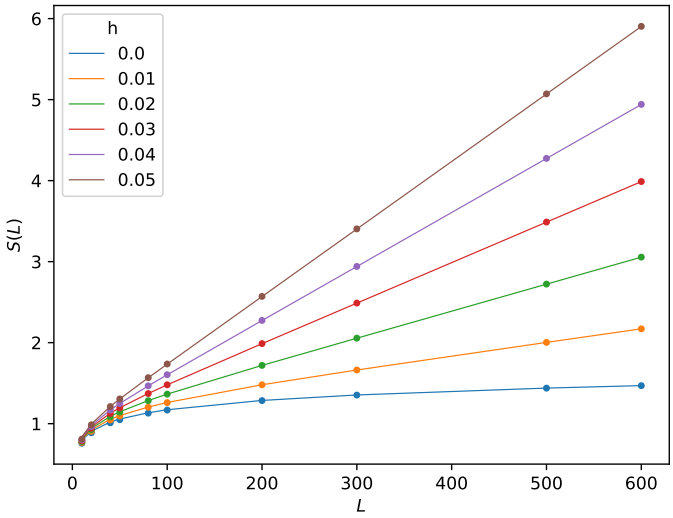

Figure 4.7: Scaling of the entanglement entropy for different values of h. The points correspond to numerical data and the lines correspond to the theoretical prediction (4.56) for $x_0 = 0$. Notice the linear behavior given by (4.58) in the regime $hL \gg 1$.

and subsequent sections. As in the case of the computation of the entanglement entropy, all the quantities which are given by CFT results can be defined on the curved background by substituting appropriately the flat-space quantities by the tilded ones. Hence, the entanglement Hamiltonian associated to a block A of a given state is (from (3.81))

$$\mathcal{H}_A = 2\pi \int_{\tilde{A}} \tilde{\beta}(\tilde{x}) T_{00}(\tilde{x}) d\tilde{x}. \tag{4.61}$$

Observe that the domain of integration has also changed. For instance, given the subsystem $A = [x_0, L]$, the domain in the curved background is $\tilde{A} = [\tilde{x_0}, \tilde{L}]$. In addition, the tilded weight function (3.82) is

$$\tilde{\beta}(\tilde{x}) = \frac{1}{\tilde{f}'(\tilde{x})},$$

where $\tilde{f}(\tilde{x})$ is the conformal transformation that maps the geometry imposed by $\tilde{A}$ into an annulus. It is possible to write it in terms of flat-space quantities

$$\beta(x) = \frac{1}{\frac{d\tilde{x}(x)}{dx}\frac{df(\tilde{x}(x))}{dx}} = \frac{\Omega(x,h)}{f'(\tilde{x}(x))}, \tag{4.62}$$

where in the last equality we have used the definition $\tilde{x}(x)$ (4.41). Let us recall that $\Omega(x,h) = J(x,h)$ is the Weyl factor. Hence, the weight function associated to the entanglement Hamiltonian of the subsystem A is obtained from (3.85)

$$\beta(x) = \Omega(x,h)\frac{2\tilde{x}(L)}{\pi}\frac{\sin\frac{\pi\tilde{x}(x)}{2\tilde{x}(L)} - \sin\frac{\pi\tilde{x}(x_0)}{2\tilde{x}(L)}}{\cos\frac{\pi\tilde{x}(x_0)}{2\tilde{x}(L)}} \tag{4.63}$$

Concerning the entanglement spectrum, we implement the tilded quantities in the expression for the entanglement gap (3.98) yielding

$$\Delta_1 = \frac{2\pi^2}{\log\left(\gamma \frac{4\tilde{x}(L)}{\pi\tilde{a}} \cos\left(\frac{\pi\tilde{x}(x_0)}{2\tilde{x}(L)}\right)\right)}, \tag{4.64}$$

where γ is a non universal constant that can be estimated through numerical analysis, and $\tilde{a}$ is the deformed cutoff (4.55).

Finally, the entanglement contour (3.105) of a block $A = [-L, 0]$ is

$$s_A^{(n)}(x) \approx \frac{1}{12}\left(1+\frac{1}{n}\right)\frac{1}{\tilde{\beta}(\tilde{x})} = \frac{c\pi}{24\tilde{x}(L)}\left(1+\frac{1}{n}\right)\frac{\Omega(x,h)}{\sin\left(\frac{\pi\tilde{x}(x)}{2\tilde{x}(L)}\right)}, \quad A = [0, L], \tag{4.65}$$

where we have particularized (4.63) for the half-chain $x_0 = 0$.

Let us conclude this chapter particularizing these results for the rainbow model.

Entanglement hamiltonian, entanglement spectrum and entanglement contour in the rainbow model.

For simplicity, let us restrict ourselves to the half chain block $A = [0, L]$. The weight function of the entanglement Hamiltonian (4.63) particularized for the tilded coordinate (4.46) and the Weyl factor (4.44) is

$$\beta_R(x) = \frac{2(e^{hL}-1)}{e^{hx}\pi h}\sin\left(\frac{\pi(e^{hx}-1)}{2(e^{hL}-1)}\right), \quad x \in [0, L]. \tag{4.66}$$

It is instructive to consider the regime $hL \gg 1$ in the above expression

$$\beta_R(x) \approx \frac{1}{h}\left(1-e^{-hx}\right) + \ldots, \tag{4.67}$$

where the dots denote subleading terms. We can distinguish between two regimes:

- If $hx \ll 1$, then $\beta(x) \approx x$ and we recover the Bisognano-Wichmann prediction (3.80).
- If $hx \gg 1$, the entanglement Hamiltonian is then

$$\mathcal{H}_A \approx \frac{2\pi}{h}\int_A T_{00}(x)dx \tag{4.68}$$

  As we mentioned, the inverse of the weight function is also called entanglement temperature. Indeed, observe that $\rho = e^{-\mathcal{H}_A}$ with $\mathcal{H}_A$ given by the above expression (4.68) describes a thermal state with temperature $T_R = h/(2\pi)$. Let us recall that we have found also this expression in the analysis of the entanglement entropy of the rainbow state in this regime (4.60). This fact makes it possible to regard the rainbow state as thermofield double (Ramírez *et al.* 2015). Given two copies l and r of a system with energies E_n and states

$|n\rangle$, a pure state $|\psi\rangle$ is said to be a thermofield double if each copy is a thermal state with temperature T (see Appendix 2.A)

$$|\psi\rangle = \sum_n e^{-\frac{E_n}{2T}} |n\rangle_l |n\rangle_r .$$

In our case, each copy corresponds to a half of the chain whose Hamiltonian is, as we have seen, a CFT Hamiltonian in curved spacetime. The thermofield double has been used to explore the connection between black holes and the EPR=ER conjecture (Hartman and Maldacena 2013; Maldacena and Susskind 2013). In this context T_R is the surface temperature corresponding to a gravitational acceleration $h = 2\pi T_R$.

In Fig. 4.8 we plot the weight function of the entanglement Hamiltonian for different configurations that keep the product $hL = const$.

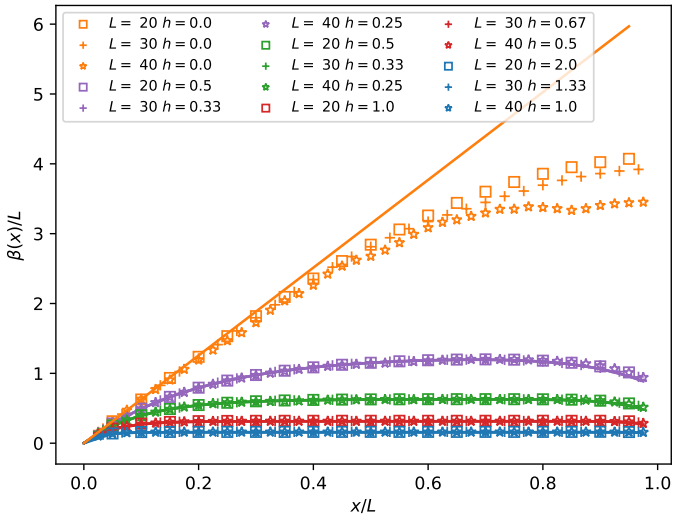

Figure 4.8: Normalized weight function $\beta(x)/L$ of the entanglement Hamiltonian associated to the right half chain, i.e. block $A = [0, L]$ for different configurations that keep $hL = const$. The numerical data are obtained with the optimization procedure (3.94). Notice the plateau for values $hL \gg 1$ which signals the thermofield double interpretation. The solid lines correspond to the prediction (4.66).

As we mentioned, the entanglement spectrum of a CFT Hamiltonian is asymptotically equispaced (3.89) (Peschel 1999). For finite and small chains, the dispersion relation shows some curvature, which is due to non-universal contributions. Particularizing (4.64) for the rainbow model yields

$$\Delta_1 = \frac{2\pi^2}{\log\left(\gamma \tilde{L}\right)} = \frac{2\pi^2}{\log\left(\gamma \frac{2}{\pi h}\left(e^{hL} - 1\right)\right)}, \tag{4.69}$$

where $\tilde{L}$ is given by (4.49) and γ accounts for all the non-universal corrections and it has been numerically found by Ramírez *et al.* (2015). Notice that in the regime

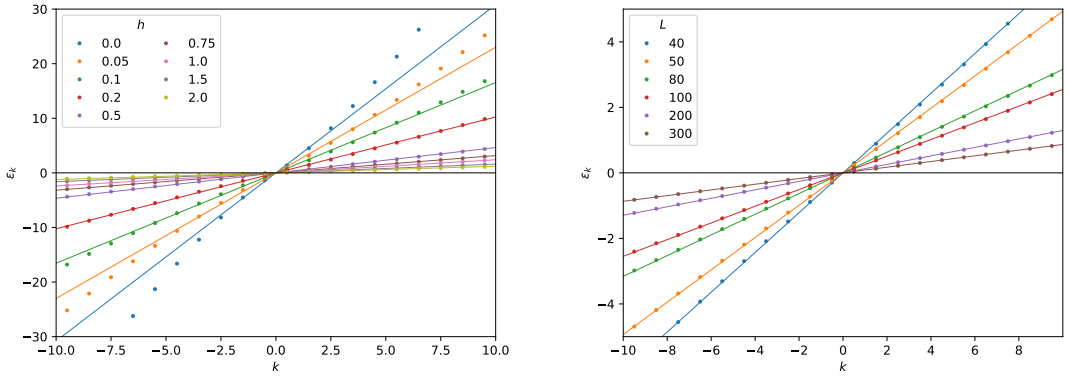

Figure 4.9: Central part of the dispersion relation ϵ_k of the entanglement spectrum. (Left) Chain with $N = 160$ sites and different values of h. Observe that the bigger h the better the linear prediction. (Right) The inhomogeneity parameter is fixed to $h = 0.75$.

$hL \gg 1$, $\tilde{L}$ is huge, meaning that

$$\Delta_1 \approx \frac{2\pi^2}{hL} = \frac{\pi\beta_R}{L}, \tag{4.70}$$

yielding a dispersion relation

$$\epsilon_k = \frac{\pi^2}{hL}k, \quad k = \pm\frac{1}{2}, \pm\frac{3}{2}, \dots \tag{4.71}$$

In Fig. 4.9 we plot the central part of dispersion relation of the entanglement spectrum corresponding to the half chain. The solid lines correspond to the linear prediction (4.71). It is important to note that since the accuracy of the CFT prediction increases with h and L, the non universal contribution γ is less relevant in this regime.

Tonni *et al.* (2018) computed the contour of the rainbow model for the block A=$[x_0, L]$. Here we review the case $x_0 = 0$. Hence, as usual, we particularize the CFT prediction of the contour in curved spacetime (4.65) for the tilded quantities (4.46)

$$s_A^{(1)} = \frac{1}{6}\frac{1}{\tilde{\beta}(\tilde{x})} = \frac{\pi e^{hx}h}{12(e^{hL}-1)}\frac{1}{\sin\frac{\pi(e^{hx}-1)}{2(e^{hL}-1)}}, \tag{4.72}$$

where we have used the weight function of the rainbow model (4.66). Observe that $s_A^{(1)} \approx h/6$ in the regime $hL \gg 1$. In Fig. 4.10 we plot the contour function for different values of h for a chain with $N = 100$. As we can see, there is a plateau at $h/6$ for those sites far enough from the boundaries. Observe that the parity oscillations deviations are expelled toward the edge as the inhomogeneity grows.

In this chapter we have studied the entanglement of connected blocks of the

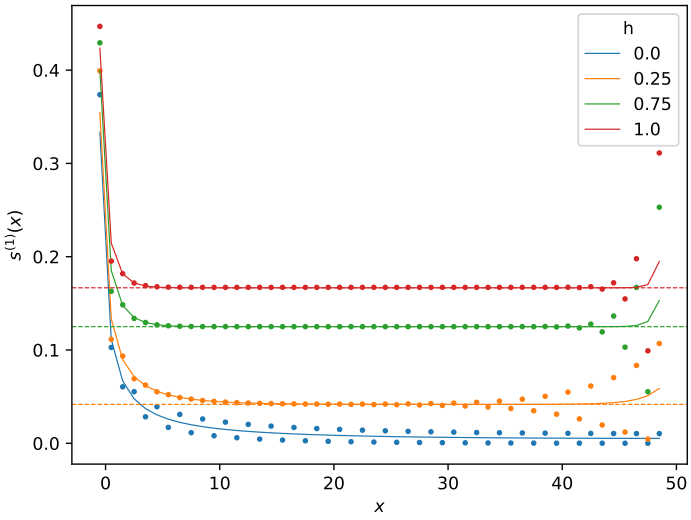

Figure 4.10: Entanglement contour for of the block $A = [0, 50]$ of a chain with $N = 100$ sites for different values of h. The dotted lines correspond to the constant $h/6$ predicted in the regime $hL \gg 1$. In turn, solid lines represent the prediction (4.72).

inhomogeneous XX model analyzing the fermionic model obtained by means of the Jordan-Wigner transformation. We have described the strong inhomogeneity $h \gg 1$ regime with the strong disorder renormalization group and the weak inhomogeneity $h \ll 1$ with a continuum limit around the Fermi point.

We have also presented the rainbow model proposed by Vitagliano *et al.* (2010) and rediscovered by Ramírez *et al.* (2014) which is a free-fermionic chain with hoppings which decay exponentially from the center. Its ground state presents a linear growth of the entanglement entropy in both the strong and weak inhomogeneity regimes. The latter is described by a geometrical deformation of the free-fermionic conformal field theory, associated to a hyperbolic spacetime metric. The strong inhomogeneity limit is described as a valence bond state with concentric bonds around the center, as it can be established using the Dasgupta-Ma renormalization group.

It is worth to say that Ramírez *et al.* (2014) generalized the rainbow model to the Heisenberg spin chain and computed numerically the entanglement with the DMRG. However, as we discussed in Chapter 1, this method is deeply connected with matrix product states, short-range entanglement and the area law. Since the rainbow model violates the area law, the effective description with the DMRG restricts the computations to small sizes. Moreover, Ramírez *et al.* (2015) considered a two dimensional version of the model, finding also a linear scaling of the entanglement entropy with logarithmic corrections.

Appendices

4.A Free fermion models

In this Appendix we shall describe the treatment of free fermion models and the obtainment of the correlation matrix. We shall distinguish between models with and without pairing terms. Consider a generic quadratic Hamiltonian.

$$H = \mathbf{\Psi}^\dagger \mathbf{H} \mathbf{\Psi} \tag{4.A.1}$$

where

$$\mathbf{\Psi} = \begin{pmatrix} c_{1,\eta_1} \\ \vdots \\ c_{N,\eta_N} \\ c^\dagger_{1,\eta_1} \\ \vdots \\ c^\dagger_{N,\eta_N} \end{pmatrix} = \begin{pmatrix} \mathbf{c} \\ \mathbf{c}^\dagger \end{pmatrix} \tag{4.A.2}$$

is called a Nambu-spinor, and η_m takes account of other possible relevant quantum numbers, such as spin. For now on, we will abuse notation and ignore the index η_m. Here H is the *many-body Hamiltonian* or *second quantized Hamiltonian* while the matrix $\mathbf{H}$ is the *single-body Hamiltonian* or *first quantized Hamiltonian*. The most general quadratic Hamiltonian can be written as:

$$H = \begin{pmatrix} \mathbf{c}^\dagger & \mathbf{c} \end{pmatrix} \left(\begin{array}{c|c} \mathbf{T} & \mathbf{P} \\ \hline -\mathbf{P}^* & -\mathbf{T}^* \end{array} \right) \begin{pmatrix} \mathbf{c} \\ \mathbf{c}^\dagger \end{pmatrix}, \tag{4.A.3}$$

where due to hermiticity $H = H^\dagger$, the hopping matrix is Hermitian $\mathbf{T} = \mathbf{T}^\dagger$ and the pairing matrix is antisymmetric $\mathbf{P} = -\mathbf{P}^T$. We can also write (4.A.3) as

$$H = \sum_{ij} \left(2T_{ij} c_i^\dagger c_j + P_{ij} c_i^\dagger c_j^\dagger + P_{ij}^* c_j c_i \right) + \operatorname{tr} T. \tag{4.A.4}$$

The spectrum and energy states of H are obtained by diagonalizing $\mathbf{H}$. There exists a unitary matrix $\mathbf{U_B} \in SU(2N)$ such that $\mathbf{U_B}^\dagger \mathbf{H} \mathbf{U_B} = \mathbf{D}$, where $\mathbf{D}$ is a diagonal matrix that contains the eigenvalues ϵ_k with $k = 1, \ldots, 2N$. Then we can write (4.A.1) as:

$$H = \mathbf{\Psi}^\dagger \mathbf{U_B} \mathbf{D} \mathbf{U_B}^\dagger \mathbf{\Psi} = \mathbf{\Phi}^\dagger \mathbf{D} \mathbf{\Phi}, \tag{4.A.5}$$

where

$$\mathbf{\Phi} = \mathbf{U_B}^\dagger \mathbf{\Psi} = \begin{pmatrix} \mathbf{b} \\ \mathbf{b}^\dagger \end{pmatrix} \tag{4.A.6}$$

is a new Nambu spinor.

The ground state $|GS\rangle$ is obtained filling all the negative energy levels. We shall distinguish two situations. If there are no pairing terms $\mathbf{P} = \mathbf{0}$ the Hamiltonian H commutes with the total number of c fermions, as we discussed in Chapter 3. As a consequence, the Fock state of the $\{c_m\}$ fermions, defined as $c_m |0\rangle = 0$ for all m, is also the Fock state of the new fermions, $b_k |0\rangle = 0$ for all k. On the contrary, if there exist pairing terms $\mathbf{P} \neq \mathbf{0}$, there is no particle number conservation and the state $|0\rangle$ is not anymore the Fock vacuum of the $\{b\}$ fermions. Let us discuss the first case.

4.A.1 Without pairing terms

If $\mathbf{P} = 0$ the Nambu spinor formalism is redundant and we can rewrite (4.A.1) as

$$H = \mathbf{c}^\dagger \mathbf{T} \mathbf{c} = \sum_{ij} T_{ij} c_i^\dagger c_j, \quad T_{ij} = T_{ji}^*. \tag{4.A.7}$$

There exists a unitary $\mathbf{U} \in SU(N)$ such that $\mathbf{U}^\dagger \mathbf{T} \mathbf{U} = \mathbf{D}$. We can thus write the Hamiltonian as

$$H = \sum_{k=1}^{N} \epsilon_k b_k^\dagger b_k, \tag{4.A.8}$$

with

$$b_k = \sum_{i=1}^{N} U_{ik}^* c_i \tag{4.A.9}$$

$$c_i = \sum_{k=1}^{N} U_{ik} b_k. \tag{4.A.10}$$

The ground state |GS⟩ is obtained by filling all the negative energy levels:

$$|GS\rangle = \prod_{k \in \Omega_{\mathrm{GS}}} b_k^\dagger |0\rangle, \quad \Omega_{\mathrm{GS}} := \{ k \mid \epsilon_k < 0 \}. \tag{4.A.11}$$

Consequently, the energy of the ground state is the sum of the negative single-body energies:

$$E_{\mathrm{GS}} = \sum_{k \in \Omega_{\mathrm{GS}}} \epsilon_k. \tag{4.A.12}$$

The number of fermions that compose the ground state is then $N_F = \#\Omega$, where $\#$ denotes the cardinal of a set.

Notice that the excited states are obtained in a similar way, i.e. filling the single-body energy levels specified by the set Ω.

Correlation matrices

It is important for us to compute also the two point correlators of the physical fermions $\langle \mathrm{GS}|c_i^\dagger c_j|\mathrm{GS}\rangle \equiv \langle c_i^\dagger c_j\rangle$ that can be arranged in a matrix $\mathbf{C}$. Using matrix notation and taking into account that $\left\langle b_k b_k^\dagger \right\rangle = 0$ for all $k \in \Omega_{\mathrm{GS}}$:

$$\left\langle \mathbf{c}\ \mathbf{c}^\dagger \right\rangle = \mathbf{U}\left\langle \mathbf{b}\ \mathbf{b}^\dagger \right\rangle \mathbf{U}^\dagger = \mathbf{U}\begin{pmatrix} \langle b_1 b_1^\dagger\rangle & \cdots & \langle b_1 b_N^\dagger\rangle \\ \vdots & \ddots & \vdots \\ \langle b_N b_1^\dagger\rangle & \cdots & \langle b_N b_N^\dagger\rangle \end{pmatrix}\mathbf{U}^\dagger = \mathbf{U}\left(\begin{array}{c|c} \mathbf{0}_{N_F} & \mathbf{0} \\ \hline \mathbf{0} & \mathbb{1}_{N-N_F} \end{array}\right)\mathbf{U}^\dagger \tag{4.A.13}$$

Finally, using the anticommutation relations, $\mathbf{C} = \mathbb{1}_N - \left\langle \mathbf{c}\ \mathbf{c}^\dagger \right\rangle$,

$$\mathbf{C} = \mathbf{U}\left(\begin{array}{c|c} \mathbb{1}_{N_F} & \mathbf{0} \\ \hline \mathbf{0} & \mathbf{0}_{N-N_F} \end{array}\right)\mathbf{U}^\dagger, \tag{4.A.14}$$

or more explicitly:

$$C_{ij} = \sum_{k=1}^{N_F} U_{ik}U_{jk}^*. \tag{4.A.15}$$

4.A.2 With pairing terms (no particle number conservation)

If $\mathbf{P} \neq \mathbf{0}$, we need to diagonalize the $2N \times 2N$ matrix (4.A.5). Notice however that the components of the Nambu spinors are not completely independent. Indeed,

$$\boldsymbol{\sigma}_x^{(N)}\boldsymbol{\Psi} = \left(\begin{array}{c|c} \mathbf{0} & \mathbb{1}_N \\ \hline \mathbb{1}_N & \mathbf{0} \end{array}\right)\begin{pmatrix} \mathbf{c} \\ \mathbf{c}^\dagger \end{pmatrix} = (\boldsymbol{\Psi}^\dagger)^T. \tag{4.A.16}$$

Indeed, the operation $\boldsymbol{\sigma}_x^{(N)}$ interchanges creation by annihilation operators and it implements a so-called particle-hole transformation. It can be shown that the Hamiltonian (4.A.1) is symmetric under this transformation. As a consequence,if $\mathbf{u}$ is an eigenvector of $\mathbf{H}$ with eigenvalue ϵ, then $(\boldsymbol{\sigma}_x^{(N)}\mathbf{u})^*$ is also an eigenvector with eigenvalue $-\epsilon$. Hence, we can write

$$\mathbf{U}_B = \left(\begin{array}{c|c} \mathbf{V} & \mathbf{W}^* \\ \hline \mathbf{W} & \mathbf{V}^* \end{array}\right), \quad \mathbf{D} = \left(\begin{array}{c|c} \boldsymbol{\epsilon} & \mathbf{0} \\ \hline \mathbf{0} & -\boldsymbol{\epsilon} \end{array}\right) = \begin{pmatrix} \epsilon_1 & & & & & \\ & \ddots & & & & \\ & & \epsilon_N & & & \\ & & & -\epsilon_1 & & \\ & & & & \ddots & \\ & & & & & -\epsilon_N \end{pmatrix} \tag{4.A.17}$$

Thus, using (4.A.5) yields

$$H = \sum_{k=1}^{N} 2\epsilon_k\left(b_k^\dagger b_k - \frac{1}{2}\right), \quad \epsilon_k > 0. \tag{4.A.18}$$

The ground state $|\mathrm{GS}\rangle$ coincides with the Fock space of the fermions $\mathbf{b}$, that are known as Bogoliubov particles (or bogoliubons):

$$b_k |\mathrm{GS}\rangle = 0, \quad \textit{for all } k \quad \Rightarrow \quad |\mathrm{GS}\rangle \propto \prod_{k=1}^{N} b_k |0\rangle . \tag{4.A.19}$$

It follows from (4.A.18) that the energy of the ground state is:

$$E_{\mathrm{GS}} = -\sum_{k=1}^{N} \epsilon_k . \tag{4.A.20}$$

Majorana fermions

It is also worth to point out that there exists an alternative formulation in terms of Majorana fermions, also known as real fermions. Let us start by defining them. A Dirac fermion or complex fermion can always be decomposed into a real and imaginary part:

$$\alpha_m = c_m + c_m^\dagger, \quad \beta_m = i(c_m^\dagger - c_m). \tag{4.A.21}$$

Notice that they are by construction their own antiparticle $\alpha_m^\dagger = \alpha_m$ ($\beta_m^\dagger = \beta_m$) and that they satisfy the following anticommutation relations

$$\{\alpha_m, \beta_m'\} = 0, \quad \{\alpha_m, \alpha_m'\} = \{\beta_m, \beta_m'\} = 2\delta_{mm'}, \tag{4.A.22}$$

provided that the anticommutation relations of the Dirac (or complex) fermions (4.A.22) are satisfied. We can thus transform the Nambu spinor $\boldsymbol{\Psi}$ into a spinor of Majorana fermions $\boldsymbol{\xi}$ by means of the matrix $\mathbf{U}_M$:

$$\boldsymbol{\Psi} = \begin{pmatrix} \mathbf{c} \\ \mathbf{c}^\dagger \end{pmatrix} = \frac{1}{2}\mathbf{U}_M \boldsymbol{\xi} \equiv \frac{1}{2}\left(\begin{array}{c|c} \mathbb{1}_N & i\mathbb{1}_N \\ \hline \mathbb{1}_N & -i\mathbb{1}_N \end{array}\right)\begin{pmatrix} \boldsymbol{\alpha} \\ \boldsymbol{\beta} \end{pmatrix}, \tag{4.A.23}$$

and write the generic Hamiltonian (4.A.1) in terms of Majorana fermions:

$$H = \boldsymbol{\Psi}^\dagger \mathbf{H} \boldsymbol{\Psi} = \frac{1}{4}\boldsymbol{\xi}^T \mathbf{U}_M \mathbf{H} \mathbf{U}_M^\dagger \boldsymbol{\xi} = \frac{i}{2}\boldsymbol{\xi}^T \mathbf{A} \boldsymbol{\xi}, \tag{4.A.24}$$

where $\mathbf{A} = (1/2)\,\mathrm{Im}(\mathbf{U}_M \mathbf{H} \mathbf{U}_M^\dagger)$ is antisymmetric[5] $\mathbf{A} = -\mathbf{A}^T$. There exists an orthogonal matrix $\mathbf{Q} \in SO(2N)$ that brings $\mathbf{A}$ to the so-called normal form $\mathbf{N}_\epsilon$:

$$\mathbf{Q}^T \mathbf{A} \mathbf{Q} \equiv \mathbf{N}_\epsilon = \left(\begin{array}{c|c} \mathbf{0}_N & \boldsymbol{\epsilon} \\ \hline \boldsymbol{\epsilon} & \mathbf{0}_N \end{array}\right) \tag{4.A.26}$$

[5] In terms of the hopping $\mathbf{T}$ and $\mathbf{P}$ of the Dirac fermions (4.A.3):

$$\mathbf{A} = \frac{1}{2}\left(\begin{array}{c|c} \mathbf{0} & 2(\mathbf{T}-\mathbf{P}) \\ \hline -2(\mathbf{T}+\mathbf{P}) & \mathbf{0} \end{array}\right), \tag{4.A.25}$$

where we have assumed that all the terms are real numbers. The antisymmetry is manifested taking into account that $\mathbf{P}^T = -\mathbf{P}$

where $\boldsymbol{\epsilon}$ is defined in (4.A.17). Let us mention that the normal form $\mathbf{N}_\epsilon$ can also be obtained by means of the real Schur decomposition. Putting (4.A.26) in (4.A.24) leads to $H = (i/2)\boldsymbol{\xi}^T\mathbf{Q}\mathbf{N}_\epsilon\mathbf{Q}^T\boldsymbol{\xi}$, allowing us to define a new spinor and write

$$H = \frac{i}{2}\boldsymbol{\chi}^T\mathbf{N}_\epsilon\boldsymbol{\chi}, \quad \mathbf{Q}^T\boldsymbol{\xi} \equiv \boldsymbol{\chi} = \begin{pmatrix}\boldsymbol{\mu}\\ \boldsymbol{\nu}\end{pmatrix}. \tag{4.A.27}$$

We recover the Bogoliubov transformations (4.A.5) by inverting appropriately (4.A.23):

$$H = \frac{i}{2}\boldsymbol{\chi}^T\mathbf{N}_\epsilon\boldsymbol{\chi} = \frac{i}{2}\boldsymbol{\Phi}\mathbf{U}_M\mathbf{N}_\epsilon\mathbf{U}_M^\dagger\boldsymbol{\Phi} = \boldsymbol{\Phi}\mathbf{D}\boldsymbol{\Phi}. \tag{4.A.28}$$

Covariance matrix

The correlation matrix (4.A.13) in terms of b fermions is particularly simple

$$\left\langle\boldsymbol{\Phi}\boldsymbol{\Phi}^\dagger\right\rangle = \left(\begin{array}{c|c}\mathbb{1}_N & \mathbf{0}\\ \hline \mathbf{0} & \mathbf{0}\end{array}\right), \tag{4.A.29}$$

where we have taken into account (4.A.11). Thus, the correlation matrix $\mathbf{C} = \langle\boldsymbol{\Psi}\boldsymbol{\Psi}^\dagger\rangle$ is

$$\mathbf{C} = \left\langle\boldsymbol{\Psi}\boldsymbol{\Psi}^\dagger\right\rangle = \mathbf{U}_B\left\langle\boldsymbol{\Phi}\boldsymbol{\Phi}^\dagger\right\rangle\mathbf{U}_B^\dagger = \left(\begin{array}{c|c}\mathbf{V}\mathbf{V}^\dagger & \mathbf{V}\mathbf{W}^\dagger\\ \hline \mathbf{W}\mathbf{V}^\dagger & \mathbf{W}\mathbf{W}^\dagger\end{array}\right), \tag{4.A.30}$$

where we have used $\mathbf{U}_B$ given by (4.A.17).

We can also express the correlators in terms of the Majorana fermions $\langle\boldsymbol{\Phi}\boldsymbol{\Phi}^\dagger\rangle = \mathbf{U}_M\langle\boldsymbol{\chi}\boldsymbol{\chi}^T\rangle\mathbf{U}_M^\dagger$ and those in terms of the physical Majorana fermions $\boldsymbol{\xi}$ given by (4.A.23)

$$\left\langle\boldsymbol{\xi}\boldsymbol{\xi}^T\right\rangle = \mathbf{Q}^T\left(\begin{array}{c|c}\mathbb{1}_N & i\mathbb{1}_N\\ \hline -i\mathbb{1}_N & \mathbb{1}_N\end{array}\right)\mathbf{Q}, \tag{4.A.31}$$

where we use the orthogonal matrix defined in (4.A.26). The symmetric part of the matrix above is given by the anticommutation relation of the Majorana fermions, while the antisymmetric part that contains all the non-trivial information is known as the covariance matrix.

$$\mathcal{C} = \mathbf{Q}^T\left(\begin{array}{c|c}\mathbf{0} & \mathbb{1}_N\\ \hline -\mathbb{1}_N & \mathbf{0}\end{array}\right)\mathbf{Q}, \tag{4.A.32}$$

Entanglement Hamiltonian of Majorana fermions

The entanglement Hamiltonian can be obtained from the covariance matrix. Consider a system of $N = 2L$ Majorana fermions given by the quadratic Hamiltonian (4.A.24). There exists a transformation $\mathbf{O} \in SO(2N)$ which brings the Hamiltonian to the canonical form $\mathbf{O}^T\mathbf{A}\mathbf{O} = \mathbf{N}'_\epsilon$, where $\mathbf{N}'_\epsilon$ is a block diagonal matrix

$$\mathbf{N}'_\epsilon = \bigoplus_k^L \begin{pmatrix} 0 & \epsilon_k \\ -\epsilon_k & 0 \end{pmatrix}, \tag{4.A.33}$$

where $\pm\epsilon_k$ with $k = 1 \dots L$ are the eigenvalues of the matrix $i\mathbf{A}$. Notice that N'_ϵ (4.A.33), and N_ϵ (4.A.26), are similar matrices meaning that $\mathbf{O}$ and $\mathbf{Q}$ differ in the order of the elements of the basis. $\mathbf{O}\boldsymbol{\xi} = \tilde{\boldsymbol{\xi}}$ with $\boldsymbol{\xi}$ given in (4.A.23) and

$$\tilde{\boldsymbol{\xi}}^T = (\alpha_1, \beta_1, \dots, \alpha_N, \beta_N)\,.$$

The transformation $\mathbf{O}$ is more convenient because the lateral blocks considered in the main text are contiguous in this basis. Thus, the Hamiltonian reads also as (4.A.27) after substituting $\mathbf{Q}$ by $\mathbf{O}$. The density matrix ρ associated with the the GS of a quadratic Hamiltonian can always be written as

$$\rho = \mathcal{K} e^{-\mathcal{H}}, \tag{4.A.34}$$

where $\mathcal{K}$ is a normalization constant and $\mathcal{H}$ is the entanglement Hamiltonian (see Section 3.3.1), given by (4.A.24). It is possible to obtain $\mathcal{H}_A$, the entanglement Hamiltonian associated to the reduced density matrix ρ_A making use of the associated partial covariance matrix (4.A.32) $(\mathcal{C}_A)_{ij} = \langle [\xi_i \xi_j] \rangle$ with $i, j \in A$.

$$\mathcal{C}_A = \mathbf{O}^T \mathbf{N}'_\lambda \mathbf{O}, \tag{4.A.35}$$

where $\mathbf{N}'_\lambda$ has the same structure as $\mathbf{N}'_\epsilon$ but contains the eigenvalues of $\mathcal{C}_A$. Since the matrix $\mathbf{O}$ brings to the normal form both $\mathcal{C}_A$ and $\mathcal{H}_A$, there is a relation between the entanglement spectrum ϵ, and the eigenvalues of the covariance matrix:

$$\lambda_k = -\tanh \frac{\epsilon_k}{2} \tag{4.A.36}$$

Hence, by inverting the above relation, it is possible to compute the entanglement Hamiltonian knowing the covariance matrix,

$$\mathcal{H} = \mathbf{O}^T \mathbf{N}'_{\epsilon(\lambda)} \mathbf{O}. \tag{4.A.37}$$

4.B Dirac equation on a curved background

Let us consider the Dirac equation on curved spacetime:

$$(i\not{D} - m)\Psi = 0, \tag{4.B.1}$$

where $\not{D} = E_a^\mu \gamma^a D_\mu$ is the slashed covariant derivative, and

$$E_a^\mu = g^{\mu\nu} \eta_{ab} e_\nu^b, \tag{4.B.2}$$

is the inverse of the vielbein or tetrad basis, actually a *zweibein* e^a_μ that satisfies

$$g_{\mu\nu} = e^a_\mu e^b_\nu \eta_{ab}. \tag{4.B.3}$$

Here η_{ab} is the flat spacetime metric with signature $(-,+)$. The covariant derivative of the two component spinor Ψ is given by

$$D_\mu \Psi = \left(\partial_\mu - \frac{1}{8}\omega^{ab}_\mu [\gamma_a, \gamma_b]\right)\Psi, \tag{4.B.4}$$

where ω^{ab}_μ is the spin-connection, which is defined in terms of the Christoffel symbols $\Gamma^\nu_{\sigma\mu}$ and the inverse of the zweibein E^μ_a,

$$\omega^{ab}_\mu = e^a_\nu \partial_\mu E^{b\nu} + e^a_\nu E^{b\sigma}\Gamma^\nu_{\sigma\mu}. \tag{4.B.5}$$

As we are considering a static system, it is reasonable to assume that the zweibein matrix e^a_μ is diagonal ($E^1_0 = E^0_1 = 0$). Expanding (4.B.1) with this assumption leads to

$$\left(iE^0_0\gamma^0\left(\partial_0 - \frac{1}{8}\omega^{ab}_0[\gamma_a,\gamma_b]\right) + iE^1_1\gamma^1\left(\partial_1 - \frac{1}{8}\omega^{ab}_0[\gamma_a,\gamma_b]\right) - m\right)\Psi = 0\,. \tag{4.B.6}$$

Taking into account that $[\gamma_0,\gamma_1] = [-\gamma^0,\gamma^1] = -2\gamma^3$ and the antisymmetry of the internal indices of the spin connection we arrive at

$$\left(\gamma^0\partial_0 + \frac{1}{2}\omega^{01}_0\gamma^0\gamma^3 + \frac{E^1_1}{E^0_0}\left(\gamma^1\partial_1 + \frac{1}{2}\omega^{01}_1\gamma^1\gamma^3\right) + i\frac{m}{E^0_0}\right)\Psi = 0\,. \tag{4.B.7}$$

Chapter 5

Piercing the rainbow: defects and inhomogeneity

In this chapter we add a tunable exchange coupling constant at the center of the rainbow model, γ, and show that it induces entanglement transitions of the ground state. At very strong inhomogeneity, the rainbow state survives for $0 \leq \gamma \leq 1$, while outside that region the ground state is a product of dimers. In the weak inhomogeneity regime the entanglement entropy satisfies a volume law, derived from CFT in curved spacetime, with an effective central charge that depends on the inhomogeneity parameter and γ. In all regimes we have found that the entanglement properties are invariant under the transformation $\gamma \longleftrightarrow 1-\gamma$, whose fixed point $\gamma = \frac{1}{2}$ corresponds to the usual rainbow model. This chapter contains content published in Samos Sáenz de Buruaga *et al.* (2020).

In the last chapter we have introduced the rainbow model (4.42) for both strong and weak inhomogeneity regimes finding that the ground state presents a linear growth of the entanglement entropy for certain subsystems. Thus, it is relevant to ask whether the weak and the strong inhomogeneity limits will match in all possible situations. We have introduced a *defect* in the center of the rainbow system and considered the entanglement structure as a function of the defect intensity and the curvature. As we will show, both the Dasgupta-Ma and the field theory approach that describes entanglement on a critical chain with a defect (Eisler and Peschel 2010; Iglói *et al.* 2009; Levine 2004; Peschel 2005) can be extended to the curved case in the strong and weak inhomogeneity regimes, respectively, providing a complete physical picture.

This chapter is organized as follows. In Section 5.1 we present the model. The strong inhomogeneity limit, studied with the Dasgupta-Ma RG, is described in detail in Section 5.2, while Sec. 5.3 considers the weak-inhomogeneity regime

through a perturbation of a conformal field theory. We characterize the entanglement structure via the entropies and the entanglement spectrum, Hamiltonian and contour.

5.1 The model

Let us consider an inhomogeneous XX spin chain with an even number $N = 2L$ whose Hamiltonian is defined as:

$$H_L(h,\gamma) = -\frac{1}{2}\sum_{m=-L+1}^{L-1} J_m S^+_{m-1/2} S^-_{m+1/2} + \text{h.c.}, \tag{5.1}$$

and by performing a Jordan-Wigner transformation, its fermionic version:

$$H_L(h,\gamma) = -\frac{1}{2}\sum_{m=-L+1}^{L-1} J_m c^\dagger_{m-1/2} c_{m+1/2} + \text{h.c.}, \tag{5.2}$$

where $c_n(c_n^\dagger)$, with $n = \pm\frac{1}{2}, \pm\frac{3}{2}\cdots\pm(L-\frac{1}{2})$ are fermionic annihilation (creation) operators that obey the standard anti-commutation relations. The coupling parameters J_m are

$$J_m = \begin{cases} e^{-h|m|} & \text{if } m \neq 0, \\ e^{-h\gamma} & m = 0, \end{cases} \tag{5.3}$$

where $h \geq 0$ is the inhomogeneity parameter, and $\gamma \in \mathbb{R}$ parametrizes the value of the central coupling. Observe that for $\gamma = 1/2$ we recover the rainbow Hamiltonian that we presented in the previous chapter. Here we will investigate how the central coupling that we shall interpret as a *defect* modify the properties of the ground state, with special focus in the entanglement characterization. Notice that sites have half-integer indices, while links have integer ones. We will follow the same scheme presented in the previous chapter. Firstly we shall consider the strong inhomogeneity regime with the SDRG and later the weak inhomogeneity regime.

5.2 Strong inhomogeneity regime

When the inhomogeneity is large enough, it can be addressed through the SDRG scheme as we discussed in Section 4.1.1. Let us recall that for a free-fermionic chain with a Hamiltonian such as (5.2), the effective coupling obtained at each RG step is

$$\tilde{J}_i = -\frac{J_{i-1}J_{i+1}}{J_i}, \qquad |J_i| \gg |J_{i\pm1}|, \tag{5.4}$$

and that the GS predicted by the SDRG is a valence-bond solid (VBS) given by (4.11)

$$|GS\rangle = \prod_{k=1}^{L} (b^{\eta_k}_{i_k,j_k})^\dagger |0\rangle\,, \tag{5.5}$$

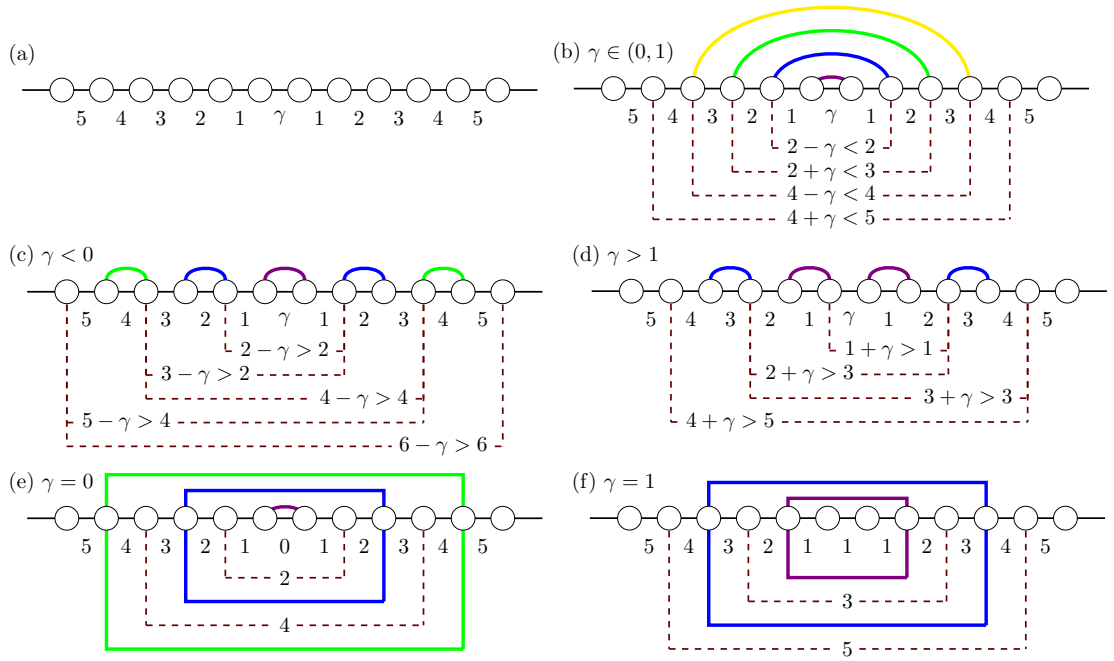

Figure 5.1: (a) Illustration of the rainbow chain with a central defect, showing the log-couplings (5.7) on each link; (b) SDRG procedure in the $\gamma \in (0,1)$ case, leading to the *rainbow phase*; (c) SDRG for the $\gamma < 0$ case; (d) SDRG for the $\gamma > 1$ case, both leading to *dimerized phases*; (e) and (f) transition cases, where the SDRG approximation is not valid; the dashed boxes mark the *ties* between the couplings, which demand a different RG approach.

where $\eta_k = \pm 1$ is a phase given by (5.4), and $b^{+}_{i,j}$ ($b^{-}_{i,j}$) are bonding (anti-bonding) operators

$$\left(b^{\pm}_{ij}\right)^{\dagger} = \frac{1}{\sqrt{2}}\left(c^{\dagger}_{i} \pm c^{\dagger}_{j}\right). \tag{5.6}$$

For our purposes, it is convenient to define the log-couplings (Rodríguez-Laguna *et al.* 2016) of the original couplings J_i (5.3):

$$t_i = -\log \frac{|J_i|}{h}, \tag{5.7}$$

where h is included for later convenience. In this language, the two fermionic sites that are integrated out on each step of the RG are those connected by the *lowest* t_i and the effective coupling (5.4) is computed in additive way:

$$\tilde{t}_i = t_{i-1} - t_i + t_{i+1}. \tag{5.8}$$

Let us consider the GS of Hamiltonian (5.2) under the light of the SDRG for $h \gg 1$. For simplicity, we will only consider even L (the case of odd L can be straightforwardly obtained), as a function of the defect parameter, γ. The different phases will be discussed along the panels of Fig. 5.1.

The different ground states obtained by means of the SDRG are presented in Table 5.1, please refer to Appendix 5.A for the details. All of them are obtained at half filling and it is important to note that the validity of the SDRG improves when the renormalized coupling is much stronger than the surrounding ones, so all the GS that we have found are better approximations for bigger h (and eventually they are exact for $h \to \infty$ as they are fixed points of the RG).

In summary, we obtain a *rainbow phase* whose GS is constituted by concentric bonds, two *dimerized phases* that are related to the two phases of the Su-Schrieffer-Heeger (SSH) model (Heeger *et al.* 1988; Su *et al.* 1979) and two *transition phases* whose structure is a blend of the two previous ones and it shall be understood in what follows.

Phase	**Fig. 5.1**	Ground State $\lvert GS\rangle$
Rainbow Phase $\gamma \in (0,1)$	(b)	$\prod_{i=0}^{L-1}\left(b^{\eta_i}_{-i-1/2,i+1/2}\right)^\dagger \lvert 0\rangle\,, \quad \eta_i = (-1)^i$
Dimerized Phase I $\gamma < 0$	(c)	$(b^-_{-L+\frac{1}{2},L-\frac{1}{2}})^\dagger \prod_{i=-\frac{L}{2}+1}^{\frac{L}{2}-1}(b^+_{2i-\frac{1}{2},2i+\frac{1}{2}})^\dagger \lvert 0\rangle$
Dimerized Phase II $\gamma > 1$	(d)	$\prod_{i=-\frac{L-1}{2}}^{\frac{L-1}{2}}(b^+_{2i-\frac{1}{2},2i+\frac{1}{2}})^\dagger \lvert 0\rangle$
Transition Phase I $\gamma = 0$	(e)	$(b^-_{-L+\frac{1}{2},L-\frac{1}{2}})^\dagger \prod_{i=1}^{\frac{L}{4}}(d^{\eta_i}_{2i+\frac{1}{2}})^\dagger (b^+_{-\frac{1}{2},\frac{1}{2}})^\dagger \lvert 0\rangle,$
Transition Phase II $\gamma = 1$	(f)	$\prod_{i=1}^{\frac{L}{2}}(d^{\eta_i}_{2i-\frac{1}{2}})^\dagger \lvert 0\rangle$

Table 5.1: All the possible ground states obtained via the SDRG in terms of the defect amplitude γ. The b operator is given by (5.6) and the d operators are defined in (5.9).

The $d^\pm_k$ operators appearing in Table 5.1 create two particles on four fermionic sites. The explicit form of these operators is given by the the two negative energy modes of the open homogeneous system that we discussed in Chapter (3), i.e. (3.26) particularized to $N = 4$ with energies $\epsilon(u) = -J\cos\frac{\pi}{5}$ and $\epsilon(v) - J\cos\frac{2\pi}{5}$,

$$\begin{aligned}
&(d^{\eta_i}_i)^\dagger = (v^{\eta_i})^\dagger (u^{\eta_{i-1}})^\dagger \lvert 0\rangle\,, \quad \eta_i = (-1)^i,\\
&u^\pm_i = \frac{1}{\sqrt{5+\sqrt{5}}}(c_{-i} \pm c_i) + \frac{1}{\sqrt{5-\sqrt{5}}}(c_{-i+1} \pm c_{i-1}),\\
&v^\pm_i = \frac{1}{\sqrt{5-\sqrt{5}}}(c_{-i} \pm c_i) + \frac{1}{\sqrt{5+\sqrt{5}}}(c_{-i+1} \pm c_{i-1}).
\end{aligned} \tag{5.9}$$

It is worth noticing the existence of a symmetry between the cases $\gamma \le 0$ and $\gamma \ge 1$. Consider a system $H_L(h, \gamma < 1)$. After performing the first RG step, the new

system is described by the renormalized Hamiltonian $H_{L-1}(h, 2-\gamma)$. If we now subtract one from all the log-couplings (or equivalently we divide by e^{-h} all the couplings) the Hamiltonian becomes $e^h H_{L-1}(h, 1-\gamma)$, which describes a system of $N-2$ sites and a defect with strength $1-\gamma$. Hence, the transformation

$$\gamma \to \tilde{\gamma} = 1 - \gamma, \tag{5.10}$$

leaves the structure invariant up to a global constant. Note that this symmetry can be considered as a local strong-weak duality of the defects, leaving the $\gamma = 1/2$ point invariant.

The aforementioned description, along with the evidences obtained by the study of the energies, the correlators and the entanglement entropy, allow us to claim that the rainbow system with a defect presents two *entanglement transitions* (Vasseur *et al.* 2019) in the strong inhomogeneity regime.

5.2.1 Energies

Let us consider the single-body energy levels $E_k(h, \gamma)$ with $k \in \{0, \cdots, N-1\}$ of $H_L(h, \gamma)$, obtained by diagonalizing the corresponding coupling matrix. Due to the particle-hole symmetry, $E_k = -E_{N-k}$, we need only consider values up to $L-1$. For large h, these single-body energy levels correspond to the couplings associated with each valence bond, thus leading us to propose that the following limits are finite,

$$\lim_{h\to\infty} -\frac{\log|E_k(h,\gamma)|}{h} = \Xi_k(\gamma). \tag{5.11}$$

Fig. 5.2 (top) plots these values, $\Xi_k(\gamma)$ as a function of γ for $L = 12$, obtained numerically using $h = 15$ (for which convergence has been achieved). Notice the clear pattern: for $\gamma > 1$, all energy levels are degenerate, $\Xi_{2k}(\gamma) = \Xi_{2k+1}(\gamma) = 2k+1$ for $k \in \{0, \cdots, L/2-1\}$, while for $\gamma < 0$ all energy levels are degenerate and constant, except the first and last which vary exponentially with γ, $\Xi_{2k-1}(\gamma) = \Xi_{2k}(\gamma) = 2k$ for $k \in \{1, \cdots, L/2-1\}$. Indeed, these values correspond to the energies associated to the successive valence bonds of the dimerized phases. On the other hand, for $\gamma \in (0, 1)$ the energy levels are not degenerate, and we can observe the same alternation of the renormalized log-couplings that we observed in the SDRG description: $\Xi_k(\gamma) = k + 1/2 + (-1)^k(\gamma - 1/2)$. Thus, the *transition points*, $\gamma = 0$ and $\gamma = 1$, correspond to the points where the degeneracy starts and ends.

The ground state energy is the sum of the energies of the occupied orbitals, $E_{GS}(h, \gamma) = \sum_{k=0}^{L-1} E_k(h, \gamma)$. Notice that for large h and $\gamma > 1$, the lowest single-body energy $E_0(h, \gamma)$ is the main contribution to $E_{GS}(h, \gamma)$ as its value grows exponentially with γ (see the lowest line of the top panel of Fig. 5.2), so we have considered instead the quantity

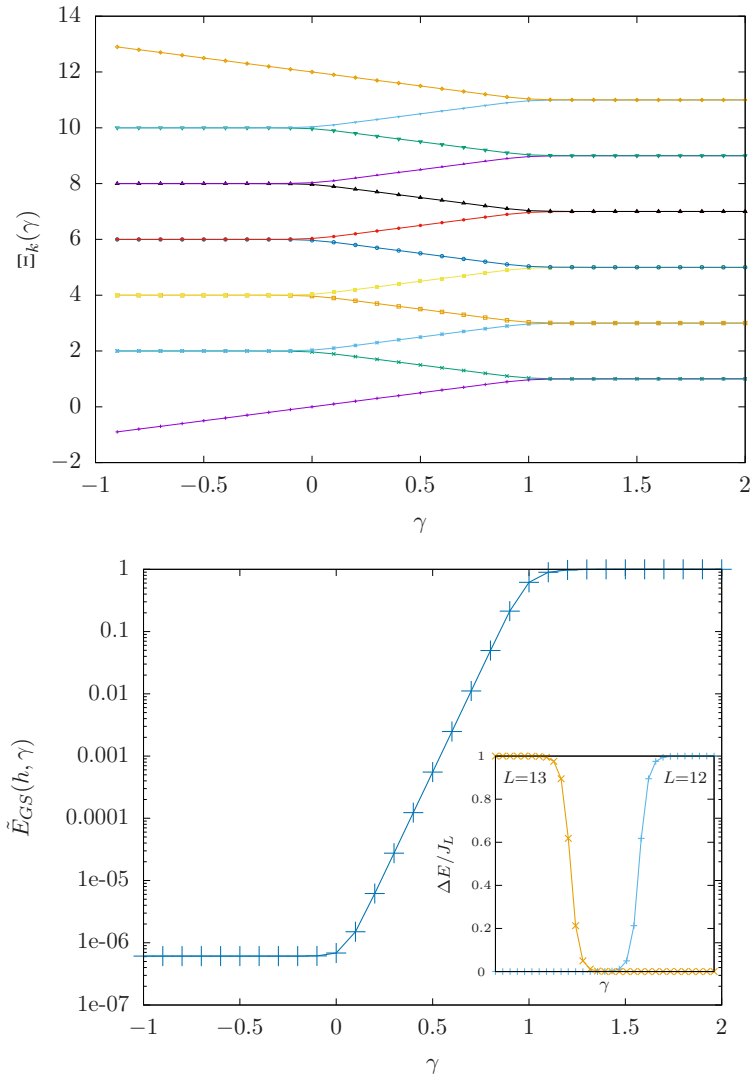

Figure 5.2: Top: plot of $\Xi_k(\gamma)$, obtained numerically for $L = 12$ and $h = 15$, see (5.11). Each curve matches the renormalized log-couplings along the SDRG procedure. Bottom: ground state energy, with the lowest single-body energy level removed, as a function of γ for the same system. Inset: energy gap in units of the lowest energy scale of the system, $\Delta E/J_L$, for $L = 12$ and $L = 13$.

$$\tilde{E}_{GS}(h,\gamma) = -E_{GS}(h,\gamma) + E_0(h,\gamma) = -\sum_{k=1}^{L-1} E_k(h,\gamma). \tag{5.12}$$

The values of $\tilde{E}_{GS}(h,\gamma)$ are plotted in Fig. 5.2 (bottom) for the same system $L = 12$ and $h = 15$, in logarithmic scale. Notice the three regions: for the dimerized phases, $\tilde{E}_{GS}(h,\gamma)$ stays constant, while for the rainbow phase it grows exponentially. Indeed, for $h \to \infty$, the energy curve $\log\big(\tilde{E}_{GS}(h,\gamma)\big)/h$ becomes non-smooth at $\gamma = 0$ and $\gamma = 1$, pointing at a phase transition.

In addition, the inset of Fig. 5.2 (bottom) plots the energy gap $\Delta E/J_L = (E_L - E_{L-1})/J_L$, normalized with the lowest energy scale of the system (the lowest coupling constant). We can see that it presents two types of behaviors, depending

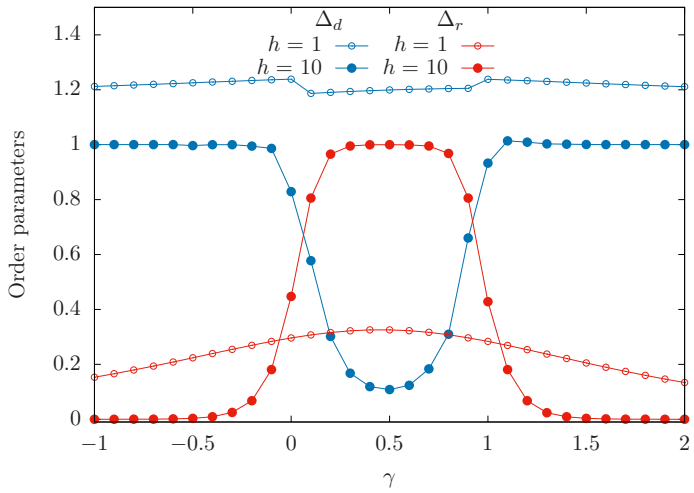

Figure 5.3: Dimerization parameter Δ_d (blue curves) and rainbow parameter Δ_r (red curves) as a function of γ, for a system of $L = 10$. As the inhomogeneity parameter h grows, Δ_d approaches one in the dimerized phases and zero in the rainbow phase, while Δ_r approaches one in the rainbow phase and zero in the dimerized phases.

whether the spectrum has a long range mode (with $E_{L-1}(h,\gamma) = e^{-Lh}$): for even L it is close to zero ($\Delta E/J_L \sim e^{-h}$) for $\gamma < 1$, while for odd L it is close to zero ($\Delta E/J_L \sim e^{-h}$) for $\gamma > 0$. For $\gamma \in [0,1]$, it is close to zero for all sizes.

5.2.2 Correlations and order parameters

In order to provide further support to our idea that there is a phase transition at $\gamma = 0$ and $\gamma = 1$ in the strong inhomogeneity limit, let us provide two order parameters, that we will call the *dimerization parameter*, Δ_d and the *rainbow parameter*, Δ_r,

$$\Delta_d = \frac{1}{N}\sum_{i=-L+\frac{1}{2}}^{L-\frac{1}{2}} |\langle\psi|c_i^\dagger c_{i+1}|\psi\rangle| \tag{5.13}$$

$$\Delta_r = \frac{1}{L}\sum_{i=-\frac{1}{2}}^{L-\frac{1}{2}} |\langle\psi|c_i^\dagger c_{-i}|\psi\rangle|. \tag{5.14}$$

Fig. 5.3 shows the behavior of these two order parameters as a function of γ, for two values of h and $L = 10$. For large h ($h = 10$ in the figure), we see that the rainbow parameter Δ_r tends to 1 in the rainbow phase ($\gamma \in (0,1)$), while it decays to zero in the dimerized phases. The opposite behavior is true for the dimerization parameter Δ_d.

5.2.3 Entanglement entropy

As we have mentioned in the previous chapter, the entanglement entropy of a VBS, can be obtained by counting the number of bonds which are broken when we detach the block from its environment, and multiplying by $\log(2)$, and the same is true for all Rényi entropies. On the other hand, the correlation matrices can be exactly obtained in the strong inhomogeneity limit, as it is shown in Appendix 5.C.

We have considered two different types of blocks: *lateral blocks* start from the extreme of the chain, while *central blocks* are symmetric with respect to the center. In the next paragraphs we will describe the behavior of their entanglement.

Lateral blocks. Half chain entropies

Lateral blocks $A_\ell = \{-L+\frac{1}{2}, \ldots, -L+\frac{1}{2}+\ell\}$ are contiguous blocks containing one of the extremes of the chain. Concretely, we will be interested in the entanglement entropy of the half chain, $S(L) = S[A_L]$ in the strong inhomogeneity regime for different values of γ. Let us remind the reader that we will only consider even L for simplicity, and that the different phases can be visualized either in Fig. 5.1 and Fig. 5.5, where the blocks contain ℓ sites from the upper leg, starting from the right end.

- *Rainbow phase,* $\gamma \in (0,1)$*:* the entanglement entropy (and all other Rényi entropies) are merely proportional to the length up to $\ell = L$, $S[A_\ell]_{\gamma\in(0,1)} = \log(2)\min(\ell, 2L+1-\ell)$.

- *Dimerized phases,* $\gamma < 0$ *or* $\gamma > 1$*:* the lateral blocks cut either zero or one bonds for $\gamma > 1$, $S[A_\ell]_{\gamma>1} = \log(2)(1-(-1)^\ell)/2$; yet, for $\gamma < 0$ there is always a long-distance bond joining both ends, thus $S[A_\ell]_{\gamma<0} = \log(2)\,(1+(1+(-1)^\ell)/2)$.

- *Transition cases:* $\gamma = 0$ *and* $\gamma = 1$*:* The state is not a VBS, so the entanglement entropy of a block can not be evaluated just by counting broken bonds. As we can see in the folded view, Fig. 5.5, the sites are grouped into plaquettes (except, maybe, for the extremes and the central link). Cutting one of these plaquettes horizontally in half contributes a finite amount of entanglement S_a, which is exactly evaluated in Appendix 5.C (see (5.9)):

$$S_a = \log 20 - \frac{4\tanh^{-1}\left(\frac{2}{\sqrt{5}}\right)}{\sqrt{5}} \approx 0.4133, \tag{5.15}$$

  we are thus led to exact expressions for the half-chain entropy:

$$S[A_L]_{\gamma=1} = S_a\, L/2,$$

$$S[A_L]_{\gamma=0} = S_a\,(L/2-1) + 2\log(2).$$

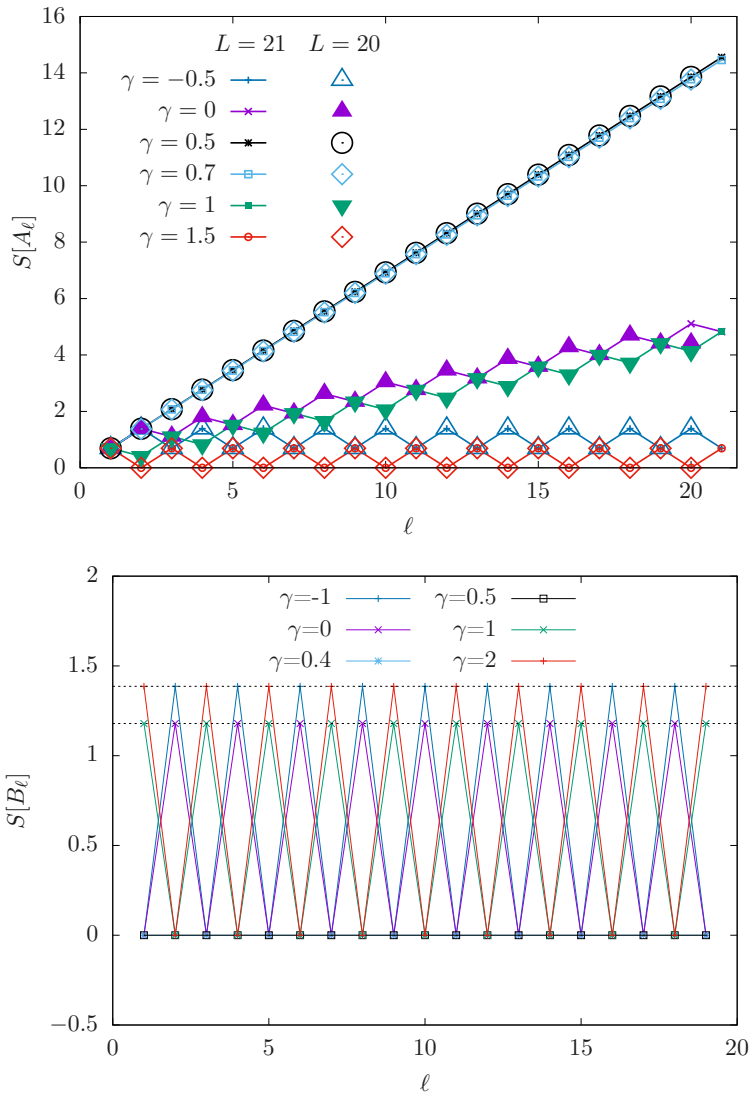

Figure 5.4: Top: Entanglement entropy of blocks of size ℓ using $h = 10$ for two systems, of size $L = 20$ and $L = 21$, for different values of γ. Bottom: entanglement entropy of the central blocks B_ℓ for $L = 20$ sites and $h = 10$. The top horizontal line marks $2 \log 2$, and the lower one marks S_b, see (5.16)

.

All these results can be checked in Fig. 5.4 (top) for two rainbow chains with $L = 20$ and $L = 21$, using $h = 10$, where $S[A_\ell]$ is plotted as a function of ℓ for different values of γ. We can see that the $\gamma = -0.5$ and $\gamma = 1.5$ cases show a properly dimerized behavior, and the $\gamma = 0.5$ values correspond to the rainbow, linear with (maximal) slope $\log(2)$. For the transition points, $\gamma = 0$ and $\gamma = 1$ we can observe a linear behavior (with parity oscillations) with a slope S_a.

Central blocks

The structure of the different phases can be properly understood if we *fold* the chain around the central link, as it is shown in Fig. 5.5 (a), converting the chain

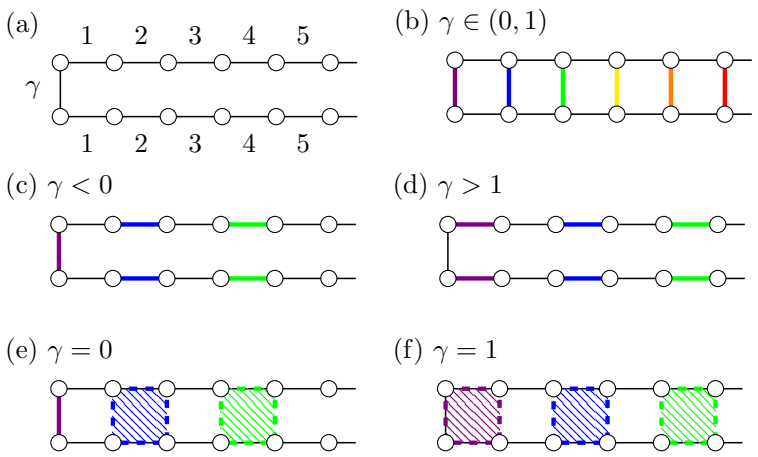

Figure 5.5: (a) Folding the rainbow into a two-rung ladder; (b) folded rainbow structure, obtained for $\gamma \in (0,1)$; (c) and (d) folded dimerized structures, for $\gamma < 0$ and $\gamma > 1$; (e) and (f) folded versions of the transition points, with the plaquettes marked where operators $d^\dagger$ act, see (5.9).

into a two-rung ladder where sites $+k$ and $-k$ face each other. This transformation converts rainbow bonds into vertical bonds and the remaining local bonds into horizontal bonds. The lower panels of Fig. 5.5 present the bond structure as a function of γ.

In this subsection we consider the entanglement entropy of central blocks, symmetrically placed around the center of the chain, $B_\ell = \{-\ell + \frac{1}{2}, \cdots, \ell - \frac{1}{2}\}$. See Fig. 5.5, where the blocks now include ℓ rungs starting from the left extreme.

- *Rainbow phase*, $\gamma \in (0,1)$*:* we always have $S[B_\ell]_{\gamma\in(0,1)} = 0$.

- *Dimerized phases*, $\gamma < 0$ *or* $\gamma > 1$*:* central blocks either cut zero or two bonds. Always using even L we have

$$S[B_\ell]_{\gamma<0} = (1 + (-1)^\ell)\log(2), \quad \text{and}$$

$$S[B_\ell]_{\gamma>1} = (1 - (-1)^\ell)\log(2).$$

- *Transition phases*, $\gamma = 0$ *or* $\gamma = 1$*:* central blocks can cut plaquettes in half vertically, in the folded view. Each such cut contributes a finite amount of entanglement, given by (See Appendix 5.C and (5.9)):

$$S_b = \log 5 - \frac{\coth^{-1}\left(\sqrt{5}\right)}{\sqrt{5}} \approx 1.1790, \tag{5.16}$$

which leads us to the expressions

$$S[B_\ell]_{\gamma=0} = (1 + (-1)^\ell)S_b, \quad \text{and}$$

$$S[B_\ell]_{\gamma=1} = (1 - (-1)^\ell)S_b.$$

All these features can be checked in Fig. 5.4 (bottom), where we can see the central blocks entropy $S[B_\ell]$ as a function of ℓ for different values of γ. Note that the entanglement entropy of the central blocks is always bounded, thus obeying the area law. Non-local fermionic operators of the type $b_{i,-i}$ and d_i (see (5.6) and (5.9)) become local with the folding operation, allowing us to describe the system state using only *short range entanglement* (Samos Sáenz de Buruaga *et al.* 2019). We will discuss this point more in detail in the next chapter.

5.3 Weak inhomogeneity regime

It is relevant to ask whether the phases described in the strong inhomogeneity limit and the corresponding entanglement transitions extend into the weak inhomogeneity regime. The answer is no, but some relevant traits do.

In Fig 5.6 we show the dependence on h of the entanglement entropy of the half chain, $S(L) = S[A_L]$, for different values of γ. We can observe a perfect symmetry between γ and $1-\gamma$, and the three different trends in the large h limit that we have explained on the previous section: for $\gamma \in (0,1)$ the EE reaches its maximal value; for $\gamma \in \{0,1\}$, it reaches an intermediate value ($S_a L/2$); for $\gamma \notin [0,1]$, it stays at $\log(2)$. Interestingly, the behavior is remarkably different for lower values of h, as we will discuss.

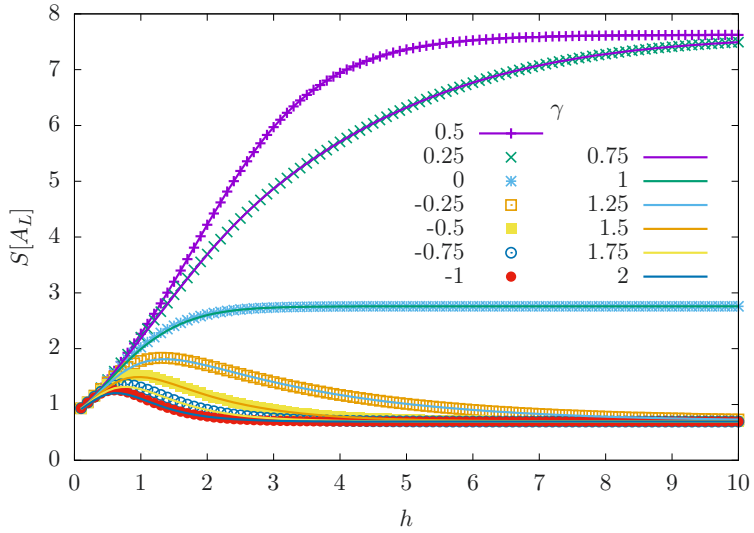

Figure 5.6: EE of the half system $N = 22$ as a function of h for different values of the defect strength γ.

For $h = 0$ the Hamiltonian (5.2) becomes the standard massless free-fermionic chain with open boundary conditions which can be described at low energies by a conformal field theory (CFT) with $c = 1$ as we shown in 3.1.3. It is interesting to discuss first such a system in presence of a defect.

5.3.1 Homogeneous chain with defect

Let us consider an open homogeneous free fermionic chain and a defect on its central link, parametrized by a coupling parameter τ,

$$H_\tau = -\frac{\tau}{2} c^\dagger_{-\frac{1}{2}} c_{\frac{1}{2}} - \frac{1}{2} \sum_{n=1/2}^{L-3/2} c^\dagger_n c_{n+1} + c^\dagger_{-n} c_{-n-1} + \text{h.c.} \tag{5.17}$$

Let us take the continuum limit of (5.17) and characterize its low-energy properties by expanding the local operators c_n into slow left/right moving components $\psi_{\{L,R\}}$ around the Fermi points, and introducing a physical coordinate $x = an$, with lattice constant $a \to 0$, while $L \to \infty$ with $\mathcal{L} = aL$ fixed.

$$c_m \approx \sqrt{a} \left(e^{ik_F x} \psi_L(x) + e^{-ik_F x} \psi_R(x) \right). \tag{5.18}$$

The boundary conditions satisfied by the fields at the edge boundaries $\psi_{L,R}(\pm\mathcal{L})$ are obtained by imposing $c_{\pm(L+\frac{1}{2})} = 0$:

$$\psi_L(\pm\mathcal{L}) = e^{i\pi(L\pm\frac{1}{2})} \psi_R(\pm\mathcal{L}). \tag{5.19}$$

In order to characterize the effect of the defect τ, we need to distinguish between the fields on the left side $\psi^I_{L,R}$ and the right side $\psi^{II}_{L,R}$ of the defect, which are related by a transfer matrix $\psi^I = T\psi^{II}$ (see Appendix 5.D):

$$\begin{pmatrix} \psi^I_L \\ \psi^I_R \end{pmatrix} = \frac{1}{2\tau} \begin{pmatrix} \tau^2+1 & -i(\tau^2-1) \\ i(\tau^2-1) & \tau^2+1 \end{pmatrix} \begin{pmatrix} \psi^{II}_L \\ \psi^{II}_R \end{pmatrix}. \tag{5.20}$$

It is important to realize that T *only* depends on the defect and a vicinity of radius a (lattice sites $\pm\frac{1}{2}$ and $\pm\frac{3}{2}$). Also notice that for $\tau = 1$, $T = \mathbb{I}$. Following Sierra (2014), we can associate this transfer matrix to the one associated with a massless Dirac fermion with a δ term associated to a mass m and to a chiral mass m',

$$T_D = \frac{1}{1 - r^2 - r'^2} \begin{pmatrix} 1 + r^2 + r'^2 & 2(ir + r') \\ 2(-ir + r') & 1 + r^2 + r'^2 \end{pmatrix}, \tag{5.21}$$

where $r \propto m$ and $r' \propto m'$ are the reflection coefficients associated to both terms. If we assume $r' = 0$ and compare with (5.20) we find that

$$r = \frac{1-\tau}{\tau+1}. \tag{5.22}$$

Hence, the field theory associated to the homogeneous system in presence of a defect (5.17) is a massless Dirac fermion with a δ potential term that mixes the left and right moving fermions generating a *local* mass placed at the center.

The entanglement properties of this system were studied by Eisler and Peschel (2010). The authors used a conformal mapping to an isotropic 2D classical model to show that the entanglement entropy of the half chain presents a logarithmic

behavior, as predicted by CFT, but with a coefficient that depends on the strength of the defect which they called *effective central charge*:

$$S(L) = \frac{c_{\text{eff}}}{6} \log L + c', \tag{5.23}$$

with

$$c_{\text{eff}} = \frac{6}{\pi^2} I(s), \tag{5.24}$$

and $I(s)$ given by (see Eq. (26) of Eisler and Peschel (2010)):

$$I(s) = -\frac{1}{2}\left[\left((1+s)\log(1+s) + (1-s)\log(1-s)\right)\log s \right. \\ \left. + (1+s)\text{Li}_2(-s) + (1-s)\text{Li}_2(s)\right],$$

with $s = \sin(2\arctan\tau)$ and $\text{Li}_2(z)$ is the dilogarithm function (Abramowitz and Stegun 1972).

5.3.2 Field theory of the rainbow model with a defect

Let us return to our rainbow model with a defect. In order to build the field theory describing the low energy physics of Hamiltonian (5.2) in the weak inhomogeneity regime we need to obtain the transfer matrix $T_{h,\gamma}$ associated to the defect. Since the defect is local, we will conjecture that $T_{h,\gamma}$ is determined by the defect and its closest vicinity (see Appendix 5.D):

$$T_{h,\gamma} = \frac{1}{2} e^{h(\gamma-\frac{1}{2})} \begin{pmatrix} e^{-2h(\gamma-\frac{1}{2})}+1 & -i\left(e^{-2h(\gamma-\frac{1}{2})}-1\right) \\ i\left(e^{-2h(\gamma-\frac{1}{2})}-1\right) & e^{-2h(\gamma-\frac{1}{2})}+1 \end{pmatrix}. \tag{5.25}$$

Note that $T_{h,\gamma} = T$ described in (5.20) if we define

$$\tau = e^{-h(\gamma-1/2)}. \tag{5.26}$$

Notice that the symmetry $\gamma \to 1-\gamma$ described in the previous section is also present in the transfer matrix: $T_{h,1-\gamma}$ is $T_{h,\gamma}$ with opposite signs in the non diagonal terms and that $\tau = 1$ if $h = 0$ but also if $\gamma = \frac{1}{2}$. This implies that the defect has no effect in $H_L(h, \frac{1}{2})$ or, in other terms, we will say that the defect is *absent*. Indeed, evaluating the continuum limit of (5.18) over (5.2) leads to the effective Hamiltonian (4.43) discussed in the previous chapter

$$H \approx i \int_{-\tilde{L}}^{\tilde{L}} d\tilde{x} \left[\tilde{\psi}_L^\dagger \partial_{\tilde{x}} \tilde{\psi}_L - \tilde{\psi}_R^\dagger \partial_{\tilde{x}} \tilde{\psi}_R\right], \tag{5.27}$$

where $\tilde{x}$ is given by (see (4.41))

$$\tilde{x} \equiv \text{sign}(x) \frac{e^{h|x|}-1}{h}, \tag{5.28}$$

As a consequence, the field theory associated to the Hamiltonian $H_L(h, \gamma \neq \frac{1}{2})$ for low energies should be described by a free Dirac theory with a local defect –which is analogous to the one studied in the previous subsection– but in the background metric described above. In what follows we show that this is the case by studying the entanglement properties such as the entanglement entropy, the entanglement spectrum, the entanglement Hamiltonian and the entanglement contour.

5.3.3 Entanglement entropy

The case of the absence of defect, $\gamma = \frac{1}{2}$, has been discussed in the previous chapter (see Section 4.2.1). The entanglement entropy can be evaluated can be evaluated for intervals of the form $A = [-L, x]$ within a 2D CFT by making an appropriate use of transformation (5.28). Let us recall that besides the transformation of L and x, we need to take into account the transformation of the UV cutoff, a, through the Weyl factor (4.55), $\tilde{a} = e^{-h|x|}a$ in our metric. We obtain the expression (4.56).

Here we will focus exclusively on the universal contribution of the entanglement entropy and we shall neglect the non-universal terms. The half chain entanglement entropy scales linearly (4.58):

$$S_{\gamma=\frac{1}{2}}(L) \approx \frac{c\,hL}{6}. \tag{5.29}$$

However, the defect ($\gamma \neq \frac{1}{2}$) creates a mass and introduces a scale, breaking the conformal invariance of the system. As a consequence, the previous formulae can not be applied to compute the EE. Nevertheless, the entanglement entropy should follow (5.24), with the modifications associated to the change of background. Indeed, we should modify (5.29) as

$$S_\gamma(L) \approx \frac{c_{\text{eff}}(\tau)\,hL}{6} \tag{5.30}$$

where τ is given by (5.26). In order to check this, we have obtained the *entropy per site*, defined for convenience as

$$s(h, \gamma) = \lim_{L\to\infty} \frac{6S[A_L]}{L}. \tag{5.31}$$

The values of $s(h, \gamma)$ are obtained through a linear fit. Fig. 5.7 (top) shows this entropy per site as a function of h for several values of γ. For very low values of h, all curves seem to collapse. Yet, for $\gamma \notin [0, 1]$, the curve $s(h)$ eventually presents a maximum and decays to zero. This is a signature that the system will obey the area law in the strong inhomogeneity limit. The validity of (5.30) can be checked with the soft continuous lines, which correspond to the theoretical prediction. Indeed, for low values of h the prediction is very accurate, losing this accuracy for large inhomogeneity ($h \approx 1.5$).

Furthermore, (5.30) suggests that the entropy per site will collapse if we plot $s(h, \gamma)/h$ as a function of a measure of the defect intensity, $h(\gamma - 1/2)$. Indeed, this

collapse can be seen in the bottom panel of Fig. 5.7, showing the universal curve for $c_{\text{eff}}(\tau)$. The high accuracy of this collapse can be checked in the inset, which shows the same data in logarithmic scale. Moreover, the circles correspond to the plot of c_{eff} in (5.24) as a function of $\log(\tau)$, for comparison.

5.3.4 Phase diagram

In Fig. (5.8) we show the relative error between the theoretical prediction and the numerics

$$\delta s(h,\gamma) = \frac{|s(h,\gamma) - h c_{\text{eff}}|}{s(h,\gamma)}, \tag{5.32}$$

in the color intensity. The white lines correspond to the theoretical values of the relative maxima of $s(h,\gamma)$ as a function of h, following (5.30). Notice that the theoretical prediction states that, for all γ, the curve $s(h)$ will present a maximum and decay to zero afterwards. Thus, weak inhomogeneity regime presents a smooth crossover into the three phases of the strong inhomogeneity regime described in the previous section. For large h lattice effects become dominant and the universal properties predicted by the field theory approach are lost.

5.3.5 Beyond entanglement entropy

Having studied the entanglement entropy, and proceeding analogously to what we did in the previous chapter, let us study the entanglement Hamiltonian, the entanglement spectrum (ES), and the contour.

Entanglement Hamiltonian

The entanglement Hamiltonian (see 3.3.1) H_A is approximately local for a 1+1D CFT (Cardy and Tonni 2016; Tonni *et al.* 2018). Indeed, it can be written as (3.93)

$$H_A \approx \sum_i \beta_A(i)\; c_i^\dagger c_{i+1}, \tag{5.33}$$

where the $\beta_A(i)$ constitute entanglement couplings and we neglect the terms that describe long-range interactions since they are expected to be very small. The estimation of the set of $\{\beta_A(i)\}$ is obtained by minimizing an error function (3.94) using standard optimization techniques (Tonni *et al.* 2018).

The numerical values of $\{\beta(i)\}$ for the left half (block A_L) of a $L = 20$ system, using $h = 0.5$ and different values of γ are shown in Fig. 5.9. For $\gamma = 1/2$ the EH of the rainbow system presents flat coefficients $\beta(i)$ everywhere except near the physical boundary (left extreme) and near the internal boundary (right extreme), where it follows the Bisognano-Wichmann prediction, that they will decay to zero linearly, with slope 1. Yet, in presence of a defect we observe an increasing *dimerization* of the EH.

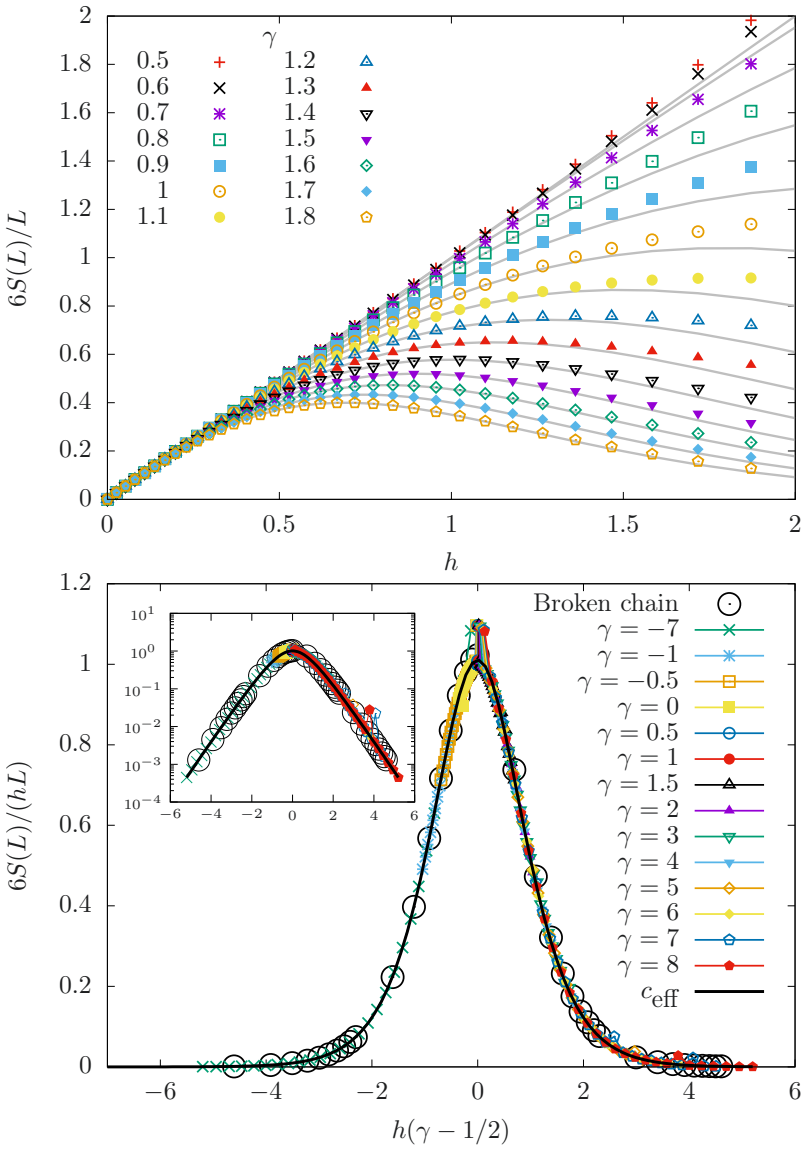

Figure 5.7: Top: Entropy per site of the rainbow model with a defect, $s(h, \gamma)$ as a function of h, for different values of γ. Soft continuous lines correspond to the theoretical prediction, (5.30). Bottom: entropy per site divided by the inhomogeneity parameter, as a function of the defect intensity, $h(\gamma - 1/2)$, showing the collapse predicted by (5.30).

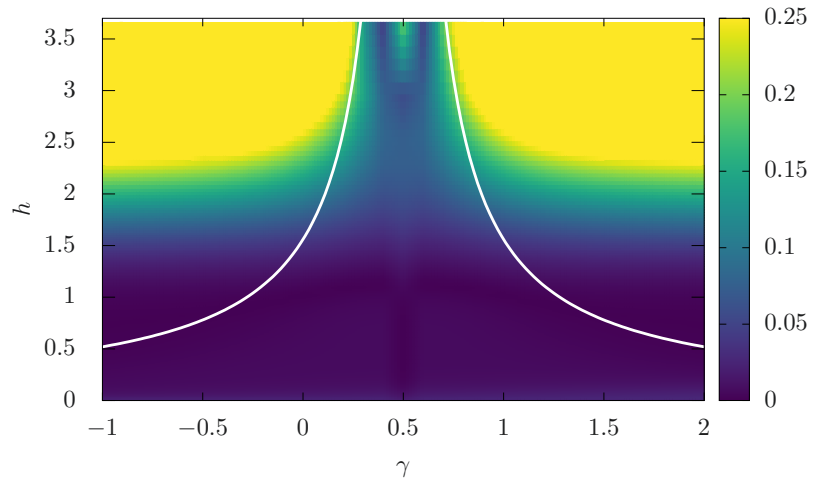

Figure 5.8: Phase diagram, absolute error of the entanglement entropy prediction; the white lines correspond to the local maximum of the entropy density, $s(h)$.

Let us remind the reader that the flat profile for $\{\beta(i)\}$ in the rainbow case accounts for the fact that the rainbow GS for all values of h resembles a *thermofield double* (see (4.68) and discussion below) as was shown by Ramírez *et al.* (2015) and Tonni *et al.* (2018)

$$|\Psi\rangle \approx \sum_n \exp(-\beta E_n/2)\,|n\rangle_L \otimes |n\rangle_R\,, \tag{5.34}$$

where E_n and $|n\rangle_{\{L,R\}}$ are the energies and eigenstates of the homogeneous free Hamiltonian on the left/right with open boundaries. Thus, we are led to the following claim: in presence of a defect, the ground state of Hamiltonian (5.2) is still approximately a thermofield double, but of a *dimerized* Hamiltonian, with dimerization parameter associated to the defect strength γ.

We would like to stress that the cases of γ and $1-\gamma$ are extremely similar, only interchanging the higher and lower values of the dimerization pattern.

Entanglement Spectrum

We have considered the full entanglement spectrum of the left half block, A_L, for different values of γ. It is obtained in terms of the eigenvalues $\{\nu_k\}_{k=1}^{L}$ of the block correlator matrix (3.89). As it can be expected, the defect preserves the particle-hole symmetry. The most salient feature is that the entanglement spectrum shows a finite gap $\Delta\epsilon$ whose width grows with γ, as can be seen in Fig. 5.10 (top). Let us recall that the entanglement gap, $\Delta\epsilon \sim 1/\log(L)$ for a CFT system, but for a deformed system such as the rainbow we should consider instead $\Delta\epsilon \sim 1/\log\big(\tilde{L}\big) \sim 1/L$. Indeed, for low h the gap decays linearly with the system size, as we can see on the bottom panel of Fig. 5.10 for $h = 0.015$, but it seems to reach a finite value for $h = 0.32$.

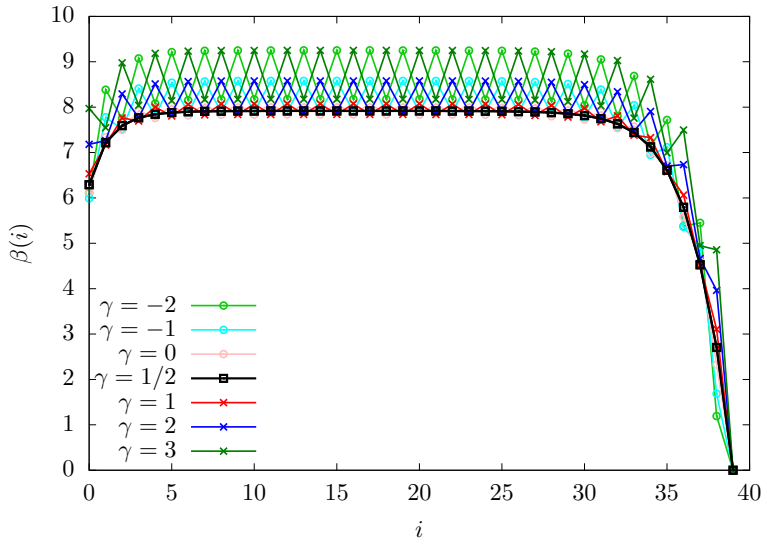

Figure 5.9: Entanglement Hamiltonian coefficients $\{\beta(i)\}$ for the left half of a $L = 20$ rainbow with a defect, using $h = 0.5$. Notice that, for $\gamma = 1/2$ the bulk is flat, as expected, but for the other values the Hamiltonian coefficients present dimerization, which changes the high and low values when we change γ for $1 - \gamma$.

Entanglement Contour

With respect to the entanglement contour (see 3.3.3), we use the expression (3.102) provided by Chen and Vidal (2014). Fig. 5.11 shows the curve of the entanglement contour for the left block of the rainbow GS using $L = 40$ and $h = 0.5$, for different values of γ, scaled with the entropy density predicted in (5.30). The collapse is very clear in the bulk region, which presents universal features, and a little bit less near the boundary, where it does not. Importantly, notice that the entanglement contour does not present any oscillations related to dimerization, with a constant entropy per site in the bulk.

5.4 Conclusions

In this chapter we have characterized a lattice model of Dirac fermions on a negatively curved background in presence of a local defect. The unperturbed lattice model is the *rainbow model* that we have introduced in Chapter 4. The presence of a defect in the center of the chain can induce an entanglement transition in the strong inhomogeneity limit, characterized by a rainbow phase of linear scaling of entanglement for intermediate defect strengths, and two dimerized phases, with alternate dimerizations in similarity with the SSH model. Further hints of the transition are provided by the ground state energy, the single-body orbitals, the energy gap (rescaled with the minimum coupling) and two order parameters: the average dimerization and the *rainbow order parameter*, which measures the average occupation of the concentric bonds.

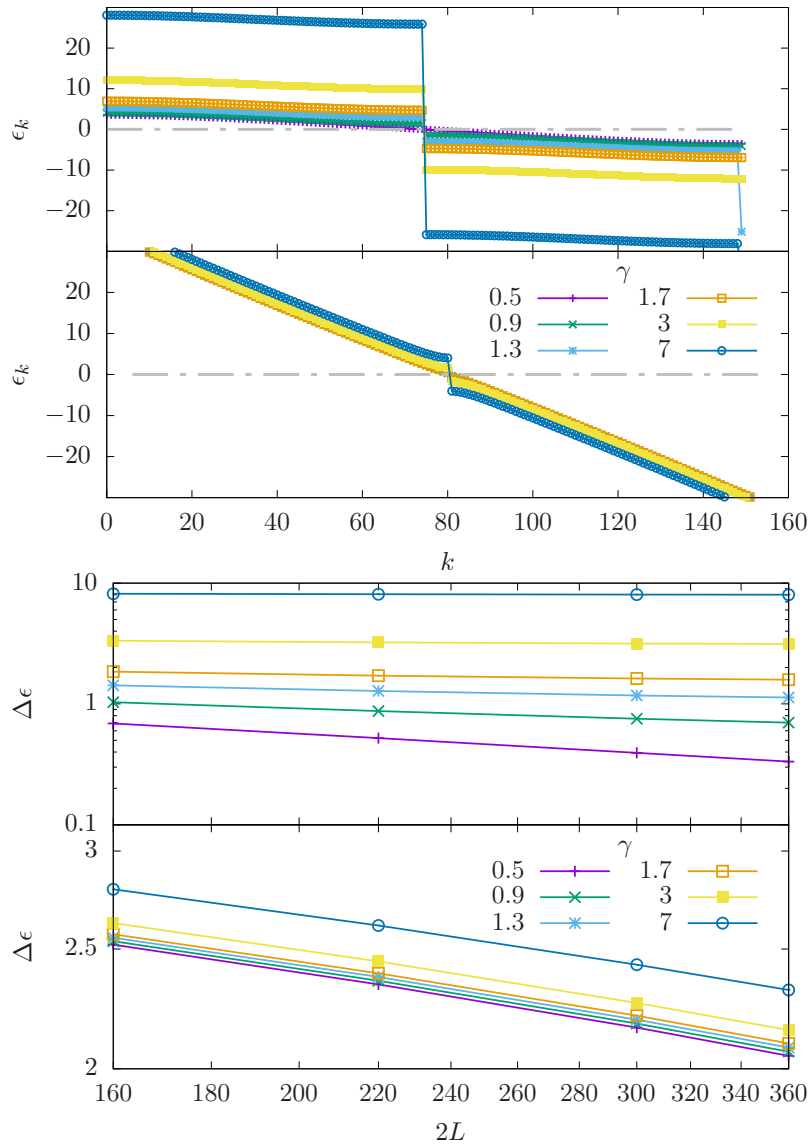

Figure 5.10: Top: Entanglement spectrum ϵ_k of the left block of a system with $L = 150$ and different values of γ. Upper panel: $h = 0.32$, lower panel: $h = 0.015$. Bottom: Scaling of the entanglement spectrum gap $\Delta\epsilon$ with size $2L$ for different values of γ. The upper panel shows the case $h = 0.32$, and the lower panel $h = 0.015$.

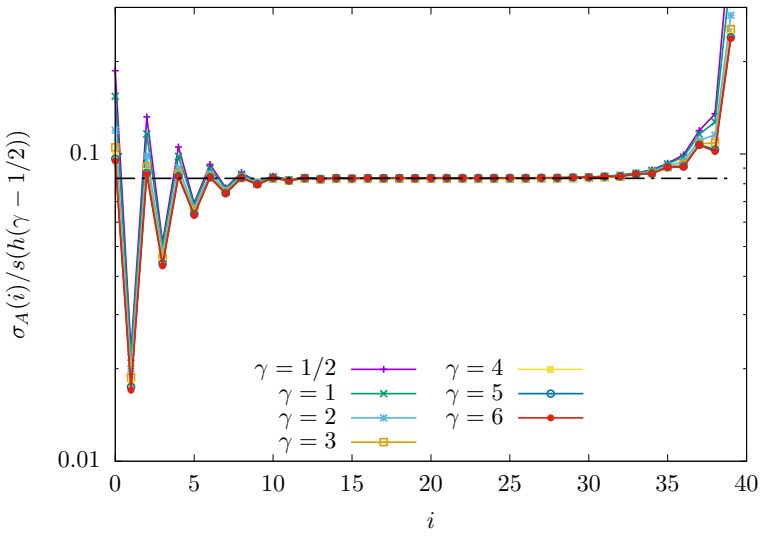

Figure 5.11: Entanglement contour of the left half (the left edge is the physical boundary while the right one is originated by the block) of the rainbow model with a defect using $L = 40$ and $h = 0.5$, scaled with the entropy per site predicted in (5.30), for different values of γ.

In the weak inhomogeneity limit, the transition gets blurred, and the ground state always presents linear entanglement, with an entropy per site that can be effectively described by a geometric deformation of the entanglement entropy of a homogeneous fermionic chain with a central defect. Analysis of the entanglement gap and the entanglement Hamiltonian allows us to claim that the system behaves as a thermofield double, as in the rainbow case, but with a dimerized Hamiltonian instead of a homogeneous one.

This work opens up several interesting questions related to the presence of geometric defects on the vacuum structure of a quantum field theory. It is interesting to ask whether such a deep modification of the entanglement properties can be found in other cases.

Appendices

5.A Details of the application of the SDRG

In this appendix we detail the obtainment of the ground states by using the SDRG. For our purposes, it is convenient to consider the log-couplings (5.7). Interestingly, the log-couplings SDRG rule (5.8) can be generalized for this type of models: whenever a bond is established between sites p and q (with $p+q$ even), the renormalized log-coupling is given by the *sum rule* (Alba *et al.* 2019):

$$\tilde{t}_{[p,q]} = \sum_{j=0}^{q-p-1} (-1)^j t_{p+j}, \tag{5.A.1}$$

or, in other words: the renormalized log-coupling can be obtained summing all log-coupling between the two extremes, with alternating signs. We shall distinguish:

- *The rainbow phase:* $\gamma \in (0,1)$, see Fig. 5.1 (b). The strongest link (lowest log-coupling) is the central one. Thus, a valence bond is established on top ($b^{+}_{-1/2,+1/2}$) and an effective log-coupling appears between its neighbors, of magnitude $\tilde{t} = 2-\gamma < 2$. Thus, the central link is again the strongest one, so we can put a valence-bond on top of it ($b^{-}_{-3/2,+3/2}$), leading to an effective log-coupling of magnitude $\tilde{t} = 2+\gamma < 3$. We can see that the procedure iterates, giving rise to the rainbow state.

$$|GS\rangle_{\gamma\in(0,1)} = \prod_{i=0}^{L-1} \left(b^{\eta_i}_{-i-1/2,i+1/2}\right)^{\dagger} |0\rangle\,, \quad \eta_i = (-1)^i. \tag{5.A.2}$$

- *The dimerized phase (I):* $\gamma < 0$, see Fig. 5.1 (c). The dominant interaction is again the central one, leading us to establish a valence bond on top. Yet, the renormalized log-coupling, $\tilde{t} = 2-\gamma > 2$ is not the strongest (lowest value) at the next SDRG iteration. On the other hand, we are led to establish two valence bonds on top of the links with log-couplings equal to 2, in any order. The renormalized central log-coupling after these two bonds have been established is $\tilde{t} = 4-\gamma > 4$ (see (5.A.1)), so we are led to the same situation, where the lateral links are always stronger than the central one, leading to a *dimerized state*. Yet, the last SDRG step leaves us with the two extreme sites of the chain, leading to a final bond connecting them. The ground state can be written as

$$|GS\rangle_{\gamma<0} = (b^{-}_{-L+\frac{1}{2},L-\frac{1}{2}})^{\dagger} \prod_{i=-\frac{L}{2}+1}^{\frac{L}{2}-1} (b^{+}_{2i-\frac{1}{2},2i+\frac{1}{2}})^{\dagger} |0\rangle \,. \tag{5.A.3}$$

Notice that the last bond is only present for even L, while it is absent for odd L.

- *The dimerized phase (II):* $\gamma > 1$, see Fig. 5.1 (d). In this case, the dominant interaction is *not* the central one, but their neighbors, with $t_{\pm 1} = 1$. Hence, we must establish first these two valence bonds, leading to a renormalized log-coupling between their extremes of $\tilde{t} = 2 + \gamma > 3$ (see (5.A.1)). Thus, we have the same situation, in which the central link is not the strongest. In this case, no long-range bond is established at the end of the procedure, and we obtain

$$|GS\rangle_{\gamma>1} = \prod_{i=-\frac{L-1}{2}}^{\frac{L-1}{2}} (b^{+}_{2i-\frac{1}{2},2i+\frac{1}{2}})^{\dagger} |0\rangle \,. \tag{5.A.4}$$

- *The transition points:* $\gamma = 1$ *and* $\gamma = 0$, see Fig. 5.1 (e) and (f). Let us start with $\gamma = 1$ (Fig. 5.1 (e)). The first SDRG step fails, because the strongest coupling is not unique. On the other hand, we obtain a *triple tie* in the three central links, with $t_{0,\pm 1} = 1$. In Appendix 5.B we have developed an extension of the SDRG for the free-fermion model when a block with 2ℓ sites is integrated out, yielding the renormalized log-coupling given by the sum rule, (5.A.1). Thus, the renormalized log-coupling between sites $-5/2$ and $+5/2$ is $\tilde{t} = 3$, leading to a new triple tie, which propagates further along the chain. For $\gamma = 0$, on the other hand, the strongest link is the central one, thus receiving a valence bond. But, on the next SDRG step, we can see that the effective central log-coupling is $\tilde{t} = 2$, equal to its neighbors in a new *triple tie*, forcing us to recourse to the extended SDRG. From that moment on, all SDRG steps lead to triple ties. The ground states take the form

$$|GS\rangle_{\gamma=0} = (b^{-}_{-L+\frac{1}{2},L-\frac{1}{2}})^{\dagger} \prod_{i=1}^{\frac{L}{4}} (d^{\eta_i}_{2i+\frac{1}{2}})^{\dagger} (b^{+}_{-\frac{1}{2},\frac{1}{2}})^{\dagger} |0\rangle \,, \tag{5.A.5}$$

$$|GS\rangle_{\gamma=1} = \prod_{i=1}^{\frac{L}{2}} (d^{\eta_i}_{2i-\frac{1}{2}})^{\dagger} |0\rangle \,, \tag{5.A.6}$$

where $d^{\pm}_{k}$ are operators creating two particles on four fermionic sites given by (5.9).

5.B Dasgupta-Ma RG extension for free fermions

In this Appendix we describe a generalization of the Dasgupta-Ma RG for inhomogeneous free fermionic chains that can be applied to systems that have an homogeneous subchain of $N = 2L$ sites embedded. The Hamiltonian H_0 that describes this subchain is given by

$$H_0 = -\frac{J}{2}\sum_{i=1}^{N-1} c_i^\dagger c_{i+1} + c_{i+1}^\dagger c_i, \tag{5.B.1}$$

and its interactions with the nearest neighbours is given by H_{lr}

$$H_{lr} = -J_l c_l^\dagger c_1 - J_r c_N^\dagger c_r + \text{h.c.}. \tag{5.B.2}$$

Assuming that $J_l \ll J$ and $\frac{J_l}{J_r} \approx 1$ the whole system can be study by means of degenerate perturbation theory. The ground state of H_0 is given in the previous Appendix (see (**??**)) $|\psi_0\rangle = \prod_{m=1}^{L} \hat{\phi}_{k_m}^\dagger |0\rangle$ with energy $E_0 = \sum_{m=1}^{L} \epsilon_{k_m} = -2\sum_{m=1}^{L} \cos\left(\frac{m\pi}{N+1}\right)$. The first order correction $\langle\psi_0; l', r'|H_{lr}|\psi_0; l, r\rangle$ (where $|\psi_i; l, r\rangle = |\psi_i\rangle \otimes |l\rangle \otimes |r\rangle$) vanishes. The matrix element $B_{l,r;l'r'}$ of the degenerate second order contribution is given by:

$$B_{l,r;l'r'} = \sum_{i\neq 0}\sum_{l''r''} \frac{\langle\psi_0; l, r|H_{lr}|\psi_i; l'', r''\rangle \langle\psi_i; l'', r''|H_{lr}|\psi_0; l', r'\rangle}{E_0 - E_i} \tag{5.B.3}$$

Expanding this product and taking into account that $\sum_{l''r''} |l'', r''\rangle \langle l'', r''| = \mathbb{I}$ we have:

$$\begin{aligned}
B_{l,r;l'r'} = J_l^2\Big(&\langle l, r|c_l^\dagger c_l|l', r'\rangle \sum_{i=1}^{N} \frac{\langle\psi_0|c_1|\psi_i\rangle \langle\psi_i|c_1^\dagger|\psi_0\rangle + \langle\psi_0|c_1^\dagger|\psi_i\rangle \langle\psi_i|c_1|\psi_0\rangle}{\epsilon_{k_i}} \\
&- \sum_{i=1}^{N} \frac{\langle\psi_0|c_1^\dagger|\psi_i\rangle \langle\psi_i|c_1|\psi_0\rangle}{\epsilon_{k_i}}\Big) + \\
J_r^2\Big(&\langle l, r|c_r^\dagger c_r|l', r'\rangle \sum_{i=1}^{N} \frac{\langle\psi_0|c_N|\psi_i\rangle \langle\psi_i|c_N^\dagger|\psi_0\rangle + \langle\psi_0|c_N^\dagger|\psi_i\rangle \langle\psi_i|c_N|\psi_0\rangle}{\epsilon_{k_i}} \\
&- \sum_{i=1}^{N} \frac{\langle\psi_0|c_N^\dagger|\psi_i\rangle \langle\psi_i|c_N|\psi_0\rangle}{\epsilon_{k_i}}\Big) + \\
J_l J_r\Bigg(&\langle l, r|c_l^\dagger c_r|l', r'\rangle \sum_{i=1}^{N} \frac{\langle\psi_0|c_1|\psi_i\rangle \langle\psi_i|c_N^\dagger|\psi_0\rangle + \langle\psi_0|c_N^\dagger|\psi_i\rangle \langle\psi_i|c_1|\psi_0\rangle}{\epsilon_{k_i}} + \\
&\langle l, r|c_r^\dagger c_l|l', r'\rangle \sum_{i=1}^{N} \frac{\langle\psi_0|c_N|\psi_i\rangle \langle\psi_i|c_1^\dagger|\psi_0\rangle + \langle\psi_0|c_1^\dagger|\psi_i\rangle \langle\psi_i|c_N|\psi_0\rangle}{\epsilon_{k_i}}\Bigg),
\end{aligned} \tag{5.B.4}$$

Where the non vanishing contributions are given by the excited states whose particle number differs by one with respect to $|\psi_0\rangle$:

$$\langle\psi_i|c_i^\dagger|\psi_0\rangle \neq 0 \quad \text{if} \quad |\psi_i\rangle = \hat{\phi}_{k_i}|\psi_0\rangle, \quad E_i = E_0 - \epsilon_{k_i}, \tag{5.B.5}$$

$$\langle\psi_i|c_i|\psi_0\rangle \neq 0 \quad \text{if} \quad |\psi_i\rangle = \hat{\phi}_{k_i}^\dagger|\psi_0\rangle, \quad E_i = E_0 + \epsilon_{k_i}\ . \tag{5.B.6}$$

Given that $c_i = \sum_{m=1}^{N} U_{im}\hat{\phi}_{k_m}$ we reach

$$\begin{aligned} B_{l,r;l'r'} =& J_l^2 \left(\langle l, r|c_l^\dagger c_l|l', r'\rangle \sum_{i=1}^{N} \frac{|U_{1m}|^2}{\epsilon_{k_m}} + \sum_{i=1}^{L} \frac{|U_{1m}|^2}{\epsilon_{k_m}} \right) \\ &+ J_r^2 \left(\langle l, r|c_r^\dagger c_r|l', r'\rangle \sum_{i=1}^{N} \frac{|U_{Nm}|^2}{\epsilon_{k_m}} + \sum_{i=1}^{L} \frac{|U_{Nm}|^2}{\epsilon_{k_m}} \right) + \\ & J_l J_r \left(\langle l, r|c_l^\dagger c_r|l', r'\rangle \sum_{i=1}^{N} \frac{U_{1m}U_{mN}^*}{\epsilon_{k_m}} + \langle l, r|c_r^\dagger c_l|l', r'\rangle \sum_{i=1}^{N} \frac{U_{Nm}U_{m1}^*}{\epsilon_{k_m}} \right). \end{aligned} \tag{5.B.7}$$

Now, particularizing for the single-body modes (3.26) we obtain that the renormalized Hamiltonian B is (up to an additive constant):

$$H_{eff} = -\frac{J_l J_r}{J} \left(c_l^\dagger c_r + \text{h.c} \right), \tag{5.B.8}$$

which is the expression used to renormalize the systems with strength defects $\gamma = 0$ and $\gamma = 1$.

5.C Correlation matrices and entanglement entropy

The correlation matrices C for the ground states (5.A.2)-(5.A.6) can be obtained using (4.A.15)

$$C_{ij} = \sum_{k=1}^{N_F} U_{ik}U_{jk}^*,$$

where we consider half filling and $\hat{\phi}_m$ are the fermionic excitations of each system ($b_{i,j}$ (5.6) and d_i (5.9) in our case) and U_{ik} is a unitary matrix.

We shall next describe the correlation matrices as a function of the defect parameter γ. All the matrices are symmetric $C_{i,j} = C_{j,i}$ and present left-right symmetry $C_{i,j} = C_{N+1-j,N+1-i}$. All the computations are done with L even.

- $\gamma < 0$:

$$\begin{cases} C_{i,i} = \frac{1}{2}, \quad i = 1, \dots, L \\ C_{1,N} = -\frac{1}{2}, \\ C_{2i,2i+1} = \frac{1}{2}, \quad i = 1, \dots \frac{L}{2}, \end{cases} \tag{5.C.1}$$

- $\gamma = 0$:

$$\begin{cases} C_{1,N} = -\frac{1}{2}, \quad C_{L,L+1} = \frac{1}{2} \\ C_{i,i} = \frac{1}{2}, \quad i = 1, \dots, L \\ C_{i,N+1-i} = (-1)^i \frac{1}{2\sqrt{5}}, \quad i = 2, \dots, L-1 \\ C_{2i,2i+1} = \frac{1}{\sqrt{5}}, \quad i = 1, \dots \frac{L}{2}, \end{cases} \tag{5.C.2}$$

- $\gamma \in (0,1)$:

$$C_{i,j} = \frac{1}{2}\delta_{i,i} + (-1)^i \frac{1}{2}\delta_{i,N+1-i}, \tag{5.C.3}$$

- $\gamma = 1$:

$$\begin{cases} C_{i,i} & = \frac{1}{2}, \quad i = 1,\dots,L \\ C_{i,N+1-i} & = (-1)^i \frac{1}{2\sqrt{5}}, \quad i = 1,\dots,L \\ C_{2i-1,2i} & = \frac{1}{\sqrt{5}}, \quad i = 1,\dots \frac{L}{2} \end{cases} \tag{5.C.4}$$

- $\gamma > 1$:

$$\begin{cases} C_{i,i} = \frac{1}{2}, & i = 1,\dots,L \\ C_{2i-1,2i} = \frac{1}{2}, & i = 1,\dots \frac{L}{2} \end{cases} \tag{5.C.5}$$

The correlation matrix of the four sites that are integrated out in the same step whose ground state is given by (5.9) is

$$C_4 = \begin{pmatrix} \frac{1}{2} & \frac{1}{\sqrt{5}} & 0 & -\frac{1}{2\sqrt{5}} \\ \frac{1}{\sqrt{5}} & \frac{1}{2} & \frac{1}{2\sqrt{5}} & 0 \\ 0 & \frac{1}{2\sqrt{5}} & \frac{1}{2} & \frac{1}{\sqrt{5}} \\ -\frac{1}{2\sqrt{5}} & 0 & \frac{1}{\sqrt{5}} & \frac{1}{2} \end{pmatrix}. \tag{5.C.6}$$

The most simple non trivial lateral block is

$$A_2 = \begin{pmatrix} \frac{1}{2} & \frac{1}{\sqrt{5}} \\ \frac{1}{\sqrt{5}} & \frac{1}{2} \end{pmatrix}, \tag{5.C.7}$$

whose eigenvalues are $\nu_1 = \frac{1}{10}\left(2\sqrt{5}+5\right), \nu_2 = \frac{1}{10}\left(5-2\sqrt{5}\right)$. The value of S_a, given in (5.15), is obtained applying (3.54). Furthermore S_b, given in (5.16), is obtained from the central block

$$B_1 = \begin{pmatrix} \frac{1}{2} & \frac{1}{2\sqrt{5}} \\ \frac{1}{2\sqrt{5}} & \frac{1}{2} \end{pmatrix}, \tag{5.C.8}$$

whose eigenvalues are $\nu_1 = \frac{1}{10}\left(\sqrt{5}+5\right), \nu_2 = \frac{1}{10}\left(5-\sqrt{5}\right)$. It can be shown that larger central blocks also have these non trivial eigenvalues and the rest are 0 and 1 which do not contribute to the entanglement entropy .

5.D Relation to the Dirac equation with δ potential

Consider an inhomogeneous free-fermion chain with a central hopping defect and bond centered symmetry described by the Hamiltonian:

$$H(\tau) = -\frac{\tau}{2}c^\dagger_{-\frac{1}{2}}c_{\frac{1}{2}} - \frac{1}{2}\sum_{m=\frac{1}{2}}^{L-\frac{3}{2}} J_m\left(c^\dagger_m c_{m+1} + c^\dagger_{-m}c_{-m+1}\right). \tag{5.D.1}$$

The single body spectrum is obtained by diagonalizing the hopping matrix. The eigenvalue equations at the center of the chain are

$$\begin{aligned} \alpha\phi_{-\frac{3}{2}} + \tau\phi_{\frac{1}{2}} &= \epsilon\phi_{-\frac{1}{2}}, & (5.D.2)\\ \tau\phi_{-\frac{1}{2}} + \alpha\phi_{\frac{3}{2}} &= \epsilon\phi_{\frac{1}{2}}, & (5.D.3) \end{aligned}$$

where ϵ is the single body energy and ϕ_m is the amplitude associated with the fermionic operator c_m and $J_{\frac{1}{2}} = \alpha$. The expansion of the local operators c_m in terms of its right and left moving components around the Fermi points (see (5.18)) leads to the equations:

$$\begin{aligned} \tau\left(\psi^{II}_L - i\psi^{II}_R\right) &= \left(-i\epsilon + \alpha\right)\psi^I_L + \left(\epsilon - i\alpha\right)\psi^I_R & (5.D.4)\\ \tau\left(\psi^{I}_L + i\psi^{I}_R\right) &= \left(i\epsilon + \alpha\right)\psi^{II}_L + \left(\epsilon + i\alpha\right)\psi^{II}_R, & (5.D.5) \end{aligned}$$

with

$$\begin{aligned} \lim_{a\to 0}\psi_{L,R}\left(-\frac{3}{2}a\right) &= \lim_{a\to 0}\psi_{L,R}\left(-\frac{1}{2}a\right) = \psi^I_{L,R}, & (5.D.6)\\ \lim_{a\to 0}\psi_{L,R}\left(\frac{3}{2}a\right) &= \lim_{a\to 0}\psi_{L,R}\left(\frac{1}{2}a\right) = \psi^{II}_{L,R}, & (5.D.7) \end{aligned}$$

Solving for ψ^I_L in (5.D.4) and putting it into (5.D.5) we have:

$$\psi^I_R = \frac{1}{2\alpha\tau}\left(i(\tau^2 - \alpha^2 - \epsilon^2)\psi^{II}_L + (\tau^2 - (\epsilon + i\alpha)^2)\psi^{II}_R\right). \tag{5.D.8}$$

Inserting this expression into (5.D.4) we arrive at

$$\psi^I_L = \frac{1}{2\alpha\tau}\left((\tau^2 + (\alpha + i\epsilon)^2)\psi^{II}_L - i(\tau^2 - \alpha^2 + \epsilon^2)\psi^{II}_R\right). \tag{5.D.9}$$

We can express these two equations as $\psi^I = T\psi^{II}$, where T is a transfer matrix:

$$\begin{pmatrix}\psi^I_L\\ \psi^I_R\end{pmatrix} = \frac{1}{2\alpha\tau}\begin{pmatrix}\tau^2 + (\alpha + i\epsilon)^2 & -i(\tau^2 - \alpha^2 + \epsilon^2)\\ i(\tau^2 - \alpha^2 - \epsilon^2) & \tau^2 - (\epsilon + i\alpha)^2\end{pmatrix}\begin{pmatrix}\psi^{II}_L\\ \psi^{II}_R\end{pmatrix}. \tag{5.D.10}$$

Furthermore, at half filling we have that $\epsilon \xrightarrow[L\to\infty]{} 0$ and the transfer matrix simplifies to:

$$T = \frac{1}{2\alpha\tau}\begin{pmatrix} \tau^2+\alpha^2 & -i(\tau^2-\alpha^2) \\ i(\tau^2-\alpha^2) & \tau^2+\alpha^2 \end{pmatrix}. \tag{5.D.11}$$

Note that this can be also written as:

$$T = \frac{1}{2\tilde{\tau}}\begin{pmatrix} \tilde{\tau}^2+1 & -i(\tilde{\tau}^2-1) \\ i(\tilde{\tau}^2-1) & \tilde{\tau}^2+1 \end{pmatrix}, \tag{5.D.12}$$

where $\tilde{\tau} = \frac{\tau}{\alpha}$. Substituting $\tau = e^{-h\gamma}$ and $\alpha = e^{-\frac{h}{2}}$ we have the expression (5.25).

Chapter 6

Symmetry protected topological phases and inhomogeneity

In this chapter we show that by folding the rainbow chain around its center, the long-range entanglement becomes short-range which can lead to topological phases protected by symmetries (SPT). The phases are trivial for bond-centered foldings, and non trivial for site-centered ones. In the latter case, the folded spin $1/2$ chain with $U(1)$ symmetry belongs to the Su-Schrieffer-Heeger class, while the folded chain with $SU(2)$ symmetry is in the Haldane phase. Finally, we extend these results to higher spin chains where we find a correspondence between the symmetry protection of gapped and gapless phases. Finally, we study the robustness of non trivial topological phases in the presence of the defect. This chapter contains content published in Samos Sáenz de Buruaga *et al.* (2019, 2020).

As we mentioned in Chapter 1, the area of Quantum Matter has emerged, where Condensed Matter Physics and Quantum Optics find a common ground to exchange ideas and techniques. Some antecedents of this area can be found in the 80's in the integer and fractional Quantum Hall effects (Tsui *et al.* 1982) that paved the way to the more recent discovery of topological insulators and superconductors (Bernevig and Hughes 2013), Weyl semimetals (Yan and Felser 2017), etc. The description of Quantum Matter goes beyond the Landau paradigm in terms of symmetry breaking and local order parameters. The fundamental concept here is that of topology which in this context means that the relevant properties of a physical system are distributed throughout its extent, whose characterization requires the use of advanced mathematical tools (Wen 1989; Wen 2002; Wen 2017).

Those states with short-range entanglement can be disentangled, i.e. turned into a product state through local unitary evolution (Chen *et al.* 2010). Yet, if we impose that the unitaries must preserve the symmetries of the system, some states

cannot be transformed into a product state because of constraints imposed by the symmetry. Thus, the states belong to *symmetry protected topological* (SPT) phases (Gu and Wen 2009; Tsui *et al.* 2015). If the system is closed (in the sense of boundary conditions), the ground state belonging to an SPT phase does not spontaneously break the symmetry, and it is not degenerate. On the contrary, if the system is open, it possesses non-trivial zero modes, that are called edge-states if they are located at the ends of the chain[1]. The presence of zero modes makes the ground state degenerate. The so-called topological invariants, such as the Chern number, are quantities that do not depend on the boundary and that take different discrete values for different topological phases. A ground state belonging to an SPT phase fulfills the so-called bulk-edge correspondence (Bernevig and Neupert 2015). A non-trivial value of the bulk invariant for the closed system implies the existence of edge-modes for the open chain.

Interacting bosonic topological insulators and topological superconductors were classified using group cohomology theory by Chen *et al.* (2013, 2011) and with matrix product states and tensor network tools by Schuch *et al.* (2011). Altland and Zirnbauer (1997) proposed the so called ten-fold way: a classification framework of non-interacting topological insulators and superconductors under the presence of time-reversal and charge conjugation symmetries, and Kitaev (2009) re-derived it by analyzing the topological invariants with the so-called K-Theory of algebraic topology. Fidkowski and Kitaev (2011) and Turner *et al.* (2011) studied the effects of interactions on the topological classification of free fermions under an entanglement perspective. Indeed, the characterization of the entanglement spectrum has proven to be a good detector of this kind of phases (Cho *et al.* 2017; Fidkowski 2010; Pollmann *et al.* 2012, 2010).

Let us consider the antiferromagnetic Heisenberg chain (AFH) of spin 1. As famously conjectured by Haldane (1983), the spin 1 AFH Hamiltonian has a unique ground state which does not break the rotational symmetry $SO(3)$, and presents a gap in the spectrum for periodic chains. This conjecture led Affleck *et al.* (1988) to propose a state whose properties are similar to those of Haldane's state, and whose many-body wave function is a matrix product state (MPS) (Orús 2014; Schollwöck 2011). The topological properties of the Haldane and the AKLT states were characterized by a string order parameter of den Nijs and Rommelse (1989) or a symmetry dependent string order parameter (Haegeman *et al.* 2012), and the existence of effective spins $1/2$ at the ends of an open chain. It was realized that the Haldane phase can be protected by several symmetries like $Z_2 \times Z_2$ (Kennedy and Tasaki 1992), time reversal and inversion symmetry (Gu and Wen 2009; Pollmann *et al.* 2012), which guarantee *independently* the degeneracy of the entanglement spectrum. More importantly, the concept of symmetry protection turns out to be the key to understand and classify the phases with short range entanglement where one can apply the MPS techniques (Chen *et al.* 2011; Schuch *et al.* 2011).

[1]The zero modes can locate at the edges for specific parameter configurations.

Here we present a new way to generate symmetry protected phases in 1D using local Hamiltonians that are inhomogeneous and without a gap in the spectrum. At first glance, one does not expect this possibility to occur because the corresponding ground states would develop long-range entanglement that violates the area-law (Hastings 2006; Vitagliano *et al.* 2010; Wolf *et al.* 2008). However, we will show that a rearrangement of the sites transforms the long-range entanglement into short-range entanglement, where standard methods can be applied to identify the possible phases (Chen *et al.* 2013, 2011). We shall consider the rainbow model presented in Chapter 4 and we will introduce a similar model in order to describe trivial and non trivial symmetry protected topological (SPT) phases. A byproduct of our construction is that it suggests a relationship between the SPT phases and the phases described by conformal field theories (CFT) in terms of global anomalies (Furuya and Oshikawa 2017). The reason is that the former are constructed from a special deformation of the latter. We shall illustrate this relation with several examples.

The chapter is organized as follows. In Sec. 6.1, we present two models that we shall analyze. One of them is the rainbow state that we introduced in Chapter 4, and the other is slightly different but whose ground state is dramatically different in the strong inhomogeneity regime. In Sec. 6.2, we shall introduce in the new model the central defect considered in the previous chapter, and analyze the strong inhomogeneity regime. In Sec. 6.3, we propose an antiferromagnetic Heisenberg version of the model, and in Sec. 6.4, we discuss the relation between the gapped and gapless topological phases.

6.1 Bond and site centered symmetries

Let us start with the rainbow model defined on the closed chain of $N = 2L$ sites

$$H = -\frac{1}{2}\sum_{n=1}^{2L} J_n c_n^\dagger c_{n+1} + h.c. \tag{6.1}$$

where $c_{2L+1} = c_1$ and the couplings J_n are given by (4.4)

$$J_{n\neq L} = e^{-h|n-L|},\ J_L = e^{-\frac{h}{2}} \tag{6.2}$$

As we mentioned, these couplings endow the model with an inversion symmetry around bond $(L, L+1)$. Hence we shall refer to it as bond-centered symmetry (bcs) model. Here we shall introduce a variant of the rainbow model discussed in Chapter 4 by proposing the couplings

$$J_{n\neq L,L+1} = e^{-h(|n-(L+\frac{1}{2})|-\frac{1}{2})},\ J_L = J_{L+1} = e^{-\frac{h}{2}}, \tag{6.3}$$

that endow the system with an inversion symmetry around the central site $L+1$, leading to define the site-centered symmetry (scs) model

$$J_n = J_{2L-n}\ (\mathrm{bcs}), \quad J_n = J_{2L+1-n}\ (\mathrm{scs}) \tag{6.4}$$

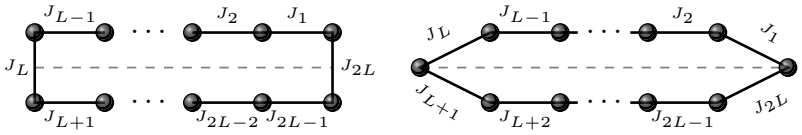

Figure 6.1: Illustrating our physical model, (6.1) with couplings given in (6.3). Symmetrical links with respect to the dashed line carry the same couplings. (a) Bond-centered symmetry (bcs); (b) Site-centered symmetry (scs).

The symmetries of the two types of chains are illustrated in Fig. 6.1. In the bcs model the highest coupling lies at the center of the chain, that is J_L, while the weakest coupling is $J_{2L} = e^{-hL}$ that connects sites 1 and $2L$. In the strong inhomogeneity limit $hL \gg 1$, one can set J_{2L} to zero which leads to the rainbow chain studied in Sec. 4.1. Let us recall that by using the Dasgupta-Ma RG method (Dasgupta and Ma 1980; Fisher 1995) the ground state of the rainbow chain takes the form (Ramírez *et al.* 2014)

$$|\text{bcs}\rangle \overset{h\to\infty}{\longrightarrow} (b_1^+)^\dagger (b_2^-)^\dagger (b_3^+)^\dagger \dots (b_L^{\eta_L})^\dagger |0\rangle\,, \tag{6.5}$$

where b_m fermions are given by the bonding/anti-bonding fermionic operators (4.12)

$$b_n^\pm \equiv b_{L+1-n,L+n}^\pm = \frac{1}{\sqrt{2}}(c_{L+1-n} \pm c_{L+n}), \quad n = 1,\dots,L\,, \tag{6.6}$$

are fermion operators on the opposite sides of the chain, that annihilate the Fock vacuum $|0\rangle$ and $\eta_L = (-1)^{L+1}$, and they satisfy the usual canonical anticommutation relations (3.10). As we have seen, the state presents a maximal violation of the entanglement entropy for the block $A = \{1, 2, \dots, \ell\}$:

$$S_A^{\text{bcs}} = \ell \log 2, \quad \ell \le L\,. \tag{6.7}$$

Let us consider now chains with site-centered symmetry. In the limit $h \gg 1$, the dominant interaction takes place between sites $L, L+1$ and $L+2$. Observe that the SDRG used for the bcs model cannot be used in this case since there are two equally strong couplings. In this situation one should use first order perturbation theory to renormalize three spins into one effective spin. See the details on the Appendix (6.A). Iterating this RG procedure one obtains the ground state,

$$|\text{scs}\rangle \overset{h\to\infty}{\longrightarrow} (d_0^+)^\dagger (d_1^-)^\dagger (d_2^+)^\dagger (d_3^-)^\dagger \dots (d_L^+)^\dagger |0\rangle\,, \tag{6.8}$$

where

$$\begin{aligned} &f_0 \equiv c_{L+1}, \quad f_L \equiv c_1, \quad f_n^\pm \equiv b_{L+1-n,L+1+n}^\pm = \frac{1}{\sqrt{2}}(c_{L+1-n} \pm c_{L+1+n}), \\ &d_0^\pm = \frac{1}{\sqrt{2}}(f_0 \pm f_1^+), \quad d_L^\pm = \frac{1}{\sqrt{2}}(f_L \pm f_{L-1}^+), \quad d_n^\pm = \frac{1}{\sqrt{2}}(f_n^\pm + f_{n+1}^\pm)\,, \end{aligned} \quad n = 1,\dots,L-1\,, \tag{6.9}$$

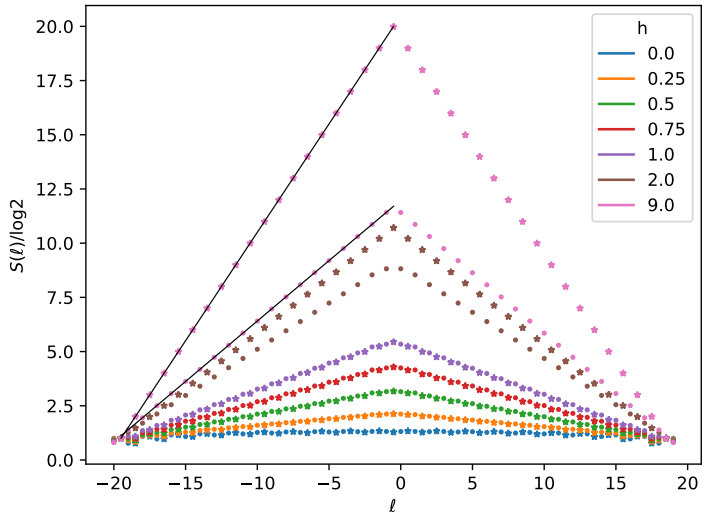

Figure 6.2: Entanglement entropy of lateral blocks belonging to the ground states of the scs ($N = 41$) and bcs ($N = 40$) models with open boundary conditions. Observe that in order to preserve the scs symmetry, the open chain presents an odd number of sites. Notice that they differentiate their behaviour in the strong inhomogeneity regime. The black lines correspond to the theoretical predictions (6.7) and (6.10). Please refer to Appendix 6.B for details of the derivation of (6.10).

where the operators $d_n^{\pm}$ also satisfy the canonical anticommutation relations (3.10) The entanglement entropy of the block A is (see Appendix 6.B)

$$S_A^{\text{scs}} = (\ell + 1)\,(2\log 2 - 1), \qquad \ell \leq L\,, \tag{6.10}$$

which is still linear but not maximal as in (6.7), as it can be seen in Fig. 6.2

The long-range entanglement of the bcs/scs states can be converted into short-range one using the basis of states generated by the operators $b_n^{\pm}$ and $f_n^{\pm}$. The b-operators are the bonding and anti-bonding combinations of the fermions located at opposite sites in the chain. They become local operators by *folding* the chain around the bond $(L, L+1)$ that transforms it into a ladder with 2 legs and L rungs, as we have seen in Sec. 5.2.3. The folding *trick* has played an important role in the study of quantum impurity problems (Büsser and Feiguin 2012; Kane and Fisher 1992; Simon and Affleck 2001). Equation (6.5) shows that the bcs state is the product of bonding and antibonding states on the rungs. Hence, the entanglement entropy of the block $C = \{L+1-\ell, \ldots, L+\ell\}$ located at the center of the chain, that corresponds to ℓ rungs in the ladder, is simply

$$S_C^{\text{bcs}} = 0, \quad \ell = 1, \ldots, L-1\,. \tag{6.11}$$

Turning to the site-centered chains we observe that the f-operators, (6.9), involve a folding transformation that leaves sites 1 and $L+1$ untouched. The chain is now transformed into a ladder with $L-1$ rungs and two isolated sites on both

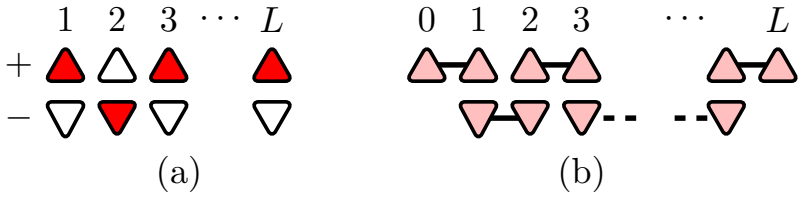

Figure 6.3: Ground states of the rainbow XX model in the limit $h \to \infty$. We use the folded representation of Fig. 6.1.

edges. The entanglement entropy of block $C = \{L+2-\ell, \ldots, L+\ell\}$ located at the center of the chain (see Fig. 6.1), that corresponds to ℓ rungs in the ladder and one site, is given by

$$S_C^{\text{scs}} = \log 2, \quad \ell = 1, \ldots, L-1\,. \tag{6.12}$$

One can verify the expressions (6.11)) and (6.12) by looking at Fig. 6.3 which shows that the GS of the bcs rainbow is a charge density wave (CDW), while that for the scs rainbow is a staggered dimer state, reminiscent of the trivial and topological phases of the well known SSH model (Su *et al.* 1979). The origin of these GS structures can be understood writing the Hamiltonian (6.1) using the operators (6.6)

$$\begin{aligned} H_{\text{bcs}} = -\frac{1}{2}\Big(\sum_{n=1}^{L-1} J_{L-n}\left((b_n^+)^\dagger b_{n+1}^+ + (b_n^-)^\dagger b_{n+1}^- + \text{h.c.}\right) \\ + J_L((b_1^+)^\dagger b_1^+ - (b_1^-)^\dagger b_1^-) + J_{2L}((b_L^+)^\dagger b_L^+ - (b_L^-)^\dagger b_L^-)\Big), \end{aligned} \tag{6.13}$$

and (6.9),

$$\begin{aligned} H_{\text{scs}} = -\frac{1}{2}\Big(\sum_{n=1}^{L-2} J_{L-n}((f_n^+)^\dagger f_{n+1}^+ + (f_n^-)^\dagger f_{n+1}^-) \\ + \sqrt{2}\, J_L\, f_0^\dagger f_1^+ + \sqrt{2}\, J_1\, f_L^\dagger f_{L-1}^+ + \text{h.c.}\Big). \end{aligned} \tag{6.14}$$

In the bcs model the chemical potential on the first rung induces, in the strong inhomogeneity limit, the full occupation of site $+1$ and the emptying of site -1. This mechanism gives rise to a CDW state (see details in Appendix 6.D). In the scs model, the hopping term between the isolated mode f_0 and the mode f_1^+ of the first rung, induces in the same limit, a hybridization that propagates along the chain producing a staggered dimer state on the ladder. These ground states are illustrated in Fig. 6.3. The bcs state is a product state in the basis $b_n^\pm$, so a MPS with bond dimension $\chi = 1$. On the other hand, the scs state is a product of dimers, with bond dimension $\chi = 2$ (Appendix 6.E.3). The entanglement spectrum is twofold degenerate with two equal eigenvalues. We shall next show that the previous topological features persist for all values of $h > 0$. Fig. 6.4 shows the entanglement entropies of the central blocks $B = [-x, x]$ with $x = n - L - \frac{1}{2}$ for bcs chain and $x = n - L - 1$ for the scs chain. They are independent of x, for sufficiently large values, so corresponding to an area law for the folded chain. Notice that when

$h \gg 1$ the entanglement entropy for the bcs chains goes to zero while that for the scs chains goes to $\log 2$, in agreement with (6.11) and (6.12). The rainbow chain has a continuum limit given by a massless Dirac fermion on a curved spacetime as we have shown in Sec. 4.2. Using CFT techniques one can find the Von Neumann entropy of the a central block (Rodríguez-Laguna *et al.* 2017) $B = [-x, x]$ is

$$S_B(x) \simeq \frac{1}{3}\log\left[\frac{4\tilde{L}}{\pi}e^{-hx}\sin\frac{\pi\tilde{x}}{\tilde{L}}\right] + \Upsilon_1 < \frac{1}{3}\log\frac{4}{h} + \Upsilon_1 \tag{6.15}$$

where $\tilde{x} = (e^{hx}-1)/h$ (4.46) and $\Upsilon_1 \simeq 0.49502$ is the non-universal constant (3.73) found by Jin and Korepin (2004). Fig. 6.4 shows that this expression reproduces the bcs and scs entropies when h is not too large, where the field theory limit applies. The upper bound in (6.15) is similar to the entanglement entropy of a massive theory in the scaling limit with $1/h$ as correlation length

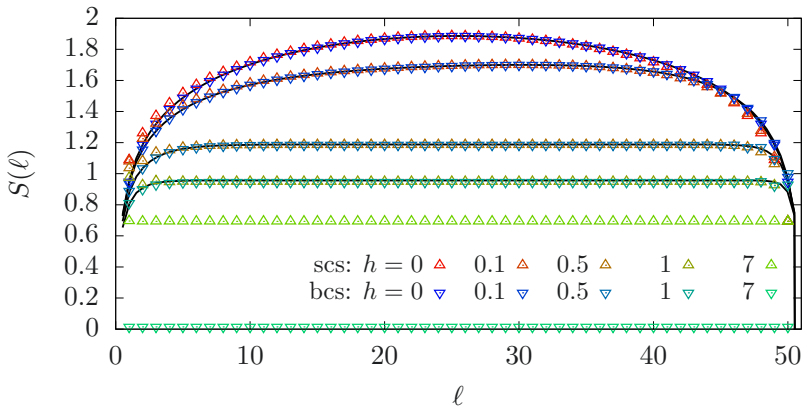

Figure 6.4: Entanglement entropy of the central block for increasing values of h shown in descending order, of the bcs and scs chains with $L = 51$. The continuum lines are the CFT prediction (6.15).

Another signature of an SPT phase is the degeneracy of the entanglement spectrum (ES) (Pollmann *et al.* 2010; Turner *et al.* 2011). For a free fermion system the entanglement energies are given by $E(\{n_p\}) = \sum_p \varepsilon_p n_p + r_0$, where $\{n_p = 0, 1\}$

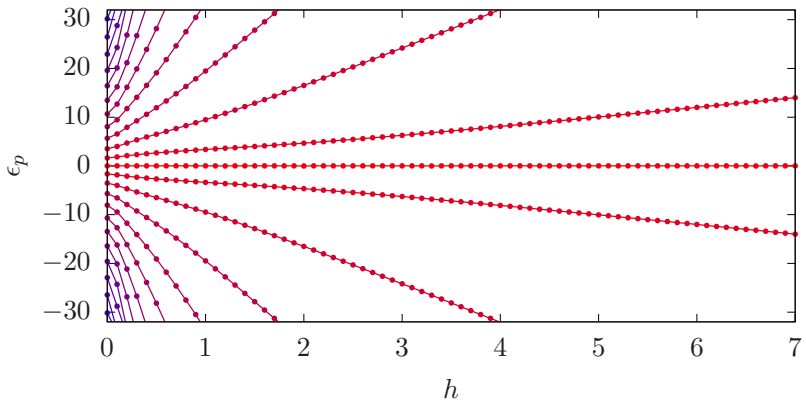

Figure 6.5: Single particle entanglement spectrum ε_p for a scs chain with $L = 51$ as a function of h.

is the set of occupation numbers of the one-body entanglement entropies ε_p that are computed from the eigenvalues of the correlation matrix (3.89) $\langle c_n^\dagger c_m \rangle$ (Peschel 2003). For scs chains there exists a zero mode, $\varepsilon_0 = 0$, for all values of h, that gives rise to a doubly degeneracy of the entanglement spectrum (see Fig. 6.5). This degeneracy is protected by the time reversal and particle-hole symmetry of the Hamiltonian. Hence, this model belongs to the symmetry class AIII for free fermions, the same as the SSH model (Bernevig and Neupert 2015; Fidkowski and Kitaev 2011; Su *et al.* 1979): a perturbation to the Hamiltonian that does not respect those symmetries will break the entanglement spectrum degeneracy.

6.2 Defect in a symmetry protected topological phase

The value of the central coupling in the systems considered so far is $e^{h/2}$ yielding a chain without a central defect, according to what we have seen in Chapter 5, where we studied the bcs model in presence of a central defect parametrized by γ. Here we shall consider the natural extension of this model for the scs symmetry and ask ourselves how the defect affect in this case. We define thus the analogous scs model

$$H_N(h,\gamma)_{\text{scs}} = -\frac{1}{2}\sum_{m=1}^{N} J_m c_m^\dagger c_{m+1} + \text{h.c.}, \tag{6.16}$$

where there are two equal central hoppings depending on γ

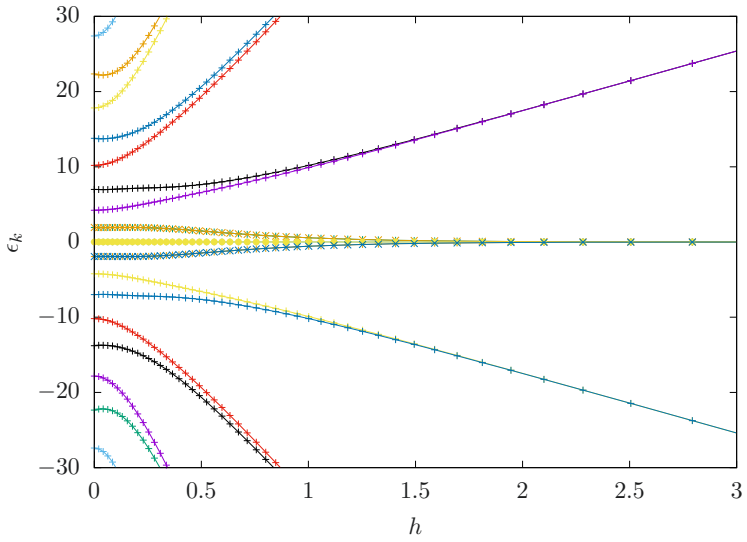

Figure 6.6: Single body entanglement spectrum ϵ_k of a block B_{11} of a system described by the Hamiltonian $H_{46}(h, \frac{17}{2})_{\text{scs}}$ as a function of h. Notice the topological zero mode, which does not depend on h.

$$J_m = \begin{cases} e^{-h(|m-(L+\frac{1}{2})|-\frac{1}{2})} & \text{if } m \neq L, L+1, \\ e^{-h\gamma} & \text{if } m \in \{L, L+1\}, \end{cases} \tag{6.17}$$

i.e., the log-couplings (5.7) present the pattern $\{\dots, 3, 2, 1, \gamma, \gamma, 1, 2, 3, \dots\}$. Since the topological nature of the state is highlighted after removing the local entanglement (Chen *et al.* 2011), it is better to study the system in the strong inhomogeneity regime. The fermionic excitations are not spread along the whole system as it is the case in the weak inhomogeneity limit. Hence, we will study the system in the strong inhomogeneity regime $H_N(h \gg 1, \gamma)_{\text{scs}}$ by means of renormalization schemes that depend on the value of γ (see details in Appendix 6.C).

Observe that $\gamma \leq 1$ corresponds to the case that we have presented above: the dominant interaction involves the three central sites, L, $L+1$ and $L+2$ and we have to employ the real space first order perturbation theory RG (see Appendix 6.A). On each step, three fermions are truncated into one which participates on the next step leading to a topological ground state with non removable entanglement that belongs to the AIII class. The case with $\gamma = 1$ differs only on the first step of the RG where 5 spins (instead of three) are truncated to one.

On the other hand, the case $\gamma > 1$ is again different. Starting from $H_N(h, \gamma)_{\text{scs}}$, the dominant interactions are two non consecutive log-couplings 1 which allows the use of the Dasgupta-Ma RG (5.4), leading to an effective system whose Hamiltonian is $H_{N-4}(h, 1+\gamma)_{\text{scs}}$. If $1+\gamma$ happens to be the dominant interaction, three fermions are involved so the Dasgupta-Ma RG is not applicable anymore and the way of procedure is described in the previous paragraph. On the contrary, if the log-couplings 2 are the dominant interaction, the Dasgupta-Ma RG can be applied again leading to a new Hamiltonian $H_{N-8}(h, 2+\gamma)_{\text{scs}}$. Hence, the same dichotomy is present in the next step. The procedure iterates and unless $\gamma > L-1$ the RG flows eventually to a dominant interaction which involves three fermions.

Therefore we see that the GS of the Hamiltonian $H_N(h, \gamma > 1)_{\text{scs}}$ is obtained via the application of two kinds of renormalization group schemes. As a consequence, the ground state of this Hamiltonian has two different phases that coexist: a dimerized phase around the defect and the AIII phase away from it. This coexistence is well captured by considering the entanglement entropy of central blocks $B_\ell = \{L-\ell, L+2+\ell\}$, with $\ell \in \{0, \dots, (L-1)\}$. Since the system is topologically non-trivial, there is entanglement that cannot be removed (the entanglement entropy in bounded by $\log 2$ for all B_ℓ) and for blocks B_ℓ with $\ell < \lfloor \gamma \rfloor$, $S(B_\ell) = 3\log 2$ due to the fact that there are two fermionic excitations $b^\dagger_{L-2(\ell-1),L-2(\ell-1)-1}|0\rangle$ and $b^\dagger_{L+2\ell,L+2\ell+1}|0\rangle$ that are not fully contained in the block B_ℓ. Furthermore, the dimerized phase appears only in the strong inhomogeneity limit $h \to \infty$ while the AIII phase is independent of the inhomogeneity parameter. This fact can be checked by considering the behaviour of the single body entanglement spectrum ϵ_k, see Fig. 6.6 and (3.89). There is a zero mode $\epsilon_0 = 0$ for all h that gives rise to a double degeneracy of the many-body entanglement spectrum and it is a signature of the topological nature of the state. There are also two additional zero modes due to the presence of the defect but they are not topological, since they depend on the

inhomogeneity.

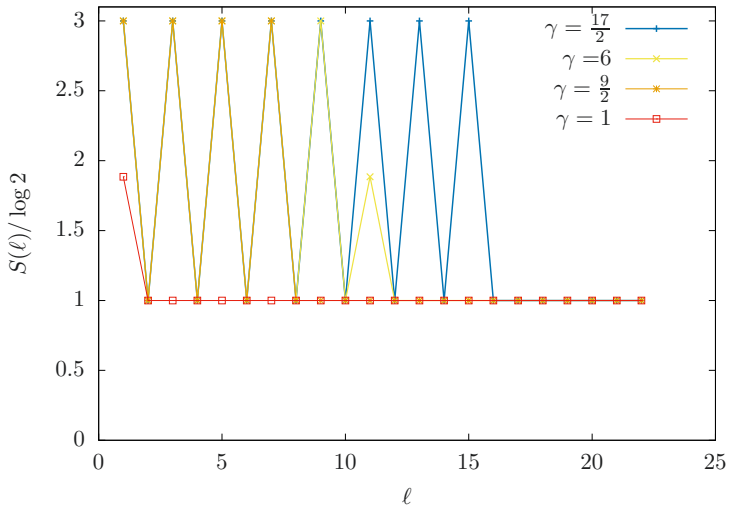

Figure 6.7: Entanglement entropy of the system with Hamiltonian $H_{46}(15,\gamma)_{\rm scs}$ partitioned with central blocks B_ℓ for different values of γ. The entropy is $S[B_\ell] = 3\log 2$ if $\ell < \lfloor\gamma\rfloor$ and it is $S[B_\ell] = \log 2$ if $\ell > \lfloor\gamma\rfloor$. If $\gamma \in \mathbb{N}$, $S[B_{\ell=\gamma}]$ takes another value which is a consequence of the quadruple tie that we have discussed in the text.

6.3 The rainbow antiferromagnetic Heisenberg model

The Hamiltonian is

$$H = \sum_{n=1}^{2L} J_n \, \mathbf{S}_n \cdot \mathbf{S}_{n+1} \,, \tag{6.18}$$

where $\mathbf{S}_n$ are the spin 1/2 matrices at site n. The couplings J_n are defined in (6.3). Let us study the phases of this model in the limit $h \gg 1$. For the bcs chain, the analysis is similar to the one of the bcs XX chain. The Dasgupta-Ma RG equation yields a GS made of spin singlets between sites n and $2L+1-n$. Folding the chain maps this state into the product of L rung singlets of the two leg ladder. In the scs chain, the highest couplings are $J_L = J_{L+1}$, and we start diagonalizing the Hamiltonian $J_L \mathbf{S}_{L+1} \cdot (\mathbf{S}_L + \mathbf{S}_{L+2})$. Its GS is obtained by forming a triplet between spins $\mathbf{S}_L$ and $\mathbf{S}_{L+2}$, that couples to spin $\mathbf{S}_{L+1}$ yielding an effective spin 1/2, denoted as $\mathbf{S}'_{L+1}$. First order perturbation theory yields the RG equations $\mathbf{S}_L, \mathbf{S}_{L+2} \to \frac{2}{3}\mathbf{S}'_{L+1}$. The next order term in the Hamiltonian is $J_{L-1}(\mathbf{S}_{L-1} \cdot \mathbf{S}_L + \mathbf{S}_{L+2} \cdot \mathbf{S}_{L+3})$ that gets renormalized into $\frac{2}{3} J_{L-1} \mathbf{S}'_{L+1} \cdot (\mathbf{S}_{L-1} + \mathbf{S}_{L+3})$, so we can repeat the same RG step done above if $h \gg 1$. Each RG step generates an effective spin 1 that couples to an effective spin 1/2 from the previous step. Completing the RG procedure yields a chain with L effective spins 1 and two spins 1/2 at the ends of the folded chain (see Fig. 6.8). This is the AKLT state (Affleck *et al.* 1988) of an open chain with $L-1$ spins 1's and two 1/2's at the ends (6.E.3). The RG method used above is valid for $h \gg 1$, but the topological nature of the GS also holds for all positive values of h.

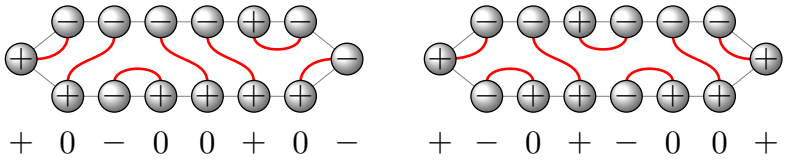

Figure 6.8: Strong inhomogeneity limit of the GS of the scs Heisenberg model. The links represent valence bonds. The ± symbols inside the balls denote the sign of σ^z of the corresponding spin, while the sign of the sum over the rung appears below. These signs display an antiferromagnetic liquid behaviour characteristic of the Haldane phase.

To verify this statement we show in Fig. 6.9 the string order parameter (den Nijs and Rommelse 1989; Girvin and Arovas 1989; White and Huse 1993).

$$g(L) = \left\langle S_1^z \, e^{i\pi \sum_{j=2}^{L-1} S_j^z} \, S_L^z \right\rangle , \tag{6.19}$$

where $S_j^z = S_{u,j}^z + S_{d,j}^z$ is the spin operator on the j^{th}- rung of the folded chain. For bcs chains all rungs are considered, while for scs chains sites 1 and $L+1$ are left out. For the bcs chains, $|g(L)|$ approaches quickly zero as $h \gg 1$, while for the scs chains $g(L)$ converges asymptotically towards $-4/9$ that corresponds to the AKLT state as was shown by den Nijs and Rommelse (1989). Fig. 6.9-bottom, shows that the entanglement entropy of the central blocks of the scs model remains constant for sufficiently large values of h, which is a signature of the area law (recall (6.15)). The entanglement spectrum is doubly degenerate (see inset of Fig. 6.9 bottom), that is another feature of the SPT phase, which in this case is protected by the time reversal symmetry (Pollmann *et al.* 2012, 2010). Moreover, if we drop the site $2N$, that is placed in the rightmost position in Fig. 6.8, this has the effect of leaving an edge spin of the effective spin 1 chain.

6.4 Gapless versus gapped topological phases

The previous results show that a strong inhomogeneous deformation of the critical spin $1/2$ AFH chain, with site centered symmetry, becomes an effective spin 1 chain in the Haldane phase. Let us now consider Heisenberg chains with higher spin. If the spin is a half-odd integer, $S = \frac{1}{2}, \frac{3}{2}, \ldots$, then the uniform AFH Hamiltonian is gapless and described by the $SU(2)_1$ Wess-Zumino-Witten (WZW) model (Affleck and Haldane 1987). Applying a strong inhomogeneous scs deformation generates, via its folding, an effective AKLT chain with spin $2S = 1, 3, \ldots$. The ground states of these spin chains possess non-trivial SPT phases (Pollmann *et al.* 2012). Let us now replace the AFH Hamiltonian by the Babujian-Takthajan (BT) Hamiltonian (Babujian 1983, 1982; Takhtajan 1982) of spin S that is integrable and described by the $SU(2)_k$ WZW model with $k = 2S$. We also expect its strong scs deformation to map into the AKLT state of spin $2S$. Hence, when k is odd, the AFH and BT

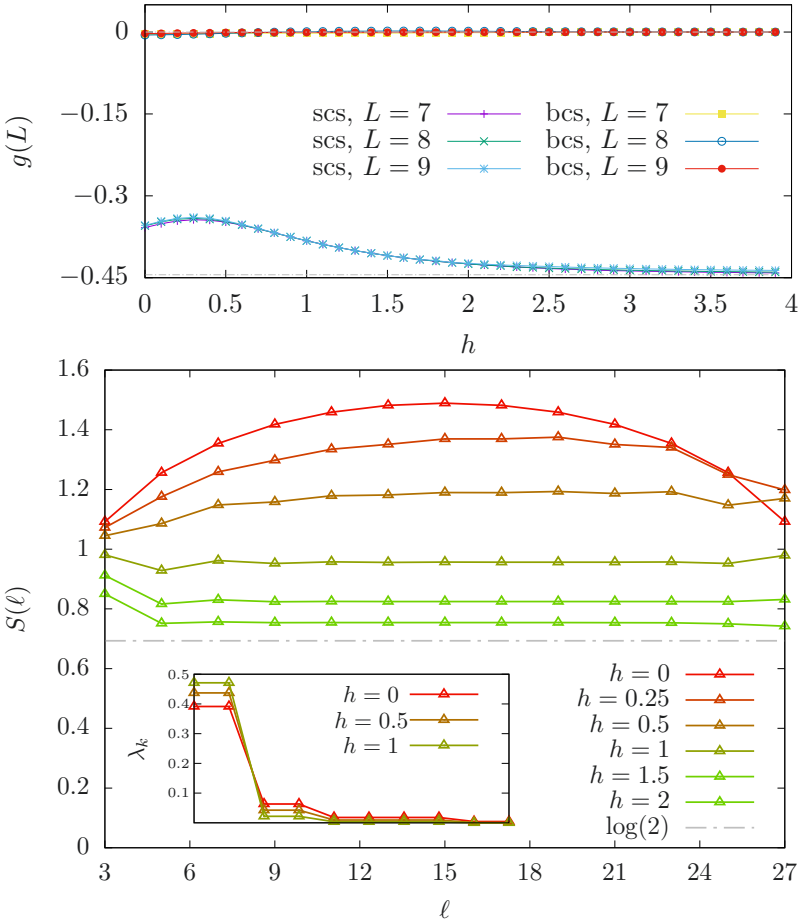

Figure 6.9: Top: Plot of the string order parameter, $g(L)$, for the Heisenberg chains with $L = 7, 8, 9$. It vanishes for the bcs chains and approaches the AKLT value $-4/9$ for the scs chains. Bottom: entanglement entropy of the central blocks of the scs Heisenberg model with $L = 15$ obtained with the DMRG (White 1992) as a function of the size and several values of h. Notice the convergence to $\log 2$ already for $h = 2$. Inset:entanglement spectrum as a function of the order for 3 values of h and central block with $x = 15$ sites.

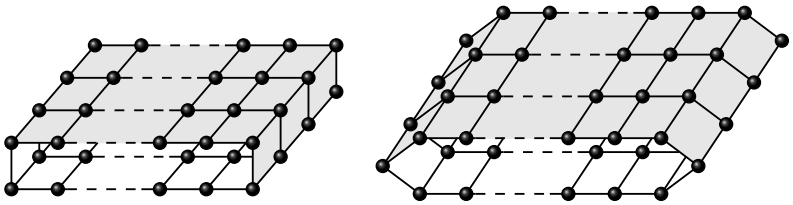

Figure 6.10: A 2D extension of the bcs (a) and scs (b). Compare with Fig. 6.1 in order to see the straightforward generalization of the folding operation.

models both end up in non-trivial SPT phases. Repeating this process for integer spin chains gives trivial SPT phases. Indeed, the AFH Hamiltonian for integer spin is gapped according to Haldane's conjecture (Haldane 1983). Its strong scs deformation gives an AKLT state with spin $2S = 2, 4, \ldots$ which is a trivial SPT phase integer (Pollmann *et al.* 2012). The same is expected to hold for the scs deformation of the BT model for integer spin. The difference between even and odd levels of critical spin chains with $SU(2)_k$ symmetry reminds the one based on global anomalies that also lies on the parity of k (Furuya and Oshikawa 2017). The mechanism of relating apparently different phases via inhomogeneities can be extended to other model in 1 and 2 dimensions. An example is the spin $1/2$ AFH model on a square lattice. A strong site-centered deformation of the exchange couplings along the X and Y-axes yields a two dimensional AKLT state with spins 2 in the bulk, spins 1 along the edges and spins $1/2$ at the corners.

SPT phases have been also related to boundary CFT (BCFT) (Cho *et al.* 2017). There, the cohomological classification of the former phases are relate to certain conditions placed on boundary states in CFT. It will be very interesting to investigate the relation between this approach and the one we have pursued here that is also based on CFT but with a different perspective.

6.5 Conclusions

In this chapter we have provided a new mechanism to generate symmetry protected topological phases in one dimensional spin chains governed by inhomogeneous local Hamiltonians. The ground states of these models have long range entanglement but by folding the chains around their center, it becomes short range. We illustrate this mechanism with the spin $1/2$ XX and antiferromagnetic Heisenberg chains whose inhomogeneous deformations, with site-centered symmetry, yield ground states in the SSH and Haldane phases respectively.

In presence of central defects, as considered in the previous chapter, the ground state possesses an interesting coexistence of a symmetry-protected topological phase near the ends and a dimerized region near the center, whose size grows as the defect intensity goes to zero.

We expect the folding mechanism to work for other 1D and 2D models. A 2D extension of the scs and bcs systems (Fig. 6.10) could be built up by joining parallel scs and bcs chains with engineered couplings in such a way that the RGs obtained above for the 1D chains are still applicable and the folding operations are the natural generalization of the 1D case: the folding for the bcs system is performed along the virtual axis that cross the central bonds $(L, L+1)$ of each chain while for the scs system the folding leaves two chains untouched: one formed by the sites 1 and the other by the sites $L+1$ of each scs chain. Nevertheless, the richness of the 2D framework offers, in principle, different folding operations that are apparently inequivalent in terms of the way that the long range entanglement becomes short range. This poses the question of which different SPT and topological phases can be constructed by playing this sort of *origami* game, and whether they could be realized experimentally for example by applying pressure to real materials, or in synthetic materials realized in optical lattices (Bloch *et al.* 2008).

Appendices

6.A Real space renormalization group for the scs model

While the bcs chain (see (6.1) and (6.3)) is tractable via the strong-disorder renormalization group (SDRG), the method is inconclusive for the scs chain. The reason is that there are two hoppings of equal magnitude $\exp\left(-\frac{h}{2}\right)$. Even if we choose one of them randomly to put a valence bond on it, the degeneracy will propagate to the next renormalization step. Thus, we have developed a different approach via a real space renormalization method à la Wilson, based on the single-particle character of this problem.

Numerical studies of the GS of the scs rainbow system show that the single-body modes are localized in the strong-inhomogeneity limit, but on *four* sites. Moreover, as the modes increase in energy, their support moves outwards from the center of the chain. This leads to a natural renormalization scheme which starts out with the central block, $B^{(1)}$, comprising the three central sites: $\bullet_{L-1}$, $\bullet_L$ and $\bullet_{L+1}$. The two internal couplings are the same, equal to $\exp(-h/2)$, so the effective Hamiltonian is:

$$H^{(1)} = -e^{-h/2}\begin{pmatrix} 0 & 1 & 0 \\ 1 & 0 & 1 \\ 0 & 1 & 0 \end{pmatrix}. \tag{6.A.1}$$

Its spectrum is composed of three values, E_i, with their associated eigenvectors, $|i^{(1)}\rangle$ where $i \in \{-, 0, +\}$. Let us select the ground state, E_-, which has the form:

$$\left|-^{(1)}\right\rangle = \frac{1}{2}(1, \sqrt{2}, 1), \tag{6.A.2}$$

and keep it as the first electronic orbital. Then we proceed to take the zero mode,

$$\left|0^{(1)}\right\rangle = \frac{1}{\sqrt{2}}(1, 0, -1), \tag{6.A.3}$$

and take it to the next RG level, along with the orbitals located on the neighboring sites to the block: sites $\bullet_{L-2}$ and $\bullet_{L+2}$. These three single-body orbitals: $|\bullet_{L-2}\rangle$, $|0^{(1)}\rangle$ and $|\bullet_{L+2}\rangle$ constitute block $B^{(2)}$. Let us build the effective Hamiltonian:

$$H^{(2)} = \begin{pmatrix} \langle \bullet_{L-2}|H|\bullet_{L-2}\rangle & \langle \bullet_{L-2}|H|0^{(1)}\rangle & \langle \bullet_{L-2}|H|\bullet_{L+2}\rangle \\ \langle 0^{(1)}|H|\bullet_{L-2}\rangle & \langle 0^{(1)}|H|0^{(1)}\rangle & \langle 0^{(1)}|H|\bullet_{L+2}\rangle \\ \langle \bullet_{L+2}|H|\bullet_{L-2}\rangle & \langle \bullet_{L+2}|H|0^{(1)}\rangle & \langle \bullet_{L+2}|H|\bullet_{L+2}\rangle \end{pmatrix} \tag{6.A.4}$$

The lowest energy eigenstate $|-^{(2)}\rangle$ is kept as a new orbital, and there appears a new zero mode, $|0^{(2)}\rangle = \frac{1}{\sqrt{2}}(1,0,1)$, which is taken to the next RG level. The n-th RG step is predicated on a block $B^{(n)}$ which contains the zero mode of the previous step, $|0^{(n-1)}\rangle$ and the next two site-orbitals, $|\bullet_{L-n}\rangle$ and $|\bullet_{L+n}\rangle$, with effective Hamiltonian:

$$H^{(n)} = \begin{pmatrix} \langle \bullet_{L-n}|H|\bullet_{L-n}\rangle & \langle \bullet_{L-n}|H|0^{(n-1)}\rangle & \langle \bullet_{L-n}|H|\bullet_{L+n}\rangle \\ \langle 0^{(n-1)}|H|\bullet_{L-n}\rangle & \langle 0^{(n-1)}|H|0^{(n-1)}\rangle & \langle 0^{(n-1)}|H|\bullet_{L+n}\rangle \\ \langle \bullet_{L+n}|H|\bullet_{L-n}\rangle & \langle \bullet_{L+n}|H|0^{(n-1)}\rangle & \langle \bullet_{L+n}|H|\bullet_{L+n}\rangle \end{pmatrix} \quad n = 1, ..., L-1 \tag{6.A.5}$$

The last step of the procedure is different: the new block is built up with the zero mode of the previous step, but there is only one remaining orbital. Hence, the effective block is a 2×2 matrix:

$$H^{(L)} = \begin{pmatrix} \langle 0^{(L-1)}|H|0^{(L-1)}\rangle & \langle \bullet_{2L}|H|0^{(L-1)}\rangle \\ \langle 0^{(L-1)}|H|\bullet_{2L}\rangle & \langle \bullet_{2l}|H|\bullet_{2L}\rangle \end{pmatrix}. \tag{6.A.6}$$

$H^{(L)}$ has two different forms depending of nature of last zero mode: if $N \equiv 0 \pmod 4$, $|0^{L-1}\rangle$ is symmetric while if $N \equiv 2 \pmod 4$ it is antisymmetric. Hence, the energy spectrum presents a double degeneracy of $E = 0$ in th former case, while in the latter it does not.

This RG procedure allows to obtain corrections in h on the step n by choosing the eigenvalue $E_-^{(n)}$. As a consequence of the growth from the center along the RG process, the method can provide corrections to the energy of every single-body mode in subsequent RG steps. Hence, the single-body operator b_1 that appears in the first RG step receives corrections at every RG step. Let us present the single-body modes computed in first order in α. Due to the periodic boundary conditions, the mode $b_L^\dagger$ possesses, at first order, the same functional form as as $d_L^\dagger$.

$$\begin{aligned}
d_0^\dagger =& \left(\frac{1}{\sqrt{2}} - \frac{e^{-h}}{8\sqrt{2}}\right) c_L^\dagger + \left(\frac{1}{2} - \frac{e^{-h}}{16}\right)\left(c_{L-1}^\dagger + c_{L+1}^\dagger\right) \\
&+ \frac{e^{-\frac{h}{2}}}{\sqrt{2}}\left(\sum_{i=1}^{L-2}\left(\frac{e^{h(2-L+i)}}{\sqrt{2}}\right)^{L-i}\left(c_i^\dagger + c_{2L-i}^\dagger\right) + 2\left(\frac{e^{\frac{L-2}{2}}}{\sqrt{2}}\right)^{L} c_{2L}^\dagger\right), \\
d_k^\dagger =& \frac{1}{2}\Big(c_{L+1-k}^\dagger + c_{L-k}^\dagger + (-1)^{k+1}(c_{L-1+k}^\dagger + c_{L+k}^\dagger) \\
&+ \sum_{l=1}^{L-2} e^{-\frac{h}{2}l(l+1)}\left(c_{L-k-i}^\dagger + (-1)^{k+1}c_{L+k+i}^\dagger\right)\Big), \quad k = 2, \cdots, L-1, \\
d_L^\dagger =& \frac{1}{2}\left(c_1^\dagger - c_{2L-1}^\dagger\right) + \frac{1}{\sqrt{2}}c_{2L}^\dagger,
\end{aligned} \tag{6.A.7}$$

$$C = \frac{1}{4}\begin{pmatrix} 2 & 1 & 0 & 0 & 0 & 0 & 0 & -1 & 0 & \sqrt{2} \\ 1 & 2 & 1 & 0 & 0 & 0 & 1 & 0 & -1 & 0 \\ 0 & 1 & 2 & 1 & 0 & -1 & 0 & 1 & 0 & 0 \\ 0 & 0 & 0 & 2 & \sqrt{2} & 0 & -1 & 0 & 0 & 0 \\ 0 & 0 & 0 & \sqrt{2} & 2 & \sqrt{2} & 0 & 0 & 0 & 0 \\ 0 & 0 & -1 & 0 & \sqrt{2} & 2 & 1 & 0 & 0 & 0 \\ 0 & 1 & 0 & -1 & 0 & 1 & 2 & 1 & 0 & 0 \\ -1 & 0 & 1 & 0 & 0 & 0 & 1 & 2 & 1 & 0 \\ 0 & -1 & -1 & 0 & 0 & 0 & 0 & 1 & 2 & \sqrt{2} \\ \sqrt{2} & 0 & 0 & 0 & 0 & 0 & 0 & 0 & \sqrt{2} & 2 \end{pmatrix} \tag{6.B.1}$$

Figure 6.B.1: Correlation matrix of a $L = 5$ scs chain in the strong coupling limit ($h \to \infty$) computed via (6.B.1) using the single body modes (6.A.7).

where $c_i^\dagger$ is the fermionic creation operator on site i. Notice that, due to particle-hole symmetry, each of these modes has a negative energy counterpart. It is important to note that the strong inhomogeneity regime is well captured with the first order on h (see (6.9)).

6.B Computation of entanglement entropy in the scs model

In this section we derive expression (6.10) of the entanglement entropy of a block B with l sites of a scs chain. As we explained in Section 3.2.1 we can compute the entanglement entropies with the eigenvalues of the block correlation matrices (CM), C_{ij}

$$C_{ij} = \sum_{k=1}^{N_F} U_{ik} U_{jk}^*,$$

where U_{ik} is the unitary matrix that diagonalizes the single-body Hamiltonian (see Appendix 4.A.2 for more details). Note that the ground state is degenerate for scs chains with $N \equiv 0 \pmod 4$, since there is a (double) zero mode in the single-body spectrum. Hence the half-filling is not well defined. In the rest of this section and on the main text we have restricted ourselves to chains with no degeneracy.

The computation of the entropies of the block B requires the diagonalization of the corresponding $l \times l$ block of the CM. In the $h \to \infty$ limit, when the block B does not include any of the sites $2L, L$ or $L \pm 1$, the submatrix of the CM is tridiagonal and translational invariant (see Fig. 6.B.1). The eigenvectors have the following form:

$$|\varphi_k\rangle = \sum_{m=1}^{l} \phi_m = \sum_{m=1}^{l} Ae^{ikm} + Be^{-ikm}, \tag{6.B.2}$$

where we have used the same ansatz that we use to diagonalize the homogeneous open XX Hamiltonian (see Section (3.1.2). The eigenvalues are given by:

$$\lambda_k = \frac{1}{2}\left(1 + \cos k\right). \tag{6.B.3}$$

It is straightforward to obtain the dispersion relation imposing the boundary conditions:

$$\sin(k(l+1)) = 2m\pi \rightarrow k = \frac{2m\pi}{N+1}. \tag{6.B.4}$$

The von Neumann entropy is given by (3.55)

$$S_{\text{scs}}(l) = -\sum_k \lambda_k \log \lambda_k + (1-\lambda_k)\log\left(1-\lambda_k\right) \tag{6.B.5}$$

This finite sum can be evaluated using the Euler-McLaurin formula, inserting a finite width in momentum space, $\Delta_k = \frac{\pi}{l+1}$. We find:

$$\begin{aligned} S_{\text{scs}}(l) &= -\frac{l+1}{\pi}\int_0^{\pi}\left(\cos^2\left(\frac{k}{2}\right)\log\left(\cos^2\left(\frac{k}{2}\right)\right) + \sin^2\left(\frac{k}{2}\right)\log\left(\sin^2\left(\frac{k}{2}\right)\right)\right)dk \\ &= (l+1)(2\log 2 - 1). \end{aligned} \tag{6.B.6}$$

The Rényi entropies (3.54) can also be computed:

$$\begin{aligned} S_2(l) &= (l+1)\log\left(24 - 16\sqrt{2}\right), \\ S_3(l) &= (l+1)2\log\frac{4}{3}, \\ S_4(l) &= (l+1)\left(7\log 2 - \log\left(17 + 8\sqrt{2} + 4\sqrt{26+17\sqrt{2}}\right)\right), \end{aligned} \tag{6.B.7}$$

and these expressions can be seen to match perfectly the numerical data for a scs rainbow chain with $h = 9.2$ and $L = 21$ in Fig. 6.B.2.

6.C Strong inhomogeneity regime of scs model with a defect

In this Appendix we derive the ground state of the Hamiltonian

$$H_N(h,\gamma)_{\text{scs}} = -\frac{1}{2}\sum_{m=1}^{N} J_m c_m^{\dagger} c_{m+1} + \text{h.c.}, \tag{6.C.1}$$

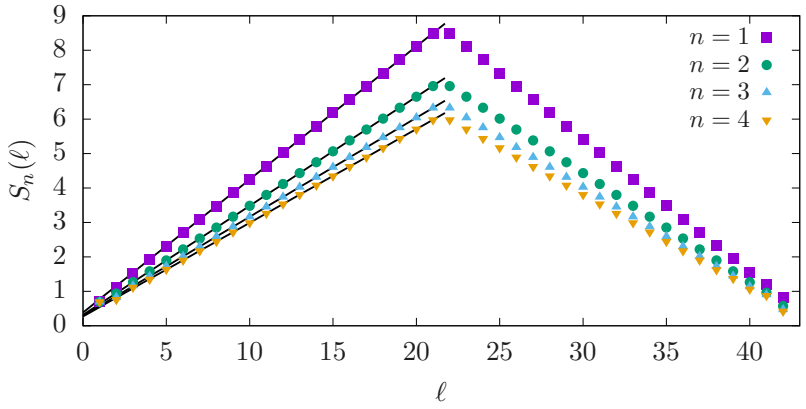

Figure 6.B.2: Different Rényi entropies for a scs system with $L = 21$ and $h = 9.2$ Black lines correspond to the theoretical expressions, (6.B.7).

with

$$J_m = \begin{cases} e^{-h(|m-(L+\frac{1}{2})|-\frac{1}{2})} & \text{if } m \neq L, L+1, \\ e^{-h\gamma} & \text{if } m \in \{L, L+1\} \end{cases} \tag{6.C.2}$$

We use the RG scheme explained in the main text. Let us recall the definition of a generic bonding operator (4.12)

$$b^{\pm}_{m,n} = \frac{1}{\sqrt{2}} \left(c_m \pm c_n \right), \tag{6.C.3}$$

that we shall use to distinguish three situations:

(1.-) Case $\gamma < 1$. The couplings present a *double tie* at the center, so that the dominant interaction involves the three central sites, L, $L+1$ and $L+2$. The Dasgupta-Ma prescription (5.8) and the sum rule (5.A.1) are not valid in this situation. We must perform a first order perturbation approach to renormalize three fermionic sites into an effective site (see Appendix 6.A), leading to a system with $N-2$ sites. The next RG step involves the effective fermion mode created on the previous one and its two nearest neighbours. Iterating this procedure one obtains the GS (6.8).

(2.-) Case $\gamma = 1$. The system presents a *quadruple tie* at the center. The five central sites involved are renormalized into an effective site on a system with $N-4$ sites. At this point the situation is equivalent to the $\gamma < 1$ case and further RG steps are the same as the ones discussed in the previous item.

(3.-) Case $\gamma > 1$. In this situation, the dominant interactions are two non-consecutive log-couplings 1, which couple respectively the sites $L-1$ and L, and the sites $L+2$ and $L+3$. Although the sum rule (5.A.1) is not valid, the Dasgupta-Ma (5.8) can be applied sequentially twice, yielding two fermionic excitations with the same energy and parity, $b^{\dagger}_{L-1,L}$ and $b^{\dagger}_{L+2,L+3}$, and leading to a effective system whose Hamiltonian is $H_{N-4}(h, 1+\gamma)_{\text{scs}}$. The next decimation step is not univocal:

- If $\gamma \in (1,2)$ the dominant interaction involves the three central sites $L-2$,L

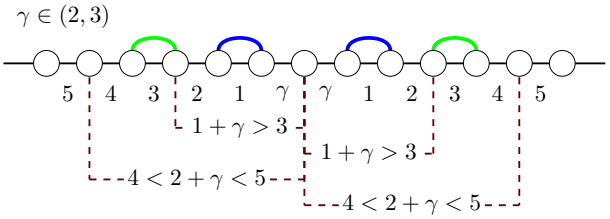

Figure 6.C.1: RG procedure for a system $H_N(h,\gamma)_{\text{scs}}$ with $h \gg 1$ and $\gamma \in (2,3)$. The system admits two Dasgupta-Ma RG steps, above links with log-coupling 1, and after those the renormalized system shows a *double tie* of lowest log-couplings, with the two central log-couplings equal to $1+\gamma$ (which must be larger than 3). At this moment, we apply the same RG procedure than for $\gamma < 1$.

and $L+4$ of the original chain and the situation is the same as the one described originally for $\gamma < 1$, with the double tie (1.).

- If $\gamma = 2$ there is a quadruple tie, same as (2.).
- If $\gamma \in (2,3)$ the dominant interactions are the two links with log-coupling 3, which is similar to the situation described in item (3.). At the end of this step there are two fermionic excitations more, $b^+_{L-3,L-2}$ and $b^+_{L+4,L+5}$, and the Hamiltonian of the decimated system is $H_{N-8}(h,2+\gamma)_{\text{scs}}$. We show in Fig. 6.C.1 this situation.

Note that unless $\gamma > L-1$ the RG flows towards the double tie situation and, if $\gamma \in \mathbb{N}$, the decimated system of the γ-th step will present a quadruple tie. Hence, the GS is:

$$|GS\rangle_{\gamma>1} = (g^-_L)^\dagger \prod_{k=1}^{L-2(1+\lfloor\gamma\rfloor)} (d^{\eta_k}_{k+2\lfloor\gamma\rfloor})^\dagger (g^-_{\lfloor\gamma\rfloor})^\dagger \prod_{m=1}^{\lfloor\gamma\rfloor} (b^+_{L-2(m-1),L-2(m-1)-1})^\dagger (b^+_{L+2m,L+2m+1})^\dagger |0\rangle, \tag{6.C.4}$$

where $\lfloor\,\rfloor$ is the floor function, $\eta_k = (-1)^{k+1}$, $\chi_k = (-1)^{k-\lfloor\gamma\rfloor}$ and

$$g^\pm_m = \frac{1}{\sqrt{2}}(c_{L+1} \pm b^+_{L-2m,L+2(m+1)}), \tag{6.C.5}$$

$$g^\pm_L = \frac{1}{\sqrt{2}}(c_1 \pm b^+_{2,2L}) \tag{6.C.6}$$

$$d^\pm_n = \frac{1}{\sqrt{2}}(b^\pm_{L+1-n,L+1+n} + b^\pm_{L-n,L+2+n}), \tag{6.C.7}$$

6.D The bcs state as a Charge Density Wave

The folding trick described in the main text allows us to transform the inhomogeneous $1D$ bcs chain into a ladder of 2 legs in terms of the bonding and antibonding states $b^\pm_n$ which are defined in (6.6):

$$H_{\text{bcs}} = -\frac{1}{2}\Big(\sum_{n=1}^{L-1} J_{L-n}\left((b_n^+)^\dagger b_{n+1}^+ + (b_n^-)^\dagger b_{n+1}^- + \text{h.c.}\right) + J_L((b_1^+)^\dagger b_1^+ - (b_1^-)^\dagger b_1^-) + J_{2L}((b_L^+)^\dagger b_L^+ - (b_L^-)^\dagger b_L^-)\Big), \tag{6.D.1}$$

In this appendix we show that the bcs state can be described by a charge density wave (CDW), when expressed on terms of these folded operators. In order to show that, we realize that the above Hamiltonian describes two independent inhomogeneous fermionic $1D$ chains with a single site endowed with non-zero chemical potential on their edges. Since they are independent, we can restrict our discussion to one of the chains and rewrite it in a more generic form:

$$H = -\mu_1 b_1^\dagger b_1 - \mu_L b_L^\dagger b_L - \sum_{m=1}^{L-1} J_m \left(b_m^\dagger b_{m+1} + \text{h.c.}\right), \tag{6.D.2}$$

where the J_m are positive numbers. Since we are dealing with an inhomogeneous system, the strong inhomogeneity regime should be well described by a decimation procedure, analogous to the SDRG. On each RG step we will only consider two fermionic modes, corresponding to the highest energy scale, either a hopping or a chemical potential. Let us consider a block Hamiltonian

$$H_B = -\mu_1 b_1^\dagger b_1 - J_1 \left(b_1^\dagger b_2 + b_2^\dagger b_1\right), \tag{6.D.3}$$

which is coupled to the rest of the system through its nearest neighbour:

$$H_I = -J_2 \left(b_2^\dagger b_3 + b_3^\dagger b_2\right). \tag{6.D.4}$$

The energies of H_B are $\epsilon = \frac{1}{2}(-\mu_1 \pm \sqrt{\mu_1^2 + 4J_1^2})$. In the regime ($|\mu_1| \gg J_1$) the energies and their corresponding eigenvectors are

$$\epsilon_1 \approx -\mu_1 - \frac{J_1^2}{\mu_1}, \quad u \approx \tfrac{1}{|\mu_1|}\left(\mu_1 b_1 + J_1 b_2\right), \tag{6.D.5}$$

$$\epsilon_2 \approx \frac{J_1^2}{\mu_1}, \quad v \approx \tfrac{1}{|\mu_1|}\left(-J_1 b_1 + \mu_1 b_2\right). \tag{6.D.6}$$

Hence we can rewrite (6.D.3) and (6.D.4) as:

$$H_B = \epsilon_1 u^\dagger u + \epsilon_2 v^\dagger v, \tag{6.D.7}$$

$$H_I \approx -\frac{J_2}{|\mu_1|}\left(\left(\mu_1 v^\dagger + J_1 u^\dagger\right) b_3 + \text{h.c.}\right). \tag{6.D.8}$$

Now we are ready to decimate. The original four-dimensional Hilbert space, $\mathcal{H}$ is spanned by the states $\{|0\rangle, u^\dagger|0\rangle, v^\dagger|0\rangle, v^\dagger u^\dagger|0\rangle\}$. The truncation operation leads to a new two-dimensional Hilbert space $\mathcal{H}'$ which is spanned by two states $\{|\tilde{0}\rangle, |\tilde{1}\rangle\}$, such that $|\tilde{1}\rangle$ contains one more particle than $|\tilde{0}\rangle$. Notice that the largest energy scale in the process is given by $|\mu_1|$. Thus, the truncation procedure depends on its sign:

- If $\mu_1 > 0$ we take $\left|\tilde{0}\right\rangle = u^\dagger |0\rangle$ and $\left|\tilde{1}\right\rangle = v^\dagger u^\dagger |0\rangle$. The new vacuum is filled with one fermion on site 1 ($u \overset{\mu_1 \gg J_1}{\longrightarrow} b_1$) and the truncated Hamiltonian $H_B^{(1)} = H_B + H_I$ takes the form:

$$H_B^{(1)} = \frac{J_1^2}{\mu_1} v^\dagger v - J_2(v^\dagger b_3 + d_3^\dagger v) + \epsilon_1. \tag{6.D.9}$$

- If $\mu_1 < 0$ we choose $\left|\tilde{0}\right\rangle = |0\rangle$ and $\left|\tilde{1}\right\rangle = v^\dagger |0\rangle$. The new vacuum state does not get any new particle, and

$$H_B^{(1)} = -\frac{J_1^2}{|\mu_1|} v^\dagger v - J_2(v^\dagger b_3 + d_3^\dagger v), \tag{6.D.10}$$

Hence in both cases the renormalized Hamiltonian has the same structure than the original one (6.D.3)

$$H_B^1 = -\mu^{(1)} v^\dagger v - J_2(v^\dagger b_3 + d_3^\dagger v), \tag{6.D.11}$$

where $\mu^{(1)} = -\frac{J_1^2}{\mu_1}$. Note that the sign of $\mu^{(1)}$ is *the opposite* of the sign of μ_1. Hence, if $|\mu^{(1)}| \gg J_2$ we have the opposite situation of above that we had in the previous step.

If we iterate this procedure, we find that after r steps the system has $L - r$ sites and the renormalized block Hamiltonian always takes the form

$$H^{(r)} = -\mu^{(r)} v^\dagger v - J_r v^\dagger b_{r+1}^\dagger, \quad r = 1 \dots L - 1,$$

where $\mu^{(r)}$ is the new effective chemical potential, whose sign is opposite to that of $\mu^{(r-1)}$. The sign alternation of the effective chemical potentials and the monotonous decay of the consecutive energy scales, $|\mu^{(r)}| \gg J_r$ for all r, imposed by (6.2) leads to a chain with an alternation on the filling of the sites. We realize that the Hamiltonian (6.D.1) describes two chains that only differ on the sign of their effective chemical potentials, and therefore its ground state presents the structure described in Fig. 6.3.

6.E XXZ Inhomogeneous model

6.E.1 Hamiltonian

In this appendix we develop an alternative renormalization approach based on the spin formalism which can be extended to the inhomogeneous XXZ model, described by:

$$H = \sum_{n=1}^{2L} J_n \left(S_n^+ S_{n+1}^- + S_n^- S_{n+1}^+ + \frac{\Delta}{2} S_n^z S_{n+1}^z \right) \equiv \sum_{n=1}^{2L} J_n (\mathbf{S_n} \cdot \mathbf{S_{n+1}})_\Delta \equiv \sum_{n=1}^{2L} h_n, \tag{6.E.1}$$

where J_n follow the rule expressed in (6.3). On the regime $h \gg 1$ it is natural to consider only the 3 spins which are coupled with the strongest hopping amplitudes, i.e. $n = L-1, L, L+1$. It can be checked that the GS of this Hamiltonian lies on the sector of the total spin $S_z^{tot} = \frac{1}{2}$, so that it is natural to renormalize the 3 spin block to an effective spin $\frac{1}{2}$, $\mathbf{S_L^{(1)}}$.

$$|\tilde{+}\rangle = \frac{1}{\mathcal{N}}(|++-\rangle - \lambda|+-+\rangle + |-++\rangle), \tag{6.E.2}$$

$$|\tilde{-}\rangle = \frac{1}{\mathcal{N}}(-|--+\rangle + \lambda|-+-\rangle - |+--\rangle), \tag{6.E.3}$$

where

$$\mathcal{N} = \sqrt{\lambda^2+2}, \quad \lambda = \frac{1}{2}(\Delta + \sqrt{\Delta^2+8}), \tag{6.E.4}$$

and the GS energy is $E_0 = -\frac{\lambda}{2}$. In order to determine how the spins $\mathbf{S}_{L-1}$ and $\mathbf{S}_{L+1}$ got renormalized we employ the Wigner-Eckhart theorem:

$$\langle \tilde{m}|S_i^a|\tilde{n}\rangle = \xi_i^a \langle \tilde{m}|S_L^{a(1)}|\tilde{n}\rangle, \tag{6.E.5}$$

which leads to:

$$\xi_{L-1}^{\pm} = \xi_{L+1}^{\pm} = \frac{2\lambda}{\mathcal{N}^2}, \qquad \xi_L^{\pm} = -\frac{2}{\mathcal{N}^2}, \tag{6.E.6}$$

$$\xi_{L-1}^{z} = \xi_{L+1}^{z} = \frac{\lambda^2}{\mathcal{N}^2}, \qquad \xi_L^{z} = \frac{2-\lambda^2}{\mathcal{N}^2}. \tag{6.E.7}$$

Note that $\sum_n \xi_n^z = 1$ for all λ and that $\sum_n \xi_n^{\pm} = \frac{4\lambda-2}{\mathcal{N}^2}$, which is 1 only if the $SU(2)$ symmetry is present. This only holds when $\lambda = 2$, i.e. $\Delta = 1$.

Hence we see that each step of the renormalization involves three spins: s_u and s_d at the edges of the block and one central s_c which is the outcome of each step except the first one, which is physical too (see Fig. 6.1 (b)).

6.E.2 Fixed Points and RG flow

The next step of the renormalization procedure involves the spins $S_{L\pm2}$. Using (6.E.7) we notice that the corresponding terms of the Hamiltonian (6.E.1), can be written in terms of the effective spin of the previous step:

$$e^{-h}((\mathbf{S_{L-2}}\cdot\mathbf{S_{L-1}})_\Delta + (\mathbf{S_{L+1}}\cdot\mathbf{S_{L+2}})_\Delta) = e^{-h}((\mathbf{S_{L-2}}\cdot\mathbf{S_L^{(1)}})_{\Delta'} + (\mathbf{S_L^{(1)}}\cdot\mathbf{S_{L+2}})_{\Delta'}), \tag{6.E.8}$$

where

$$\Delta' = \frac{\Delta}{4}(\Delta + \sqrt{8+\Delta^2}). \tag{6.E.9}$$

Imposing $\Delta' = \Delta$, we determine the existence of two fixed points: $\Delta_f = 0$ (XX) and $\Delta_f = 1$ (AFH). Furthermore, iterating this equation while replacing $\Delta \to \Delta \pm \epsilon$ with $\epsilon \ll 1$ it is straightforward to see that the former is stable ($|\Delta'| < |\Delta|, \Delta < 1$) while the latter is unstable ($\Delta' \geq \Delta, \Delta \geq 1$), as is depicted on Fig. 6.E.1.

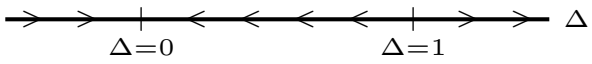

Figure 6.E.1: RG flow in terms of the anisotropy parameter Δ.

6.E.3 MPS form

As it has been described along the RG procedure, each step only considers three spins: two physical ones, s_u, s_d placed on the edges of the block, and an effective spin, s_c placed on the center, which arises from the previous step. These three spins are renormalized into a new effective spin $\frac{1}{2}$, s_c'. Hence, (6.E.3) can be written compactly in the form:

$$|s_c'\rangle = \sum_{s_u,s_c,s_d} A^{s_c'}_{s_u s_c s_d} |s_u s_c s_d\rangle \,, \tag{6.E.10}$$

with

$$A^{s}_{\bar{s}ss} = A^{s}_{ss\bar{s}} = \frac{s}{\mathcal{N}}, \qquad A^{s}_{s\bar{s}s} = -\frac{s\lambda}{\mathcal{N}}, \qquad s = \pm, \bar{s} = -s. \tag{6.E.11}$$

We can rewrite this elementary block of the MPS in another more familiar form where central spins are now indices of the auxiliary space.

$$A^{s_c'}_{s_u s_c s_d} \to A^{s_u+s_d}_{s_c s_c'}, \tag{6.E.12}$$

so that

$$A^{-} = \frac{\lambda}{\mathcal{N}}\begin{pmatrix} 0 & 0 \\ 1 & 0 \end{pmatrix}, \quad A^{+} = \frac{\lambda}{\mathcal{N}}\begin{pmatrix} 0 & -1 \\ 0 & 0 \end{pmatrix}, \quad A^{0} = \frac{1}{\mathcal{N}}\begin{pmatrix} 1 & 0 \\ 0 & -1 \end{pmatrix}. \tag{6.E.13}$$

If we particularize for the Heisenberg model, we recover (up to an overall constant) the usual matrices that describe the MPS form of the AKLT state (Schollwöck 2011). It is straightforward also to build the basis used in Pollmann *et al.* (2012, 2010) to prove the degeneracy of the entanglement spectrum due to the presence of the time reversal symmetry.

Chapter 7

Ising Rainbow Model in and out of criticality

We propose the rainbow analogue of the critical Ising chain in a transverse field. In the strong inhomogeneity limit we apply Fisher's renormalization group to show that the ground state is formed by concentric singlets similar to those of the rainbow state of the XX model. In the weak inhomogeneity limit we map the model to a massless Majorana fermion living in a hyperbolic spacetime, where, using CFT techniques, we derive the entanglement entropy that is violated linearly. We also study an inhomogeneous non-critical Ising model that for weak inhomogeneity is mapped to a massive Majorana fermion, while for strong inhomogeneity regime it exhibits trivial and non-trivial topological phases and a separation between regions with high and low entanglement. We also present the entanglement Hamiltonian of the model. This chapter contains content published in Samos Sáenz de Buruaga *et al.* (2021).

The aim of the present chapter is twofold. First, to characterize the emergence of a rainbow state as a ground state of an inhomogeneous transverse field Ising (ITF) Hamiltonian, when the couplings and the external fields are allowed to decay in a certain way, by mapping it to a (1+1)D massless Majorana field on curved spacetime. Then, we will describe the structure of the model away from the critical point, showing that it reduces to a massive Majorana field in the same setup. Moreover, we shall also consider the relation between our model and the Kitaev chain (Kitaev 2001).

The chapter is organized as follows. In Section 7.1 we introduce an inhomogeneous version of the ITF model and describe its entanglement structure. The strong inhomogeneity regime is discussed by means of RG schemes, and the weak inhomogeneity regime is characterized via field theory methods. In Section 7.2 we

propose a variation of the previous model by adding a new parameter that shifts it away from the critical point, and we describe its entanglement properties in the strong and weak inhomogeneity regimes.

7.1 The Ising rainbow model

Let us consider an inhomogeneous ITF open spin $1/2$ chain with an even number of sites $N = 2L$ whose Hamiltonian is defined as:

$$H_I = -\sum_{m=-L+1/2}^{L-3/2} J_m \sigma_m^z \sigma_{m+1}^z - \sum_{m=-L+1/2}^{L-1/2} \Gamma_m \sigma_m^x, \tag{7.1}$$

Notice that the spins are indexed by half-odd integers for later convenience, $m = -L + 1/2, \ldots, L - 1/2$. We shall apply a Jordan-Wigner transformation (see (3.6)) and write (7.1) in terms of Dirac fermions $c_m^\dagger$ which satisfy the usual anti-commutation relations $\{c_m^\dagger, c_n\} = \delta_{mn}$, and then decompose them in terms of Majorana fermions

$$c_m = \frac{1}{2}(\alpha_m + i\beta_m), \tag{7.2}$$

that satisfy the anti-commutation relations

$$\{\alpha_m, \alpha_n\} = \{\beta_m, \beta_n\} = 2\delta_{mn}, \quad \{\alpha_m, \beta_n\} = 0.$$

In terms of these Majorana fermions (7.1) reads:

$$\begin{aligned} H = -i\Big(& \sum_{m=1/2}^{L-1/2} \Gamma_m \left(\alpha_m \beta_m + \alpha_{-m}\beta_{-m}\right) \\ & + \sum_{m=1/2}^{L-3/2} J_m \left(\beta_m \alpha_{m+1} + \beta_{-(m+1)}\alpha_{-m}\right) + J_{-1/2}\beta_{-1/2}\alpha_{1/2}\Big), \end{aligned} \tag{7.3}$$

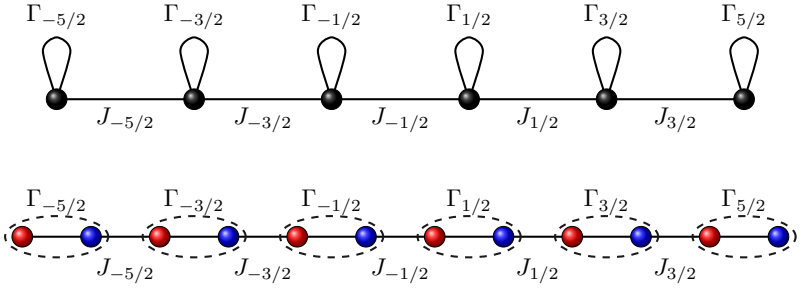

Figure 7.1: Spin (top) and Majorana fermion (bottom) representations of the inhomogeneous ITF model. The red (blue) points correspond to α (β) Majorana fermions.

Notice that the same system is described by $2L$ spins and $4L$ Majorana fermions. In Fig. 7.1 we present a schematic representation of the model in terms of spins

(top) and Majorana fermions (bottom). The transverse field Γ_m couples two Majorana fermions with the same index (α_m, β_m), while the coupling constants J_m link Majorana fermions with different indices (β_m, α_{m+1}). The dashed lines that encircle the Majorana fermions represent the Dirac fermions c_m in (7.2).

Notice that if $J_m = \Gamma_m = 1$ for all m we recover the critical ITF model whose low-energy behaviour is described by the two dimensional Ising CFT with central charge $c = 1/2$. In addition, if $J_m = 0$ for all m, the ground state becomes a trivial product state built upon the physical fermions c_m. On the contrary, if $\Gamma_m = 0$ for all m, the Majorana fermions placed at the edges of the Majorana chain, $\alpha_{-L+1/2}$ and $\beta_{L-1/2}$, do not appear in the Hamiltonian, (7.3). Moreover, they correspond to Majorana zero modes and the GS belongs to the topologically non-trivial phase of the Kitaev model (Kitaev 2001).

Let us consider both the spin (7.1) and the Majorana fermion (7.3) Hamiltonians under the following choice of coupling constants J_m and Γ_m:

$$\begin{aligned} J_m &= \begin{cases} e^{-2h|m+1/2|} & \text{if } m \neq -1/2, \\ e^{-h/2} & m = -1/2, \end{cases} \\ \Gamma_m &= e^{-2h|m|}, \end{aligned} \tag{7.4}$$

where $h \geq 0$ is the inhomogeneity parameter. Notice that for $h > 0$ the intensity of the couplings decreases from the center towards the edges, with $J_{-1/2}$ corresponding to the strongest coupling. Also, the system is symmetric under reflections around the central bond, satisfying $J_{-(m+1)} = J_m$ and $\Gamma_m = \Gamma_{-m}$. In the remainder of this section, we shall describe the strong ($h \gg 1$) and weak ($h \ll 1$) inhomogeneity regimes.

7.1.1 Strong inhomogeneity

In the limit $h \gg 1$ we can characterize the GS of (7.3) using the strong disorder renormalization scheme (SDRG) developed by Fisher (1995, 1994) for the ITF. It was devised for finding the ground states of random ITF chains but, as we have shown, the SDRG can be applied to non-disordered inhomogeneous systems. Fisher's RG proceeds by finding the strongest interaction coupling, either Γ or J, which gets sequentially decimated. If it corresponds to a magnetic field, Γ_i, the i-th spin is integrated out, leaving the system with one spin less and a new coupling term between the spins $i-1$ and $i+1$,

$$\tilde{J}_{i-1}\sigma^z_{i-1}\sigma^z_{i+1}, \qquad \text{with} \quad \tilde{J}_{i-1} = \frac{J_{i-1}J_i}{\Gamma_i}. \tag{7.5}$$

On the other hand, if the coupling J_i is the strongest interaction at a given RG step, the spins i and $i+1$ get renormalized into a single spin with effective Hamiltonian

$$\tilde{\Gamma}_i \sigma_i^x, \qquad \text{with } \tilde{\Gamma}_i = \frac{\Gamma_i \Gamma_{i+1}}{J_i}. \tag{7.6}$$

Notice that renormalizing a J term entangles two neighboring spins, while the renormalization of a Γ term freezes that spin along the direction of the magnetic field, and decouples it from the chain.

It can be shown that the fusion rules of Majorana fermions correspond to the $SU(2)_{k=2}$ algebra (Bonesteel and Yang 2007; Lahtinen and Pachos 2017; Nayak *et al.* 2008), which in turn coincide with those of the quantum-group $U_{q=i}(su(2))$ with the relation $q = e^{i2\pi/(k+2)}$ (Gómez *et al.* 1996). The non-univocal fusion rule

$$\frac{1}{2} \times \frac{1}{2} = 0 + 1, \tag{7.7}$$

corresponds to the pairing of two Majorana fermions, for instance $\alpha_m \beta_m$, which in terms of of Dirac fermions is $2\,(c_m^\dagger c_m - 1/2)$, see (7.2), and we can attach the fusion channel 0 (1) to the -1 $(+1)$ eigenvalue. Indeed, notice that (7.7) reminds the composition of two $1/2$ spins. Thus, we may call the less energetic channel a *generalized singlet state* (Bonesteel and Yang 2007; Fidkowski *et al.* 2008), and the other channel as a *generalized triplet* (albeit there is no S_z degeneracy). Notice that while the $1/2$ spins obey the $SU(2)$ algebra and the singlet states span the total $S_z = 0$ Hilbert space sector, Majorana fermions obey the $SU(2)_{k=2}$ algebra and the generalized singlet state spans the Hilbert space sector for the fusion channel 0.

With this parallelism in mind, we can devise an SDRG specially suited for an inhomogeneous Majorana chain (Devakul *et al.* 2017; Motrunich *et al.* 2001), as it is done in Appendix 7.A. At each RG step, the two Majorana fermions linked through the strongest coupling (notice that in terms of Majorana fermions the J and Γ terms are equivalent) are fused into their less energetic channel, forming a generalized singlet state or *bond*, and leaving a renormalized coupling between their closest neighbors. This scheme is completely equivalent to Fisher's RG, (7.5) and (7.6). In this case, the SDRG becomes analogous to the Dasgupta-Ma technique for spin-1/2 XX chains (Dasgupta and Ma 1980), for which it can be proved that the bonds never cross (Rodríguez-Laguna *et al.* 2016).

Let us apply this RG scheme to the Majorana Hamiltonian given in (7.3). The first Majorana pair to be decimated is $(\beta_{-1/2}, \alpha_{1/2})$, because $J_{-1/2}$ is the strongest coupling. Hence, these two Majorana fermions fuse into a Dirac fermion,

$$b_{1/2} = \frac{1}{2}\left(\beta_{-1/2} + i\alpha_{1/2}\right), \tag{7.8}$$

which becomes decoupled. Using (7.6) we can find an effective Hamiltonian with $2(N-1)$ Majorana fermions, whose new central term $\tilde{\Gamma}_{1/2}\alpha_{-1/2}\beta_{1/2}$ is given by

$$\tilde{\Gamma}_{1/2} = \frac{\Gamma_{-1/2}\Gamma_{1/2}}{J_{-1/2}} = e^{-\frac{3h}{2}}. \tag{7.9}$$

The strongest coupling is now $\tilde{\Gamma}_{1/2}$. We apply the RG again, and the decimated Majorana fermions fuse into a Dirac fermion,

$$d_{1/2} = \frac{1}{2}\left(\alpha_{-1/2} + i\beta_{1/2}\right). \tag{7.10}$$

The new effective Hamiltonian of $2(N-2)$ Majorana fermions has a central term $\tilde{J}_{3/2}$ which is given by (7.5),

$$\tilde{J}_{3/2} = \frac{J_{-3/2}J_{1/2}}{\tilde{\Gamma}_{1/2}} = e^{-\frac{5h}{2}}, \tag{7.11}$$

which is again the strongest coupling in the chain. Given the symmetry of the coupling constants, (7.4), all RG steps decimate the central pair of Majorana fermions, fusing them alternatively into b and d Dirac fermions. Hence, the ground state, that we shall call the Majorana rainbow state $|\text{MRS}\rangle$, is annihilated by the following Dirac operators:

$$b_m\,|\text{MRS}\rangle = 0, \quad d_m\,|\text{MRS}\rangle = 0, \quad m = \frac{1}{2}, \ldots, L - \frac{1}{2}, \tag{7.12}$$

with

$$b_m = \frac{1}{2}\left(\beta_{-m} + i\alpha_m\right), \quad d_m = \frac{1}{2}\left(\alpha_{-m} + i\beta_m\right). \tag{7.13}$$

$|\text{MRS}\rangle$ is a concentric generalized singlet state, shown in Fig. 7.2.

It is worth to compare the Majorana rainbow state (7.12) with its Dirac counterpart presented in Chapter 4, which emerges as the GS of the inhomogeneous XX chain and its fermionic version. As we have shown, this state can be seen as a singlet state of concentric bonding and antibonding operators (see (4.17)). The alternation is therefore similar to that of b and d Dirac fermions in (7.13).

Let us compute the entanglement entropy of a subsystem A, with length L_A, for the Majorana RS, (7.12). The entanglement entropy of any partition of a ground state formed by $SU(2)$ singlet states can be estimated by counting the number of bonds which cross the partition boundary, and multiplying by $\log(2)$. The procedure is the same when we deal with generalized singlet states. The entanglement entropy of any subsystem A can be estimated by counting the number of bonds which cross the partition boundary and multiplying by $\log d$ (Bonesteel and Yang 2007), where $d = \sqrt{2}$ is the quantum dimension of the spin $1/2$ representation of the algebra $SU(2)_2$.

Alternatively, the entanglement entropy of a Gaussian state can be obtained from its covariance matrix (CM), $\mathcal{C}$,

$$\mathcal{C}_{ab} = \langle[\gamma_a, \gamma_b]\rangle, \tag{7.14}$$

where we have arranged the Majorana operators in a vector form

$$\boldsymbol{\gamma}^T = (\alpha_{-L+1/2}, \beta_{-L+1/2}, \ldots, \alpha_{L-1/2}).$$

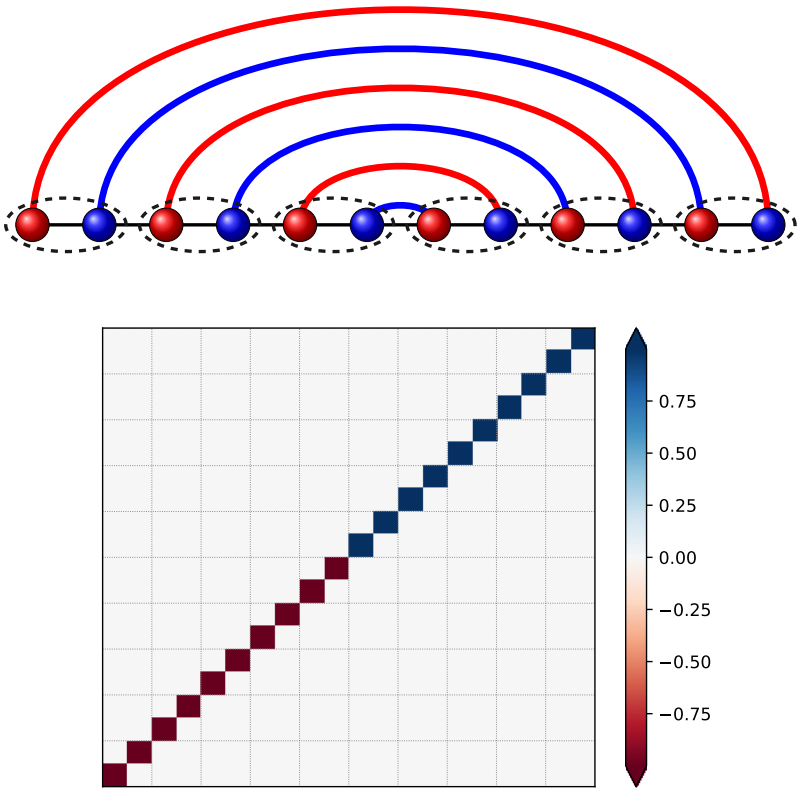

Figure 7.2: Top: schematic representation of the outcome of the RG for a chain of 6 spins. Blue bonds stand for b-type Dirac fermions, while red ones represent d-type fermions, see (7.13), which can also be considered as generalized singlet states corresponding to the less energetic fusion channel. Bottom: covariance matrix of the RS for $N = 20$ and $h = 10$. Notice that the non-zero elements are in the anti-diagonal, as it is dictated by the structure of the b and d fermions.

In Appendix 4.A.2 we provide a brief derivation of this expression. The structure of the GS obtained through the decimation procedure shows up in the CM, as we can see in Fig. 7.2 (b). The entanglement entropy of a subsystem A with size L_A can be computed through the eigenvalues $\pm\lambda_k$, $k \in \{1, \cdots, L_A/2\}$ of the appropriate restriction $\mathcal{C}_A$ of the CM (Peschel 2003), through

$$S_A = -\sum_{k=1}^{L_A} \nu_k \log \nu_k, \qquad \nu_k = \frac{1}{2}\left(1 + \lambda_k\right). \tag{7.15}$$

We can now compute the entanglement entropy of a lateral block of the system, $A_\ell = \{-L + 1/2 \cdots - L + 1/2 + 2\ell\}$, with $\ell = 1, \cdots, L$. Notice that a block with an odd number of Majorana operators has no physical sense. Thus, A_ℓ must contain an even number of Majorana fermions, which correspond to the physical fermions (dotted boxes) or the spins (black balls) of Fig. 7.1. We can obtain the entanglement entropy by counting the number of bonds n_b (reds and blues) that A_ℓ cuts in Fig. 7.2 and multiply it by $\log d$.

$$S_A = n_b \log \sqrt{2}. \tag{7.16}$$

Hence, we have that the entanglement entropy of the MRS grows linearly,

$$S(A_\ell) = 2\ell \log \sqrt{2} = \ell \log 2, \tag{7.17}$$

and the maximal entanglement entropy corresponds to the half chain block $S(A_L) = L \log 2$.

7.1.2 Weak inhomogeneity

In this section we shall consider the GS of (7.1) with couplings given by (7.4), in the low inhomogeneity regime, $h \ll 1$. The equations of motion associated to the lattice Hamiltonian in the Heisenberg picture are given by $i\partial_t \alpha_{\pm m} = [H, \alpha_{\pm m}]$ and $i\partial_t \beta_{\pm m} = [H, \beta_{\pm m}]$. Using (7.3) we have

$$\begin{aligned} \partial_t \alpha_n &= -2e^{-2h|n|}\left(\beta_n - e^{\mathrm{sign}(n)h}\beta_{n-1}\right), \\ \partial_t \beta_n &= 2e^{-2h|n|}\left(\alpha_n - e^{\mathrm{sign}(n)h}\alpha_{n+1}\right). \end{aligned} \tag{7.18}$$

Now, we define the fields

$$\alpha_m = \sqrt{a}\alpha(x), \quad \beta_m = \sqrt{a}\beta(x), \tag{7.19}$$

where a is the lattice spacing between the Dirac fermions c_m, $x = ma$, which satisfy the usual anticommutation relations, $\{\alpha(x), \alpha(x')\} = \{\beta(x), \beta(x')\} = 2\delta(x - x')$ and $\{\alpha(x), \beta(x)\} = 0$. We find the continuum limit of the lattice equations of motion by plugging these fields into (7.18) and requiring $a \to 0$ and $L \to \infty$ with both $\mathcal{L} = aL$ and $\hat{h} = h/a$ kept constant,

$$\begin{aligned}\partial_t\alpha(t,x) &\approx -2ae^{-2\hat{h}|x|}\left(\partial_x - \text{sign}(x)\hat{h}\right)\beta(t,x)\\ \partial_t\beta(t,x) &\approx -2ae^{-2\hat{h}|x|}\left(\partial_x - \text{sign}(x)\hat{h}\right)\alpha(t,x),\end{aligned} \tag{7.20}$$

where we made the approximation $e^{\text{sign}(x)h} \approx (1+\text{sign}(x)h)$. If $h = 0$ the equations of motion (7.20) correspond to the massless Dirac equation $i\partial\!\!\!/\Psi = (i\gamma^0\partial_0 + i\gamma^1\partial_1)\Psi = 0$, where we have introduced the spinor

$$\Psi^T = (\alpha(x^0,x^1),\beta(x^0,x^1)), \quad (x^0,x^1) = (2t,x). \tag{7.21}$$

Our choice for the γ matrices is $\gamma^0 = -\sigma_2$, $\gamma^1 = i\sigma_3$ and $\gamma^3 = \sigma_1$, where σ_i, $i = 1$, 2, 3, are the Pauli matrices. Hereafter, we choose $a = 1$ that sets the Fermi velocity $v_F = 1$, so we can simplify $\hat{h} = h$, $\mathcal{L} = L$, and rewrite the equations of motion of the inhomogeneous system, (7.20), as

$$\left(-\sigma_2\partial_0 + e^{-2h|x^1|}i\sigma_3\left(\partial_1 - \text{sign}(x^1)h\right)\right)\Psi = 0\ . \tag{7.22}$$

The previous equation corresponds to the massless Dirac equation in a curved spacetime whose metric depends on the inhomogeneity h, see Appendix 4.B for details. The Dirac equation on a generic metric can be written as (4.B.7),

$$\left(-\sigma_2\partial_0 + \frac{i}{2}\omega_0^{01}\sigma_3 + \frac{E_1^1}{E_0^0}\left(i\sigma_3\partial_1 - \frac{i}{2}\omega_1^{01}\sigma_2\right)\right)\Psi = 0, \tag{7.23}$$

where ω_μ^{ab} is the spin connection and E_a^μ is the inverse of the *zweibein*. Comparing (7.23) with our equations of motion (7.22), we obtain

$$\frac{E_1^1}{E_0^0} = e^{-2h|x^1|}, \tag{7.24}$$

$$\omega_0^{01} = -2e^{-2h|x^1|}h\text{sign}(x^1), \tag{7.25}$$

$$\omega_1^{01} = 0. \tag{7.26}$$

The solution of these equations gives rise to the spacetime metric:

$$g_{00} = -e^{-4h|x|}, \quad g_{11} = 1\ , \tag{7.27}$$

whose Euclidean version is

$$ds^2 = e^{-4h|x|}dt^2 + dx^2 = \Omega^2(x)dzdz, \tag{7.28}$$

where $\Omega(x) = e^{-2h|x|}$ is the Weyl factor and

$$z = \tilde{x} + it, \quad \text{with} \quad \tilde{x} = \int_0^x \frac{dy}{\Omega(y)} = \frac{\text{sign}(x)}{2h}\left(e^{2h|x|} - 1\right). \tag{7.29}$$

The non-zero Christoffel symbols are

$$\Gamma^0_{01} = -2h\,\mathrm{sign}(x), \quad \Gamma^1_{00} = -2h\,\mathrm{sign}(x)e^{-4h|x|}, \tag{7.30}$$

and the non-zero components of the Ricci tensor are

$$R_{00} = -e^{-4h|x|}\left(4h\delta(x) - 4h^2\right), \quad R_{11} = 4h\delta(x) - 4h^2. \tag{7.31}$$

The scalar of curvature $R = g^{\mu\nu}R_{\mu\nu}$ is

$$R = 8\left(h\delta(x) - h^2\right), \tag{7.32}$$

where we have used the general result (4.38). Thus, R is singular at the origin and constant and negative everywhere else, thus allowing for the holographic interpretation of the rainbow state that has been discussed in the literature (MacCormack *et al.* 2019). Observe that these are the same expressions that we have obtained in the study of the continuum limit of the rainbow model in Section 4.2 by replacing $h \to 2h$.

Entanglement entropies

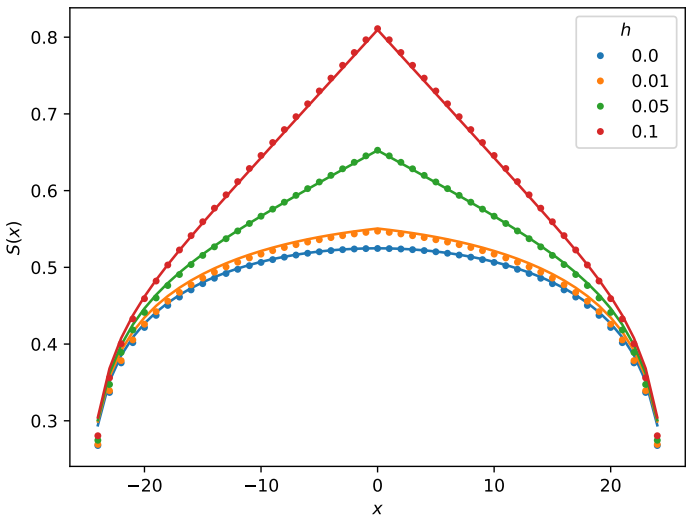

Figure 7.3: Entanglement entropy of lateral blocks of the GS of (7.1) with couplings (7.4) for different values of h and $L = 40$. The dots represent the numerical values obtained by exact diagonalization and the lines correspond to the predictions of (7.33) using (7.B.3).

We have shown that the continuum limit of the lattice model (7.3) corresponds to a Majorana field in curved spacetime, described by a conformal field theory with central charge $c = 1/2$. We can obtain the entanglement entropy of a block within this state employing the standard procedures (Calabrese and Cardy 2004)

discussed in Chapter 4: via the Weyl transformation of the correlation function of twist operators in an n-times replicated worldsheet. Hence, the entanglement entropy of the lateral blocks considered in the previous section is (see details of the derivation in Ref. (Rodríguez-Laguna *et al.* 2017)):

$$S(x) = \frac{1}{12}\log\left(\Omega(x)\frac{8\tilde{L}}{\pi}\cos\left(\frac{\pi\tilde{x}}{4\tilde{L}}\right)\right) + c_I'(\tilde{x}), \tag{7.33}$$

where the deformed quantities, $\tilde{x}$ and $\tilde{L}$, are computed using (7.29). The non universal function $c_I'(\tilde{x})$ can be found using the relation between the entanglement entropies of an XX chain of length $2L$ and an ITF chain of length L (Iglói and Juhász 2008), and is given in (7.B.3) of Appendix 7.B. Fig. 7.3 shows the numerical values of the entanglement entropy for different values of h, showing the agreement with (7.33). In the limit $hL \gg 1$, (7.33) implies for the half chain

$$S(x = 0) \approx \frac{1}{6}hL, \tag{7.34}$$

which scales linearly with the system size, thus presenting a smooth crossover between the weak and the strong inhomogeneity regimes for which the entanglement entropy is given by (7.17), i.e. $S_{A_L} = L\log 2$. In addition, this value of the entanglement entropy can be interpreted as that of a thermal state with an effective temperature h/π (Rodríguez-Laguna *et al.* 2017).

Entanglement Hamiltonian

Let us now characterize the entanglement Hamiltonian (see Section 3.3.1 associated to the reduced density matrix of the half chain, that we shall denote $\mathcal{H}_L$. In Appendix 4.A.2 we discuss the standard procedure to obtain the entanglement Hamiltonian using the covariance matrix C_L (Peschel 2003; Peschel and Eisler 2009). The entanglement Hamiltonian describes a local inhomogeneous system with the weakest couplings near the center, which is the internal boundary between the block and its environment. Moreover, if the physical system is critical and infinite, it can be shown that $\mathcal{H}_L$ is given by (3.81)

$$\mathcal{H}_L = 2\pi L\int_0^L dx\; J(x)\; T_{00}(x), \tag{7.35}$$

where $T_{00}(x)$ is the Hamiltonian density of the physical system and $J(x)$ is a weight function[1]. The Bisognano-Wichmann theorem predicts $J(x) \approx x$ for a semi-infinite line, thus being approximately applicable for our case. Moreover, when the original system is placed on a static metric, the weight function in (7.35) $J(x)$ should be appropriately deformed following (7.29) (Tonni *et al.* 2018) as we discussed in (4.2.2). In our case, we obtain

[1]Observe that we have relabelled the weight function $\beta(x) \to J(x)$ in order to avoid possible confusions with the Majorana fermion field $\beta(x)$.

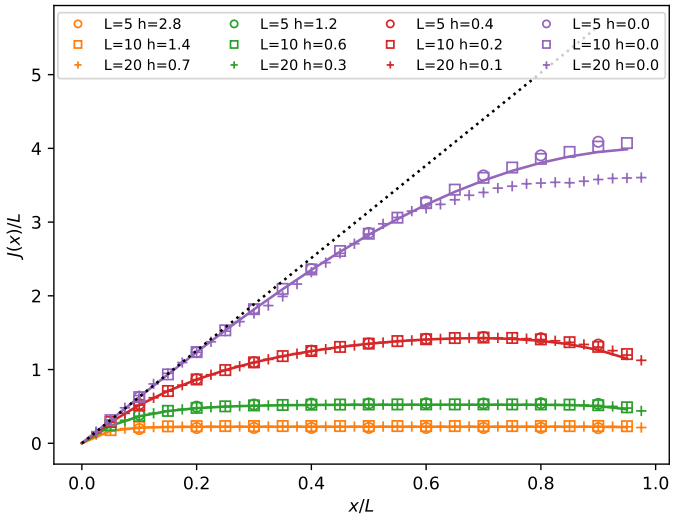

Figure 7.4: Normalized weight functions $J(x)/L$ determining the entanglement Hamiltonian for different values of $\lambda = 2hL$. Continuous lines correspond to the theoretical prediction, (7.36). The dotted black straight line corresponds to the Bisognano-Wichmann prediction for a semi-infinite system.

$$J(x) = \frac{2L}{\pi}\frac{e^{\lambda}-1}{\lambda}e^{-\lambda\frac{x}{L}}\sin\left(\frac{\pi}{2}\frac{e^{\lambda\frac{x}{L}}-1}{e^{\lambda}-1}\right), \tag{7.36}$$

where $\lambda = 2hL$. Near the internal boundary, which corresponds to the center of the chain, the weight function $J(x)$ grows linearly $J(x) \simeq 2\pi x$, as predicted by Bisognano and Wichmann. Far from $\tilde{x} = 0$, the weight function develops a plateau, as it can be seen in Fig. 7.4 where $J(x)$ is plotted for different values of λ.

7.2 Out of criticality

Let us consider an inhomogeneous ITF model described by the Hamiltonian (7.1) or, equivalently, (7.3), with a modification of the coupling constants (7.4) studied in the previous section,

$$J_m = \begin{cases} e^{-2h|m+1/2|+\delta} & \text{if } m \neq -1/2, \\ e^{-h/2+\delta} & m = -1/2, \end{cases} \tag{7.37}$$

$$\Gamma_m = e^{-2h|m|-\delta}, \tag{7.38}$$

where $\delta \in \mathbb{R}$. Notice that if $h = 0$ and $\delta \ll 1$, then $J_m = 1 + \delta$ and $\Gamma_m = 1 - \delta$, and our system describes a Majorana chain with alternating couplings, thus showing a relation to the Kitaev chain and the Su-Schrieffer-Heeger (SSH) model describing a dimerized chain of Dirac fermions (Heeger *et al.* 1988; Su *et al.* 1979). Indeed, the

alternating term $e^{\pm\delta}$ pushes the system described in Section 7.1 out of criticality, as we will describe throughout this section.

7.2.1 Strong inhomogeneity

Let us consider the Hamiltonian given in (7.3) in the limit $h \gg 1$. We can apply the same SDRG of the previous section, making use of the parameter

$$\kappa = \delta/h. \tag{7.39}$$

The RS is obtained when all the RG steps decimate the Majoranas at the center of the chain, but we will show that other structures may be obtained, depending on the value of κ. In order to decimate the central pair we need $J_{1/2}$ to be the strongest coupling of the chain. In other words, $J_{-1/2} > \Gamma_{1/2}$ which implies that $e^{-h(1/2-\kappa)} > e^{-h(1+\kappa)}$. Hence, we arrive at the condition

$$\frac{1}{2} - \kappa < 1 + \kappa \Rightarrow \kappa > -\frac{1}{4}. \tag{7.40}$$

Thus, if $\kappa > -1/4$ the Majorana fermions $\beta_{-1/2}$ and $\alpha_{1/2}$ fuse into the Dirac fermion $b_{1/2}$, defined in (7.8) and, using (7.6), we obtain a renormalized coupling

$$\tilde{\Gamma}_{1/2} = e^{-3h\left(\frac{1}{2}+\kappa\right)}, \tag{7.41}$$

which will couple $\alpha_{-1/2}$ and $\beta_{1/2}$. These Majorana fermions are decimated at the second RG step fusing into $d_{1/2}$, (7.10), if $\tilde{\Gamma}_{1/2} > J_{1/2}$, implying that

$$3\left(\frac{1}{2} + \kappa\right) < 2 - \kappa \Rightarrow \kappa < \frac{1}{8}, \tag{7.42}$$

and then a new term appears in the effective Hamiltonian of the form $\tilde{J}_{3/2}\beta_{-3/2}\alpha_{3/2}$, where $\tilde{J}_{3/2}$ follows from (7.5),

$$\tilde{J}_{3/2} = e^{-5h\left(\frac{1}{2}-\kappa\right)}. \tag{7.43}$$

Summarizing, the first central decimation requires $\kappa > -1/4$ while the second requires $\kappa < 1/8$. We can iterate this procedure and find that the bound on κ associated with exactly n consecutive central decimations is given by

$$\begin{aligned} &\kappa > -\frac{1}{4n}, \text{ if } n \text{ odd}, \\ &\kappa < \frac{1}{4n}, \text{ if } n \text{ even}. \end{aligned} \tag{7.44}$$

The state with exactly n central decimations will be called $|n\rangle$. With this notation, the RS corresponds to $|n = 2L\rangle$, and satisfies

$$|\kappa| < \frac{1}{8L}. \tag{7.45}$$

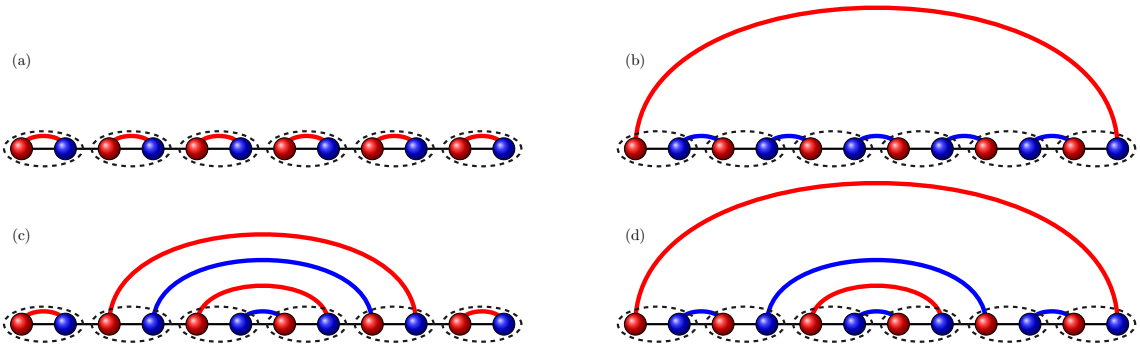

Figure 7.5: Schematic representation of different ground states of (7.3) obtained with the SDRG scheme. The trivial (a) and non-trivial (b) local pairings correspond to the states $|n = 0\rangle$ and $|n = 1\rangle$, the two possible ground states of the Kitaev chain. Panels (c) and (d) illustrate ground states with coexistence between non-local rainbow-like and local fermions. The topological type of the local pairing depends on the parity of n. Hence, we have a trivial pairing (c) $|n = 4\rangle$ and a non trivial one $|n = 3\rangle$ in (d).

Whenever a central decimation fails, the SDRG must choose the strongest couplings between two identical links, symmetrically placed with respect to the center of the chain. That is not a problem for the algorithm, because the links are not consecutive. More relevantly, from that moment on the RG will always proceed by *dimerizing* the chain towards the extremes, except perhaps for a final long distance bond, depending on the parity of the system, related to the Kitaev phase (Kitaev 2001).

Thus, we are led to the following physical picture, which is illustrated in Fig. 7.5. In panel (a) we can see the GS for $\kappa < -1/4$. No central bonds are created, and we obtain the state $|n = 0\rangle$. Panel (b) shows the GS for $\kappa > 1/8$, in which a single central bond is created. Due to parity reasons, a second bond must appear between the extremes of the chain, thus leading to the non-trivial Kitaev chain, which we call the state $|n = 1\rangle$. Panel (c) shows the state $|n = 4\rangle$ and panel (d) the state $|n = 3\rangle$, which can be obtained within fixed ranges of $\kappa \in (-1/12, -1/20)$ and $\kappa \in (1/24, 1/16)$ respectively, which can be found through (7.44).

This physical picture can be confirmed through the analysis of the covariance matrices, which are depicted using a color code in Fig. 7.6. Indeed, we can see the CM for $N = 20$ spins and $h = 10$, in the suitable range for $|n = 4\rangle$ (left) and $|n = 5\rangle$ (right). The central patterns show $n = 4$ and $n = 5$ central arcs, respectively. As predicted, the $n = 5$ case presents an extra bond between the extremes of the system, showing that it belongs to the non-trivial Kitaev phase.

Furthermore, we examine the entanglement entropy of lateral blocks, $S(A_\ell)$ in the top panel of Fig. 7.7, which has been computed from the CM using the same systems, with $N = 10$ spins and $h = 10$. As predicted in our physical picture, the

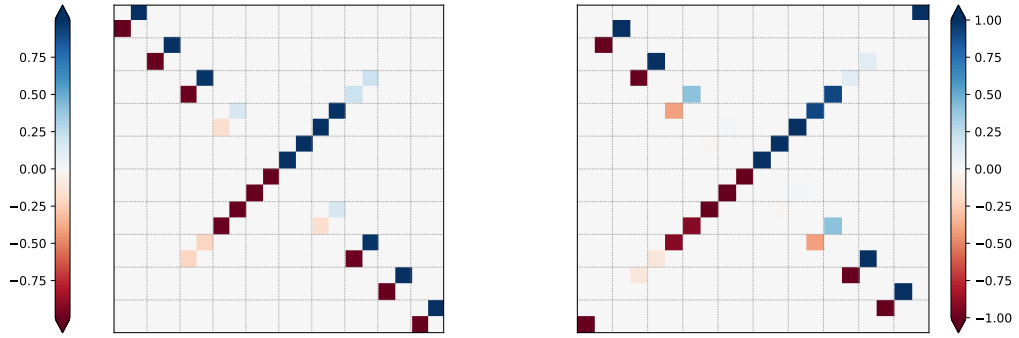

Figure 7.6: Covariance matrices of states $|n = 4\rangle$ and $|n = 5\rangle$ for $h = 10$ and $N = 20$. The short-range single states populate the secondary diagonals while the long-range singlet states correspond to the antidiagonal.

entanglement entropy for the smallest block begins at 0 or $\log(2)$ depending on the sign of κ, and presents a linear tent-shape at the center, within a block of $\lfloor n/2 \rfloor$ spins and reaching an entanglement entropy $n\log(2)/2$. The topological nature of the states is clarified in Appendix 7.C, where we present a graphical way to distinguish the trivial and topological phases by overlaying each state with the trivial state $|n = 0\rangle$ and counting the total number of loops.

We can also consider the energy gap around the Fermi level to capture the differences between ground states. Defining the energy gap in an inhomogeneous system presents some challenges, since it should be expressed in units of the typical energy scale. We can proceed in a similar way to what was done in section 5.2.1 and rescale the energy gap with the lowest coupling of the system, which in this case becomes $\Gamma_{L-1/2} \approx e^{-2hL}$. Hence, the scaled gap

$$\hat{\Delta}^{(0)} \equiv \frac{E_{N+1} - E_N}{\Gamma_{L-1/2}}, \tag{7.46}$$

becomes constant ($\hat{\Delta}^{(0)} = 2$), as it can be seen in Fig.7.7 (b). The states $|n \text{ odd}\rangle$ present a zero mode at the edge, and the system is strictly gapless, $\hat{\Delta}^{(0)} = 0$. Therefore, it is convenient to consider the second gap, defined as

$$\hat{\Delta}^{(1)} \equiv \frac{E_N - E_{N-1}}{J_{L-1/2}}, \tag{7.47}$$

which can also be seen in Fig. 7.7 (b). If $n \leq (2L-3)$ there is a short-range Majorana singlet state and the gap is finite, $\hat{\Delta}^{(1)} = 2$. Yet, both gaps fall to zero for the rainbow state, $|n = N\rangle$.

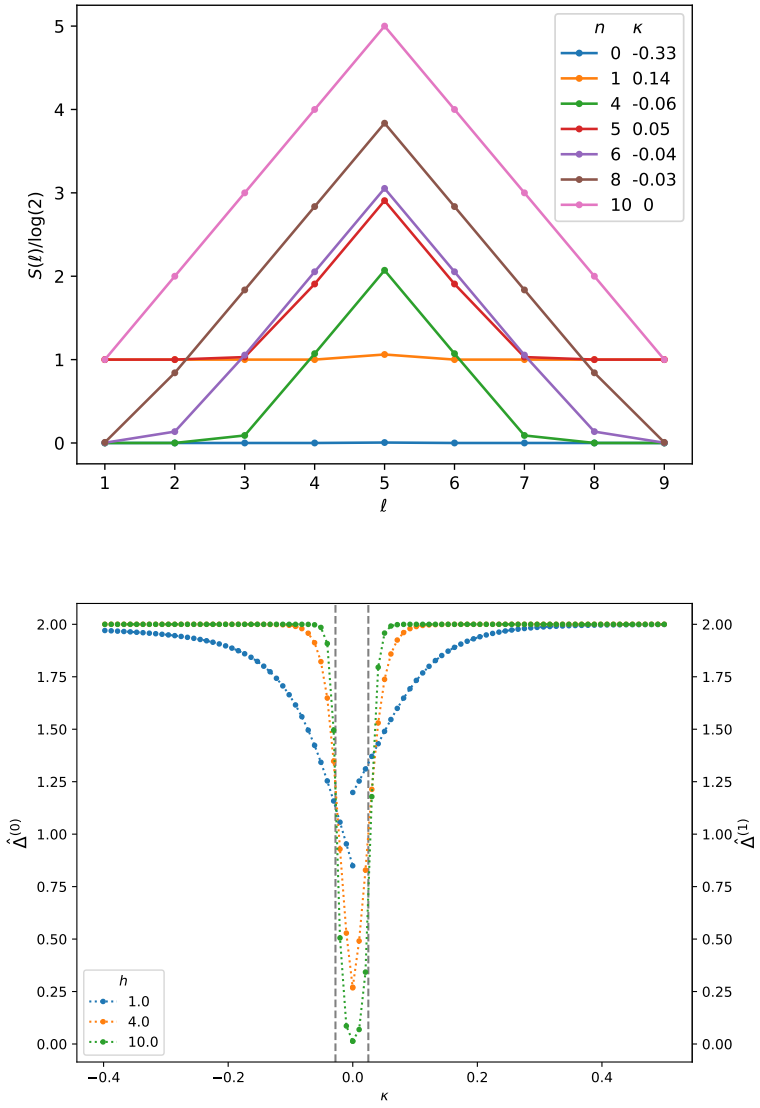

Figure 7.7: Top: entanglement entropy of lateral blocks of a chain of $N = 10$ spins for different values of κ, using $h = 10$. For $\kappa = -0.33$ and $\kappa = 0.14$ we obtain respectively the $|n = 0\rangle$ and $|n = 1\rangle$ states, for which the entropy is flat. On the other extreme, the $\kappa = 0$ curve corresponds to the rainbow state, $|n = 10\rangle$, which presents maximal entanglement entropy growth. The intermediate values of κ are chosen following (7.44) and present different numbers of central bonds. The entanglement entropy for the half-chain, $\ell = 5$, agrees with (7.16). Bottom: scaled energy gaps ($\hat{\Delta}^{(0)}$ for $\kappa < 0$ and $\hat{\Delta}^{(1)}$ for $\kappa > 0$) of the same chain for different values of h. The vertical gray lines delimit the rainbow state region for this chain size ($n > 2(L-1)$).

7.2.2 Weak inhomogeneity

Proceeding in the same way as in the previous section, we can obtain the equations of motion from the Hamiltonian (7.3) and describe the continuum limit defining $x = am$, $a \to 0$, $h \to 0$, with $\hat{h} = h/a$ and $\mathcal{L} = La$ kept constant, in terms of the fields $\alpha(x,t)$ and $\beta(x,t)$,

$$\begin{aligned}\partial_t \alpha &\approx -2ae^{-2\hat{h}|x|}\Big(ae^{\delta}\partial_x - \Big(\mathrm{sign}(x)he^{\delta} + 2\sinh\delta\Big)\Big)\beta,\\ \partial_t \beta &\approx -2ae^{-2\hat{h}|x|}\Big(ae^{\delta}\partial_x - \Big(\mathrm{sign}(x)he^{\delta} - 2\sinh\delta\Big)\Big)\alpha,\end{aligned} \tag{7.48}$$

where we will use $a = 1$ for convenience. These equations can be rewritten in terms of a spinor field Ψ, (7.21), using the same γ matrices, obtaining

$$\Big(-\sigma_2\partial_0 + e^{-2h|x^1|}\big(i\sigma_3 e^{\delta}\partial_1 - i\sigma_3 \mathrm{sign}(x^1)he^{\delta} + 2i\sinh\delta\big)\Big)\Psi = 0, \tag{7.49}$$

And, then, we can compare this equation with that representing the dynamics of a Dirac field in a curved spacetime.

$$\left(-\sigma_2\partial_0 + \frac{i}{2}\omega_0^{01}\sigma_3 + \frac{E_1^1}{E_0^0}\left(i\sigma_3\partial_1 - \frac{i}{2}\omega_1^{01}\sigma_2\right) + i\frac{m}{E_0^0}\right)\Psi = 0. \tag{7.50}$$

where ω_μ^{ab} is again the spin connection and E_a^μ the inverse of the *zweibein*. From the above identification we find that:

$$\begin{aligned} E_0^0 &= e^{2h|x^1|}, \quad E_1^1 = e^{\delta}\\ \omega_0^{01} &= -2e^{-2h|x^1|}e^{\delta}h\,\mathrm{sign}(x^1)\\ \omega_1^{01} &= 0,\\ m &= 2\sinh\delta, \end{aligned} \tag{7.51}$$

that leads to a (1+1)D metric whose non-zero terms are

$$g_{00} = -e^{-4h|x|}, \qquad g_{11} = e^{-2\delta}. \tag{7.52}$$

However, $g_{11} \simeq 1$ if $\delta \ll 1$, and thus the associated metric coincides with the one found in the previous section, see (7.28). Thus, the field theory associated with the system described by the Hamiltonian (7.3) is described by a massive Majorana fermion, with $m \approx 2\delta$, placed in the curved background described by the metric (7.28).

Entanglement entropies

Let us first consider the case $h = 0$, i.e. the massive fermion on a flat space. The entanglement entropy of this system has been obtained previously by evaluating

the associated two-dimensional classical model via the corner transfer matrix (CTM) formalism (Davies 1988; Peschel and Eisler 2009). For $\delta > 0$ one obtains

$$S(\delta) = \frac{1}{12}\left(\log\left(\frac{k^2}{16k'^2}\right) + \left(1 - \frac{k^2}{2}\right)\frac{4I(k)I(k')}{\pi}\right) + \log 2, \tag{7.53}$$

while for $\delta < 0$ we get

$$S(\delta) = \frac{1}{12}\left(\log\left(\frac{4}{kk'}\right) + \frac{1}{2}\left(k^2 - k'^2\right)\frac{4I(k)I(k')}{\pi}\right), \tag{7.54}$$

where $I(x)$ is the complete elliptic integral of the first kind (Abramowitz and Stegun 1972) and

$$k = e^{-2|\delta|}, \qquad k' = \sqrt{1 - k^2}. \tag{7.55}$$

Notice that if $|\delta| \ll 1$, $k \approx (1 - |\delta|)/(1 + |\delta|)$ which is the value used in Refs. (Eisler *et al.* 2020; Peschel and Eisler 2009). Although (7.54) is only exact for the infinite chain, it is still valid provided that $1/\delta \ll L$, i.e. when the cluster decomposition principle is satisfied. Near the critical point, $\delta \ll 1$, (7.54) are simplified to

$$S \approx \frac{c}{6}\log\left(\frac{1}{1-k}\right) = \frac{c}{6}\log\xi, \tag{7.56}$$

where the quantity inside the logarithm can be interpreted as a correlation length ξ (Calabrese and Cardy 2004) with the appropriate units of length,

$$\xi = \frac{1}{1-k} \approx \frac{1}{2|\delta|}, \tag{7.57}$$

which corresponds to the inverse of the mass, $m = 2\delta$, (7.51). To end this brief summary of the homogeneous non critical case, let us write the entanglement entropy for the half chain of a *finite* system as

$$S(\delta, L) = \frac{c}{6}\log\frac{\xi_E(\delta, L)}{2} + b(\delta), \tag{7.58}$$

where $\xi_E(\delta, L)$ shall be called the *entangled length*, because it plays the role of an effective correlation length in order to compute the entanglement entropy, even though its value is upper bounded by the size of the system, $N = 2L$. If $\delta = 0$, the system is critical and $\xi_E(0, L)$ saturates this bound, thus leading to the logarithmic scaling predicted by CFT. On the other hand, if $|\delta|$ is large enough then $\xi_E(\delta, L) \ll 2L$, finite-size effects are not important and the cluster decomposition principle holds. Thus, the results for the infinite chain can be applied, and the area law is satisfied. Hence, we see that in this case (7.58) is just a reparametrization of (7.54).

Moreover, when we introduce inhomogeneity in the system through the parameter h, we find that the entanglement entropy can be obtained merely *deforming* the entangled length $\xi_E(\delta, L)$ according to the same prescription used before, given in (7.29), giving rise to the ansatz

$$S(L,\delta,h) = \frac{c}{6}\log\left(\tilde{\xi}_E(\delta,L)\right) + b(\delta), \tag{7.59}$$

where

$$\tilde{\xi}_E(h,\delta,L) = \frac{1}{2h}\left(e^{h\xi_E(\delta,L)} - 1\right), \tag{7.60}$$

is the deformed entangled length, corresponding to the curved spacetime.

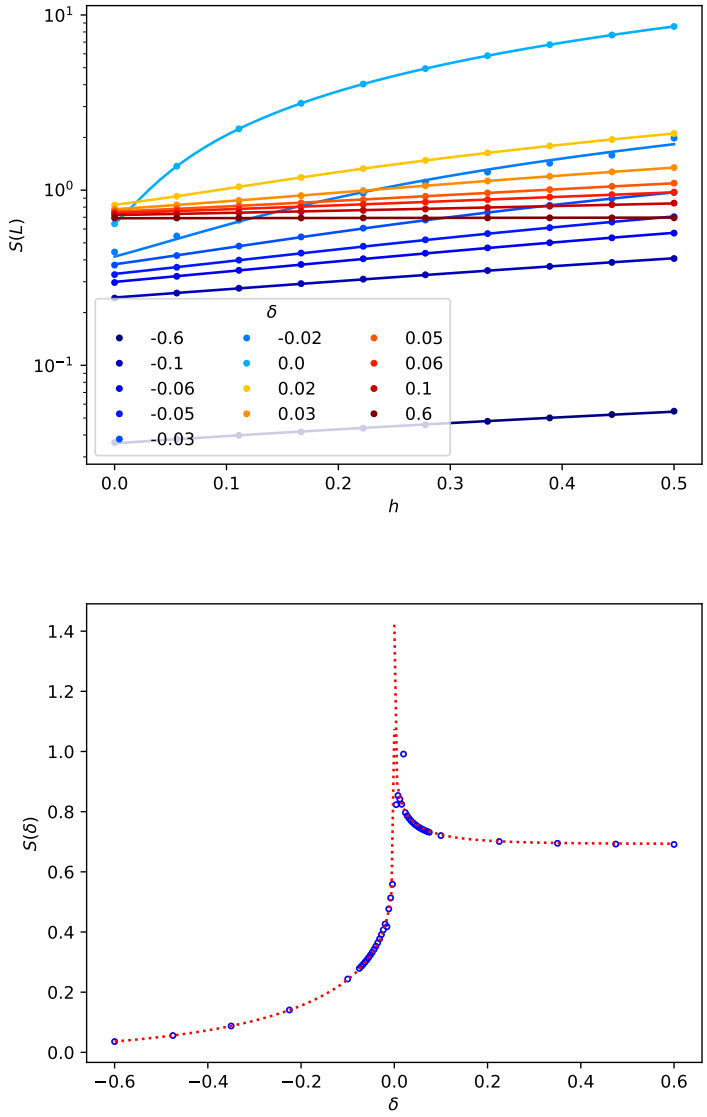

Figure 7.8: Top: Plot of the fits (lines) performed with expression (7.60) of the numerical results for the half chain entanglement entropy (points) for different values of δ. Bottom: The dotted red line corresponds to (7.54) and the blue dots to (7.59), where $\xi_E(\delta, L)$ has been obtained by fitting (7.60) to the numerical half chain entanglement entropy of a system with $L = 100$.

We have fitted expression (7.59) to the numerical values for the entanglement entropy of the half chain for different values of δ and h, using $\xi_E(\delta, L)$ and $b(\delta)$

as fitting parameters. The agreement between the fits and the numerical results can be seen in the top panel of Fig. 7.8. Hence, we obtain a single value for the entangled length for each L and δ, which accounts for the entanglement entropy under different degrees of inhomogeneity h. In the bottom panel of Fig. 7.9 we can see the good agreement between the infinite chain prediction, (7.54), and the output of (7.58) having used the values $\xi_E(\delta, L)$ and $b(\delta)$ that were obtained from the previous fits.

In Fig. 7.9 we present the fitted values $\xi_E(\delta, L)$ for different system sizes. The system presents universal behavior as long as the correlation length is much smaller than the system size.

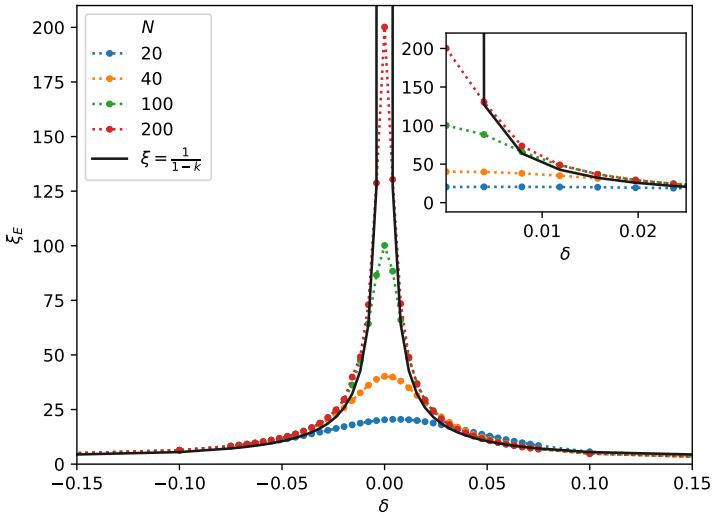

Figure 7.9: Entanglement correlation length $\xi_E(\delta, L)$ for different chain sizes $2L$. Near the critical point we have $\xi_E \approx \xi$, (7.57).

It is worth to ask whether the weak and strong inhomogeneity regimes match smoothly. Let us consider the limit $h \gg 1$ in (7.59),

$$S(L, \delta, h) \approx \frac{c}{6} h \xi_E(\delta, L). \tag{7.61}$$

If $\delta = 0$ we have $S(L, 0, h) \approx \frac{c}{3} hL$, as it was discussed in the previous section. On the other hand, if $\delta \ll 1$ but $1/\delta \ll L$, $\xi_E(\delta, L) = \xi$ from (7.57). Hence,

$$S(L, \delta, h) \approx \frac{h}{12\delta} = \frac{1}{12\kappa}, \tag{7.62}$$

which is a manifestation of the area law given by the interplay between the inhomogeneity h and the dimerization δ. Thus, we see that the weak and strong inhomogeneity regimes match.

Entanglement Hamiltonian and entanglement spectrum

The reduced density matrix ρ_A of a half infinite chain can be written in terms of the generator of the Baxter corner matrix,

$$\rho_A = e^{-H_{CTM}}, \tag{7.63}$$

Since the model is integrable, we can simplify and state that $H_{CTM} = \epsilon H_{\mathcal{N}}$, where $H_{\mathcal{N}}$ is a Hermitian operator with integer spectrum. Thus, the entanglement spectrum ϵ_l, with $l = 1 \dots L$, is equally spaced and we may focus on the level spacing ϵ. For the ITF model we have

$$\epsilon = \pi \frac{I(k')}{I(k)}, \tag{7.64}$$

where k and k' are given by (7.55). The entanglement Hamiltonian of the half infinite chain can be identified with the generator of the CTM (Eisler *et al.* 2020). Thus, in the case of the ITF chain the first neighbor couplings grow linearly from the internal boundary towards the bulk with a parity oscillation between 1 and k,

$$\mathcal{H} = \sum_{l=1}^{\infty} J^{EH}_{2\ell-1} \alpha_\ell \beta_\ell + J^{EH}_{2\ell} \beta_\ell \alpha_{\ell+1}, \tag{7.65}$$

with

$$\begin{aligned} J^{EH}_{2\ell-1} &= I(k')(2\ell-1), \quad J^{EH}_{2\ell} = I(k')2\ell k, \quad \delta < 0 \\ J^{EH}_{2\ell-1} &= I(k')(2\ell-1)k, \quad J^{EH}_{2\ell} = I(k')2\ell, \quad \delta > 0 \end{aligned} \tag{7.66}$$

where α_ℓ and β_ℓ correspond to the lattice Majorana fermions. Fig. 7.10 (a) shows the nearest neighbor coupling constants of the entanglement Hamiltonian, J^{EH}_ℓ, slightly modified in order to improve the visualization: for odd values of ℓ, J^{EH}_ℓ has been divided by k in order to remove the parity oscillation, leaving a linear growth with slope $2I(k')$, in similarity to (Eisler *et al.* 2020). If we switch on the inhomogeneity, setting $h = 0.5$, we can observe the same entanglement Hamiltonian couplings in Fig. 7.10 (b): a linear increase of the couplings with a parity oscillation between values 1 and $\hat{k}(h)$, which depends on the inhomogeneity. Notice that $\hat{k}(0) = k$.

7.3 Conclusions

In this chapter, we have characterized the entanglement properties of an inhomogeneous transverse field Ising critical spin-1/2 chain for which both the couplings and external fields fall exponentially from the center with a rate h, which defines the rainbow ITF model. It can be analytically solved by mapping into a Majorana chain, which suggests to treat the couplings and the external fields on an equal

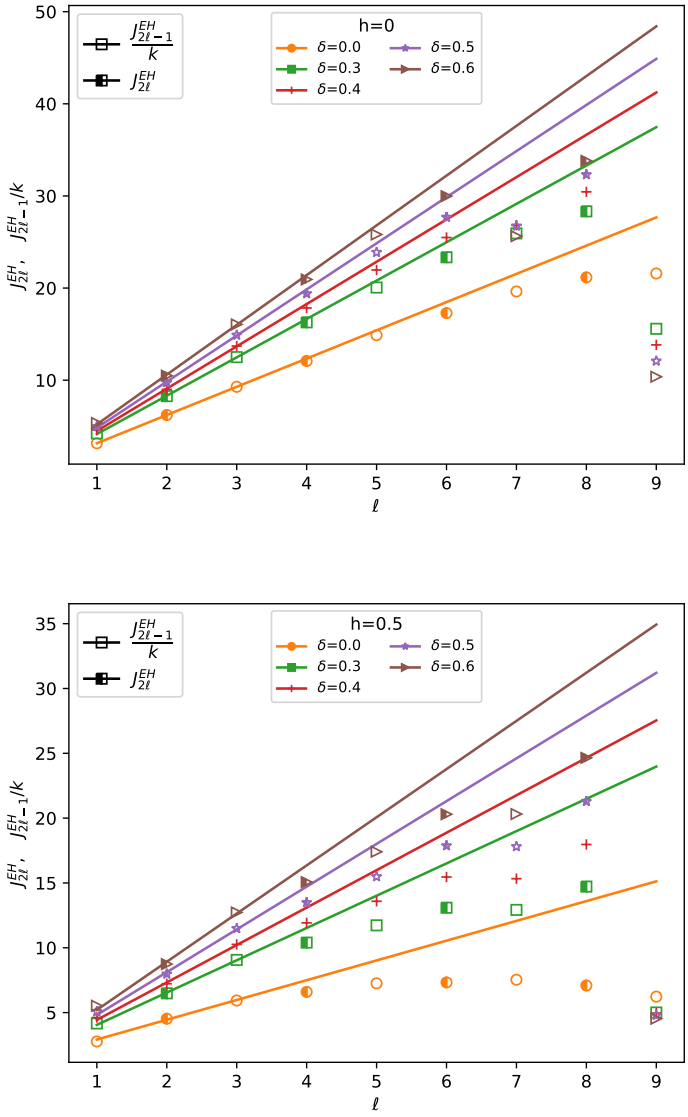

Figure 7.10: Nearest neighbor couplings of a chain of $2N = 20$ Majorana fermions, J^{EH}_{ℓ}, with a parity compensation: odd values of ℓ are divided by k. (a) Case $h = 0$. We can see that, despite the small size of the chain, we recover the behaviour of the infinite chain near the boundary for strong dimerizations. Empty symbols correspond to even couplings while the filled ones are for $J^{EH}_{2\ell-1}/k$, see 7.66. (b) In the case $h = 0.5$ we observe the same initial behavior for low values of ℓ.

footing. Applying the strong disorder renormalization method we find that the ground state can be expressed in terms of generalized singlet states which are displayed concentrically around the center, similarly to the rainbow state. The weak inhomogeneity regime can be characterized by taking the continuum limit and showing that the resulting field theory corresponds to a free massless Majorana fermion field on a curved spacetime. Thus, we are able to predict the behaviour of the entanglement entropy deforming appropriately the known CFT results for Minkowski spacetime, which turns the characteristic logarithmic growth into a

linear growth with the block size. Moreover, there is a smooth crossover between both regimes. The nearest neighbor coefficients of the entanglement Hamiltonian present the standard linear growth as we move away from the internal boundary, in agreement with the Bisognano-Wichmann theorem, showing that the state can be interpreted as a thermofield double for large enough inhomogeneity.

Out of criticality, we introduce a parity-dependent term whose strength δ competes with h, attempting to destroy the linear entanglement. Strong-disorder renormalization arguments show that for each value of $\kappa \equiv \delta/h$ we obtain a fixed number of concentric singlets around the center of the chain, also showing that the trivial and non-trivial Kitaev phases are obtained for positive and negative values of κ, although with a substantial deformation. The weak inhomogeneity regime with small δ is described by a massive Majorana field theory placed over the curved spacetime that we found in the case of the critical model. We have computed the entanglement entropy by defining an effective correlation length $\xi_E(\delta, L)$ which is deformed with the metric, see (7.58). Near the entangling point, the entanglement Hamiltonian presents a linear growth of the couplings with a parity oscillation that can be accounted for using CTM results for the infinite systems. The amplitude of the oscillation and the slope depends on the inhomogeneity parameter.

In Chapter 6, we found a connection between the rainbow antiferromagnetic Heisenberg spin chain with the Haldane phase, and another between the rainbow XX spin chain and the AIII SPT phases, by means of a folding transformation around the center of the symmetry of the chain. It could be interesting to extend this approach to the models considered here and, more generally, to address the entanglement characterization of inhomogeneous 2D systems. In addition, it could be relevant to consider an experimental realization of the rainbow state in terms of a Rydberg atoms chain whose effective Hamiltonian is an inhomogeneous ITF model with an additional longitudinal field (Schauss 2018). It is possible to extend Fisher's RG to this model and find the conditions under which a rainbow is formed. Also, it could be interesting to consider strongly inhomogeneous anyon models and study them harnessing their relation with $SU(2)_k$ Chern-Simons theories (Bonesteel and Yang 2007; Nayak *et al.* 2008).

Appendices

7.A SDRG for Majorana chains

In this appendix we explain the SDRG scheme applied to an inhomogeneous chain of Majorana fermions. Let us consider a system of 4 Majorana fermions whose Hamiltonian is given by:

$$H = i\left(g_{ia}\gamma_i\gamma_a + g_{ib}\gamma_i\gamma_b + g_{ab}\gamma_a\gamma_b + g_{aj}\gamma_a\gamma_j + g_{bj}\gamma_b\gamma_j\right), \tag{7.A.1}$$

with $\{\gamma_m, \gamma_n\} = 2\delta_{mn}$. Let us assume that g_{ab} is larger than the rest so we can use use perturbation theory to diagonalize (7.A.1).

$$H_0 = ig_{ab}\gamma_a\gamma_b, \tag{7.A.2}$$

$$H_I = i\left(g_{ia}\gamma_i\gamma_a + g_{ib}\gamma_i\gamma_b - g_{ja}\gamma_j\gamma_a - g_{jb}\gamma_j\gamma_b\right) . \tag{7.A.3}$$

Defining the Dirac fermion $b = \frac{1}{2}\left(\gamma_a + i\gamma_b\right)$, we have that $H_0 = 2g_{ab}\left(b^\dagger b - 1/2\right)$ whose spectrum is $\pm|g_{ab}|$ and eigenvectors $|0\rangle, |1\rangle$ such that $b|0\rangle = 0$. The H_I can be written as:

$$H_I = i\left\{\left[\left(g_{ia} - ig_{ib}\right)\gamma_i - \left(g_{aj} - ig_{bj}\right)\gamma_j\right]b + \left[\left(g_{ia} + ig_{ib}\right)\gamma_i - \left(g_{aj} + ig_{bj}\right)\gamma_j\right]b^\dagger\right\} \tag{7.A.4}$$

Note that we must extend the Hilbert space: $|0\rangle \to |0\rangle \otimes |\psi\rangle$ where $|\psi\rangle$ is an unknown state of the Majorana fermions γ_i, γ_j. In the same way $|1\rangle \to |1\rangle \otimes |\varphi\rangle$. However we shall make an abuse of notation and write γ_i instead of $\langle\psi|\gamma_i|\varphi\rangle$. The first order corrections are zero so we compute the second order:

$$\Delta E_0 = \frac{\langle 0|H_I|1\rangle\ \langle 1|H_I|0\rangle}{E_0 - E_1}. \tag{7.A.5}$$

Using (7.A.4) we find the same corrections for $g_{ab} > 0$ and $g_{ab} < 0$

$$\Delta E_0 = i\left(\frac{g_{ia}g_{bj}}{g_{ab}} - \frac{g_{ib}g_{aj}}{g_{ab}}\right)\gamma_i\gamma_j + \tilde{E}, \tag{7.A.6}$$

with $\tilde{E}_0 = 1/(2|g_{ab}|)\left(g_{ia}^2 + g_{ib}^2 + g_{bj}^2 + g_{aj}^2\right)$. Thus, an effective Hamiltonian $H_{eff} = ig_{ij}\gamma_i\gamma_j$ emerge with the hopping term given by

$$g_{ij} = \frac{g_{ia}g_{bj}}{g_{ab}} - \frac{g_{ib}g_{aj}}{g_{ab}}. \tag{7.A.7}$$

Particularizing for the ITF spin chain, $g_{ib} = g_{aj} = 0$ and we recover (7.5) and (7.6). In Ref. Bonesteel and Yang (2007) the authors provide the same result with a graphical derivation. The matrix elements are computed by counting the loops obtained by overlaying the (generalized) singlet states. See Appendix 7.C.

7.B Non-universal function of the entanglement entropy

The relation between the entanglement entropies of the XX and ITF models is given by Iglói and Juhász (2008):

$$S_{\mathrm{XX}}(2x, 2L) = 2S_{\mathrm{ITF}}(x, L). \tag{7.B.1}$$

We will compute the non-universal part of the entanglement entropy (7.33) with the above expression. The entanglement entropy of the XX model is computed in Chapter 4 (see (4.52) particularized for the rainbow model)

$$\begin{aligned} S_{XX}(2x, 2L) &= S_{cft}(2x, 2L) + \frac{\gamma_1}{2} + S_{oscl}(2x, 2L), \\ S_{cft}(2x, 2L) &= \frac{1}{6}\log\left(e^{-h|2x|}\frac{8(e^{h2L}-1)}{h\pi}\cos\left(\frac{\pi(e^{h|2x|}-1)}{2(e^{h2L}-1)}\right)\right) \\ S_{oscl}(2x, 2L) &= (-1)^{2x+2L}\left(\frac{8(e^{h2L}-1)}{h\pi}\cos\left(\frac{\pi(e^{h|2x|}-1)}{2(e^{h2L}-1)}\right)\right)^{-1}, \end{aligned} \tag{7.B.2}$$

and $\gamma_1 \approx 0.4950 + 1/3\log 2$ (Jin and Korepin 2004). Hence, by using relation (7.B.1) we have

$$c'_I(x, L) = \frac{\gamma_1}{4} + \frac{1}{6}\log 2 + (-1)^L\left(\frac{16(e^{2hL}-1)}{h\pi}\cos\left(\frac{\pi(e^{2h|x|}-1)}{4(e^{2hL}-1)}\right)\right)^{-1}. \tag{7.B.3}$$

7.C Pictorial representation of the topological phases

The trivial and topological ground states $|n\rangle$ of (7.3) can be distinguished graphically. We start by overlapping the GS with the trivial Majorana singlet state $\langle n|n = 0\rangle$ and connecting the Majorana fermions (red and blue balls) with their opposites, leading to the formation of closed loops.

In Fig. 7.C.1 we show the same GS that we presented in Fig. 7.5 overlapping with $|n = 0\rangle$, which we will call $\langle n = 0|n = 0\rangle$, that leads to N loops matching with the N Dirac fermions of kind c, see (7.2). This can be seen in panel (b). On the other side, the overlapping $\langle n = 1|n = 0\rangle$ leads to just one big loop as it can be seen in panel (c). Thus, the topological phase is characterized by a big loop that encloses all the Majorana fermions. Considering $1 < n < L - 2$ central decimations, the

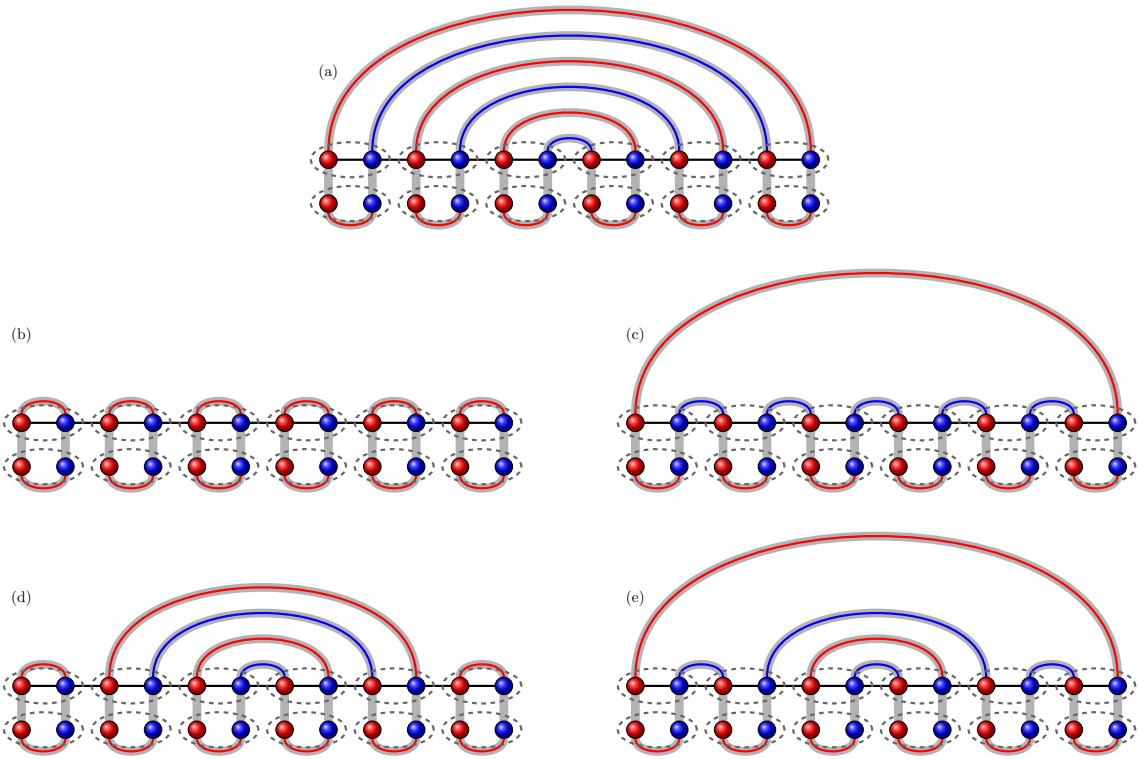

Figure 7.C.1: Overlapping of the same states considered in Fig. 7.5. Discussion on the main text.

overlapping $\langle n = 2m|n = 0\rangle$ with $m = 0, \cdots, L-1$ decreases the total number of loops to $N - m$ while the overlapping $\langle n = 2m-1|n = 0\rangle$ with $m = 1, \cdots, L-1$ increases them up to m. For instance, in Fig. 7.C.1 (d) we see the overlapping $\langle n = 4|n = 0\rangle$ that leads to $6-2 = 4$ bonds. In panel (e) there are 2 loops, because the overlapping corresponds to $\langle n = 3|n = 0\rangle$. Finally, as it can be seen in panel (a), the overlaying of a rainbow state $|\text{RS}\rangle$ $n = 0$ leads to $N/2$ loops. This is another way of unveiling the criticality of the RS since it corresponds to the intermediate situation.

The loops can also be interpreted in terms of spins and Fisher's RG (Bonesteel and Yang 2007). Each loop contains those spins that were hybridized in consecutive RG steps with dominant J. Hence, the state $|n = 1\rangle$ is a *superspin* while the RS can be seen as a collection of hybridized pairs of spins. However, notice that they do not form a $SU(2)$ singlets as it occurs with the Dasgupta-Ma method applied to antiferromagnetic spin $1/2$ chains.

Chapter 8

Conclusions

This is the final chapter of the thesis. Let us make a brief summary of the conclusions and the work done. The basic principle behind this thesis is the improvement of the understanding of new phases of matter through the study of quantum entanglement. We have characterized the entanglement in ground states of local Hamiltonians that describe inhomogeneous quantum chains by means of different tools such as Rényi entropies and the entanglement Hamiltonian among others.

On the one hand, we have studied the strong inhomogeneity regime $h \gg 1$ with the strong Disorder Renormalization Group or with expressly designed real-space renormalization schemes. On the other hand, we have approached the weak inhomogeneity regime $h \ll 1$ taking an appropriate continuum limit of the lattice model. Hence, in Chapter 4, we have seen that those models whose inhomogeneous couplings vary smoothly can be interpreted as a quantum field theory of a fermion on a curved spacetime. Thus, all the known results for Minkowski can be used with the proper deformation imposed by the curved spacetime metric.

The rainbow state violates maximally the area law of the entanglement entropy in the strong inhomogeneity regime because the ground state is a collection of concentric Bell pairs. In the weak inhomogeneity regime, the linear growth of the entanglement entropy is explained by the hyperbolic deformation of the typical logarithmic behavior associated with a critical model.

In Chapter 5 we have studied the interplay between the inhomogeneity and a local defect. Thus, we have modified the rainbow model by adding a local central defect with a tunable intensity.

- In the strong inhomogeneity regime, the presence of the defect modifies dramatically the entanglement properties of the ground state, giving rise to two transitions between states that fulfill the area law of entanglement entropy and states that violate it.

- The weak inhomogeneity regime is described by a conformal field theory in curved background with a central charge that depends on the defect intensity.

Thus, the entanglement entropy grows with the system size and we do not observe the area law behaviour predicted in the strong inhomogeneity regime.

In Chapter 6 we have considered the relation between symmetry protected topological (SPT) phases and the inhomogeneity.

- We have found a new mechanism for generating SPT phases in inhomogeneous spin chains described by local Hamiltonians. A folding transformation around the center of the chain converts the long range entanglement into short range entanglement. Then, we use the degeneracy of the entanglement spectrum to distinguish between topologically trivial and non trivial phases.

- A strong deformation of the gapless antiferromagnetic Heisenberg spin $s = 1/2$ becomes an effective spin $s = 1$ chain in the Haldane phase by means of the folding transformation. We propose a generalization of this result to rational conformal field theories. A local Hamiltonian of spin s is in correspondence through the folding transformation with a Wess-Zumino-Witten model with symmetry $SU(2)_k$ with level $k = 2s$. If k is odd, the physical chain belongs to a non-trivial SPT, whereas if k is even, the chain is topologically trivial.

In Chapter 7 we have proposed an inhomogeneous transverse field Ising model whose ground state in the strong inhomogeneity regime is a rainbow state of Majorana fermions: an state formed by concentric generalized singlet states. Moreover, the weak inhomogeneity regime is described by a conformal field theory in curved background with central charge $c = 1/2$. Furthermore, we have studied the model outside the critical point, modifying the couplings between Majorana fermions with a parity dependent term, i.e. dimerizing the chain.

- In the strong inhomogeneity regime, the ground state is formed by generalized singlet states. Its structure is completely fixed by a relation between the inhomogeneity and the dimerization parameter. It is possible to interpolate between the trivial and non-trivial fully dimerized phases of the Kitaev chain with states having a central rainbow-like zone, i.e. with concentric generalized singlets. Notice the difference between these states and those obtained with the tunable central defect in Chapter 5 where the entire chain is dimerized or is in the rainbow phase as a function of the intensity of the central defect.

- The weak inhomogeneity regime is described by a massive field theory in the same curved background: there is a parity dependent term that yields a mass, and therefore an effective correlation length $\xi_E(\delta, L)$ which must be deformed accordingly with the metric.

Conclusiones

Este es el capitulo final de la tesis. Hagamos un breve resumen de las conclusiones y del trabajo realizado. El principio básico detrás de esta tesis es el de la mejora de la comprensión de nuevas fases de la materia a través del estudio del entrelazamiento cuántico. Hemos caracterizado el entrelazamiento en estados fundamentales de Hamiltonianos locales que describen cadenas cuánticas inhomogéneas por medio de diferentes herramientas como las entropías de Rényi y el Hamiltoniano de entrelazamiento entre otras.

Por un lado, hemos estudiado el régimen de inhomogeneidad fuerte $h \gg 1$ con el grupo de Renormalizacion de Fuerte Desorden o con esquemas de renormalización en espacio real diseñados expresamente. Por otro, hemos abordado el régimen de inhomogeneidad débil $h \ll 1$ tomando un límite al contínuo apropiado. Así, en el Capítulo 4 hemos visto que, aquellos modelos cuyos acoplos inhomogéneos varían suavemente, pueden ser interpretados como una teoría cuántica de campos de un fermión en un espacio-tiempo curvo. Así, todos los resultados conocidos para Minkowski pueden ser empleados con la pertinente deformación impuesta por la métrica del espacio-tiempo curvo.

El estado arco-iris viola máximamente la ley del área de la entropía de entrelazamiento en el régimen de fuerte inhomogeneidad debido a que el estado fundamental es una colección de pares de Bell concéntricos. En el régimen de inhomogeneidad débil, el crecimiento lineal se explica por la deformación hiperbólica del típico comportamiento logarítmico asociado a un modelo crítico.

En el Capítulo 5 hemos estudiado la interacción entre la inhomogeneidad y un defecto local. Así, hemos modificado el modelo arco-iris añadiendo un defecto central con intensidad variable.

- En el régimen de fuerte inhomogeneidad la presencia del defecto modifica drásticamente las propiedades de entrelazamiento del estado fundamental, dando lugar a dos transiciones entre estados que verifican y violan la ley del área de la entropía de entrelazamiento.

- El régimen de baja inhomogeneidad es descrito por una teoría de campos conformes en espacio curvo con una carga central que depende de la intensidad del defecto. Así, la entropía de entrelazamiento crece volumétricamente y no se observa la ley del área predicha en el régimen de fuerte inhomogeneidad.

En el Capítulo 6 hemos estudiado la relación entre las fases topológicas protegidas por simetría (fases SPT) y la inhomogeneidad.

- Hemos encontrado un nuevo mecanismo para generar fases SPT en cadenas de espín inhomogéneas gobernadas por Hamiltonianos locales. Una transformación de plegado en torno al centro de la cadena convierte el entrelazamiento de largo alcance en entrelazamiento de corto alcance. La degeneración del espectro de entrelazamiento es usada entonces para diferenciar fases topologicamente triviales y no triviales.

- Una deformación fuerte del modelo de Heisenberg antiferromagnético sin gap de espín $s = 1/2$ se convierte, mediante el plegado, en una cadena efectiva de espín $s = 1$ en la fase de Haldane. Se plantea entonces la generalización de este resultado a teorías conformes racionales. Un Hamiltoniano local de espín s en el régimen de alta inhomogeneidad está en correspondencia a través del plegado con un modelo Wess-Zumino-Witten con simetría $SU(2)_k$ con nivel $k = 2s$. Si k es impar, la cadena original es una SPT no trivial, mientras que si k es par, la cadena original es topologicamente trivial.

En el Capítulo 7 hemos propuesto un modelo inhomogéneo de Ising con campo magnético transverso cuyo estado fundamental en el régimen de fuerte inhomogeneidad es un estado arco-iris de fermiones de Majorana: un estado formado por singletes generalizados dispuestos de forma concéntrica. Asimismo, el régimen de baja inhomogeneidad es descrito por una teoría de campos conformes en espacio-tiempo curvo con carga central $c = 1/2$. Además, hemos investigado el modelo fuera del punto crítico, modificando los acoplos entre los fermiones de Majorana con un término dependiente de la paridad, es decir, dimerizando la cadena.

- En el régimen fuerte inhomogeneidad, el estado fundamental está formado por singletes generalizados. Su estructura está completamente determinada por una relación entre dimerización e inhomogeneidad. Es posible interpolar entre las fases completamente dimerizadas triviales y no triviales de la cadena de Kitaev con estados que tienen un una zona central tipo arco-iris, i.e. con singletes generalizados concéntricos. Observe la diferencia entre estos estados y los obtenidos con el defecto central variable en el Capítulo 5 donde toda la cadena es dimerizada o está en fase arco-iris en función de la intensidad del defecto central.

- El régimen de baja inhomogeneidad viene descrito por una teoría de campos masiva en el mismo espacio-tiempo que el caso crítico. El término dependiente de la paridad genera una masa, y por tanto una longitud de correlación efectiva $\xi_E(\delta, L)$ que debe ser deformada adecuadamente con la métrica.

Bibliography

1. Abanin, D. A., Altman, E., Bloch, I., and Serbyn, M. "Colloquium: Many-body localization, thermalization, and entanglement". *Reviews of Modern Physics* **91,** 021001 (2019) [In p. 7].
2. Abramowitz, M. and Stegun, I. *Handbook of Mathematical Functions, With Formulas, Graphs, and Mathematical Tables,* | *Guide books* (Dover Publications, Inc., 1972) [In pp. 87, 143].
3. Adesso, G., Bromley, T. R., and Cianciaruso, M. "Measures and applications of quantum correlations". *Journal of Physics A: Mathematical and Theoretical* **49,** 473001 (2016) [In p. 13].
4. Affleck, I. and Haldane, F. D. M. "Critical theory of quantum spin chains". *Physical Review B* **36,** 5291 (1987) [In p. 113].
5. Affleck, I., Kennedy, T., Lieb, E. H., and Tasaki, H. "Valence bond ground states in isotropic quantum antiferromagnets". *Communications in Mathematical Physics 1988 115:3* **115,** 477–528 (1988) [In pp. 7, 104, 112].
6. Affleck, I. and Ludwig, A. W. W. "Universal noninteger "ground-state degeneracy" in critical quantum systems". *Physical Review Letters* **67,** 161 (1991) [In p. 33].
7. Alba, V. *et al.* "Unusual area-law violation in random inhomogeneous systems". *Journal of Statistical Mechanics: Theory and Experiment* **2019,** 023105 (2019) [In p. 95].
8. Altland, A. and Zirnbauer, M. R. "Nonstandard symmetry classes in mesoscopic normal-superconducting hybrid structures". *Physical Review B* **55,** 1142 (1997) [In p. 104].
9. Amico, L., Fazio, R., Osterloh, A., and Vedral, V. "Entanglement in many-body systems". *Reviews of Modern Physics* **80,** 517 (2008) [In p. 5].
10. Anderson, P. W. "Absence of Diffusion in Certain Random Lattices". *Physical Review* **109,** 1492 (1958) [In p. 8].
11. Arias, R. E., Blanco, D. D., Casini, H., and Huerta, M. "Local temperatures and local terms in modular Hamiltonians". *Physical Review D* **95,** 065005 (2017) [In pp. 37, 40].

12. Babujian, H. M. "Exact solution of the isotropic Heisenberg chain with arbitrary spins: Thermodynamics of the model". *Nuclear Physics B* **215,** 317–336 (1983) [In p. 113].

13. Babujian, H. M. "Exact solution of the one-dimensional isotropic Heisenberg chain with arbitrary spins S". *Physics Letters A* **90,** 479–482 (1982) [In p. 113].

14. Basor, E. L. and Tracy, C. A. "The Fisher-Hartwig conjecture and generalizations". *Physica A: Statistical Mechanics and its Applications* **177,** 167–173 (1991) [In p. 36].

15. Bednorz, J. G. and Muller, K. A. "Possible high Tc superconductivity in the BaLaCuO system". *Zeitschrift fur Physik B Condensed Matter* **64,** 189–193 (1986) [In p. 9].

16. Bekenstein, J. D. "Black Holes and Entropy". *Physical Review D* **7,** 2333 (1973) [In p. 5].

17. Belavin, A. A., Polyakov, A. M., and Zamolodchikov, A. B. "Infinite conformal symmetry in two-dimensional quantum field theory". *Nuclear Physics B* **241,** 333–380 (1984) [In p. 3].

18. Bell, J. S. "On the Einstein Podolsky Rosen paradox". *Physics Physique Fizika* **1,** 195 (1964) [In p. 4].

19. Bernevig, A. and Neupert, T. "Topological Superconductors and Category Theory" (2015) [In pp. 104, 110].

20. Bernevig, B. A. and Hughes, T. L. *Topological insulators and topological superconductors* (Princeton University Press, 2013) [In p. 103].

21. Bernien, H. *et al.* "Probing many-body dynamics on a 51-atom quantum simulator". *Nature 2017 551:7682* **551,** 579–584 (2017) [In p. 11].

22. Bethe, H. "Zur Theorie der Metalle". *Zeitschrift für Physik 1931 71:3* **71,** 205–226 (1931) [In p. 2].

23. Bisognano, J. J. and Wichmann, E. H. "On the duality condition for a Hermitian scalar field". *Journal of Mathematical Physics* **16,** 985 (1975) [In p. 37].

24. Bisognano, J. J. and Wichmann, E. H. "On the duality condition for quantum fields". *Journal of Mathematical Physics* **17,** 303 (1976) [In p. 37].

25. Bloch, I., Dalibard, J., and Nascimbène, S. "Quantum simulations with ultracold quantum gases". *Nature Physics 2012 8:4* **8,** 267–276 (2012) [In p. 11].

26. Bloch, I., Dalibard, J., and Zwerger, W. "Many-body physics with ultracold gases". *Reviews of Modern Physics* **80,** 885 (2008) [In p. 116].

27. Boada, O., Celi, A., Latorre, J. I., and Lewenstein, M. "Dirac equation for cold atoms in artificial curved spacetimes". *New Journal of Physics* **13,** 035002 (2011) [In p. 11].

28. Bombelli, L., Koul, R. K., Lee, J., and Sorkin, R. D. "Quantum source of entropy for black holes". *Physical Review D* **34,** 373 (1986) [In p. 5].

29. Bonesteel, N. E. and Yang, K. "Infinite-Randomness Fixed Points for Chains of Non-Abelian Quasiparticles". *Physical Review Letters* **99,** 140405 (2007) [In pp. 130, 131, 148, 150, 151].

30. Bravyi, S., Caha, L., Movassagh, R., Nagaj, D., and Shor, P. W. "Criticality without Frustration for Quantum Spin-1 Chains". *Physical Review Letters* **109,** 207202 (2012) [In p. 8].

31. Büsser, C. A. and Feiguin, A. E. "Designing a symmetry-protected molecular device". *Physical Review B* **86,** 165410 (2012) [In p. 107].

32. Calabrese, P., Campostrini, M., Essler, F., and Nienhuis, B. "Parity Effects in the Scaling of Block Entanglement in Gapless Spin Chains". *Physical Review Letters* **104,** 095701 (2010) [In p. 35].

33. Calabrese, P. and Cardy, J. "Entanglement entropy and quantum field theory". *Journal of Statistical Mechanics: Theory and Experiment* **2004,** P06002 (2004) [In pp. 8, 31–33, 47, 58, 135, 143].

34. Cardy, J. "Scaling and Renormalization in Statistical Physics". *Scaling and Renormalization in Statistical Physics,* 1–238 (1996) [In p. 3].

35. Cardy, J. and Calabrese, P. "Unusual corrections to scaling in entanglement entropy". *Journal of Statistical Mechanics: Theory and Experiment* **2010,** P04023 (2010) [In p. 35].

36. Cardy, J. and Tonni, E. "Entanglement Hamiltonians in two-dimensional conformal field theory". *Journal of Statistical Mechanics: Theory and Experiment* **2016,** 123103 (2016) [In pp. 37, 42, 60, 89].

37. Chen, X., Gu, Z.-C., Liu, Z.-X., and Wen, X.-G. "Symmetry protected topological orders and the group cohomology of their symmetry group". *Physical Review B* **87,** 155114 (2013) [In pp. 104, 105].

38. Chen, X., Gu, Z.-C., and Wen, X.-G. "Classification of gapped symmetric phases in one-dimensional spin systems". *Physical Review B* **83,** 035107 (2011) [In p. 104].

39. Chen, X., Gu, Z.-C., and Wen, X.-G. "Complete classification of one-dimensional gapped quantum phases in interacting spin systems". *Physical Review B* **84,** 235128 (2011) [In pp. 104, 105, 111].

40. Chen, X., Gu, Z.-C., and Wen, X.-G. "Local unitary transformation, long-range quantum entanglement, wave function renormalization, and topological order". *Physical Review B* **82,** 155138 (2010) [In pp. 10, 103].

41. Chen, Y. and Vidal, G. "Entanglement contour". *Journal of Statistical Mechanics: Theory and Experiment* **2014,** P10011 (2014) [In pp. 42, 43, 92].

42. Cho, G. Y., Shiozaki, K., Ryu, S., and Ludwig, A. W. W. "Relationship between symmetry protected topological phases and boundary conformal field theories via the entanglement spectrum". *Journal of Physics A: Mathematical and Theoretical* **50,** 304002 (2017) [In pp. 104, 115].

43. Coser, A., Nobili, C. D., and Tonni, E. "A contour for the entanglement entropies in harmonic lattices". *Journal of Physics A: Mathematical and Theoretical* **50,** 314001 (2017) [In p. 43].

44. Dalmonte, M., Vermersch, B., and Zoller, P. "Quantum simulation and spectroscopy of entanglement Hamiltonians". *Nature Physics 2018 14:8* **14,** 827–831 (2018) [In p. 39].

45. Dasgupta, C. and Ma, S.-k. "Low-temperature properties of the random Heisenberg antiferromagnetic chain". *Physical Review B* **22,** 1305 (1980) [In pp. 11, 49, 106, 130].

46. Davies, B. "Corner transfer matrices for the Ising model". *Physica A: Statistical Mechanics and its Applications* **154,** 1–20 (1988) [In p. 143].

47. Degen, C. L., Reinhard, F., and Cappellaro, P. "Quantum sensing". *Reviews of Modern Physics* **89,** 035002 (2017) [In p. 5].

48. Deift, P., Its, A., and Krasovsky, I. "Toeplitz Matrices and Toeplitz Determinants under the Impetus of the Ising Model: Some History and Some Recent Results". *Communications on Pure and Applied Mathematics* **66,** 1360–1438 (2013) [In p. 35].

49. Den Nijs, M. and Rommelse, K. "Preroughening transitions in crystal surfaces and valence-bond phases in quantum spin chains". *Physical Review B* **40,** 4709 (1989) [In pp. 104, 113].

50. Devakul, T., Majumdar, S. N., and Huse, D. A. "Probability distribution of the entanglement across a cut at an infinite-randomness fixed point". *Physical Review B* **95,** 104204 (2017) [In p. 130].

51. Dowling, J. P. and Milburn, G. J. "Quantum technology: the second quantum revolution". *Philosophical Transactions of the Royal Society of London. Series A: Mathematical, Physical and Engineering Sciences* **361,** 1655–1674 (2003) [In p. 5].

52. Dukelsky, J., Martín-Delgado, M. A., Nishino, T., and Sierra, G. "Equivalence of the variational matrix product method and the density matrix renormalization group applied to spin chains". *Europhysics Letters (EPL)* **43,** 457 (1998) [In p. 6].

53. Einstein, A., Podolsky, B., and Rosen, N. "Can Quantum-Mechanical Description of Physical Reality Be Considered Complete?" *Physical Review* **47,** 777 (1935) [In p. 4].

54. Eisert, J., Cramer, M., and Plenio, M. B. "Colloquium: Area laws for the entanglement entropy". *Reviews of Modern Physics* **82,** 277 (2010) [In p. 5].

55. Eisler, V. and Peschel, I. "Entanglement in fermionic chains with interface defects". *Annalen der Physik* **522,** 679–690 (2010) [In pp. 75, 86, 87].

56. Eisler, V., Giulio, G. D., Tonni, E., and Peschel, I. "Entanglement Hamiltonians for non-critical quantum chains". *Journal of Statistical Mechanics: Theory and Experiment* **2020,** 103102 (2020) [In pp. 40, 143, 146].

57. Eisler, V. and Peschel, I. "Analytical results for the entanglement Hamiltonian of a free-fermion chain*". *Journal of Physics A: Mathematical and Theoretical* **50,** 284003 (2017) [In p. 40].

58. Eisler, V., Tonni, E., and Peschel, I. "On the continuum limit of the entanglement Hamiltonian". *Journal of Statistical Mechanics: Theory and Experiment* **2019,** 073101 (2019) [In p. 40].

59. Fagotti, M., Calabrese, P., and Moore, J. E. "Entanglement spectrum of random-singlet quantum critical points". *Physical Review B* **83,** 045110 (2011) [In pp. 36, 37, 59].

60. Fannes, M., Nachtergaele, B., and Werner, R. F. "Finitely correlated states on quantum spin chains". *Communications in Mathematical Physics 1992 144:3* **144,** 443–490 (1992) [In p. 7].

61. Fidkowski, L., Refael, G., Bonesteel, N. E., and Moore, J. E. "c-theorem violation for effective central charge of infinite-randomness fixed points". *Physical Review B* **78,** 224204 (2008) [In p. 130].

62. Fidkowski, L. "Entanglement Spectrum of Topological Insulators and Superconductors". *Physical Review Letters* **104,** 130502 (2010) [In p. 104].

63. Fidkowski, L. and Kitaev, A. "Topological phases of fermions in one dimension". *Physical Review B* **83,** 075103 (2011) [In pp. 104, 110].

64. Fisher, D. S. "Critical behavior of random transverse-field Ising spin chains". *Physical Review B* **51,** 6411 (1995) [In pp. 11, 50, 106, 129].

65. Fisher, D. S. "Random antiferromagnetic quantum spin chains". *Physical Review B* **50,** 3799 (1994) [In pp. 50, 129].

66. Fisher, M. E. and Hartwig, R. E. "Toeplitz Determinants: Some Applications, Theorems, and Conjectures". *Stochastic Processes in Chemical Physics*, 333–353 (1969) [In p. 35].

67. Freedman, S. J. and Clauser, J. F. "Experimental Test of Local Hidden-Variable Theories". *Physical Review Letters* **28,** 938 (1972) [In p. 4].

68. Furuya, S. C. and Oshikawa, M. "Symmetry Protection of Critical Phases and a Global Anomaly in (1+1) Dimensions". *Physical Review Letters* **118,** 021601 (2017) [In pp. 105, 115].

69. Girvin, S. M. and Arovas, D. P. "Hidden topological order in integer quantum spin chains". *Physica Scripta* **T27,** 156–159 (1989) [In p. 113].

70. Giudici, G., Mendes-Santos, T., Calabrese, P., and Dalmonte, M. "Entanglement Hamiltonians of lattice models via the Bisognano-Wichmann theorem". *Physical Review B* **98,** 134403 (2018) [In p. 39].

71. Giustina, M. *et al.* "Significant-Loophole-Free Test of Bell's Theorem with Entangled Photons". *Physical Review Letters* **115,** 250401 (2015) [In p. 4].

72. Gómez, C., Ruiz-Altaba, M., and Sierra, G. "Quantum Groups in Two-Dimensional Physics". *Quantum Groups in Two-Dimensional Physics* (1996) [In p. 130].

73. Gori, G., Paganelli, S., Sharma, A., Sodano, P., and Trombettoni, A. "Explicit Hamiltonians inducing volume law for entanglement entropy in fermionic lattices". *Physical Review B* **91,** 245138 (2015) [In p. 8].

74. Gu, Z.-C. and Wen, X.-G. "Tensor-entanglement-filtering renormalization approach and symmetry-protected topological order". *Physical Review B* **80,** 155131 (2009) [In p. 104].

75. Haegeman, J., Pérez-García, D., Cirac, I., and Schuch, N. "Order Parameter for Symmetry-Protected Phases in One Dimension". *Physical Review Letters* **109,** 050402 (2012) [In p. 104].

76. Haldane, F. D. M. "Nonlinear Field Theory of Large-Spin Heisenberg Antiferromagnets: Semiclassically Quantized Solitons of the One-Dimensional Easy-Axis Néel State". *Physical Review Letters* **50,** 1153 (1983) [In pp. 7, 104, 115].

77. Hartman, T. and Maldacena, J. "Time evolution of entanglement entropy from black hole interiors". *Journal of High Energy Physics 2013 2013:5* **2013,** 1–28 (2013) [In p. 63].

78. Hastings, M. B. "An area law for one-dimensional quantum systems". *Journal of Statistical Mechanics: Theory and Experiment* **2007,** P08024 (2007) [In p. 7].

79. Hastings, M. B. "Solving gapped Hamiltonians locally". *Physical Review B* **73,** 085115 (2006) [In p. 105].

80. Hawking, S. W. "Particle creation by black holes". *Communications in Mathematical Physics 1975 43:3* **43,** 199–220 (1975) [In p. 5].

81. Heeger, A. J., Kivelson, S., Schrieffer, J. R., and Su, W. .-P. "Solitons in conducting polymers". *Reviews of Modern Physics* **60,** 781 (1988) [In pp. 78, 137].

82. Heisenberg, W. "Zur Theorie des Ferromagnetismus". *Zeitschrift für Physik 1928 49:9* **49,** 619–636 (1928) [In p. 2].

83. Holzhey, C., Larsen, F., and Wilczek, F. "Geometric and renormalized entropy in conformal field theory". *Nuclear Physics B* **424,** 443–467 (1994) [In pp. 8, 31, 32].

84. Horodecki, M., Horodecki, P., and Horodecki, R. "Separability of mixed states: necessary and sufficient conditions". *Physics Letters A* **223,** 1–8 (1996) [In p. 15].

85. Horodecki, R., Horodecki, P., Horodecki, M., and Horodecki, K. "Quantum entanglement". *Reviews of Modern Physics* **81,** 865 (2009) [In p. 5].

86. Hubbard, J. "Electron correlations in narrow energy bands". *Proceedings of the Royal Society of London. Series A. Mathematical and Physical Sciences* **276,** 238–257 (1963) [In p. 3].

87. Iglói, F. and Juhász, R. "Exact relationship between the entanglement entropies of XY and quantum Ising chains". *EPL (Europhysics Letters)* **81,** 57003 (2008) [In pp. 136, 150].

88. Iglói, F. and Monthus, C. "Strong disorder RG approach of random systems". *Physics Reports* **412,** 277–431 (2005) [In pp. 10, 50].

89. Iglói, F., Szatmári, Z., and Lin, Y.-C. "Entanglement entropy with localized and extended interface defects". *Physical Review B* **80,** 024405 (2009) [In p. 75].

90. Ising, E. "Beitrag zur Theorie des Ferromagnetismus". *Zeitschrift für Physik 1925 31:1* **31,** 253–258 (1925) [In p. 2].

91. Jin, B.-Q. and Korepin, V. E. "Quantum Spin Chain, Toeplitz Determinants and the Fisher—Hartwig Conjecture". *Journal of Statistical Physics 2004 116:1* **116,** 79–95 (2004) [In pp. 8, 34, 35, 59, 109, 150].

92. Jordan, P. and Wigner, E. "Über das Paulische Äquivalenzverbot". *Zeitschrift für Physik 1928 47:9* **47,** 631–651 (1928) [In pp. 23, 45].

93. Kadanoff, L. P. "Scaling laws for ising models near Tc". *Physics Physique Fizika* **2,** 263 (1966) [In p. 3].

94. Kane, C. L. and Fisher, M. P. A. "Transport in a one-channel Luttinger liquid". *Physical Review Letters* **68,** 1220 (1992) [In p. 107].

95. Karlsson, A. and Bourennane, M. "Quantum teleportation using three-particle entanglement". *Physical Review A* **58,** 4394 (1998) [In p. 13].

96. Kennedy, T. and Tasaki, H. "Hidden symmetry breaking and the Haldane phase inS=1 quantum spin chains". *Communications in Mathematical Physics 1992 147:3* **147,** 431–484 (1992) [In p. 104].

97. Kitaev, A. Y. "Unpaired Majorana fermions in quantum wires". *Physics-Uspekhi* **44,** 131 (2001) [In pp. 127, 129, 139].

98. Kitaev, A. "Periodic table for topological insulators and superconductors". *AIP Conference Proceedings* **1134,** 22 (2009) [In p. 104].

99. Kondo, J. "Resistance Minimum in Dilute Magnetic Alloys". *Progress of Theoretical Physics* **32,** 37–49 (1964) [In p. 3].

100. Laflorencie, N. "Quantum entanglement in condensed matter systems". *Physics Reports* **646,** 1–59 (2016) [In p. 5].

101. Lahtinen, V. T. and Pachos, J. K. "A short introduction to topological quantum computation". *SciPost Phys* **3,** 21 (2017) [In p. 130].

102. Lambert, N., Emary, C., and Brandes, T. "Entanglement and the Phase Transition in Single-Mode Superradiance". *Physical Review Letters* **92,** 073602 (2004) [In p. 8].

103. Landau, L. "The Theory of a Fermi Liquid". *Sov.Phys.JETP* **3,** 920 (1957) [In p. 1].

104. Landau, L. D. "On the theory of phase transitions." *Zh. Eksp. Teor. Fiz.* **11,** 19 (1937) [In p. 9].

105. Lange, C., Klümper, A., and Zittartz, J. "Exact groundstates for antiferromagnetic spin-one chains with nearest and next-nearest neighbour interactions". *Zeitschrift für Physik B Condensed Matter 1994 96:2* **96,** 267–270 (1994) [In p. 7].

106. Latorre, J. I., Rico, E., and Vidal, G. "Ground state entanglement in quantum spin chains". *Quantum Information and Computation* **4,** 48–92 (2003) [In pp. 8, 47].

107. Läuchli, A. M. "Operator content of real-space entanglement spectra at conformal critical points" (2013) [In p. 41].

108. Laughlin, R. B. "Anomalous Quantum Hall Effect: An Incompressible Quantum Fluid with Fractionally Charged Excitations". *Physical Review Letters* **50,** 1395 (1983) [In p. 10].

109. Levine, G. C. "Entanglement Entropy in a Boundary Impurity Model". *Physical Review Letters* **93,** 266402 (2004) [In p. 75].

110. Li, H. and Haldane, F. D. M. "Entanglement Spectrum as a Generalization of Entanglement Entropy: Identification of Topological Order in Non-Abelian Fractional Quantum Hall Effect States". *Physical Review Letters* **101,** 010504 (2008) [In pp. 5, 15, 41].

111. Lieb, E., Schultz, T., and Mattis, D. "Two soluble models of an antiferromagnetic chain". *Annals of Physics* **16,** 407–466 (1961) [In p. 23].

112. Lugiato, L. A., Gatti, A., and Brambilla, E. "Quantum imaging". *Journal of Optics B: Quantum and Semiclassical Optics* **4,** S176 (2002) [In p. 5].

113. Ma, S.-k., Dasgupta, C., and Hu, C.-k. "Random Antiferromagnetic Chain". *Physical Review Letters* **43,** 1434 (1979) [In p. 11].

114. MacCormack, I., Liu, A., Nozaki, M., and Ryu, S. "Holographic duals of inhomogeneous systems: the rainbow chain and the sine-square deformation model". *Journal of Physics A: Mathematical and Theoretical* **52,** 505401 (2019) [In pp. 57, 135].

115. Maldacena, J. and Susskind, L. "Cool horizons for entangled black holes". *Fortschritte der Physik* **61,** 781–811 (2013) [In p. 63].

116. Maldacena, J. and Stanford, D. "Remarks on the Sachdev-Ye-Kitaev model". *Physical Review D* **94,** 106002 (2016) [In p. 11].

117. Modi, K., Brodutch, A., Cable, H., Paterek, T., and Vedral, V. "The classical-quantum boundary for correlations: Discord and related measures". *Reviews of Modern Physics* **84,** 1655 (2012) [In p. 13].

118. Motrunich, O., Damle, K., and Huse, D. A. "Griffiths effects and quantum critical points in dirty superconductors without spin-rotation invariance: One-dimensional examples". *Physical Review B* **63,** 224204 (2001) [In p. 130].

119. Movassagh, R. and Shor, P. W. "Supercritical entanglement in local systems: Counterexample to the area law for quantum matter". *Proceedings of the National Academy of Sciences* **113,** 13278–13282 (2016) [In p. 8].

120. Nayak, C., Simon, S. H., Stern, A., Freedman, M., and Sarma, S. D. "Non-Abelian anyons and topological quantum computation". *Reviews of Modern Physics* **80,** 1083 (2008) [In pp. 130, 148].

121. Nielsen, M. A. and Chuang, I. L. "Quantum Computation and Quantum Information: 10th Anniversary Edition". *Quantum Computation and Quantum Information* (2010) [In pp. 5, 52].

122. Onsager, L. "Crystal Statistics. I. A Two-Dimensional Model with an Order-Disorder Transition". *Physical Review* **65,** 117 (1944) [In p. 3].

123. Orús, R. "A practical introduction to tensor networks: Matrix product states and projected entangled pair states". *Annals of Physics* **349,** 117–158 (2014) [In pp. 7, 104].

124. Östlund, S. and Rommer, S. "Thermodynamic Limit of Density Matrix Renormalization". *Physical Review Letters* **75,** 3537 (1995) [In p. 6].

125. Page, D. N. "Average entropy of a subsystem". *Physical Review Letters* **71,** 1291 (1993) [In p. 7].

126. Peres, A. "Separability Criterion for Density Matrices". *Physical Review Letters* **77,** 1413 (1996) [In p. 15].

127. Peschel, I. "Calculation of reduced density matrices from correlation functions". *Journal of Physics A: Mathematical and General* **36,** L205 (2003) [In pp. 28, 110, 133, 136].

128. Peschel, I. *Density-matrix spectra for integrable models.* 1999 [In p. 63].

129. Peschel, I. “Entanglement entropy with interface defects”. *Journal of Physics A: Mathematical and General* **38,** 4327 (2005) [In p. 75].

130. Peschel, I. “On the reduced density matrix for a chain of free electrons”. *Journal of Statistical Mechanics: Theory and Experiment* **2004,** P06004 (2004) [In p. 41].

131. Peschel, I. and Eisler, V. “Reduced density matrices and entanglement entropy in free lattice models”. *Journal of Physics A: Mathematical and Theoretical* **42,** 504003 (2009) [In pp. 136, 143].

132. Pollmann, F., Berg, E., Turner, A. M., and Oshikawa, M. “Symmetry protection of topological phases in one-dimensional quantum spin systems”. *Physical Review B* **85,** 075125 (2012) [In pp. 104, 113, 115, 126].

133. Pollmann, F., Turner, A. M., Berg, E., and Oshikawa, M. “Entanglement spectrum of a topological phase in one dimension”. *Physical Review B* **81,** 064439 (2010) [In pp. 10, 41, 104, 109, 113, 126].

134. Powell, M. J. D. “An efficient method for finding the minimum of a function of several variables without calculating derivatives”. *The Computer Journal* **7,** 155–162 (1964) [In p. 40].

135. Preskill, J. “Quantum information and physics: Some future directions”. *Journal of Modern Optics* **47-2,** 127–137 (2000) [In p. 5].

136. Rachel, S., Haque, M., Bernevig, A., Laeuchli, A., and Fradkin, E. *Special Issue: Quantum Entanglement in Condensed Matter Physics - Journal of Statistical Mechanics: Theory and Experiment.* 2015 [In p. 5].

137. Ramírez, G., Rodríguez-Laguna, J., and Sierra, G. “Entanglement in low-energy states of the random-hopping model”. *Journal of Statistical Mechanics: Theory and Experiment* **2014,** P07003 (2014) [In p. 65].

138. Ramírez, G., Rodríguez-Laguna, J., and Sierra, G. “Entanglement over the rainbow”. *Journal of Statistical Mechanics: Theory and Experiment* **2015,** P06002 (2015) [In pp. 9, 48, 56, 62, 63, 65, 91].

139. Ramírez, G., Rodríguez-Laguna, J., and Sierra, G. “From conformal to volume law for the entanglement entropy in exponentially deformed critical spin 1/2 chains”. *Journal of Statistical Mechanics: Theory and Experiment* **2014,** P10004 (2014) [In pp. 9, 48, 65, 106].

140. Refael, G. and Moore, J. E. “Criticality and entanglement in random quantum systems”. *Journal of Physics A: Mathematical and Theoretical* **42,** 504010 (2009) [In p. 52].

141. Refael, G. and Moore, J. E. “Entanglement Entropy of Random Quantum Critical Points in One Dimension”. *Physical Review Letters* **93,** 260602 (2004) [In p. 8].

142. Rényi, A. "On Measures of Entropy and Information". *Proceedings of the Fourth Berkeley Symposium on Mathematical Statistics and Probability, Volume 1: Contributions to the Theory of Statistics,* 547–561 (1961) [In p. 16].

143. Rodríguez-Laguna, J., Dubail, J., Ramírez, G., Calabrese, P., and Sierra, G. "More on the rainbow chain: entanglement, space-time geometry and thermal states". *Journal of Physics A: Mathematical and Theoretical* **50,** 164001 (2017) [In pp. 9, 47, 56–58, 109].

144. Rodríguez-Laguna, J., Santalla, S. N., Ramírez, G., and Sierra, G. "Entanglement in correlated random spin chains, RNA folding and kinetic roughening". *New Journal of Physics* **18,** 073025 (2016) [In pp. 77, 130].

145. Rodríguez-Laguna, J., Tarruell, L., Lewenstein, M., and Celi, A. "Synthetic Unruh effect in cold atoms". *Physical Review A* **95,** 013627 (2017) [In p. 136].

146. Rosenfeld, W. *et al.* "Event-Ready Bell Test Using Entangled Atoms Simultaneously Closing Detection and Locality Loopholes". *Physical Review Letters* **119,** 010402 (2017) [In p. 4].

147. Ryu, S. and Takayanagi, T. "Holographic Derivation of Entanglement Entropy from the anti–de Sitter Space/Conformal Field Theory Correspondence". *Physical Review Letters* **96,** 181602 (2006) [In p. 8].

148. Samos Sáenz de Buruaga, N., Santalla, S. N., Rodríguez-Laguna, J., and Sierra, G. "Symmetry protected phases in inhomogeneous spin chains". *Journal of Statistical Mechanics: Theory and Experiment* **2019,** 093102 (2019) [In pp. 85, 103].

149. Samos Sáenz de Buruaga, N., Santalla, S. N., Rodríguez-Laguna, J., and Sierra, G. "Entanglement in noncritical inhomogeneous quantum chains". *Physical Review B* **104,** 195147 (2021) [In p. 127].

150. Samos Sáenz de Buruaga, N., Santalla, S. N., Rodríguez-Laguna, J., and Sierra, G. "Piercing the rainbow state: Entanglement on an inhomogeneous spin chain with a defect". *Physical Review B* **101,** 205121 (2020) [In pp. 75, 103].

151. Schauss, P. "Quantum simulation of transverse Ising models with Rydberg atoms". *Quantum Science and Technology* **3,** 023001 (2018) [In p. 148].

152. Schollwöck, U. "The density-matrix renormalization group in the age of matrix product states". *Annals of Physics* **326,** 96–192 (2011) [In pp. 7, 104, 126].

153. Schuch, N., Pérez-García, D., and Cirac, I. "Classifying quantum phases using matrix product states and projected entangled pair states". *Physical Review B* **84,** 165139 (2011) [In p. 104].

154. Schultz, T., Lieb, E., and Mattis, D. "Two-Dimensional Ising Model as a Soluble Problem of Many Fermions". *Reviews of Modern Physics* **36,** 856 (1964) [In p. 3].

155. Shannon, C. E. "A Mathematical Theory of Communication". *Bell System Technical Journal* **27,** 379–423 (1948) [In p. 16].

156. Shiba, N. and Takayanagi, T. "Volume law for the entanglement entropy in non-local QFTs". *Journal of High Energy Physics 2014 2014:2* **2014,** 1–16 (2014) [In p. 8].

157. Sierra, G. "The Riemann zeros as energy levels of a Dirac fermion in a potential built from the prime numbers in Rindler spacetime". *Journal of Physics A: Mathematical and Theoretical* **47,** 325204 (2014) [In p. 86].

158. Simon, P. and Affleck, I. "Persistent currents through a quantum dot". *Physical Review B* **64,** 085308 (2001) [In p. 107].

159. Srednicki, M. "Entropy and area". *Physical Review Letters* **71,** 666 (1993) [In pp. 6, 8].

160. Streltsov, A., Adesso, G., and Plenio, M. B. "Colloquium: Quantum coherence as a resource". *Reviews of Modern Physics* **89,** 041003 (2017) [In p. 13].

161. Su, W. P., Schrieffer, J. R., and Heeger, A. J. "Solitons in Polyacetylene". *Physical Review Letters* **42,** 1698 (1979) [In pp. 78, 108, 110, 137].

162. Swingle, B. "Entanglement renormalization and holography". *Physical Review D* **86,** 065007 (2012) [In p. 8].

163. Takhtajan, L. A. "The picture of low-lying excitations in the isotropic Heisenberg chain of arbitrary spins". *Physics Letters A* **87,** 479–482 (1982) [In p. 113].

164. Tonni, E., Rodríguez-Laguna, J., and Sierra, G. "Entanglement hamiltonian and entanglement contour in inhomogeneous 1D critical systems". *Journal of Statistical Mechanics: Theory and Experiment* **2018,** 043105 (2018) [In pp. 40, 47, 60, 64, 89, 91, 136].

165. Tsui, D. C., Stormer, H. L., and Gossard, A. C. "Two-Dimensional Magnetotransport in the Extreme Quantum Limit". *Physical Review Letters* **48,** 1559 (1982) [In pp. 9, 103].

166. Tsui, L., Wang, F., and Lee, D.-H. "Topological versus Landau-like phase transitions" (2015) [In p. 104].

167. Turner, A. M., Pollmann, F., and Berg, E. "Topological phases of one-dimensional fermions: An entanglement point of view". *Physical Review B* **83,** 075102 (2011) [In pp. 104, 109].

168. Vasseur, R., Potter, A. C., You, Y.-Z., and Ludwig, A. W. W. "Entanglement transitions from holographic random tensor networks". *Physical Review B* **100,** 134203 (2019) [In p. 79].

169. Verstraete, F. and Cirac, J. I. "Matrix product states represent ground states faithfully". *Physical Review B* **73,** 094423 (2006) [In p. 7].

170. Verstraete, F. and Cirac, J. I. "Renormalization algorithms for Quantum-Many Body Systems in two and higher dimensions" (2004) [In p. 7].

171. Verstraete, F., Porras, D., and Cirac, J. I. "Density Matrix Renormalization Group and Periodic Boundary Conditions: A Quantum Information Perspective". *Physical Review Letters* **93,** 227205 (2004) [In p. 6].

172. Vidal, G. "Efficient Classical Simulation of Slightly Entangled Quantum Computations". *Physical Review Letters* **91,** 147902 (2003) [In p. 7].

173. Vidal, G. "Entanglement Renormalization". *Physical Review Letters* **99,** 220405 (2007) [In p. 8].

174. Vidal, G., Latorre, J. I., Rico, E., and Kitaev, A. "Entanglement in Quantum Critical Phenomena". *Physical Review Letters* **90,** 227902 (2003) [In p. 8].

175. Vitagliano, G., Riera, A., and Latorre, J. I. "Volume-law scaling for the entanglement entropy in spin-1/2 chains". *New Journal of Physics* **12,** 113049 (2010) [In pp. 9, 48, 65, 105].

176. Wehrl, A. "General properties of entropy". *Reviews of Modern Physics* **50,** 221 (1978) [In p. 16].

177. Wen, Q. "Formulas for partial entanglement entropy". *Physical Review Research* **2,** 23170 (2020) [In p. 43].

178. Wen, X. G. "Vacuum degeneracy of chiral spin states in compactified space". *Physical Review B* **40,** 7387 (1989) [In p. 103].

179. Wen, X. G. "Quantum orders and symmetric spin liquids". *Physical Review B* **65,** 165113 (2002) [In p. 103].

180. Wen, X.-G. "Colloquium:Zoo of quantum-topological phases of matter". *Reviews of Modern Physics* **89,** 041004 (2017) [In pp. 10, 103].

181. White, S. R. "Density matrix formulation for quantum renormalization groups". *Physical Review Letters* **69,** 2863 (1992) [In pp. 4, 114].

182. White, S. R. "Density-matrix algorithms for quantum renormalization groups". *Physical Review B* **48,** 10345 (1993) [In p. 4].

183. White, S. R. and Huse, D. A. "Numerical renormalization-group study of low-lying eigenstates of the antiferromagnetic S". *Physical Review B* **48,** 3844 (1993) [In p. 113].

184. Wilson, K. G. "The renormalization group: Critical phenomena and the Kondo problem". *Reviews of Modern Physics* **47,** 773 (1975) [In p. 3].

185. Wolf, M. M. "Violation of the Entropic Area Law for Fermions". *Physical Review Letters* **96,** 010404 (2006) [In p. 8].

186. Wolf, M. M., Verstraete, F., Hastings, M. B., and Cirac, J. I. "Area Laws in Quantum Systems: Mutual Information and Correlations". *Physical Review Letters* **100,** 070502 (2008) [In p. 105].

187. Wong, G., Klich, I., Zayas, L. A. P., and Vaman, D. "Entanglement temperature and entanglement entropy of excited states". *Journal of High Energy Physics 2013 2013:12* **2013,** 1–24 (2013) [In p. 37].

188. Xavier, J. C. and Alcaraz, F. C. "Rényi entropy and parity oscillations of anisotropic spin-<span class". *Physical Review B* **83,** 214425 (2011) [In p. 35].

189. Yan, B. and Felser, C. "Topological Materials: Weyl Semimetals". *Annual Reviews* **8,** 337–354 (2017) [In p. 103].

190. Zeng, B., Chen, X., Zhou, D.-L., and Wen, X.-G. "Quantum Information Meets Quantum Matter". *Quantum Science and Technology* (2019) [In p. 5].